Anisotropic Phenomena in Gauge/Gravity Duality

Dissertation by Hansjörg Zeller

Anisotropic Phenomena in Gauge/Gravity Duality

Dissertation
an der Fakultät für Physik
der Ludwig–Maximilians–Universität
München

vorgelegt von
Hansjörg Zeller
aus Neuendettelsau

München, den 26. Mai 2014

Dissertation

submitted to the faculty of physics of the
Ludwig–Maximilians–Universität München

by Hansjörg Zeller

supervised by Prof. Dr. Johanna Karen Erdmenger
Max-Planck-Institut für Physik, München

1st Referee: Prof. Dr. Johanna Karen Erdmenger
2nd Referee: Prof. Dr. Dieter Lüst

Date of submission: 26 May 2014
Date of oral examination: 18 July 2014

Zusammenfassung

Diese Dissertation untersucht anisotrope Effekte verschiedener Materialien mit Hilfe der Dualität zwischen Eich- und Gravitationstheorien. Wir interessieren uns einerseits für die hydrodynamischen Eigenschaften holographischer Systeme mit gebrochener Rotationssymmetrie. Andererseits analysieren wir Geometrien, die eine duale Interpretation als infrarot Fixpunkte von Theorien haben, welche die Festkörper beschreiben.

Die Dualität setzt eine Gravitationstheorie in Anti-de Sitter Raum in Beziehung zu einer Quantenfeldtheorie in einem niedriger dimensionalen Minkowski Raum. Während des letzten Jahrzehntes konnten mit Hilfe der Dualität viele Eigenschaften stark gekoppelter Systeme, wie zum Beispiel Eigenschaften des Quark-Gluon Plasmas und quantenkritischer Punkte in Festkörperphysiktheorien, untersucht werden.

Ein sehr wichtiges Ergebnis, das in diesem Zusammenhang berechnet wurde, ist das Verhältnis zwischen Viskosität und Entropiedichte in stark gekoppelten Theorien. Der berechnete Wert stimmt sehr gut mit den Messungen dieser Größe im Quark-Gluon Plasma überein. Allerdings ist dieses Verhältnis temperaturunabhängig, falls die duale Gravitationstheorie, in der es berechnet wurde, höchstens zweifache Ableitungsterme beinhaltet und isotrop ist. Wir zeigen in dieser Arbeit, dass bereits durch eine Brechung der Rotationssymmetrie eine Temperaturabhängigkeit der Viskosität über Entropiedichte erzeugt werden kann. Dies ist ein wichtiges Ergebnis um der Beschreibung realer Substanzen näher zu kommen.

Zusätzlich berechnen wir verschiedenste hydrodynamische Eigenschaften stark gekoppelter anisotroper Systeme im Rahmen der oben beschriebenen Dualität. Unter den wichtigsten Ergebnissen ist das Niedrigfrequenzverhalten der elektrischen Leitfähigkeit, welches der eines Drude Models ähnlich ist. Letzteres ist von Leitern mit gebrochener Translationsinvarianz bekannt. Allerdings wurde diese Brechung nicht explizit in unsere Theorie eingebaut. Des Weiteren beobachten wir Effekte, die aus Flüssigkristallen bekannt sind, nämlich den Flexo- und den Piezoelektrischen Effekt.

Im zweiten Teil untersuchen wir eine Geometrie mit nicht trivialen Skalierungseigenschaften um infrarot Fixpunkte von Theorien aus der Festkörperphysik zu modellieren. Wir berechnen die UV Vervollständigigung dieser Geometrie und ermitteln ihre Eigenschaften durch die Berechnung der sogenannten holographischen Verschränkungsentropie für verschieden geformte verschränkte Regionen: einem Streifen, einer Scheibe und einem Ring. Die Verschränkungsentropie ist sensitiv auf die mikroskopischen Freiheitsgrade einer Theorie. Deshalb ist es sehr interessant,

dass der Streifen und der Ring, im Gegensatz zur Scheibe, einen Phasenübergang für einen bestimmten Wert der relevanten typischen Längen aufweisen. Außerdem gibt es einen Zusammenhang zwischen den kritischen Längen der ersten beiden Formen. Die Geometrien, in denen das seltsame Verhalten der Scheibe bereits beobachtet wurde, sind gekennzeichnet durch eine endliche Masse, die zu einer diskreten Anregungsenergie führt. Bezeichnenderweise ist in unserem System das nicht der Fall.

Diese Dissertation basiert auf den Ergebnissen, die der Autor unter der Betreuung von Prof. Dr. J. K. Erdmenger während der Zeit zwischen Juni 2011 und Mai 2014 am Max-Planck-Institut für Physik in München, Deutschland erzielt hat. Die relevanten Veröffentlichungen sind:

1. J. Erdmenger, P. Kerner, and H. Zeller, "Non-universal shear viscosity from Einstein gravity," *Phys.Lett.* **B699** (2011) 301–304, `arXiv:1011.5912 [hep-th]`.

2. J. Erdmenger, P. Kerner, and H. Zeller, "Transport in Anisotropic Superfluids: A Holographic Description," *JHEP* **1201** (2012) 059, `arXiv:1110.0007 [hep-th]`.

3. J. Erdmenger, D. Fernandez, and H. Zeller, "New Transport Properties of Anisotropic Holographic Superfluids," *JHEP* **1304** (2013) 049, `arXiv:1212.4838 [hep-th]`.

4. J. Erdmenger, D.-W. Pang, and H. Zeller, "Holographic entanglement entropy of semi-local quantum liquids," *JHEP* **1402** (2014) 016, `arXiv:1311.1217 [hep-th]`.

Abstract

In this thesis we use gauge/gravity duality to model anisotropic effects realised in nature. Firstly we analyse transport properties in holographic systems with a broken rotational invariance. Secondly we discuss geometries dual to IR fixed points with anisotropic scaling behaviour, which are related to quantum critical points in condensed matter systems.

Gauge/gravity duality relates a gravity theory in Anti-de Sitter space to a lower dimensional strongly coupled quantum field theory in Minkowski space. Over the past decade this duality provided many insights into systems at strong coupling, e.g. quark-gluon plasma and condensed matter close to quantum critical points.

One very important result computed in this framework is the value of the shear viscosity divided by the entropy density in strongly coupled theories. The quantitative result agrees very well with measurements of the ratio in quark-gluon plasma. However, for isotropic two derivative Einstein gravity it is temperature independent. We show that by breaking the rotational symmetry of a system we obtain a temperature dependent shear viscosity over entropy density. This is important to make contact with real world systems, since substances in nature display such dependence.

In addition, we derive various transport properties in strongly coupled anisotropic systems using the gauge/gravity dictionary. The most notable results include an electrical conductivity with Drude behaviour in the low frequency region. This resembles conductors with broken translational invariance. However, we did not implement the breaking explicitly. Furthermore, our analysis shows that this setup models effects, resembling the piezoelectric and flexoelectric effects, known from liquid crystals.

In a second project we discuss a geometry with non-trivial scaling behaviour in order to model an IR fixed point of condensed matter theories. We construct the UV completion of this geometry and analyse its properties by computing the holographic entanglement entropy for different entangling shapes, namely a strip, a disc and an annulus. The entanglement entropy is a quantity sensitive to the microscopic degrees of freedom of a theory. Thus it is interesting that the strip and the annulus undergo a phase transition for certain values of the relevant length of the shape, while the disc does not. In addition, the critical lengths at which the former two shapes change their behaviour are related to each other. The backgrounds, where the awkwardly behaving disc shape was observed before, are characterised by a mass gap. Remarkably this is not the case here.

The results presented in this thesis were obtained by the author under the supervision of Prof. Dr. J. K. Erdmenger between June 2011 and May 2014 at the Max-Planck-Institute for Physics in Munich, Germany. The relevant publications are:

1. J. Erdmenger, P. Kerner, and H. Zeller, "Non-universal shear viscosity from Einstein gravity," *Phys.Lett.* **B699** (2011) 301–304, `arXiv:1011.5912 [hep-th]`.

2. J. Erdmenger, P. Kerner, and H. Zeller, "Transport in Anisotropic Superfluids: A Holographic Description," *JHEP* **1201** (2012) 059, `arXiv:1110.0007 [hep-th]`.

3. J. Erdmenger, D. Fernandez, and H. Zeller, "New Transport Properties of Anisotropic Holographic Superfluids," *JHEP* **1304** (2013) 049, `arXiv:1212.4838 [hep-th]`.

4. J. Erdmenger, D.-W. Pang, and H. Zeller, "Holographic entanglement entropy of semi-local quantum liquids," *JHEP* **1402** (2014) 016, `arXiv:1311.1217 [hep-th]`.

Contents

Chapter 1

Introduction

Superconductors model quantum aspects of black holes. This sentence was hardly imaginable before the advent of holography. However, the holographic principle not only blurs the borders between different fields of physics, but it also lays out a new path in our understanding of quantum gravity. At the centre of this principle stands the description of a quantum gravitational system in a bounded volume by a quantum field theory living at its boundary.

A first hint at this remarkable correspondence occurred through the identification of black hole entropy. Bekenstein and Hawking showed that the entropy is proportional to the area of the black hole horizon in Planck units rather than its volume [5,6]. This is as opposed to non-gravitational quantum systems, where the entropy scales with the latter. From this result 't Hooft and Susskind developed the holographic principle, which relates the number of quantum states of a gravity theory to the Fock space of a lower dimensional quantum field theory [7, 8]. By now there are quantitative realisations of holography in terms of string theories in Anti-de Sitter space and quantum field theories in one dimension less. This was first proposed by Maldacena in [9] and shortly afterwards made precise by Gubser, Klebanov, Polyakov and Witten [10, 11].

Understanding quantum gravity is one of the biggest challenges in physics of our time. From a theoretical point of view, string theory already provides some very good insight. However, direct experimental input is rather unlikely at present. The energies needed to directly probe gravity in this regime are far out of reach (of order of the Planck scale) and black holes obscure this aspect with a horizon. However, shortly before the time of this writing a notable measurement was published, which may cast some light on this realm. The experiment in question is BICEP2 (Background Imaging of Cosmic Extragalactic Polarization), which measures the polarisation of the cosmic microwave background (CMB). They claim to

have detected gravitational waves originating from the early universe [12], i.e. primordial gravitational waves. If true, the data seems to strongly favour theoretical descriptions of the early universe in a framework known as cosmic inflation [13–15]. The models attributed to this concept describe a very fast (inflationary) expansion of space over a very brief amount of time just at the beginning of the universe. These theories explain, for instance, the surprising overall homogeneity and isotropy of the temperature distribution of the CMB. Remarkably, even the very small anisotropies of the latter are accounted for. Since cosmic inflation, if true, took place at very high energies (BICEP2 favours inflation to end at roughly $\mathcal{O}(10^{16}\,\mathrm{GeV})$) and is very sensitive to the conditions before it started, it encodes quantum gravitational effects. Thus measurements may find some hints of these.

There is a second approach to gaining insight into gravitational theories at very high energies from theory as well as, perhaps, experiment. The holographic principle tells us that gravitational theories can be described by lower dimensional quantum field theories. While both theories are very different from each other, they are very successful in their own domain of validity.

Quantum field theories are very precise descriptions of the microscopic world. One of the greatest achievements in this context is the Standard Model of particle physics [16–19]. It describes to a very high accuracy the properties of the most elementary particles, leptons and quarks, that are known to date. These particles interact via three forces, the electromagnetic, the weak and the strong force. All of them are mediated via gauge bosons, namely photons, W- and Z-bosons and gluons, respectively. Recently another boson known as the Higgs particle was measured by two experiments, Atlas and CMS, at the Large Hadron Collider (LHC) in Geneva [20, 21]. Therefore, how the spontaneous symmetry breaking at a fundamental level is realised is now unchallenged. It comes about in the same way as observed before on a non-fundamental level in materials which become superconducting below a certain temperature, with the Higgs mechanism. This mechanism also provides an explanation as to how elementary particles dynamically become massive. In 2013 the Nobel Prize was awarded to some of its inventors, namely to François Englert and Peter Higgs[1] [23–25]. With the measurement of this boson all predicted particles of the Standard Model are experimentally accounted for. Moreover, many of the other predictions originating from this model agree to a very high precision with data at the energies reachable to date ($\mathcal{O}(1\mathrm{TeV})$). The next step is to go beyond these energies. It is an experimental and theoretical challenge of our time to find the correct models that describe the physics at the higher scales.

[1] In 1964 Robert Brout, François Englert, Peter Higgs, Gerald Guralnik, C. Richard Hagen and Tom Kibble published on this topic nearly at the same time [22–25].

On the other end of the microscopic world, quantum field theories describe, also very successfully, condensed matter systems. Examples are fermi-liquids and conventional superconductors. The difference to the high energy world, where one model (Lagrangian) predominates, is the use of different Lagrangians depending on the problem of interest. Here the concept of effective theories is more accentuated[2]. Instead of fundamental particles one deals with quasiparticle excitations. These are excitations which can effectively be described in a particle language, i.e. they are long-lived enough. In addition, there is a clear UV cut off, for instance a lattice spacing. Next we make a huge jump to the other end of the length scale.

At macroscopic distances, roughly around the size of the solar system, the effects from the general theory of relativity, developed by Einstein at the beginning of the last century and published in 1916 [26], become increasingly important[3]. This theory geometrises the concept of a gravitational force. Many of the predicted effects, such as gravitational lensing, are accounted for experimentally. A missing piece, the gravitational waves, may have been observed by BICEP2 (see above). Interestingly, the equations of general relativity also allow for black hole solutions. Classically, these are objects that bend spacetime so strongly that nothing comes out of them, not even light. They are geometrically bounded by a horizon, the black hole horizon. However, to properly describe black holes, quantum mechanics has to be taken into account, since they radiate with a Planckian black body radiation spectrum, leading to a temperature and an unusually behaving entropy (see second paragraph) [5, 6, 27].

To take quantum mechanical effects of a black hole into account, without the knowledge of quantum gravity, one has to rely on certain approximations. Usually it is reasonable to assume that quantum field theory in not too strongly curved backgrounds is a valid description. This way it is possible to compute the vacuum that an observer hovering just over the black hole sees, namely a thermal ensemble [27]. This leads to the Hawking temperature T_H of a black hole, measured by an observer far away. Taking the laws of thermodynamics into account, one concludes that an object with temperature also has an entropy [5, 6]. This is the entropy that turns out to be proportional to the area of the horizon, rather than the black hole volume. In addition, since it radiates energy, the black hole should fully evaporate at some point [6]. Assuming that the principles of quantum mechanics are also valid for this process, an observer outside the black hole sees

[2]Note that the Standard Model Lagrangian is also an effective theory, since it is not UV complete.

[3]Depending on the precision needed, GR effects are already visible at much smaller length scales, for instance in global navigational satellite systems (e.g. Galileo).

its creation and evaporation as a unitary process, governed by a well defined S matrix. That is, no information should be lost along the line. Besides these three assumptions (i.e. quantum field theory is valid in weakly curved backgrounds, thermodynamics applies to black holes and quantum mechanics is not violated) there is a fourth assumption, namely that an observes freely falling through a big black hole[4] does not feel anything out of the ordinary. It is noteworthy that such a horizon is a global concept, i.e. even though some matter has not yet collapsed to form a black hole it is possible to fall through the corresponding horizon, so the last assumption seems reasonable (cf. [28]). It is difficult to combine these four assumptions, while not violating any physical law, for instance information conservation [28]. One proposed way goes under the name of black hole complementarity, which claims that no observer should see any violation of the laws of nature[5]. However, without the knowledge of a theory of quantum gravity many of these subtleties are very difficult to study quantitatively. But the holographic principle provides some handles to tackle these issues. Since the gravity degrees of freedom are equivalent to the states of a quantum field theory, it may turn out to be possible to study, e.g., the formation and evaporation of black holes from a QFT point of view. Therefore it would be interesting to study an explicit example of the holographic principle, as we now introduce.

The best understood example of the holographic principle is the AdS/CFT duality [9–11]. This duality is the reason for the first sentence of this introduction as we will see below. In addition it is the main framework of this thesis. As the name already suggests it relates a gravity theory living in Anti-de Sitter space to a conformal field theory in one dimension lower. It originally arose from low energy limits of superstring theory, more specifically when considering a stack of N D3-branes in type IIB superstring theory. The perturbative description for $g_sN \ll 1$ (g_s is the string coupling) is well described by the effective D3-brane DBI-action, whereas in the limit of $g_sN \gg 1$ a black 3-brane[6] with (Ramond) charge N turns out to be the correct viewpoint [31]. In the low energy limit the DBI-action turns into a supersymmetric $U(N)$ gauge theory in four dimensions, while from the black 3-brane we obtain supergravity theory in $\mathrm{AdS}_5 \times \mathrm{S}^5$. Now, the claim of the duality is that the supergravity theory is equivalent to the gauge theory in the $\lambda \gg 1$ limit, i.e. at strong coupling. Thus the AdS/CFT duality states that[7]

[4] Big black holes guarantees that the curvature at the horizon is small.

[5] Recently a vivid discussion started after a few authors claimed that the complementarity was violated for old black holes. To solve the issue they proposed a firewall right behind the horizon which would break any entanglement between the particle falling into the black hole and some particle outside its horizon [29, 30].

[6] Black branes are generalised black holes in higher dimensions, with a planar, infinitely extended horizon.

[7] The modern interpretation relates a full superstring theory in $\mathrm{AdS}_5 \times \mathrm{S}^5$ to some gauge theory

$$\text{type IIB superstring theory on } \mathrm{AdS}_5\times\mathrm{S}^5$$
$$\equiv$$
$$\mathcal{N}=4 \text{ } SU(N) \text{ super Yang-Mills theory in 4 dimensions}\,.$$

A few remarks are in order: this duality not only agrees on the level of symmetries but also on the level of dynamics. Furthermore, the gauge theory is a conformal field theory, thus the name AdS/CFT. Even though the original form was derived using the large N limit, nowadays it is assumed that it holds for all values of N and λ [33]. Note that N is the number of colours of the field theory. In addition the duality passed many non-trivial tests (see [34, 35] and references therein) and by now is considered to be robust, even though no strict mathematical proof is known. Finally one can think of the gauge theory living on the 4 dimensional boundary of the AdS_5 space. We will stick to the last picture through out this thesis.

Assuming that the duality above is in its full generality true, then we have found a complete description of a theory of quantum gravity, namely string theory, in terms of a non-gravitational supersymmetric gauge theory in four dimensions. To date string theory is the only known consistent theory of quantum gravity[8]. Hence, even though the full quantisation of string theory has not been worked out, in principle we can describe the full quantum gravity structure from a dual gauge theory point of view. Note that on a technical level this is still very hard.

In this thesis we mainly use a form of the duality known as gauge/gravity duality. It basically assumes that every gravity theory in $\mathrm{AdS}_{\mathrm{D}+1}$ spacetime has a dual description in terms of a quantum field theory living on the D dimensional AdS boundary. In addition, since the duality is best understood for a weakly coupled classical gravity theory dual to some strongly coupled QFT with a large number of colours, i.e. in the large N and large λ limit, we also stick to this limit here. We hope that by better understanding this easier case we may at some point be able to draw precise conclusions concerning quantum gravity. On the way there we can learn about strongly coupled systems that are dual to classical gravity, which is by no means less important. Examples of strongly coupled systems found in nature are the quark-gluon plasma, which is a state of matter at high densities and high temperatures, or condensed matter systems at criticality, i.e. close to a quantum phase transition. Finally, it is not unthinkable that once this case is well understood, it will be feasible to design a condensed matter tabletop experiment

in four dimensional space. That is, the full spectrum of string theory can be described from a dual field theoretic perspective [32].

[8] Using string theory it is, e.g., possible to derive the Bekenstein-Hawking entropy of a black hole with quantum statistical methods. That is, string theory correctly describes the microstates of black holes [36].

which models a field theory known to be dual to some black hole solution[9]. This will open a window to determine the quantum properties of these black holes, or to even simulate the creation and evaporation of one.

Applications of gauge/gravity duality

By now there are many different applications of gauge/gravity duality. Since for most of the computations performed in this framework N is considered to be large, it is difficult to draw quantitative conclusions. However, universal behaviour is excluded from this fact. This behaviour may be realised by dimensionless quantities that do not depend on the number of colours N. In addition we can obtain valuable insight into quantum phase transitions, which are governed by conformal field theories and are independent of the underlying microscopic theory and therefore can be classified into different universality classes [38].
Another very beautiful application is hydrodynamics. It turns out that the Navier-Stokes equation of a D dimensional theory is encoded in Einstein equations. This development is known as the fluid/gravity correspondence [39, 40]. It provides a framework that allows for an algorithmic derivation of the dissipative terms of the energy-momentum tensor and currents in the field theory.

Many of the applications consider a field theory at finite temperature and charge density (finite chemical potential). Solutions of the gravity theory with black holes add temperature to the duality, namely the Hawking temperature, which we already introduced above. The temperature and related to it the entropy of the dual QFT take exactly the corresponding values of the black hole. Interestingly, already at this stage, some quantum properties of a black hole enter the duality. In addition, finite charge density, which is especially interesting for condensed matter applications, is generated by gauge fields present in Einstein-Maxwell or Einstein-Yang-Mills setups. To realise both, finite temperature and finite charge density, the Reissner-Nordström solution in AdS space is a good starting point [41]. Interestingly for a certain parameter range this solution is unstable. However, it is possible to generate new stable solutions by considering, for instance, the condensation of an additional field. The reason for the instability is a finite, very large, entropy at zero temperature. We will make use of this fact in the following chapters.

The most famous universal result computed in the context of gauge/gravity duality is the ratio between shear viscosity and entropy density, η/s. It was first derived

[9]Note that there are already condensed matter experiments modelling high energy physics Lagrangians [37].

by Kovtun, Son and Starinets in [42], who calculated its value to be

$$\frac{\eta}{s} = \frac{\hbar}{4\pi k_B}\,, \tag{1.1}$$

with $\hbar$ the reduced Planck constant and k_B the Boltzmann constant. Later it was shown to be generically true for any field theory dual to an isotropic two derivative Einstein gravity minimally coupled to matter [43–45]. The property of isotropy, or rather how to break it, will play a major role in this thesis. Surprisingly, this result fits to the findings in quark-gluon plasma measured by RHIC in Brookhaven and by the Alice experiment at LHC in Geneva [46]. That is, opposed to the expectations quark-gluon plasma seems to be a strongly coupled phase of QCD. Note that in [42] (1.1) was conjectured to be a lower bound, known as the KSS bound, for all substances found in nature.

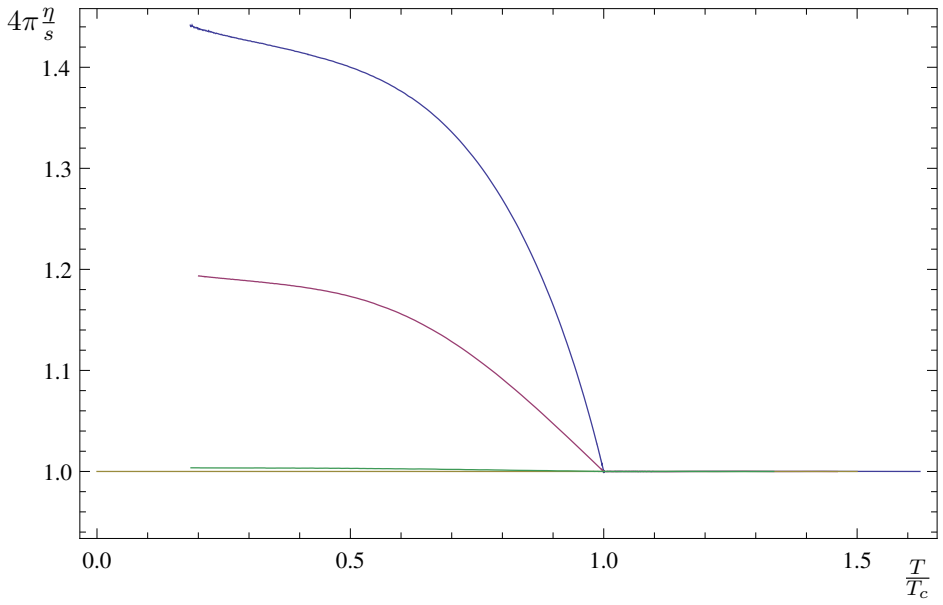

Figure 1.1: Ratio of shear viscosities η_{yz} and $\eta_{x\perp}$ to entropy density s over the reduced temperature T/T_c for different values of the ratio of the gravitational coupling constant to the Yang-Mills coupling constant α. The colour coding is as follows: In yellow, η_{yz}/s for all values of α; while the curve for $\eta_{x\perp}/s$ is plotted in green for $\alpha = 0.032$, red for $\alpha = 0.224$ and blue for $\alpha = 0.316$. The shear viscosities coincide and are universal in the normal phase $T \geq T_c$. However in the superfluid phase $T < T_c$, the shear viscosity η_{yz} has the usual universal behavior while the shear viscosity $\eta_{x\perp}$ is non-universal. Source: [1, 2]

The universality of this result implies that it is temperature independent. However since most, if not all, substances found in nature have a ratio η/s which varies with temperature, it would be nice to model such a behaviour holographically. We show in this thesis that by considering solutions to two derivative Einstein gravity with broken rotational symmetry this can be achieved (see figure 1.1). This was the first example of a deviation from the "universal" value for the ratio of shear

viscosity and entropy density in field theories dual to Einstein gravity [1, 2]. To break the rotational symmetry we consider solutions with a vector condensate. That is the condensate chooses a preferred direction in the system, with the rotational symmetry around that direction still unbroken. A way to implement this is to consider $SU(2)$ gauge fields, with the $SU(2)$ symmetry explicitly broken to a $U(1)$, which is generated by a chemical potential μ. The condensate now corresponds to a non-trivial solution of A^1_x. This was first realised holographically in [47] and coined the holographic p-wave superconductor (superconductor because a $U(1)$ symmetry is broken spontaneously). A top-down (string theoretic) model followed, where the authors of [48,49] considered two probe D7-branes to generate the $SU(2)$ gauge fields. In [50] the backreaction of the condensate onto the geometry was included, while before only the probe approximation was considered, i.e. the gravitational part of the solutions was kept fixed to a uncharged black hole, the AdS Schwarzschild black hole. In the background with full backreaction we computed the fluctuations of the metric and gauge fields. One of these modes can be related using the gauge/gravity dictionary to the shear mode in the field theory. Now, the reason for the temperature dependence of η/s lies in the non-trivial coupling between graviton modes and gauge field modes. That is, after the symmetry breaking, the relevant graviton mode does not transform as a tensor under the remaining $SO(2)$ symmetry, but rather as a vector and can thus couple to gauge fields. Finally, we find that with decreasing temperature the ratio of shear viscosity to entropy density increases. This means that our result does not go below $1/4\pi$ and thus respects the KSS bound introduced above (see chapter 4 and [1,2]).

Besides the shear viscosity it is possible to derive many transport properties of a dual field theory, either by using the fluid/gravity correspondence or by computing Green's functions related to transport coefficients via Kubo's formula. One of the most remarkable coefficient derived this way is related to vorticities in fluids [51, 52]. This term was first computed using gauge/gravity duality and only later confirmed from a pure field theoretic approach [53]. In the latter it is related to triangle anomalies and thus may be measured in a quark-gluon plasma through separation of right-handed and left-handed mesons by a magnetic field.

In the holographic p-wave superconductor, discussed in chapter 4, we derive many interesting transport properties (cf. [2, 3]). The richness of this system arises due to the many broken symmetries and thus many interacting modes. Aside from the non-universal ratio discussed above, we find two distinct electrical conductivities[10], and related to that an effect known as the thermoelectric effect. The conductivity in the preferred direction shows characteristics of broken translational invariance,

[10]We denote conductivities related to the fluctuations of the gauge field, which is uncharged under the $U(1)$, as electrical due to the analogy to Maxwell theories.

that is a Drude-like frequency dependence. Note that this is not expected, since our solution does not seem to break any translational invariance. In addition we can identify couplings similar to the piezoelectric and flexoelectric effect. These are effects known from nematic crystals [54], which are liquid crystals with broken rotational symmetry, similar to our solution.

The last paragraph already indicates that apart from QCD, condensed matter setups may provide interpretations to the effects found in holographic computations. In condensed matter physics there are a rich selection of materials with strongly coupled phases, for instance, high-T_c superconductors and different kinds of non-Fermi liquids. The first computation of a superconductor using holographic methods (see [55, 56]) generated a huge interest and many attempts to construct condensed matter systems followed. In this model it is convenient to interpret the flow along the radial AdS direction as an RG-flow of the dual field theory. Many new IR fixed points of this theory were constructed by considering different geometries in the bulk of the gravitational spacetime [57–59]. Note that all these solutions live in asymptotically AdS space, i.e. the region close to the AdS boundary is pure AdS. Thus the UV fixed point of all theories is still governed by a relativistic conformal field theory. The different IR fixed points, which were constructed are characterised by, among others, non-trivial critical scalings, anisotropic and lattice ground states [58, 60, 61]. Unfortunately no unaccounted experimental result has been convincingly modelled yet. Nevertheless, many results already incorporate some typical features seen in condensed matter, as for example the frequency dependence of the conductivity for certain materials close to quantum criticality [57, 60] and the appearance of Fermi surfaces [62].

In chapter 5 we examine one IR fixed point with non-trivial critical scaling (see also [4]). In this special case we consider a geometry, where the time direction t scales as λt, while the spatial field theory directions do not scale at all. Nevertheless, the entropy has a temperature dependence $S \sim T^\eta$, with $\eta > 0$, which guarantees for a vanishing of the entropy in the zero temperature limit, as opposed to the AdS Reissner-Nordström case mentioned before. Thus we expect that this scaling geometry describes a stable IR fixed point of the dual field theory. Note that due to the different scaling of the time and spatial directions this geometry naturally behaves in a very fermionic way. That is, low energy excitations are possible at finite momenta. This resembles the properties of Fermi surfaces [63]. To analyse this last claim further, we compute the entanglement entropy of different shapes in this theory. The entanglement entropy is a measure of how quantum a system behaves, or alternatively how strongly different regions of a system are entangled. There are claims that a Fermi surface may be seen in a logarithmic dependence on the typical length of the aforementioned shapes (see discussion in

chapter 5). However, the latter is still vividly debated. We also can not find any logarithmic behaviour in this background. Another important feature of the entanglement entropy is its sensitivity to phase transitions of the system. Interestingly in the geometry discussed in chapter 5 we find phase transitions only for certain entangling shapes. It is still not resolved why this is the case (for similar results see [64]).

Main results of this thesis

This thesis is mainly concerned with fluctuations in anisotropic holographic superconductors, especially the holographic p-wave superconductor. In addition to computing the different transport properties we can identify them in terms of known effects in condensed matter systems (see chapter 4 and [1–3]). The following points summarise the important findings:

1. **Non-universal shear viscosity** In section 4.2.7.5 we show the temperature dependence of the ratio between shear viscosity and entropy density. Such a dependence has not been observed holographically before [1, 2] in a two derivative Einstein gravity. The reason behind this behaviour is the breaking of a rotational symmetry, which leads to a non-trivial coupling between a gauge field and the relevant gravity mode.

2. **Electrical conductivities** Due to the different symmetries present in the p-wave setup, we find two distinct electric conductivities, namely one parallel and one perpendicular to the condensate. The perpendicular conductivity behaves as expected from computations in holographic superconductors without rotational symmetry breaking. The conductivity parallel to the condensate shows an unexpected behaviour. It resembles a broad Drude-peak, known from, e.g., metals with impurities, for a certain temperature range before it turns into a pole (see section 4.2.7.1 and 4.2.7.2).

3. **Other transport effects** Besides the shear viscosity and the electrical conductivities we find many effects known from condensed matter systems. One is the thermoelectric effect (sections 4.2.7.1 and 4.2.7.2), which relates charge and energy transport. The flexoelectric effect relating off-diagonal stress and flavour currents can be found in section 4.2.7.5. Finally the coupling between diagonal stress and flavour currents, which resembles the piezoelectric effect, is described in section 4.2.7.6.

The second part of this thesis involves the dual geometry to an IR fixed point with non-trivial scaling behaviour (see chapter 5 and [4]). We analyse the following points:

4. **Scaling geometry** In section 5.1 we show that this special scaling geometry is a solution to an Einstein-Maxwell-Dilaton system. Apart from that we

construct the UV-completion, that is, we embed the IR scaling geometry in asymptotically AdS space.

5. **Entanglement entropy** Finally in section 5.3 we compute the entanglement entropy in this geometry for the following entangling surfaces: a strip, a disc and an annulus. Surprisingly, we find that the strip and the annulus display a phase transition, whereas the disc does not.

Structure of this thesis

This thesis includes 6 chapters. They cover the following subjects:

- This chapter gives a general overview to the topics of this thesis.
- In chapter 2 we give a general, more mathematical, introduction to AdS/CFT and gauge/gravity duality.
- Chapter 3 is about conventional superfluids and superconductors followed by a discussion of their holographic counterparts.
- Chapter 4 is one of our main chapters, in which we discuss the holographic p-wave superconductor and especially its transport properties.
- The second main part is covered by chapter 5, where we discuss scaling geometries and the holographic entanglement entropy.
- Finally in chapter 6 we conclude.
- In appendix A we present some large formulae.

Conventions

In this thesis we set the reduced Planck constant $\hbar = 1$, the speed of light $c = 1$ and Boltzmann constant $k_B = 1$. In addition capital Latin letters denote gravitational spacetime, whereas small Greek letters denote the boundary coordinates. We use the metric with the mainly plus convention.

Chapter 2

Gauge/Gravity Duality

The main goal of this chapter is to show the intimate relation between AdS spacetime and conformal field theories. Thus we start with a brief review of both areas. Afterwards a brief derivation of the AdS/CFT duality is given followed by its generalisation, gauge/gravity duality.

2.1 Conformal Field Theories

In this section we give a brief review of conformal field theories (CFT). CFTs play an important role in many different areas of theoretical physics. For instance string theory can be formulated in terms of a two dimensional CFT living on the string worldsheet[1]. Another important application of CFTs is related to quantum critical points in condensed matter systems. More generally, at fixed points of the renormalisation group flow, i.e. where the β function vanishes, the theory is described by a CFT. In this thesis we are mainly concerned with CFTs which allow for a dual description in terms of a higher dimensional gravitational theory. We start by defining conformal transformations.

2.1.1 Conformal Transformations in D dim Minkowski Space

Consider local transformations, $x^\mu \to x'^\mu(x) = x^\mu + v^\mu$, in general D dimensional spacetime which preserve angles. Under these operations the metric transforms as

$$g'_{\mu\nu}(x') = \Omega^2(x) g_{\mu\nu}(x)\,, \tag{2.1}$$

with μ, ν running from 1 to $\mathrm{D}-1$ and $g_{\mu\nu}(x)$ being the original metric. We see that the metric remains the same up to an overall scale $\Omega^2(x)$.

[1] The string worldsheet is the area covered by the motion of the string through spacetime (c.f. [65]).

translations	$x'_\mu = x_\mu + a_\mu$	$P_\mu = -\mathrm{i}\partial_\mu$	4
rotations and boosts	$x'_\mu = M_\mu{}^\nu x_\nu$	$L_{\mu\nu} = \mathrm{i}(x_\mu\partial_\nu - x_\nu\partial_\mu)$	6
dilatations	$x'_\mu = \lambda x_\mu$	$D = \mathrm{i}x^\mu\partial_\mu$	1
special conformal transformations	$x'_\mu = \frac{x_\mu + b_\mu x^2}{1+2b\cdot x+(b\cdot x)^2}$	$K_\mu = \mathrm{i}(2x_\mu x^\nu\partial_\nu - x^2\partial_\mu)$	4

Table 2.1: Overview of the conformal transformations and the corresponding infinitesimal generators. a_μ and b_μ are constant vectors and $M_\mu{}^\nu$ is the matrix of Lorentz transformations. In the last column we give the corresponding conserved charges in D = 4.

For the rest of this thesis we only need conformal transformations in D dimensional Minkowski space. Thus the flat metric $g_{\mu\nu} = \eta_{\mu\nu}$ is used from now on. The conformal group is a generalisation of the Poincaré group including dilatations and special conformal transformations. In table 2.1 the finite form of the conformal transformations and the corresponding infinitesimal generators are shown. The generators obey the conformal algebra

$$\begin{aligned}
[L_{\mu\nu}, L_{\rho\sigma}] &= -\mathrm{i}\eta_{\mu\rho}L_{\nu\sigma} \pm \text{permutations}\,,\\
[L_{\mu\nu}, P_\rho] &= -\mathrm{i}(\eta_{\mu\rho}P_\nu - \eta_{\nu\rho}P_\mu)\,,\\
[L_{\mu\nu}, K_\rho] &= -\mathrm{i}(\eta_{\mu\rho}K_\nu - \eta_{\nu\rho}K_\mu)\,,\\
[D, P_\mu] &= -\mathrm{i}P_\mu\,,\\
[D, K_\mu] &= +\mathrm{i}K_\mu\,,\\
[D, L_{\mu\nu}] &= 0\,,\\
[P_\mu, K_\nu] &= 2\mathrm{i}L_{\mu\nu} - 2\mathrm{i}\eta_{\mu\nu}D\,,
\end{aligned} \tag{2.2}$$

with all other commutators vanishing. Note that it is possible to rewrite these generators so that the algebra is manifestly isomorphic to $SO(\mathrm{D}, 2)$ (see e.g. [34]).

2.1.2 Aspects of Conformal Field Theories

Conformal field theories are highly constrained by their symmetries. Therefore it is possible to write down many of its dynamical properties directly by demanding the correct behaviour under these symmetries. Furthermore CFTs do not posses an S-matrix, since it is not possible to define asymptotic states in the usual manner[2].

In this thesis we are interested in the adjoint representations of the conformal group, i.e.

$$[D, \mathcal{O}] = \mathrm{i}\left(-\Delta + x^\mu\partial_\mu\right)\mathcal{O}\,, \tag{2.3}$$

[2]In [66] the authors show that there is no bosonic generalisation of the Poincaré Group with a non-trivial S-matrix.

with $\mathcal{O}$ a local operator of the CFT with scaling dimension Δ. Note that under the scaling transformation $x \to x' = \lambda x$ this operator has to transforms as $\mathcal{O}(x) \to \mathcal{O}'(x) = \lambda^{\Delta}\mathcal{O}(\lambda x)$.

From the commutators involving P_μ and K_μ with D in (2.2) it is apparent that P_μ and K_μ rises and lowers, respectively, the scaling dimension of the operator $\mathcal{O}$. The main operators we are concerned with in this thesis are known as primary operators, which are defined to be the ones annihilated by K_μ.

As remarked above, the high amount of symmetry severely constrains the 2- and 3-point correlation function for operators $\mathcal{O}_i$ with scaling dimension Δ_i:

$$\begin{aligned} &\langle \mathcal{O}_i(x)\mathcal{O}_j(y)\rangle = \delta_{ij}\frac{\text{const.}}{|x-y|^{2\Delta_i}}\,, \\ &\langle \mathcal{O}_1(x_1)\mathcal{O}_2(x_2)\mathcal{O}_3(x_3)\rangle = \\ &\qquad = \frac{\text{const.}}{|x_1-x_2|^{\Delta_1+\Delta_2-\Delta_3}|x_1-x_3|^{\Delta_1+\Delta_3-\Delta_2}|x_2-x_3|^{\Delta_2+\Delta_3-\Delta_1}}\,. \end{aligned} \tag{2.4}$$

The final important property we need later on relates to the trace of the energy-momentum-tensor $T_{\mu\nu}$ of a CFT. It can easily be shown that it is traceless, i.e. $T_\mu{}^\nu = 0$ (see e.g. [65]). Note that this may not be true in a quantised theory, since Weyl anomalies contribute to the trace of the energy-momentum-tensor.

2.2 Anti de-Sitter Space

Most of the calculations in this thesis are performed in Anti de-Sitter (AdS) space or in spaces which asymptote to AdS space (asymptotically AdS will be defined bellow). Next we define the AdS spacetime.

2.2.1 Definition

The AdS space is a maximally symmetric space, i.e. it is homogeneous as well as isotropic (c.f. [34]). Other examples of maximally symmetric spaces are the sphere and de-Sitter space. The isometry group of a $\mathrm{D}+1$ dimensional AdS space is $SO(\mathrm{D},2)$[3]. We define the space by the following embedding in $\mathrm{D}+2$ dimensional flat space ($\mathbb{R}^{\mathrm{D}+2}$)

$$L^2 = X_0^2 + X_{\mathrm{D}+1}^2 - \sum_{i=1}^{\mathrm{D}} X_i^2\,. \tag{2.5}$$

[3]Note that here we already see a first hint of the connection between CFTs living in D dimensional flat space and a $\mathrm{AdS}_{\mathrm{D}+1}$ spacetime, since both have the same symmetries (c.f. section 2.1.1).

This is the equation of a hyperboloid and it defines $\mathrm{AdS}_{\mathrm{D}+1}$ spacetime with an AdS radius L. The resulting metric in Cartesian coordinates reads

$$\mathrm{d}s^2 = -\mathrm{d}X_0^2 - \mathrm{d}X_{\mathrm{D}+1}^2 + \sum_{i=1}^{\mathrm{D}} \mathrm{d}X_i^2 \,. \tag{2.6}$$

Furthermore $\mathrm{AdS}_{\mathrm{D}+1}$ is a solution to the vacuum Einstein equations

$$R_{\mu\nu} - \frac{1}{2} g_{\mu\nu}(R - \Lambda) = 0 \,, \tag{2.7}$$

with a negative cosmological constant

$$\Lambda = \frac{\mathrm{D}-1}{\mathrm{D}+1} R = -\frac{\mathrm{D}(\mathrm{D}-1)}{L^2} \,. \tag{2.8}$$

For this space the Riemann curvature tensor and the Ricci scalar are given by

$$\begin{aligned} R_{\mu\nu\lambda\rho} &= -\frac{1}{L^2} \left(g_{\mu\lambda} g_{\nu\rho} - g_{\mu\rho} g_{\nu\lambda} \right) \,, \\ R &= -\frac{\mathrm{D}(\mathrm{D}+1)}{L^2} \,. \end{aligned} \tag{2.9}$$

2.2.2 Different Parametrisations

There are different ways to parametrise AdS spaces, following the literature (see e.g. [34]) we call them global AdS coordinates and Poincaré coordinates. The former parametrises the whole hyperboloid defined by equation (2.5), the latter covers only half of it.

2.2.2.1 Global AdS Coordinates

The Cartesian coordinates defined earlier (see (2.5) and (2.6)) can be expressed as

$$\begin{aligned} X_0 &= L \cosh\rho \cos\tau \,, \\ X_{\mathrm{D}+1} &= L \cosh\rho \sin\tau \quad \text{and} \\ X_{\mathrm{i}} &= L \sinh\rho \; \Omega_{\mathrm{i}}, \quad \text{with} \;\; \mathrm{i} \in \{1, ..., \mathrm{D}\} \;\; \text{and} \;\; \sum_{\mathrm{i}} \Omega_{\mathrm{i}}^2 = 1 \,, \end{aligned} \tag{2.10}$$

which leads to the metric

$$\mathrm{d}s^2 = L^2(-\cosh^2\rho \; \mathrm{d}\tau^2 + \mathrm{d}\rho^2 + \sinh^2\rho \; \mathrm{d}\Omega^2) \,. \tag{2.11}$$

The hyperboloid (2.5) is covered once, if $\rho \in \mathbb{R}_{\geq 0}$ and $\tau \in [0, 2\pi)$. In this coordinates the topology of the space is easily recognisable by looking at the limit $\rho \ll 1$, whereby the metric becomes $\mathrm{d}s^2 = L^2(-\mathrm{d}\tau^2 + \mathrm{d}\rho^2 + \rho^2 \; \mathrm{d}\Omega^2)$. Thus the topology of global $\mathrm{AdS}_{\mathrm{D}+1}$ is $S^1 \times \mathbb{R}^{\mathrm{D}}$.

To have a well-defined causal structure we unwrap the S^1 by defining τ from $-\infty < \tau < \infty$, leading to the universal cover of $\mathrm{AdS}_{\mathrm{D}+1}$. Note that AdS can be conformally mapped into one half of the Einstein static universe[4]. Spaces with

[4]The Einstein static universe is defined as $\mathbb{R} \times S^{\mathrm{D}-1}$, for details see e.g. [34].

an asymptotic region which can be conformally mapped into half of the Einstein static universe are called asymptotically AdS.

2.2.2.2 Poincaré Coordinates

The second parametrisation we consider are the Poincaré coordinates. All of the computations in this thesis are performed in these.

They are defined as

$$\begin{aligned} X_0 &= \frac{1}{2r}\left(1 + r^2\left(L^2 + \sum_{\mathrm{i}=1}^{\mathrm{D}-1} x_\mathrm{i}^2 - t^2\right)\right), \\ X_\mathrm{D} &= \frac{1}{2r}\left(1 - r^2\left(L^2 - \sum_{\mathrm{i}=1}^{\mathrm{D}-1} x_\mathrm{i}^2 + t^2\right)\right), \\ X_{\mathrm{D}+1} &= Lrt \quad \text{and} \\ X_\mathrm{i} &= Lrx_\mathrm{i}, \quad \text{with i} \in \{1, ..., \mathrm{D}-1\}, \end{aligned} \tag{2.12}$$

with $r > 0$ and x_i, $t \in \mathbb{R} \forall \mathrm{i} \in \{1, ..., \mathrm{D}-1\}$. This leads to

$$\mathrm{d}s^2 = L^2\left(\frac{\mathrm{d}r^2}{r^2} + r^2\left(-\mathrm{d}t^2 + \sum_{\mathrm{i}=1}^{\mathrm{D}-1} \mathrm{d}x_\mathrm{i}^2\right)\right). \tag{2.13}$$

The AdS boundary is situated at $r \to \infty$. This form is our first choice through out chapter 4.
By performing the coordinate transformation $r = 1/z$ we get

$$\mathrm{d}s^2 = \frac{L^2}{z^2}\left(\mathrm{d}z^2 - \mathrm{d}t^2 + \sum_{\mathrm{i}=1}^{\mathrm{D}-1} \mathrm{d}x_\mathrm{i}^2\right). \tag{2.14}$$

Here $z = 0$ corresponds to the AdS boundary. We are going to use this coordinates in chapters 3 and 5.

2.3 The AdS/CFT Correspondence

The AdS/CFT correspondence describes a one to one map between a supergravity theory in $AdS_5 \times S^5$ spacetime and a conformal field theory living in $3 + 1$ dimensional Minkowski space. It was first conjectured by Maldacena in his seminal paper [9] in 1997 and soon afterwards made precise by Gubser, Klebanov, Polyakov and Witten in their papers [10] and [11]. Before we come to the correspondence we introduce a central element needed for it, the D-brane.

2.3.1 Two Complementary Pictures of D-branes

In the following we give a rough derivation of the correspondence based on [34]. In string theory[5] there are non-perturbative objects called D-branes[6]. There are two possible ways to interpret D-branes:

1. **Open string picture:** Dp-branes are p-dimensional surfaces where open strings end. The open string excitations are described by a so called DBI-action,
$$S^{(\mathrm{p})}_{\mathrm{DBI}} = -T_{\mathrm{p}} \int \mathrm{d}^{\mathrm{p}+1}\xi \mathrm{e}^{-\phi} \sqrt{\det(g_{ab} + B_{ab} + 2\pi\alpha' F_{ab})} \tag{2.15}$$
where the fieldcontent of this action lives in the $\mathrm{p}+1$-dimensional worldvolume of the Dp-brane. g_{ab} is the pullback metric of the worldvolume, B_{ab} the induced Kalb-Ramond field, ϕ the dilaton related to the string coupling g_s and F_{ab} the field strength tensor of gauge fields living on the brane. This gauge fields are directly related to the excitations of the open strings. Note that if we consider N branes lying on top of each other we get a non-abelian generalization of S_{DBI} with the gauge fields being in the adjoint representation of the $U(N)$ group. Finally T_{p} is the brane tension and $\alpha' = l_s^2$ the square of the string length.

2. **Closed string picture:** Dp-branes are also solitonic solutions to ten dimensional supergravity theories[7]. They are electrically and magnetically charged under Ramond-Ramond fields, i.e. they are governed by the action
$$S_{\mathrm{RR}} \sim \mu_{\mathrm{p}} \int_{\mathcal{M}_{\mathrm{p}+1}} C_{(\mathrm{p}+1)}\,, \tag{2.16}$$
where μ_{p} is the RR charge under the $\mathrm{p}+1$ form $C_{(\mathrm{p}+1)}$. Furthermore the D-branes are massive objects which curve the spacetime and therefore couple to closed strings. For a more detailed analysis see for instance [65].

In general all the actions presented above have to be added up to get a full low energy description of D-branes. However, in certain limits the one or the other term provides a sensitive low energy description. We will come back to this in order to "derive" the AdS/CFT correspondence. But first, we examine the D3-branes, i.e. branes with a four dimensional worldvolume, which are of central interest for the duality as we are using it in this thesis.

2.3.2 N D3-branes

Take a stack of N coincident D3-branes. As we saw above there are two low energy perspectives onto these branes. However, there are two possibilities to take

[5] For a nice review of string theory see e.g. [67]
[6] For a detailed account of D-branes see the book by Johnson [65].
[7] Supergravity theories emerge as the low energy limit of superstring theory.

the low energy limit. The first way is to consider energies much smaller than the inverse string length $1/l_s$, alternatively one can fix the energy and send $l_s \to 0$ (this is equivalent to sending $\alpha' \to 0$). In the following we use the latter approach.

From the open string viewpoint onto the N D3-branes in the $l_s \to 0$ limit, we find that the open string massless excitations are described by a $\mathcal{N} = 4$ $SU(N)$ super Yang-Mills theory living on the $3+1$ dimensional worldvolume of the branes (see [34]). This is a conformal theory, i.e. its β-function vanishes identically for all values of the coupling constant, which we call $\lambda = g^2_{\mathrm{YM}} N$. λ is the 't Hooft coupling. The vanishing of the β function is of great importance for different checks of the correspondence. We present one of this checks in a later section. Additionally there is a decoupled supergravity theory living in 10 dimensional spacetime. Summing up we have a gauge theory living in 4 flat spacetimes dimensions and a decoupled supergravity theory in 10 dimensions. This is a valid perturbative point of view if $\lambda = g^2_{\mathrm{YM}} N = g_s N \sim L^4/l_s^4 \ll 1$. Note that the last relation will become clearer in the following.

From a closed string perspective the N D3-branes are massive charged objects which bend spacetime, i.e. black 3-branes. The corresponding (extremal) solution[8] to the supergravity equations of motion is (c.f. [34])

$$\begin{aligned} \mathrm{d}s^2 &= H(r)^{-1/2}\left(-\mathrm{d}t^2 + \mathrm{d}x^2 + \mathrm{d}y^2 + \mathrm{d}z^2\right) + H(r)^{1/2}\left(\mathrm{d}r^2 + r^2 \mathrm{d}\Omega_5^2\right) , \\ F_5 &= (1+\star)\mathrm{d}t\,\mathrm{d}x\,\mathrm{d}y\,\mathrm{d}z\,\mathrm{d}H(r)^{-1} , \text{ with} \\ H(r) &= 1 + \frac{L^4}{r^4} \text{ and } L^4 = 4\pi g_s \alpha'^2 N , \end{aligned} \tag{2.17}$$

with $\star$ being the Hodge star operator. For the supergravity solutions to be a sensible description we need $L^4/\alpha'^2 = L^4/l_s^4 \gg 1$. There is a nice way to picture this criteria. Since the string length is much smaller than the relevant scale in the gravity theory we can treat the strings as point particles and hence the supergravity theory is the correct description. Using the last equation in (2.17) leads to $g_s N \gg 1$, since we always work in the perturbative string regime $g_s \ll 1$. To meet this demands we need N to be very large.

Next we can ask what are the low energy excitations a observer at spatial infinity sees in such a background. For once the energy E, observed at spatial infinity, is redshifted in comparison to the energies E_r measured at a constant value of r. The relation between both energies is

$$E = H(r)^{-1/4} E_r = \left(\frac{r^4}{r^4 + L^4}\right)^{1/4} E_r , \tag{2.18}$$

[8] This solution is not the most general one. We already took the extremal limit, where the inner and outer horizon of the black 3-brane agree. This is a half BPS solution since the BPS bound is saturated and half of the supercharges is annihilated by the solution.

i.e. that the closer we come to $r = 0$ the lower the energy observed at spatial infinity is. Hence one type of low energy excitation are excitations of arbitrary energy very close to $r = 0$. The second low energy excitation are massless particles in the bulk (away from $r = 0$). The two kind of low energy excitations decouple from each other. With lower and lower energies it becomes harder and harder for the excitations close $r = 0$ to go into the bulk. On the other hand the large wavelength $\gg L$ of the massless particles in the bulk makes them blind to the size of the brane. Therefore we end up with a supergravity theory close to $r = 0$ (this region is called the near-horizon region) decoupled from free supergravity theory in the bulk.

We can examine the near-horizon region closer. Taking the limit $r \ll L$ in (2.17) leads to

$$\begin{aligned} \mathrm{d}s^2 &= \frac{r^2}{L^2}\left(-\mathrm{d}t^2 + \mathrm{d}x^2 + \mathrm{d}y^2 + \mathrm{d}z^2\right) + \frac{L^2}{r^2}\left(\mathrm{d}r^2 + r^2\mathrm{d}\Omega_5^2\right) \\ &= \frac{r^2}{L^2}\left(-\mathrm{d}t^2 + \mathrm{d}x^2 + \mathrm{d}y^2 + \mathrm{d}z^2\right) + \frac{L^2}{r^2}\mathrm{d}r^2 + L^2\mathrm{d}\Omega_5^2\,. \end{aligned} \tag{2.19}$$

This is the metric of $\mathrm{AdS}_5 \times \mathrm{S}^5$ (cf. (2.13) up to a rescaling of r).

Now we have all ingredients to formulate the AdS/CFT correspondence.

2.3.3 The Correspondence

In the section above we saw that there are two ways to see a stack of N coincident D3-branes. For values of $g_s N = \lambda \ll 1$, the coupling constant of the field theory, the low energy excitations of the brane are described by gauge theory in $3 + 1$ dimensions plus a free supergravity theory in 10 dimensions. On the other hand for values of $g_s N \gg 1$ (however, g_s still small) two decoupled supergravity theories emerge, one lives in $\mathrm{AdS}_5 \times \mathrm{S}^5$ the other one is a free theory in 10 dimensions. Since in both limits of $g_s N$, we get in the low energy limit a free supergravity theory in 10 dimensions it was conjectured by Maldacena in [9] that the other two resulting theories are also equivalent (dual) to each other, i.e.

type IIB superstring theory compactified on $\mathbf{AdS}_5 \times \mathbf{S}^5$
corresponds to (is dual to)
$\mathcal{N} = 4$ $SU(N)$ super-Yang-Mills theory in $3 + 1$ dimensions [9].

There are different forms of this correspondence (c.f. [35]). The best understood and most tested form, called the *weakest form*, relates the two theories in the $N \to \infty$ and $g_s \to 0$ limit. In this case the gravity theory is a classical supergravity theory in $\mathrm{AdS}_5 \times \mathrm{S}^5$ dual to a strongly coupled, $\lambda \gg 1$, $\mathcal{N} = 4$ $SU(N)$ super-Yang-Mills theory, in $3 + 1$ dimensions. In this thesis we work in this limit

of the correspondence.

The *weak form* of the duality is understood in terms of the 't Hooft limit, i.e. $\lambda = g_{\mathrm{YM}}^2 N = g_s N$ is fixed to a finite large value, while $N \to \infty$. This allows for the inclusion of $1/N$ corrections on the field theory side and string loop corrections (g_s corrections) of the classical type IIB string theory on $\mathrm{AdS}_5 \times \mathrm{S}^5$.

Finally, in the *strongest form* of the correspondence the full quantum type IIB superstring theory on $\mathrm{AdS}_5 \times \mathrm{S}^5$, with the AdS and five sphere radius L being identified with $L^4 = 4\pi g_s N \alpha'^2$, is dual to $\mathcal{N} = 4$ $SU(N)$ super-Yang-Mills theory for all values of N and g_s, i.e. for all values of λ.

For a more detailed discussion and subtleties in taking the different limits see e.g. [35].

This correspondence works on the level of global symmetries and dynamics. The matching of the bosonic symmetries is straight forward, i.e. the isometries of AdS_5 correspond exactly to the conformal group in 3+1 dimensions ($SO(4,2)$ cf. sections 2.1.1 and 2.2.1) and the $SO(6)$ rotational symmetry of the S^5 corresponds to the $SU(4)$ R-symmetry in the field theory. In the following section we discuss the mapping between the dynamics of both sides. Note that under inclusion of fermions the symmetries also agree. In addition, one maps exactly the objects, which transform in the irreducible representation of the symmetries in one theory, to the objects with the same transformation behaviour in the other theory.

2.3.4 The Field-Operator Map (Dictionary)

In order to use the duality we need a well-defined map between the degrees of freedom on both sides of the correspondence. More concretely, the fields on the gravity side are identified with operators on the field theory side. We start this discussion by giving the result followed by a very heuristic derivation.

The "mathematical" realisation of the AdS/CFT duality is (see e.g. [10, 11, 34])

$$\mathcal{Z}_{\mathrm{String}}\left[\phi(z,\vec{x})|_{z\to 0} = \phi_\Delta(\vec{x})\right] = \left\langle \mathrm{e}^{\int \mathrm{d}^{\mathrm{D}} x\, \phi_\Delta(\vec{x}) \mathcal{O}_\Delta(\vec{x})} \right\rangle_{\mathrm{CFT}} . \tag{2.20}$$

In plain words, this means that the superstring theory partition function $\mathcal{Z}_{\mathrm{String}}$ with a field $\phi(r,\vec{x})$, which at the AdS boundary $z = 0$ takes the value $\phi_\Delta(\vec{x})$, is equal to the generating functional of a CFT with an operator $\mathcal{O}_\Delta(\vec{x})$ sourced by $\phi_\Delta(\vec{x})$. In principle we are now able to compute any correlation function of $\mathcal{O}_\Delta$ in the strongly coupled field theory by simply differentiating the left hand side of (2.20) with respect to the boundary value of ϕ_Δ. But before the boundary value

of ϕ has to be thoroughly defined.

Close to the AdS boundary $z = 0$ the fields living on the gravity side, we call them $\phi_\Delta(z, \vec{x})$, generically behave as

$$\phi_\Delta(z,\vec{x}) \xrightarrow[z\to 0]{} \begin{cases} z^\Delta & \text{normalisable solution} \\ z^{\mathrm{D}-\Delta} & \text{non-normalisable solution} \end{cases} . \tag{2.21}$$

In [10] it was proposed that the normalisable mode be identified with the vacuum expectation value of the dual operator $\mathcal{O}_\Delta$ while the non-normalisable mode $\bar{\phi}_\Delta$ corresponds to the source. Therefore close to the boundary we may write the solution for $\phi_\Delta(z, \vec{x})$ as

$$\begin{gathered} \phi_\Delta(z,x) \xrightarrow[z\to 0]{} \langle \mathcal{O}_\Delta \rangle z^\Delta + \bar{\phi}_\Delta z^{\mathrm{D}-\Delta}, \\ \text{with} \quad \bar{\phi}_\Delta := \lim_{z\to 0} \phi_\Delta(z,x) z^{\Delta-\mathrm{D}}. \end{gathered} \tag{2.22}$$

On the gravity side Δ is related to the mass of the field m in $\mathrm{AdS}_{\mathrm{D}+1}$. Depending on the field we get the following relations [34]:

- scalar: $\Delta_\pm = \frac{1}{2}\left(\mathrm{D} \pm \sqrt{\mathrm{D}^2 + 4m^2L^2}\right)$,
- spinor: $\Delta = \frac{1}{2}\left(\mathrm{D} + 2|mL|\right)$,
- vector: $\Delta_\pm = \frac{1}{2}\left(\mathrm{D} \pm \sqrt{(\mathrm{D}-2)^2 + 4m^2L^2}\right)$,
- massless spin 2: $\Delta = \mathrm{D}$.

From a dual field-theoretic point of view, Δ is the scaling dimension of the operator $\mathcal{O}_\Delta$. We will show that this is true in the next section. Note that the demand for a unitary CFT constraints the value of the scaling dimension to be

$$\Delta \geq \frac{\mathrm{D}}{2} - 1\,, \tag{2.23}$$

where in principle Δ can be chosen to be either Δ_+ or Δ_-. While Δ_+ always fulfils the bound, the case of Δ_- is more subtle. Since the two values of Δ are related by $\Delta_- = \mathrm{D} - \Delta_+$, only in special cases this bound is not violated for Δ_-. In this special case we are free to choose which of the expansion coefficients close to the boundary (cf. (2.22)) are the source and the expectation value of the dual operator, if at the same time Δ_- does not violate the Breitenlohner-Freedman bound [68]

$$m^2L^2 \geq -\frac{\mathrm{D}^2}{4}\,. \tag{2.24}$$

This translates into the constraint $\Delta_- \leq \mathrm{D}/2$.

2.3.5 Correlators from AdS/CFT

After having defined the dictionary, we now determine the correlation functions on the CFT side by performing a gravity theory computation. From this section on we use the "weakest form" of the duality introduced before, i.e. our computations are in the context of classical supergravity theory in AdS space, while we interpret the results from a strongly coupled CFT point of view.

Our goal is to compute the time order correlation function

$$\langle \mathrm{T}\mathcal{O}_\Delta(x')\mathcal{O}_\Delta(x)\rangle \tag{2.25}$$

of the CFT operator $\mathcal{O}_\Delta$ dual to the scalar field $\phi_\Delta(z,\vec{x})$.

First consider a scalar field $\phi_\Delta(z,\vec{x})$ in $\mathrm{AdS}_{\mathrm{D}+1}$. Its boundary expansion is given by equation (2.22). The bulk-to-bulk propagator, for the points $(z',\vec{x}')$ and $(z,\vec{x})$ far apart from each other, is given by (see e.g. [33])

$$\left\langle \mathrm{T}\phi_\Delta(z',\vec{x}')\phi_\Delta(z,\vec{x})\right\rangle \sim \left(\frac{z'z}{z'^2+z^2+(x'-x)^2}\right)^\Delta . \tag{2.26}$$

Note that in principle this computation can be performed in either, Lorentzian or Euclidean, signature, without notable adjustments. To be concise we stick to the Euclidean signature, i.e. $(x'-x)^2=\sum_{i=1}^{\mathrm{D}}(x'^i-x^i)^2$. Furthermore we choose Δ in (2.22) to be Δ_+ and we set $\bar{\phi}_\Delta=0$. The latter is a consistent boundary condition on the gravity side, which allows us to easily derive (2.25). Note that when using this boundary condition the dual operator $\mathcal{O}_\Delta$ is defined through (c.f. equation (2.22))

$$\mathcal{O}_\Delta(\vec{x}) = \lim_{z\to 0}\phi_\Delta(z,x)z^{-\Delta}\,. \tag{2.27}$$

Now it is easy to see that by combining (2.25), (2.27) and (2.26) we obtain

$$\begin{aligned}
\langle \mathrm{T}\mathcal{O}_\Delta(x')\mathcal{O}_\Delta(x)\rangle &= \lim_{z,\,z'\to 0}\left\langle \mathrm{T}\, z'^{-\Delta}z^{-\Delta}\phi_\Delta(z',\vec{x}')\phi_\Delta(z,\vec{x})\right\rangle = \\
&= \lim_{z,\,z'\to 0} z'^{-\Delta}z^{-\Delta}\left\langle \mathrm{T}\phi_\Delta(z',\vec{x}')\phi_\Delta(z,\vec{x})\right\rangle \\
&\sim \lim_{z,\,z'\to 0} z'^{-\Delta}z^{-\Delta}\left(\frac{z'z}{z'^2+z^2+(x'-x)^2}\right)^\Delta = \frac{1}{(x'-x)^{2\Delta}}\,.
\end{aligned} \tag{2.28}$$

This is precisely the behaviour seen for a 2-point function of an operator $\mathcal{O}_\Delta(x)$ with scaling dimension Δ in a CFT (see section 2.1.2).

For a more precise and thorough, yet, still brief review of the computation of correlation functions in AdS/CFT we recommend [33]. In this review, Polchinski shows that by not setting $\bar{\phi}_\Delta=0$, as we do here, but just by fixing it, one obtains the same result as we did above, however with the interpretation of $\bar{\phi}_\Delta$ as the

source of $\mathcal{O}_\Delta$, in the sense of (2.20). We will use this way of determining field theory correlators in chapters 3 and 4.

Finally, there are many subtleties regarding renormalisation, correlators at finite temperature, advanced or retarded propagators and many others, which we do not address here (see e.g. [69]). In this work we only need real-time retarded thermal Green's functions which we introduce in section 3.2.4. For an extensive study of correlators see [69] and references therein.

2.4 Generalisations of AdS/CFT: Gauge/Gravity Duality

In the sections above we introduced the original form of the AdS/CFT duality. It is derived from ten dimensional string theory and both sides of the duality are known explicitly. In this section we generalise the AdS/CFT correspondence to a general duality between gravity theories and gauge theories. The basic assumption governing the generalisations is that there always exists a field theory in D spacetime dimensions dual to a gravity theory living in asymptotically $\mathrm{AdS}_{\mathrm{D}+1}$ spacetime. As opposed to the AdS/CFT case in most of the examples of the generalised duality the Lagrangian of the field theory is not known, since we do not derive the theory from string theory[9]. Rather, the field theory is defined by its operator spectrum and its correlators, which can be derived from the gravity side.

In this approach it is common to interpret the additional coordinate on the gravity side as an RG scale [70]. Einstein's equations in AdS are thought of describing the RG flow of the dual field theory. Thus, the asymptotically AdS geometry close to the boundary characterises the UV fixed point of the field theory. On the other hand, the IR of the field theory is mapped into the bulk of AdS.

Looking at pure $\mathrm{AdS}_{\mathrm{D}+1}$ solution described by the metric (cf. (2.14))

$$\mathrm{d}s^2 = \frac{L^2}{z^2}\left(\mathrm{d}z^2 - \mathrm{d}t^2 + \sum_{\mathrm{i}=1}^{\mathrm{D}-1}\mathrm{d}x_{\mathrm{i}}^2\right), \tag{2.29}$$

where the AdS boundary is situated at $z = 0$, we see that this metric is invariant under rescaling

$$z \to \lambda z \text{ and } t,\, x_i \to \lambda t,\, \lambda x_i\,. \tag{2.30}$$

The t, x_i coordinates are regarded as the field theory coordinates. By rescaling these coordinates, we move into the bulk of AdS space. However, in pure AdS

[9] We call the constructions which do not arise from consistent truncations of superstring theory as *bottom-up* models, while theories which arise from string theory are coined *top-down* models.

spacetime the geometry at every z-slice looks the same, i.e. it is conformal to flat space. This is in agreement with the interpretation that the dual field theory is conformal at all scales, i.e. the β function vanishes identically. For asymptotically AdS, the dual field theory is conformal at the UV fixed point, while its couplings run, away from this point. Depending on the geometry and the parameters in the bulk, the field dual theory can flow to different IR fixed point. In addition we can model phase transitions holographically by spontaneously breaking symmetries. This is of major interest for the application of the duality to systems found in nature, e.g. phases of condensed matter systems or the quark-gluon plasma. In this thesis we will examine such a phase transition from a "normal", non-superfluid, fluid to a holographic superfluid (chapters 3 and 4). To study this more complex systems we have to deform the pure AdS space, e.g. by adding matter to the theory or considering black hole geometries. In the following we present two simple examples where the effect of black holes and gauge fields is analysed.

2.4.1 D + 1 dimensional AdS Schwarzschild Solution

Following [57], the simplest example of a theory which admits above (pure AdS) solution is Einstein gravity with a negative cosmological constant (see section 2.2.1)

$$S_L = \frac{1}{2\kappa^2}\int \mathrm{d}^{\mathrm{D}+1}x\sqrt{-g}\,(R-\Lambda) - \frac{1}{2\kappa^2}\int_{\partial\mathrm{AdS}} \mathrm{d}^{\mathrm{D}}x\sqrt{-\gamma}\left(-2K + \frac{2(\mathrm{D}-1)}{L}\right), \tag{2.31}$$

with $\Lambda = -\mathrm{D}(\mathrm{D}-1)/L^2$, g_{AB} the 5 dimensional metric, R the Ricci scalar, K the trace of the extrinsic curvature $K_{\mu\nu}$, $\gamma_{\mu\nu}$ the induced metric on the AdS boundary and $\kappa^2 \propto G_N^{\mathrm{D}+1}$, while $G_N^{\mathrm{D}+1}$ is the D + 1 dimensional Newton's constant. The second term above is the Gibbons-Hawking term (see e.g. [65]), which does not affect the equations of motion, however it renders the action finite and gives the correct Dirichlet boundary conditions at the AdS boundary. The corresponding field equations,

$$R_{AB} - \frac{1}{2}g_{AB}(R-\Lambda) = 0\,, \tag{2.32}$$

admit, besides pure AdS, another solution, the AdS Schwarzschild black hole, i.e.

$$\begin{aligned} \mathrm{d}s^2 &= \frac{L^2}{z^2}\left(-f(z)\mathrm{d}t^2 + \frac{1}{f(z)}\mathrm{d}z^2 + \sum_{\mathrm{i}=1}^{\mathrm{D}-1}\mathrm{d}x_{\mathrm{i}}^2\right), \\ \text{with } f(z) &= 1 - \left(\frac{z}{z_H}\right)^{\mathrm{D}}. \end{aligned} \tag{2.33}$$

This solution is still AdS in the UV, i.e. for $z \to 0$. However, in the bulk we have a planar black hole, with black hole horizon z_H, which distorts the pure AdS geometry. According to Hawking [6], a black hole radiates. Therefore a temperature of the black hole, the so called Hawking temperature T_H, can be defined. In order

to compute that temperature we change to Euclidean coordinates, i.e. $t = i\tau$ and we demand the spacetime to be regular at the horizon, which places a constraint onto τ. This constraint translates into periodically identifying τ,

$$\tau \sim \tau + \frac{4\pi}{|f'(z_H)|} = \tau + \frac{1}{T}\,. \tag{2.34}$$

The last equality arises from the fact that thermal field theory identifies the inverse of the period of Euclidean time with the temperature T i.e.

$$T = \frac{|f'(z_H)|}{4\pi} = \frac{\mathrm{D}}{4\pi z_H}\,. \tag{2.35}$$

This temperature corresponds to the Hawking temperature $T_H = T$ of the black hole[10]. It is defined as the temperature measured at spatial infinity of a field theory living in a black hole geometry (c.f. [28]).

Wick rotating the action (2.31) and evaluating it at the Wick rotated solution (2.33), leads to a saddle point approximation of the supergravity partition function

$$\mathcal{Z}_{\mathrm{SUGRA}} \simeq \mathrm{e}^{-S_E[g_{\mu\nu}]}\,, \tag{2.37}$$

where by S_E we denote the Euclidianised on-shell action (2.31), which is

$$S_E = -\frac{L^{\mathrm{D}-1}}{2\kappa^2}\frac{1}{z_H^{\mathrm{D}}}\frac{V_{\mathrm{D}-1}}{T} = -\frac{(4\pi)^{\mathrm{D}}L^{\mathrm{D}-1}}{2\kappa^2\mathrm{D}^{\mathrm{D}}}V_{\mathrm{D}-1}T^{\mathrm{D}-1}\,. \tag{2.38}$$

Note the factor of $1/T$ comes from the compactification of the Euclidean time direction with a period of $1/T$. S_E describes a system in thermodynamic equilibrium at a temperature $T = T_H$, with a free energy given by

$$F = -T\ln\mathcal{Z} = TS_E = -\frac{(4\pi)^{\mathrm{D}}L^{\mathrm{D}-1}}{2\kappa^2\mathrm{D}^{\mathrm{D}}}V_{\mathrm{D}-1}T^{\mathrm{D}}\,, \tag{2.39}$$

and a entropy by

$$S = \frac{\partial(T\ln\mathcal{Z})}{\partial T} = -\frac{\partial F}{\partial T} = \frac{(4\pi)^{\mathrm{D}}L^{\mathrm{D}-1}}{2\kappa^2\mathrm{D}^{\mathrm{D}-1}}V_{\mathrm{D}-1}T^{\mathrm{D}-1}\,. \tag{2.40}$$

The entropy can also be derived using the usual Bekenstein-Hawking formula [5,6]

$$S_{\mathrm{BH}} = \frac{2\pi}{\kappa^2}A_H\,, \tag{2.41}$$

where A_H is the area of the black hole horizon.

[10] An alternative way to compute the Hawking temperature of a black hole is by using

$$T = \frac{\kappa}{2\pi}\,, \tag{2.36}$$

while $\kappa = \sqrt{\partial_M\xi\partial^M\xi}\Big|_{z_H}$ is the surface gravity of the black hole and $\xi = \sqrt{-g_{tt}\xi^t\xi^t}$ the norm of the timelike Killing vector $\xi^\mu = (1,0,0,0,0)$.

Now we can use the gauge/gravity dictionary which relates the partition function of the supergravity theory to the partition function of the dual field theory by

$$\mathcal{Z}_{\text{SUGRA}} = \mathcal{Z}_{\text{FT}} \,. \tag{2.42}$$

This equation tells us, that the dual theory of a Schwarzschild AdS black hole in thermal equilibrium is precisely described by temperature T, free energy F and entropy S just derived above. Note that the temperature dependence of the free energy is exactly as expected for a relativistic field theory with the temperature being the only scale. In terms of field theory quantities we can relate $L^{\text{D}-1}/(2\kappa^2) \propto N^\alpha$ with $\alpha > 0$. In the usual $\text{AdS}_5 \times \text{S}^5$ version of the gauge/gravity duality $\alpha = 2$. Finally since the dual theory is scale invariant, and there is no second scale to compare the temperature to, all the temperatures are equivalent and the theory can only differentiate between zero and non-zero temperature. This is also visible in the gravity theory since we can always set $z_H = 1$ by rescaling z. In the next section we introduce a second scale, the chemical potential μ, to which we can compare the temperature.

2.4.2 D + 1 dimensional AdS Reissner-Nordström Solution

To render gauge/gravity duality interesting for condensed matter and also for particle physics applications we have to introduce charged matter. The first step into this direction is to introduce a $U(1)$ gauge group on the gravity side which translates into a global $U(1)$ symmetry on the field theory side. Note that this identification of the symmetries is true for all symmetries in gauge/gravity duality. For example, the local diffeomorphism invariance of the AdS_5 under the $SO(4,2)$ symmetry group is dual to the global conformal invariance, $SO(4,2)$, in 4 dimensional Minkowski space (cf. section 2.3.3). The simplest way to add a $U(1)$ gauge symmetry is to consider the Einstein-Maxwell system with the action

$$S_L = \int \text{d}^{\text{D}+1}x \, \sqrt{-g} \left(\frac{1}{2\kappa^2} \left(R + \frac{\text{D}(\text{D}-1)}{L^2} \right) - \frac{1}{4g^2} F_{AB} F^{AB} \right) + S_{\text{bdry}} \,, \tag{2.43}$$

with the same definitions as in the AdS Schwarzschild solution above. In addition we have g the Maxwell coupling, $F_{AB} = \partial_A A_B - \partial_B A_A$ the field strength tensor associated to the $U(1)$ gauge field $A_A(z, x_\mu)$ and S_{bdry} the boundary terms as defined in equation (2.31). Note that we do not need additional boundary terms since the gauge field falls of quickly enough towards the AdS boundary.

The corresponding equations of motion are

$$\begin{aligned} &R_{AB} - \frac{1}{2} g_{AB} \left(R + \frac{\text{D}(\text{D}-1)}{L^2} \right) = \kappa^2 T_{AB} \,, \\ &\qquad \text{with } T_{AB} = \frac{1}{4g^2} \left(4 F_{AC} F_B{}^C - g_{AB} F_{CD} F^{CD} \right) \text{ and} \\ &\nabla_A F^{AB} = 0 \,. \end{aligned} \tag{2.44}$$

These equations admit the AdS Reissner-Nordström solution

$$\begin{aligned} \mathrm{d}s^2 &= \frac{L^2}{z^2}\left(-f(z)\mathrm{d}t^2 + \frac{1}{f(z)}\mathrm{d}z^2 + \sum_{\mathrm{i}=1}^{\mathrm{D}-1}\mathrm{d}x_{\mathrm{i}}^2\right), \\ \text{with}\quad f(z) &= 1 - \left(1+\frac{z_H^2\mu^2}{\gamma^2}\right)\left(\frac{z}{z_H}\right)^{\mathrm{D}} + \frac{z_H^2\mu^2}{\gamma^2}\left(\frac{z}{z_H}\right)^{2(\mathrm{D}-1)}, \\ \gamma^2 &= \frac{(\mathrm{D}-1)L^2g^2}{(\mathrm{D}-2)\kappa^2}, \\ \text{and}\quad A_t(z) &= \mu\left(1-\left(\frac{z}{z_H}\right)^{\mathrm{D}-2}\right). \end{aligned} \tag{2.45}$$

μ is, in principle, a free parameter of the theory which defines the boundary value of the gauge field component $A_t(z=0)$. We can identify this value with the chemical potential of the dual field theory. This follows from the identification of the dual operator of a gauge field, which is associated to a local symmetry on the gravity side, with a conserved global current $\langle \mathcal{J}^\mu \rangle$. The time component of the current, a density, naturally couples to the chemical potential from a field theory point of view. Thus μ is considered to be the chemical potential of the QFT.

Using the same reasoning as in the AdS Schwarzschild case we can compute the thermodynamic quantities which describe this system in the saddle point approximation. The temperature is

$$T = \frac{|f'(z_H)|}{4\pi} = \frac{1}{4\pi z_H}\left(\mathrm{D} - \frac{(\mathrm{D}-2)z_H^2\mu^2}{\gamma^2}\right), \tag{2.46}$$

while the Euclidianised version of the on-shell action (2.43) is

$$S_E = -\frac{L^{\mathrm{D}-1}}{2\kappa^2}\frac{1}{z_H^{\mathrm{D}}}\left(1+\frac{z_H^2\mu^2}{\gamma^2}\right)\frac{V_{\mathrm{D}-1}}{T}, \tag{2.47}$$

with $1/T$ being the period of the compact Euclidean time direction.

The equivalent to the free energy in this model, the grand potential Ω, is given by

$$\Omega = -T\ln\mathcal{Z} = TS_E = -\frac{L^{\mathrm{D}-1}}{2\kappa^2}\frac{1}{z_H^{\mathrm{D}}}\left(1+\frac{z_H^2\mu^2}{\gamma^2}\right)V_{\mathrm{D}-1}. \tag{2.48}$$

We do not compute the free energy, since by holding the chemical potential fixed we automatically changed to the grand canonical potential[11].

[11] Grand canonical ensemble means that we are keeping a system in thermal equilibrium with a particle and energy reservoir attached. Thus, if we change the chemical potential μ or the temperature T and wait long enough the system will be in a new equilibrium state with possibly changed total energy and particle number.

Next the entropy density $s = S/V_{\mathrm{D}-1}$ of this configuration is computed. Using the Bekenstein-Hawking formulae (2.41), we find

$$s = \frac{2\pi}{\kappa^2}\frac{L^{\mathrm{D}-1}}{z_H^{\mathrm{D}-1}}\,. \tag{2.49}$$

This result, even not apparent yet, bares some surprises. In the vanishing temperature limit the AdS Reissner-Nordström black hole does not vanish, but it turns into a extremal black hole. An extremal black hole is a black hole which does not radiate Hawking radiation, i.e. it has zero temperature, however its horizon does not vanish, but the inner and outer horizon are coincident. Note that the blackening factor $f(z)$ has more than one root. The root separating the black hole from the bulk defines the outer horizon z_H. We denote the other root as the inner horizon z_-. If $z_H = z_-$, we get $T_H = 0$, however due to the existence of a horizon entropy density s is still non-vanishing. This is possible in the AdSRN case but not in the Schwarzschild case studied before, since we introduced a second scale μ to which we can compare the temperature. Examining (2.46) we see that for

$$z_H = \sqrt{\frac{\mathrm{D}}{\mathrm{D}-2}}\frac{\gamma}{\mu} \tag{2.50}$$

the temperature vanishes. Plugging this into (2.49) results in

$$s_{T=0} = 2\pi\frac{L^{\mathrm{D}-1}}{\kappa^2}\left(\frac{(\mathrm{D}-2)\mu^2}{\mathrm{D}\gamma^2}\right)^{\mathrm{D}-1}\,. \tag{2.51}$$

As we remarked at the end of last section $L^{\mathrm{D}-1}/\kappa^2$ is proportional to some positive power of N. Thus this entropy is not only not vanishing, but it is very big. From a dual field theoretic point of view, this means that the ground state has a non-zero entropy at zero temperature, i.e. it is highly degenerate. We will see later that this behaviour can be regarded as a sign of instability of the system, leading us to new IR geometries, which correspond to different ground states of the dual theory. For a detailed discussion of the thermodynamics of the AdSRN solution see [41].

The next quantity relevant to our discussion is the charge density ρ. To compute it we use the thermodynamic relation

$$\rho = -\frac{1}{V_{\mathrm{D}-1}}\frac{\partial\Omega}{\partial\mu}\,. \tag{2.52}$$

Note that it has to be taken into account that $z_H \equiv z_H(\mu, T)$, i.e. using equation (2.46) we get

$$\frac{\partial z_H}{\partial\mu} = -\frac{2(\mathrm{D}-2)z_H^3\mu}{\mathrm{D}\gamma^2 + (\mathrm{D}-2)z_H^2\mu^2}\,. \tag{2.53}$$

Putting everything together results in

$$\rho = \frac{(\mathrm{D}-1)L^{\mathrm{D}-1}}{\kappa^2\gamma^2}\frac{\mu}{z_H^{\mathrm{D}-2}} = \frac{(\mathrm{D}-2)L^{\mathrm{D}-3}}{g^2}\frac{\mu}{z_H^{\mathrm{D}-2}}\,. \tag{2.54}$$

Using (2.42), we identify the values for the grand potential Ω and the charge density ρ with the corresponding quantities in the dual strongly coupled field theory. There is a second way to compute the value of ρ without resorting to thermodynamic relations, but by explicitly relaying on the gauge/gravity dictionary.

Following the discussion in section 2.3.4 we examine the behaviour of $A_A(z,\vec{x})$ at the AdS boundary, which is

$$A_t(z,\vec{x}) \xrightarrow[z\to 0]{} \mu + \frac{-\mu}{z_H^{\mathrm{D}-2}} z^{\mathrm{D}-2}\,, \tag{2.55}$$

and considering equation (2.22), we can identify

$$\langle \mathcal{J}_t \rangle \sim \frac{\mu}{z_H^{\mathrm{D}-2}}\,. \tag{2.56}$$

The global $U(1)$ charge current $\langle \mathcal{J}^\mu \rangle(\vec{x})$ is the field theory dual operator to $A_A(z,\vec{x})$. As stated before, to every gauge symmetry on the gravity side there is a corresponding global symmetry on the field theory side. The associated conserved (Noether) current to the global symmetry is the dual operator to the gauge field living in AdS. In this example we see the duality between a $U(1)$ global and local symmetry. However, there is another very simple example present in every gauge/gravity correspondence model, the graviton $h_{AB}(z,\vec{x})$. It is related to the diffeomorphism invariance on the gravity side and it is dual to the conserved field theory energy momentum tensor $\langle \mathcal{T}_{\mu\nu} \rangle(\vec{x})$. However, in this case to compute the dual field theory tensor one has to be more careful, due to the appearance of divergences and renormalisation terms. We will analyse this later on, see section 3.2.4.

Coming back to the the example studied here, note that the overall normalisation of $\langle \mathcal{J}^t \rangle$ has to be fixed by plugging the AdS Reissner-Nordström solution into the action and then in the spirit of gauge/gravity (cf. equation (2.42)) duality take the functional derivative with respect to the boundary value of $A_t(z=0,\vec{x})$. The relevant part of the action is

$$\begin{aligned} S_L \sim & -\frac{1}{4g^2}\int \mathrm{d}^{\mathrm{D}+1}x\sqrt{-g}F_{AB}F^{AB} = \\ & = -\frac{1}{4g^2}\int \mathrm{d}^{\mathrm{D}}x \int_0^{z_H} \mathrm{d}z \sqrt{-g} g^{AC} g^{BD} F_{AB} F_{CD} = \\ & = -\frac{1}{2g^2}\int \mathrm{d}^{\mathrm{D}}x \int_0^{z_H} \mathrm{d}z \Bigg(\partial_A \left(\sqrt{-g} g^{AC} g^{BD} A_B F_{CD} \right) \\ & \qquad\qquad - A_B \underbrace{\partial_A \left(\sqrt{-g} F^{AB} \right)}_{=0 \text{ e.o.m.}} \Bigg) = \end{aligned}$$

$$
\begin{aligned}
&= -\frac{1}{2g^2}\int \mathrm{d}^{\mathrm{D}}x\left(\sqrt{-g}g^{zz}g^{BD}A_B F_{zD}\right)\Big|_{z=0}^{z_H} = \\
&\overset{(2.45)}{=} \lim_{z\to 0}\frac{1}{2g^2}\int \mathrm{d}^{\mathrm{D}}x\left(\frac{L^{\mathrm{D}+1}}{z^{\mathrm{D}+1}}\frac{z^2 f(z)}{L^2}\frac{-z^2}{L^2 f(z)}A_t(z)\partial_z A_t(z)\right) = \\
&= -\lim_{z\to 0}\frac{L^{\mathrm{D}-3}}{2g^2}\int \mathrm{d}^{\mathrm{D}}x\left(\frac{1}{z^{\mathrm{D}-3}}\frac{-(\mathrm{D}-2)z^{\mathrm{D}-3}}{z_H^{\mathrm{D}-2}}\mu^2 + \mathcal{O}(z)\right) = \\
&= \frac{L^{\mathrm{D}-3}}{2g^2}\int \mathrm{d}^{\mathrm{D}}x\frac{\mathrm{D}-2}{z_H^{\mathrm{D}-2}}\mu^2\,.
\end{aligned}
$$

Note that since $A_t(z_H) = 0$ we only get contributions from the boundary.

Now we can use the dictionary (2.42) to determine $\langle \mathcal{J}^t \rangle$ by varying the on-shell action, we just obtained, with respect to the boundary value of $A_t(z \to 0, \vec{x}) = A_t^b(\vec{x}) = \mu$, which sources $\langle \mathcal{J}^t \rangle$, i.e.

$$
\langle \mathcal{J}^t(\vec{x}) \rangle = \frac{\delta S_L^{\text{on-shell}}}{\delta A_t^b(\vec{x})} = \frac{(\mathrm{D}-2)L^{\mathrm{D}-3}}{g^2}\frac{\mu}{z_H^{\mathrm{D}-2}} \tag{2.57}
$$

Comparing this result to (2.54), we see that both agree. This has to be the case, since $\langle \mathcal{J}^t \rangle$ is the charge density in the field theory.

The AdS Reissner-Nordström system is the starting point for the following chapters. In the next chapter we add a scalar field to this setup and show how to spontaneously break the $U(1)$ symmetry. This leads us to holographic superconductors. In chapter 4, we examine the phase transition between AdSRN and a phase with spontaneously broken $U(1)$ and rotational symmetry. Afterwards, we add the effect of relevant operators at the UV fixed point dual to AdSRN, which results in a flow to a new IR fixed point. This fixed point has desirable properties for the modelling of condensed matter systems (see chapter 5).

Chapter 3

Holographic Superfluids and Superconductors

In this chapter we start with a recapitulation of conventional superfluids and superconductors. Afterwards we implement the concept in a holographic framework by examining the holographic s-wave superconductor.

3.1 Superfluids and Superconductors

Superfluidity and superconductivity are remarkable macroscopic effects arising from the quantum properties of the underlying microscopic theory. There are many surprising consequences of superfluidity and superconductivity, for instance, helium 4 in the superfluid phase can climb up the walls of a vessel, if there is a lower lying basin which can be reached. The most famous characteristic of superconductors is its zero electrical resistivity, a property which is heavily used in many technical applications where large electrical currents are of need (e.g. to generate strong magnetic fields). In this section we present a very brief review of superfluidity and superconductivity based on [71–73], where we concentrate on the effective description of these phenomena. The description of superconductivity will be an effective description, i.e. close to a critical temperature T_c where the theory undergoes a phase transition from a normal[1] to a superconducting phase. This theory is known as the Ginzburg-Landau theory of superconductivity [74].

3.1.1 Superfluidity

The easiest setup to study superfluidity is ϕ^4 theory. The corresponding well-known scalar field Lagrangian is

$$\mathcal{L} = -D_\mu\phi(D^\mu\phi)^* - m^2|\phi|^2 - \lambda|\phi|^4\,, \tag{3.1}$$

[1] With normal we denote a phase without superfluidity and superconductivity.

where $m^2 > 0$ is the mass of the scalar field ϕ, $\lambda > 0$ a coupling constant and $D_\mu = \partial_\mu - \mathrm{i}A_\mu$, with $A_t = \mu$ the (constant) chemical potential and $A_a = 0$. This theory is invariant under a global $U(1)$ symmetry, which transforms

$$\phi(x^\mu) \to \phi(x^\mu)\mathrm{e}^{\mathrm{i}\alpha} \text{ and } \phi^*(x^\mu) \to \phi^*(x^\mu)\mathrm{e}^{-\mathrm{i}\alpha}\,. \tag{3.2}$$

Including the chemical potential we get an effective potential

$$V(\phi, \phi^*) = (\mu^2 - m^2)|\phi|^2 - \lambda|\phi|^4\,. \tag{3.3}$$

To compute the vacuum expectation value of $\langle\phi\rangle$ in this theory we vary the potential with respect to ϕ^* [2] demand this to vanish, i.e.

$$0 = (\mu^2 - m^2)\phi - 2\lambda|\phi|^2\phi = \left((\mu^2 - m^2) - 2\lambda|\phi|^2\right)\phi\,. \tag{3.4}$$

One solution is always $\langle\phi_0\rangle = 0$. However, depending on the value of the chemical potential μ this solution is either stable or unstable. By choosing a chemical potential $\mu > m$, then $\langle\phi\rangle = 0$ is an unstable state of the theory and the lower lying stable ground states are given by $|\langle\phi\rangle|^2 = \frac{\mu^2 - m^2}{2\lambda}$. Note that there is some freedom left in the choice of $\langle\phi\rangle$, namely its phase. The freedom in the choice of ground state corresponds exactly to the $U(1)$ symmetry of the Lagrangian. That is

$$\langle\phi_\theta\rangle = \sqrt{\frac{\mu^2 - m^2}{2\lambda}}\mathrm{e}^{\mathrm{i}\theta}\,, \tag{3.5}$$

where θ is the phase. However, once θ is fixed, the solution is not invariant under the $U(1)$ transformation anymore and the $U(1)$ symmetry is spontaneously broken. This has far reaching consequences and is also the reason for the appearance of superfluidity. For concreteness we choose $\theta = 0$.
To derive the effects of this new ground state $\langle\phi_{\theta=0}\rangle \equiv \langle\phi\rangle \in \mathbb{R}$, we consider fluctuations around it, i.e. $\phi = \langle\phi\rangle + \frac{1}{\sqrt{2}}(\rho_1 + \mathrm{i}\rho_2)$. Plugging this ansatz into the Lagrangian (3.1) and expanding up to quadratic order in the fluctuations (and using the corresponding equations of motion) results in

$$\begin{aligned}\mathcal{L}^{(2)} = &-\frac{1}{2}\left(\partial_\mu\rho_1\partial^\mu\rho_1 + \partial_\mu\rho_2\partial^\mu\rho_2\right) + \mu\left(\rho_2\partial_t\rho_1 - \rho_2\partial_t\rho_1\right)\\ &-\frac{1}{2}(m^2 - \mu^2)\left(\rho_1^2 + \rho_2^2\right) - \lambda\langle\phi\rangle^2\left(3\rho_1^2 + \rho_2^2\right)\,.\end{aligned} \tag{3.6}$$

Note that there are higher contributions in the fluctuations neglected above [73]. However, they are not of interest for the simple analyses of interest here. It is easier to work in momentum space, thus we take the Fourier transform

$$\rho_i(x^\mu) = \int \frac{\mathrm{d}^\mathrm{D}k}{(2\pi)^\mathrm{D}}\mathrm{e}^{\mathrm{i}k_\mu x^\mu}\rho_i(k_\mu)\,. \tag{3.7}$$

[2] In order to do so we take ϕ and ϕ^* to be independent fields.

The fields ρ_i in real and momentum space are differentiated only by their arguments. Plugging this into the action $S \sim \int \mathrm{d}^{\mathrm{D}} x \mathcal{L}^{(2)}$ leads to

$$S \sim \int \frac{\mathrm{d}^{\mathrm{D}} k}{(2\pi)^{\mathrm{D}}} \Big(\rho_1(-k_\mu), \rho_2(-k_\mu)\Big) G^{-1}(k_\mu) \begin{pmatrix} \rho_1(k_\mu) \\ \rho_2(k_\mu) \end{pmatrix}, \tag{3.8}$$

with $G^{-1}(k_\mu)$ the inverse tree level propagator, given by

$$G^{-1}(k_\mu) = \begin{pmatrix} -k^2 - m^2 + \mu^2 - 6\lambda\langle\phi\rangle^2 & 2\mathrm{i}\omega\mu \\ -2\mathrm{i}\omega\mu & -k^2 - m^2 + \mu^2 - 2\lambda\langle\phi\rangle^2 \end{pmatrix}, \tag{3.9}$$

with $k^2 = k_\mu k^\mu$. The dispersion relation is obtained from the zeros of the determinant of $G^{-1}(k_\mu)$, i.e.

$$\begin{aligned} \omega_{\vec{k}}^{\pm} &= \sqrt{\vec{k}^2 + m^2 + \mu^2 + 4\lambda\langle\phi\rangle^2 \mp \sqrt{4\mu^2\left(\vec{k}^2 + m^2 + 4\lambda\langle\phi\rangle^2\right) + 4\lambda^2\langle\phi\rangle^4}} = \\ &= \sqrt{\vec{k}^2 - m^2 + 3\mu^2 \mp \sqrt{4\mu^2\vec{k}^2 + (3\mu^2 - m^2)^2}}, \end{aligned} \tag{3.10}$$

where in the last step the solution for the condensate (3.5) was used. Next we expand these solutions for small values of $|\vec{k}|$, i.e.

$$\begin{aligned} \omega_{\vec{k}}^{+} &\simeq \sqrt{\frac{\mu^2 - m^2}{3\mu^2 - m^2}}|\vec{k}| + \mathcal{O}(|\vec{k}|^2), \\ \omega_{\vec{k}}^{-} &\simeq \sqrt{6\mu^2 - 2m^2} + \frac{5\mu^2 - m^2}{(2(3\mu^2 - m^2))^{3/2}}|\vec{k}|^2 + \mathcal{O}(|\vec{k}|^3). \end{aligned} \tag{3.11}$$

The ω^+ solution vanishes linearly for $|\vec{k}| \to 0$, i.e. this is a massless mode, known as the Goldstone mode, which corresponds to fluctuations along the minimum of the potential (3.3). Being massless means that it can be excited with a minimal amount of energy. This are clearly the fluctuations of the phase $\delta\theta$ around our vacuum choice $\theta = 0$, since $\langle\phi_\theta\rangle$ for all values of θ corresponds to the same energy. Thus a change in the phase barely costs any energy. The second solution describes a massive mode, which corresponds to the fluctuation of the modulus of $\langle\phi_\theta\rangle$ [3]. Clearly the just derived dispersion relations are only valid for $\mu > m$, i.e. in the phase with a condensate. For the solutions with $\mu < m$ and therefore without a condensate, we can immediately obtain the relations by setting $\langle\phi\rangle = 0$ in equation (3.10).The well-known solution is

$$\omega_{\vec{k}}^{\pm} = \sqrt{\vec{k}^2 + m^2} \mp \mu. \tag{3.12}$$

[3]This mode is the Higgs particle. A corresponding mode coming from the spontaneous breaking of a $SU(2) \times U(1)$ symmetry was recently observed at the LHC at CERN in Geneva, Switzerland [20, 21].

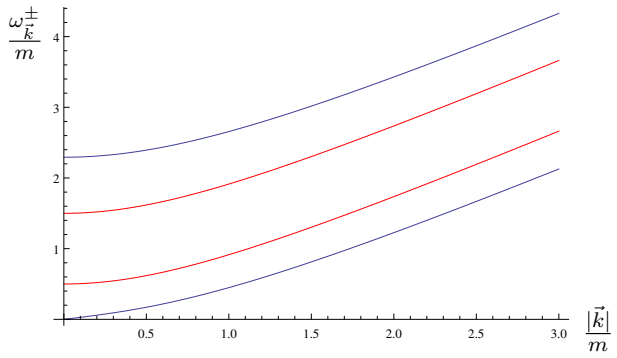

Figure 3.1: Dispersion relation $\omega_{\vec{k}}^{\pm}$ for the case with condensate, i.e. $\mu > m$ (blue lines) and without a condensate (red lines). Note that in the case without a condensate the difference between $\omega_{\vec{k}}^{-} - \omega_{\vec{k}}^{+} = 2\mu$, where for this plot $\mu = 0.5m$.

From the discussion above we saw that the particle spectrum in the unbroken and broken phase changes. In the unbroken phase positively and negatively charged particles are the correct degrees of freedom, whereas in the broken phase a massive and a massless mode take over. However, this does not yet explain why superfluidity in the hydrodynamic limit of such a setup is expected. In order to explain this effect, we closely follow [71].

Let us consider a non-relativistic fluid through a pipe with a velocity $\vec{V}$ everywhere. A part of the fluid with mass M then carries a kinetic energy $E_1 = MV^2/2$. Taking the friction between the pipe walls and the fluid into account leads to an elementary excitation in the fluid resulting in a kinetic energy $E_2 = MV^2/2 + \vec{p}\vec{V} + e(\vec{p})$, where $\vec{p}$ and $e(\vec{p})$ is the momenta and the energy, respectively, of this excitation. Since the energy for the excitation has to come from the fluid itself, energy conservation tells that $E_1 = E_2$ and thus $e(\vec{p}) = -\vec{p}\vec{V}$. Since $\vec{p}\vec{V} = V\,p\,\cos(\theta) \geq -V\,p$ we obtain that $e(\vec{p}) \leq V\,p$.

Massless excitations, which are not Goldstone modes, have dispersion relations with $e(\vec{p}) \propto p^2$. In this case for every given fluid velocity V we can find a momentum small enough to fulfil the inequality derived above. For massive excitations, i.e. $e(p \to 0) = \text{const}$, on the other hand or massless excitations of the Goldstone kind, i.e. $e(\vec{p}) \propto p$ there are values of V for which the above inequality is violated. The massive case is clear, however, for the massless case let us call v the constant of proportionality between e and p, thus $e = v\,p$. Plugging this into $e(\vec{p}) \leq V\,p$, we see that as soon as $V < v$ the inequality is violated and it is not possible to dissipate energy due to friction into elementary excitations anymore. Therefore, for fluid velocities slower than v the flow has to be dissipationless.

There is one issue we still have to comment on. Until now everything was computed at zero temperature. However, we expect superfluidity to appear below a finite temperature T_c. As shown in [72, 73] for small temperatures $T \ll \langle\phi\rangle$ all the

considerations above are still valid. For increasing temperatures one finds that the condensate has a temperature dependence. Finally for temperatures comparable to the size of the zero temperature condensate one obtains that the condensate takes the form

$$\begin{aligned} &\langle\phi\rangle(T) \propto \left(1-\frac{T}{T_c}\right)^{1/2}\,, \text{ with} \\ &T_c^2 = \frac{3(\mu^2-m^2)}{\lambda} + \text{higher order corrections}\,. \end{aligned} \tag{3.13}$$

T_c is the critical temperature below which a solution with a condensate spontaneously breaks the $U(1)$ symmetry. The condensate $\langle\phi\rangle(T)$ is the so-called order parameter of this phase transition. By analysing the pressure and entropy density of the system one finds that they are continuous across the phase transition, however, they are not differentiable. Thus, this is a second order phase transition [72]. We will see similar transitions in later sections and chapters arising from holographic computations.

Finally we would like to remark that in the spontaneously broken phase the mass of the Goldstone mode vanishes for all temperatures smaller than T_c and the massive mode has a non-vanishing mass everywhere except right at the phase transition where $\mu = m$ [72]. The last point hints to the fact that directly at the phase transition the system is described by a conformal field theory, i.e. there is no scale (mass) present.

3.1.2 Superconductivity from Ginzburg-Landau Theory

The microscopic theory of superconductivity is very different from the description of superfluidity presented. However, here we concentrate on the effective description following [75], which is again very similar, up to a certain extent, to the formalism in the last section. The description developed here is known as the Ginzburg-Landau theory [74], which was proposed before the microscopic theory, the BCS theory[4], was known.

The starting point is the Lagrangian (3.1) from the last section. However, this time the field ϕ is understood as a composite particle, composed for example of two electrons[5]. In addition, this prescription is only valid close to the phase transition between the normal and the superconducting phase, i.e. for $T \lesssim T_c$. The next change is to promote the global $U(1)$ symmetry to a gauge symmetry. Thus the transformation under which the theory is invariant reads

$$\phi(x^\mu) \to \phi(x^\mu)\mathrm{e}^{\mathrm{i}\alpha(x^\mu)} \text{ and } \phi^*(x^\mu) \to \phi^*(x^\mu)\mathrm{e}^{-\mathrm{i}\alpha(x^\mu)}\,. \tag{3.14}$$

[4] BCS stands for J. Bardeen, L. Cooper and J. Schrieffer, which published their theory in [76].

[5] In order to understand this pairing mechanism we need BCS theory. Good explanations of this process can be found in [71, 73]

Since the phase is spacetime dependent, another transformation has to be added, namely

$$A_\mu \to A_\mu + \partial_\mu \alpha(x^\mu)\,. \tag{3.15}$$

It can easily be checked that the Lagrangian in (3.1) is invariant under these transformations. The next assumption is that we are in a static situation. Thus all time derivatives are set to zero and we choose the gauge $A_t = 0$. Finally the Lagrangian

$$\mathcal{L}_{GL} = -\left(\vec{\nabla} - \mathrm{i}\vec{A}\right)\phi\left(\vec{\nabla} + \mathrm{i}\vec{A}\right)\phi^* - m^2|\phi|^2 - \lambda|\phi|^4 - \frac{1}{2}\left(\vec{\nabla}\times\vec{A}\right)^2\,, \tag{3.16}$$

is obtained, where the last term comes from the addition of a kinetic term for the gauge field A_μ in the static case. It can easily be computed by starting from

$$\begin{aligned} \mathcal{L}_{EM} &= \frac{1}{4}F_{\mu\nu}F^{\mu\nu} \text{ with} \\ F_{\mu\nu} &= \partial_\mu A_\nu - \partial_\nu A_\mu\,. \end{aligned} \tag{3.17}$$

Putting everything together we get

$$\mathcal{L}_{EM} = -\frac{1}{2}\left(\vec{\nabla}\times\vec{A}\right)^2\,. \tag{3.18}$$

Since the ansatz above is valid close to the phase transition, we can linearise with respect to the temperature dependence and use $m^2 = a(T - T_c)$. Note that in this section m is not a mass of an elementary particle but rather a parameter of the theory. For $T \leq T_c$ there is again a non-trivial value for the expectation value of ϕ. Taking the conventions we use in this section into account, it turns out to be

$$\langle\phi\rangle = \sqrt{-\frac{m^2}{2\lambda}} = \sqrt{\frac{aT_c}{2\lambda}\left(1 - \frac{T}{T_c}\right)}\,. \tag{3.19}$$

This is the same expectation value as in the superfluid case (see the end of section 3.1.1). Apart from that, all other conclusions we drew in the last section from this result are also valid here. Thus $\langle\phi\rangle$ is the order parameter of a second order phase transition between a "normal" (Fermi-liquid-like) and a superconducting phase.

Next small fluctuations around this ground state are considered. Using Noether's theorem[6], the conserved current is

$$\vec{j} = -\mathrm{i}\left(\phi^*\vec{\nabla}\phi - \phi\vec{\nabla}\phi^*\right) - 2|\phi|^2\vec{A}\,, \tag{3.20}$$

which is related to the $U(1)$ symmetry of the theory. The next simplifying assumption we make is that the scalar field varies slowly along the spatial directions

[6]Nother's theorem: For every continuous symmetry of the fields we find a conserved current [77].

around the expectation value (3.19) and it is allowed to linearise in the fluctuations. Therefore the first term in the conserved current above can be neglected and we set ϕ to its expectation value. This gives the London equation

$$\vec{j} = \frac{m^2}{2\lambda}\vec{A}\,. \tag{3.21}$$

The vanishing resistance R can be seen from Ohm's law, $\vec{E} = R\,\vec{j}$, where $\vec{E} = -\partial_t \vec{A} = 0$ is the vanishing electric field in the static case. Thus we conclude that $R = 0$.

Next we derive the Meissner effect. This effect describes the expulsion of the magnetic fields from the superconductor. We start with one of the Maxwell's equations, namely Ampère's law,

$$\vec{\nabla} \times \vec{B} = \vec{j}\,, \tag{3.22}$$

with $\vec{B} = \vec{\nabla} \times \vec{A}$ in our conventions. Taking the curl of this equation and using (3.21) we obtain

$$\vec{\nabla}^2 \vec{B} = -\frac{m^2}{2\lambda}\vec{B}\,, \tag{3.23}$$

where $\vec{\nabla}\,\vec{B} = 0$. Choosing the magnetic field to only have a component in x direction leads to

$$B_x = B_0 \mathrm{e}^{-\sqrt{-\frac{m^2}{2\lambda}}x} \tag{3.24}$$

as the solution to the equation above. Note that the term under the square root is positive. This result tells us that a magnetic field is exponentially suppressed when entering the superconductor. Imagine a material at a temperature slightly above its critical temperature T_c placed in a small magnetic field. Lowering the temperature continuously below T_c leads to a phase transition in the material to the superconducting phase. At T_c the magnetic field cannot go through the material anymore, but it is exponentially suppressed. Since the flux is conserved the magnetic field has to flow around the material.

By rewriting eq. (3.23) in a covariant form in terms of the gauge field A_μ we get

$$\Box A_\mu = -\frac{m^2}{2\lambda}A_\mu\,, \tag{3.25}$$

where the term in front of A_μ on the right hand side of the equation corresponds to a squared mass term of the photon. This mass term arises from the Higgs mechanism associated to the spontaneous breaking of a gauged symmetry. It is noteworthy that the Meissner effect, as well as the superconductivity itself, is strongly related to the fact that this theory has a local (gauged) symmetry, rather

than a global symmetry as for instance in the discussion of the superfluid in section 3.1.1.

With the effective approach presented in this section some of the effects seen in "conventional" superconductors were derived. It is important to stress that superconductivity does not arise due to a superflow of charged particles, with the superflow originating from the linear dispersion relation of Goldstone modes, but from the Higgs mechanism which makes the photon massive. Note that the critical temperature $T_c \propto \Delta_0$, where Δ_0 is the zero temperature energy gap $\Delta(T \to 0) = \Delta_0$ between the ground state and the first excited state in the quasi-particle picture of BCS theory (cf. [71]). In our effective description, around $T \lesssim T_c$, the energy gap is $\langle\phi\rangle = \Delta(T)$. Finally, this description only applies to conventional, weakly coupled, superconductors. For high-T_c superconductors a theoretical description is still missing. It may be that holography can close this gap. Thus in the next section we describe holographic superfluids and superconductors.

3.2 Holographic Superfluids

In this section we study the holographic realisation of superfluids (superconductors)[7]. Our main source for this section is the presentation in [55,57]. Furthermore most of the technical details, which are needed to solve the equations of the system discussed below, are obscured. Nevertheless, in chapter 4 all details and subtleties involved in this kind of computations are explicitly shown. Here we wish to concentrate on the overall picture and the physical interpretations.

To realise a holographic superconductor $U(1)$ symmetry has to be broken spontaneously. To realise that some of the fields in the corresponding theory have to be charged under this $U(1)$. A very easy holographic setup we can study to model this effect is the Einstein-Maxwell theory in asymptotically AdS space with a charged scalar field in the bulk. The action reads

$$S_L = \int \mathrm{d}^{\mathrm{D}+1}x\, \sqrt{-g}\left(\frac{1}{2\kappa^2}\left(R-\Lambda\right) - \frac{1}{4g^2}F^2 - |D_A\psi|^2 - V(\psi)\right), \tag{3.26}$$

with $\Lambda = -\mathrm{D}(\mathrm{D}-1)/L^2$, $F^2 = F_{AB}F^{AB}$, $|D_A\psi|^2 = (D_A\psi)\left(D^A\psi\right)^*$, where $D_A = \nabla_A - iqA_A$ and q being the charge of the scalar field ψ, and $V(\psi) = m^2|\psi|^2$, where m is the scalar mass. The remaining terms have the same definition as in section 2.4.2. Again boundary terms S_{bdry} are needed to render the on-shell action and Green's functions finite. However, for the sake of legibility they are suppressed

[7] In the holographic literature superconductors and superfluids are used very loosely. From the knowledge to date, one can consider a holographic superconductor to be a weakly gauged superconductor. In this thesis we do not differentiate between holographic superconductors and superfluids.

here.

The equations of motion of this system are

$$\begin{aligned}
&-\left(\nabla_A - iqA_A\right)\left(\nabla^A - iqA^A\right)\psi + \frac{1}{2}\frac{\psi}{|\psi|}V'|\psi| = 0\,,\\
&\frac{1}{g^2}\nabla^A F_{AB} = iq\left(\psi^*\left(\nabla_B - iqA_B\right)\psi - \psi\left(\nabla_B + iqA_B\right)\psi^*\right)\,,\\
&R_{AB} - \frac{1}{2}g_{AB}\left(R + \frac{\mathrm{D}(\mathrm{D}-1)}{L^2}\right) = \kappa^2 T_{AB}\,,
\end{aligned} \tag{3.27}$$

with

$$\begin{aligned}
T_{AB} =& \frac{1}{4g^2}\left(4F_{AC}F_B{}^C - g_{AB}F_{CD}F^{CD}\right)\\
&- g_{AB}\left(V(|\psi|) + |D_A\psi|^2\right) + \left(\left(D_A\psi\right)\left(D_B\psi\right)^* + \left(D_B\psi\right)\left(D_A\psi\right)^*\right)\,,
\end{aligned} \tag{3.28}$$

where D_A is defined above.

Following [55, 57, 78] we choose the ansatz

$$\begin{aligned}
&\mathrm{d}s^2 = g_{AB}\mathrm{d}x^A\mathrm{d}x^b = -N(r)\mathrm{e}^{-\chi(r)}\mathrm{d}t^2 + \frac{1}{N(r)}\mathrm{d}r^2 + r^2\left(\sum_{i=1}^{\mathrm{D}-1}\mathrm{d}x_i^2\right)\,,\\
&A = \phi(r)\mathrm{d}t\,,\\
&\psi = \psi(r)\,.
\end{aligned} \tag{3.29}$$

In the case of vanishing scalar field the AdS Reissner-Nordström black hole solution, studied in section 2.4.2, is the correct description, i.e.

$$\begin{aligned}
&\psi = 0\,,\\
&\phi(r) = \mu\left(1 - \left(\frac{r_H}{r}\right)^{\mathrm{D}-2}\right)\,,\\
&\chi(r) = 0\,,\\
&N(r) = \left(\frac{r^2}{L^2} - \left(\frac{r_H^2}{L^2} + \frac{L^2\mu^2}{\gamma^2}\right)\left(\frac{r_H}{r}\right)^{\mathrm{D}-2} + \frac{L^2\mu^2}{\gamma^2}\left(\frac{r_H}{r}\right)^{2\mathrm{D}-4}\right)\,,\\
&\qquad \text{with } \gamma^2 = \frac{(\mathrm{D}-1)L^2g^2}{(\mathrm{D}-2)\kappa^2}\,.
\end{aligned} \tag{3.30}$$

This result looks slightly different than (2.45), since here we took the coordinates $r = L^2/z$, with z as defined in chapter 2. At the same time the spatial field theory directions was rescaled by $x_i \to L\,x_i$. The boundary value of $A_t(r_B) = \mu$ is again interpreted as the chemical potential of the dual field theory.

From here on we work in 4 dimensional gravity, i.e. in a field theory living in $D = 2 + 1$ dimensions. In this case the equations of motion for a non-vanishing scalar field (primes denote ∂_r) are

$$\begin{aligned}
&\psi'' + \left(\frac{N'}{N} - \frac{\chi'}{2} + \frac{2}{r}\right)\psi' + \left(\frac{q^2 e^{\chi}\phi^2}{N^2} - \frac{m^2}{N}\right) = 0\,,\\
&\phi'' + \left(\frac{\chi'}{2} + \frac{2}{r}\right)\phi' - \frac{2g^2q^2\psi^2}{N}\phi = 0\,,\\
&\chi' + \frac{2\kappa^2 q^2 r e^{\chi}\psi^2\phi^2}{N^2} + 2\kappa^2 r\psi'^2 = 0\,,\\
&\frac{1}{2}\psi'^2 - \frac{3}{2\kappa^2L^2N} + \psi^2\left(\frac{m^2}{2N} + \frac{q^2e^{\chi}\phi^2}{2N^2}\right) + \frac{N'}{2\kappa^2 rN} + \frac{e^{\chi}\phi'^2}{4g^2N} + \frac{1}{2\kappa^2r^2} = 0\,.
\end{aligned} \tag{3.31}$$

This correspond to the equations (3.3) to (3.6) given in [55], with the difference that there $\kappa^2 = 1/2$ and $g = 1$.

3.2.1 Instabilities

To find the instabilities of the AdSRN setup, we start by linearising the equations with respect to the scalar field ψ, i.e. all terms which are not linear in ψ are thrown away. The resulting equations correspond exactly to the AdSRN case with one additional one for ψ, namely

$$\psi'' + \left(\frac{N'}{N} + \frac{2}{r}\right)\psi' + \left(\frac{q^2\mu^2}{N^2}\left(1 - \frac{r_H}{r}\right)^2 - \frac{m^2}{N}\right) = 0\,. \tag{3.32}$$

Since the other fields are still governed by the AdSRN equations of motion, we can consider the scalar field as a probe in the Reissner-Nordström background and just use the solution (3.30) for the remaining fields in the equation above. Close to the boundary, the scalar field falls off as $\psi \sim r^{-\Delta}$ with Δ a positive number. Using this ansatz in the equation for ψ and expanding close to the boundary results in the relation

$$m^2L^2 = \Delta\,(\Delta - 3) \tag{3.33}$$

between the mass and the fall-off behaviour. This is exactly the relation between the mass of a scalar field and the scaling dimension of the dual operator stated before, at the end of section (2.3.4). The next step is to analyse this equation at zero temperature close to the horizon. Remember that in the AdSRN case $T = 0$ corresponds to an extremal black hole. Thus even though the temperature vanishes, there is still a horizon. First we rewrite the temperature derived in the last chapter for the AdSRN solution (cf. eq. (2.46)) in terms of the conventions used in this section, i.e.

$$T = \frac{3r_H}{4\pi L^2}\left(1 - \frac{\kappa^2L^2}{g^2}\frac{\mu^2}{6r_H^2}\right)\,. \tag{3.34}$$

Zero temperature means that $\mu = \sqrt{6}gr_H/(\kappa L)$. Furthermore in this limit one obtains near the horizon a geometry which is $AdS_2 \times \mathbb{R}^2$ with an AdS radius

$L_2^2 = L^2/6$. Plugging this into the linearised equation for the scalar field and evaluating it close to the horizon leads to a new effective mass of the scalar field in the AdS_2 geometry, namely $m_2^2 = m^2 - q^2 g^2/\kappa^2$. Due to the negative cosmological constant AdS space allows for negative mass squared of the scalar field down to a certain value without becoming unstable. The lower stability bound for the mass, the Breitenlohner-Freedman (BF) bound [68], is (c.f. section 2.3.4)

$$L^2 m^2 \geq -\frac{\mathrm{D}^2}{4}\,. \tag{3.35}$$

Putting everything together, i.e. $\mathrm{D} = 1$ in the extremal near horizon AdS_2 case, the scalar field becomes unstable if

$$-\frac{1}{4} \geq (L_2 m_2)^2 = \frac{L^2}{6}\left(m^2 - q^2 g^2/\kappa^2\right)\,. \tag{3.36}$$

It is noteworthy that also in the $q = 0$ case, i.e. the scalar field is uncharged, by a certain choice of m^2 the system could become unstable, since squared masses which are perfectly fine in AdS_4 may render the AdS_2 region unstable [55, 57].

At finite temperature and due to the covariant derivative the effective mass reads

$$m_{\text{eff}}^2 = m^2 + q^2 g^{tt} A_t^2 = m^2 - q^2 \frac{1}{N(r)}\phi(r)^2\,. \tag{3.37}$$

By tuning the chemical potential, or alternatively, the temperature we can get m_{eff}^2 smaller than the BF bound, which renders the AdSRN solution unstable.

The instabilities described above at $T = 0$ and $T \neq 0$ result in a phase transition from AdSRN to a new vacuum with a condensed scalar field $\phi(r) \neq 0$, which breaks the $U(1)$ symmetry spontaneously. In the following we concentrate on the $T \neq 0$ case. Since the effective mass square m_{eff}^2 depends on q and Δ (or alternatively $L^2 m^2$) a phase transition from the AdSRN solution to a phase with a condensate can be triggered by changing these values. The phase transition takes place at a critical values of $(T/\mu)_c$, where the numerical value depends on the parameters chosen. A plot relating the different values of $(T/\mu)_c$, q and Δ is shown in figure 1 in [79].

3.2.2 The Superconducting Solution

After having examined the conditions for instabilities of the system (3.26) in the AdSRN phase, we go on to discuss the corresponding stable solution. Again the results were derived in [55, 57]. In chapter 4 we compare these results to the ones we find in a holographic superconductor with an additional rotational symmetry broken.

The relevant quantities are presented in terms of the coefficients of the expansion of the fields close to the AdS boundary[8]. These coefficients are related to the expectation values of the dual field theory operators[9], as was pointed out in section 2.3.4. The expansions at the AdS boundary of the different fields in the broken phase are

$$\begin{aligned}
\phi(r\to\infty) &\simeq \mu + \frac{L}{r}\phi_1^B + \mathcal{O}(r^{-2})\,,\\
\psi(r\to\infty) &\simeq \frac{L}{r}\psi_1^B + \frac{L^2}{r^2}\psi_2^B + \mathcal{O}(r^{-3})\,,\\
N(r\to\infty) &\simeq \frac{r^2}{L^2} + \kappa^2\psi_1^B + \frac{L}{r}N_1^B + \mathcal{O}(r^{-2}) \text{ and}\\
\chi(r\to\infty) &\simeq \frac{\kappa^2 L^2}{r^2}\left(\psi_1^B\right)^2 + \mathcal{O}(r^{-3})\,,
\end{aligned} \tag{3.38}$$

where μ denotes the chemical potential, ϕ_1^B is proportional to the charge density of the dual field theory and $\chi_0^B = 0$. The latter fixes the space to be asymptotically AdS. In addition we set $L^2m^2 = -2$. This choice of mass leads to $\Delta_+ = 2$ and $\Delta_- = 1$, in agreement with the boundary expansion above (cf. (2.22)). Note that this choice for the mass is special since both modes, the normalisable one, with $\Delta_+ = 2$, and the non-normalisable one, with $\Delta_- = 1$ have a fall-off behaviour, which does not violate the unitarity bound

$$\frac{3}{2} - 1 = \frac{1}{2} \leq \Delta\,. \tag{3.39}$$

See also the discussion at the end of section 2.3.4. Hence we are free to choose which of the coefficients to interpret as the expectation value of the dual operator and which one as its source. However, to break the $U(1)$ symmetry spontaneously on the field theory side, the source term has to vanish, since a term in the field theory Hamiltonian of the form $\sim \int \bar{\psi}_2^B\langle\mathcal{O}_1\rangle$ would break the symmetry explicitly. Therefore, if we choose to set $\psi_1^B \sim \langle\mathcal{O}_1\rangle$, ψ_2^B has to vanish or vice versa. Thus, from a field theoretic point of view the operator $\mathcal{O}_1$ obtains a vacuum expectation value dynamically, i.e. the $U(1)$ symmetry is broken spontaneously.

From the dual field theory, this new solution with a non-vanishing condensate presents a new stable thermal equilibrium state for certain regions of parameter space, i.e. for certain values of T/μ for given q and m^2. Thus, in the same way the grand potential, the entropy density and charge density was computed for the AdS Reissner-Nordström solution at the end of last chapter, this could be redone for

[8] With boundary expansion we denote the expansion close to the AdS boundary. For the coordinates used in this chapter, this means that the fields are expanded in negative powers of r for $r \to \infty$.

[9] In section 3.2.4 a second method is derived to compute the expectation value of a dual operator.

this new solution. Below $(T/\mu)_c$ the grand potential of the solution with condensate is lower than the AdSRN one. Therefore the broken phase, for values of the temperature below $(T/\mu)_c$, is thermodynamically preferred and describes the correct state of the theory. In addition the entropy density at this point is continuous but not differentiable which hints to a second order phase transition between both solutions (cf. [55, 57] and discussions in the sections 3.1.1 and 3.1.2). In the dual field theory, $\langle \mathcal{O}_i \rangle$ acts as an order parameter of the phase transition. Therefore it is of interest to study its temperature dependence. For both choices of boundary conditions this dependence is presented in figure 3.2, see also [55]. Note that above a certain critical temperature T_c [10] the condensate vanishes and the AdSRN solution is obtained. Close, but below T_c, for both choices of boundary conditions the order parameter has a mean field behaviour, i.e. $\langle \mathcal{O}_i \rangle \sim (1 - T/T_c)^{1/2}$, which is in agreement with the postulated second order phase transition. Note that the mean field behaviour and the similarities to classical Ginzburg-Landau theory is due to the large N limit of the dual field theory. This is also the reason why there is an ordered phase in $2 + 1$ dimensions, which in principle is excluded by the Mermin-Wagner theorem [80].

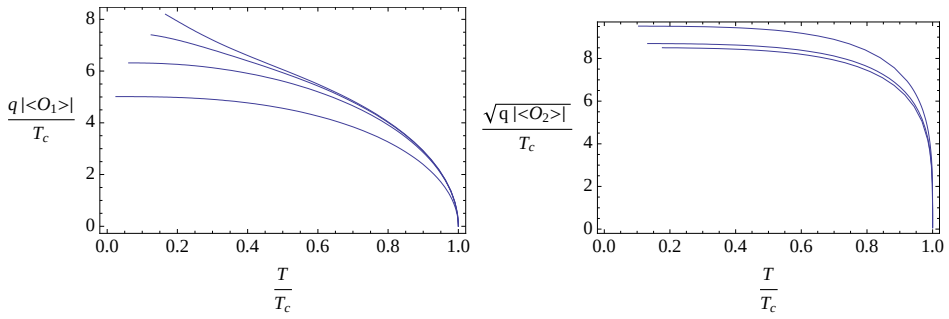

Figure 3.2: Vacuum expectation value of the operators $\mathcal{O}_1$ and $\mathcal{O}_2$, respectively, as a function of the temperature. The different curves correspond to different values of q. Source: [55]

3.2.3 Perturbations and Hydrodynamic Transport

Important quantities which on the one hand can be compared to experiment and on the other hand are very sensible to many characteristics of a theory are the transport coefficients. These coefficients determine the behaviour of a system close to thermal equilibrium, i.e. it has been slightly perturbed. These perturbations depend on time and in general also on the spatial coordinates. We start the discussion from a field theoretic point of view in general dimensions D and then make contact to the holographic computation of the relevant quantities in the next sec-

[10] Note that this is short for $(T/\mu)_c$. For a more intuitive presentation of the results we can always rewrite T/μ as $T/T_c = (T/\mu)/(T/\mu)_c$, by fixing $\mu = 1$ for instance.

tion. For a very nice introduction to hydrodynamics we refer the interested reader to [81].

While the form of an effective theory describing the thermodynamic equilibrium and small fluctuations about this state is fully determined by the symmetries of the system, i.e. by its conserved currents

$$\begin{aligned} &\text{the energy-momentum tensor } T_{\mu\nu} \text{ and} \\ &\text{conserved charge current } J_\mu\,, \end{aligned} \tag{3.40}$$

the transport coefficients appearing in this currents are determined by the underlying microscopic theory. For instance the dual field theory of the AdSRN solution, which is isotropic and includes a conserved $U(1)$ current, is effectively described by

$$\begin{aligned} \langle T_{\mu\nu}\rangle &= e u_\mu u_\nu + P\, P_{\mu\nu} + \Pi_{\mu\nu} \text{ and} \\ \langle J_\mu\rangle &= \rho u_\mu + \Upsilon_\mu\,, \end{aligned} \tag{3.41}$$

with u^μ the four velocity, $P_{\mu\nu} = g_{\mu\nu} - u_\mu u_\nu$ the projector transverse to the four velocity. Note that by using $g_{\mu\nu}$ these equations also apply to curved spaces. For computations in Minkowski space choose $g_{\mu\nu} = \eta_{\mu\nu}$. In addition, we work in the fluid rest frame, i.e. $u^t = 1$, while $u^a = 0$. The coefficients e, the energy density, P, the pressure, and ρ, the charge density, are determined by the underlying theory (see section 2.4.2 for the corresponding AdSRN values of these coefficients). In $\Pi_{\mu\nu}$ and Υ_μ the first order dissipative contributions to the energy-momentum tensor and the current are hidden. These arise due to small fluctuations about the thermal equilibrium. There is some ambiguity in how the energy density of a system including fluctuations is defined. To resolve this issue, we use the Landau frame choice throughout this thesis, i.e. $u_\mu u_\nu T^{\mu\nu} \equiv e$ is always the energy density and does not get perturbative contributions, therefore $u_\mu \Pi^{\mu\nu} = 0$ and $u_\mu \Upsilon^\mu = 0$. The fluctuations are organised in terms of an expansion series in gradients of the four velocity u^μ, the temperature T and the chemical potential μ (in case of a charged fluid), see e.g. [40]. Taking the symmetries of the AdS Reissner-Nordström solution into account we expect the dissipative terms up to linear order to have the form [82]

$$\begin{aligned} \Pi_{\mu\nu} &= -\eta\, P_\mu{}^\alpha P_\nu{}^\beta \left(\nabla_\alpha u_\beta + \nabla_\beta u_\alpha\right) \text{ and} \\ \Upsilon_\mu &= \sigma\, u^\alpha F_{\alpha\mu} - \sigma T\, P_\mu{}^\alpha \nabla_\alpha \left(\frac{\mu}{T}\right) - \alpha\, P_\mu{}^\alpha \nabla_\alpha T\,, \end{aligned} \tag{3.42}$$

where η, the shear viscosity, σ, the electrical conductivity, and α the thermoelectric conductivity are transport coefficients. $F_{\mu\nu} = \nabla_\mu A_\nu - \nabla_\nu A_\mu$ is the field-strength tensor of a external vector field acting on the $U(1)$ charge, μ the chemical potential associated to the $U(1)$ and T the temperature. Note that $E_\mu = u^\alpha F_{\alpha\mu}$

corresponds to an external electrical field. Since the AdSRN solution describes a dual conformal field theory the trace of the energy-momentum tensor has to vanishes implying that there is no bulk viscosity.

The transport coefficients introduced above can be computed using linear response theory [72]. For the coefficients of interest here, it is enough to consider fluctuations up to linear order. We start with an unperturbed Hamiltonian H_0 and consider small perturbations[11]

$$H_{\text{pert}}(t) = \int \mathrm{d}^{\mathrm{D}-1}x\, \mathcal{O}_m(t,\vec{x})\, \delta j_m(t,\vec{x})\,, \tag{3.43}$$

i.e. an operator $\mathcal{O}_m$ coupled to some external source j_m. Following, e.g. [72], the reaction of the expectation value of the other operators to this perturbation is given by

$$\delta\langle\mathcal{O}_n\rangle(t,\vec{x}) \simeq \int_{-\infty}^{\infty} \mathrm{d}t' \int \mathrm{d}^{\mathrm{D}-1}x'\, G^R_{\mathcal{O}_n\mathcal{O}_m}(t,\vec{x};t',\vec{x}')\, \delta j_m(t',\vec{x}')\,, \tag{3.44}$$

with

$$G^R_{\mathcal{O}_n\mathcal{O}_m}(t,\vec{x};t',\vec{x}') = -\mathrm{i}\theta(t-t')\langle\big[\mathcal{O}_n(t,\vec{x}),\mathcal{O}_m(t',\vec{x}')\big]\rangle\,. \tag{3.45}$$

$G^R_{\mathcal{O}_n\mathcal{O}_m}$ is the retarded Green's function computed in the unperturbed system. Note that at finite temperature the vacuum expectation value has to be replaced by the corresponding thermal average, i.e.

$$\langle\mathcal{O}\rangle = \frac{\mathrm{tr}\,\left(\mathrm{e}^{-\beta H}\mathcal{O}\right)}{\mathrm{tr}\,\left(\mathrm{e}^{-\beta H}\right)}\,, \tag{3.46}$$

where $\beta = 1/T$. Since the Green's function is computed with regard to the unperturbed Hamiltonian, describing the thermal equilibrium, it does not depend on the coordinates $(t,\vec{x})$ and $(t',\vec{x}')$ separately, but rather only on their difference $(t-t',\vec{x}-\vec{x}')$. Therefore, the equivalent to (3.44) in momentum space is simply

$$\delta\langle\mathcal{O}_n\rangle(\omega,\vec{k}) = G^R_{\mathcal{O}_n\mathcal{O}_m}(\omega,\vec{k})\, \delta j_m(\omega,\vec{k})\,. \tag{3.47}$$

In the last step the retarded Green's function is related to the corresponding transport coefficient. This goes under the name Kubo's formulae [83]. For the shear viscosity, for instance, this is

$$\eta = -\lim_{\omega\to 0}\frac{1}{\omega}\mathrm{Im}\left(G^R_{T^{xy}T^{xy}}\right)\,. \tag{3.48}$$

We postpone the derivation of this result to section 4.2.7.3. Here we concentrate on the $U(1)$ current.

[11] We present the general results in arbitrary dimensions D and only comeback to the D = 3 case when relating it to the holographic s-wave superconductor.

A very important quantity in a superconductor is the optical, or electrical, conductivity σ_{ab}, where a, b run over the spatial directions in the field theory. It is defined as the answer of the $U(1)$ current to an external electrical field E_a, i.e. Ohm's law

$$\langle J^a \rangle = \sigma^{ab} E_b \,. \tag{3.49}$$

Choosing a gauge where the gauge potential $\delta A_t = 0$ and considering a vector potential dependent on time only, $\delta A_b(t) \sim \delta A_b \mathrm{e}^{-\mathrm{i}\omega t}$ [12], Ohm's law can be rewritten by using $E_b = u^\mu F_{\mu b} = \mathrm{i}\omega \delta A_b$ resulting in

$$\delta\langle J^a \rangle = \mathrm{i}\omega \sigma^{ab}\, \delta A_b \,. \tag{3.50}$$

Now we have all ingredients to apply the just developed linear response theory to Ohm's law (3.49). Small fluctuations of a vector potential δA_a about some background photon field source a electrical current J^a. Using (3.47) we obtain

$$\delta\langle J^a \rangle(\omega, \vec{0}) = G^R_{J^a J^b}(\omega, \vec{0})\, \delta A_a(\omega, \vec{0}) \,. \tag{3.51}$$

Using the same choices as mentioned above equation (3.50) and comparing it with (3.50) leads to

$$\sigma^{ab}(\omega) = -\frac{\mathrm{i}}{\omega} G^R_{J^a J^b}(\omega, \vec{0}) \,. \tag{3.52}$$

This is Kubo's formula for the electrical conductivity. Note that until now the α term in eq. (3.42) was omitted. To include this term it has to be taken into account that charged particles not only transport charge but also energy. Therefore Ohm's law (3.49) has to be generalised to [57]

$$\begin{pmatrix} \langle J^a \rangle \\ \langle Q^a \rangle \end{pmatrix} = \begin{pmatrix} \sigma^{ab} & T\alpha^{ab} \\ T\alpha^{ab} & T\bar{\kappa}^{ab} \end{pmatrix} \begin{pmatrix} E_b \\ -(\nabla_b T)/T \end{pmatrix} , \tag{3.53}$$

where α is the thermoelectric conductivity, $\bar{\kappa}$ is the thermal conductivity and $\langle Q_a \rangle = \langle T_{ta} \rangle - \mu \langle J_a \rangle$ is the heat current. Without magnetic fields there are no off-diagonal matrix entries for the different transport coefficients, e.g. $\sigma^{ab} = 0$ for $a \neq b$. Similarly to the connection between E_b and the fluctuation of the vector potential, the fluctuations about a background metric are related to the temperature gradient. We follow the procedure presented in [57] to derive this relation. First rescale the time $t \to \bar{t} = tT$, thus the period of the Euclidean time τ is 1 instead of $1/T$. This also redefines the metric to $g_{\overline{tt}} = -1/T^2$. Small fluctuations of the temperature $x^a \nabla_a T$ lead to small fluctuations of the $\overline{tt}$ component of the metric,

$$g_{\overline{tt}} - \delta g_{\overline{tt}} = -\frac{1}{T^2} + \frac{2x^a \nabla_a T}{T^3} \,. \tag{3.54}$$

[12] A mathematically more rigorous approach would be to work in Fourier space. Doing so we would automatically obtain the $\mathrm{e}^{-\mathrm{i}\omega t}$ factor. We pursue this approach in the next chapter.

As in the pure Ohm's law case, we again choose the following time dependence $\mathrm{e}^{-\mathrm{i}\bar{\omega}\bar{t}}$ of the fluctuations.
Taking into account that fluctuations of the metric can be seen as diffeomorphisms,

$$\begin{aligned} \delta g_{\mu\nu} &= \partial_\mu \xi_\nu + \partial_\nu \xi_\mu \text{ and} \\ \delta A_\mu &= A_\nu \partial_\mu \xi^\nu + \xi^\nu \partial_\nu A_\mu \,, \end{aligned} \tag{3.55}$$

acting on the background fields, we can set $\delta g_{\bar{t}\bar{t}} = 0$ by a choosing certain ξ_μ, namely $\xi_{\bar{t}} = \mathrm{i}x^a \nabla_a T/(\bar{\omega} T^3)\mathrm{e}^{-\mathrm{i}\bar{\omega}\bar{t}}$ and $\xi_a = 0$. This leads to

$$\begin{aligned} \delta g_{ta} &= \mathrm{i}\frac{\nabla_a T}{\omega T}\mathrm{e}^{-\mathrm{i}\omega t} \text{ and} \\ \delta A_a &= -\mathrm{i}\mu\frac{\nabla_a T}{\omega T}\mathrm{e}^{-\mathrm{i}\omega t} \,, \end{aligned} \tag{3.56}$$

where we changed back to the original coordinates t, used that the background vector field is $A_t = \mu$ and the background metric is flat. Finally one obtains

$$\begin{aligned} -\frac{\nabla_a T}{T} &= \mathrm{i}\omega \delta g_{ta} \text{ and} \\ E_a &= \mathrm{i}\omega \left(\delta A_a + \mu \delta g_{ta}\right) \,. \end{aligned} \tag{3.57}$$

Switching on the fluctuations δA_a and δg_{ta} in a theory in thermal equilibrium leads to the following additional terms in the action (similar to eq. (3.43))

$$\begin{aligned} S_{\text{pert}} &= \int \mathrm{d}^{\mathrm{D}} x \sqrt{-g} \left(T^{ta}\delta g_{ta} + J^a \delta A_a\right) = \\ &\overset{(3.57)}{=} \int \mathrm{d}^{\mathrm{D}} x \sqrt{-g} \left(\left(T^{ta} - \mu J^a\right)\left(\mathrm{i}\frac{\nabla_a T}{\omega T}\right) + J^a \frac{E_a}{\mathrm{i}\omega}\right) \,. \end{aligned} \tag{3.58}$$

This has exactly the format claimed in (3.53). Now Kubo's formula for all the coefficients in (3.53) are

$$\begin{aligned} \sigma(\omega) &= -\frac{\mathrm{i}}{\omega} G^R_{J^a J^a}(\omega, \vec{0}) \,, \\ \alpha(\omega) T &= -\frac{\mathrm{i}}{\omega} G^R_{J^a Q^a}(\omega, \vec{0}) \text{ and} \\ \bar{\kappa}(\omega) T &= -\frac{\mathrm{i}}{\omega} G^R_{Q^a Q^a}(\omega, \vec{0}) \,. \end{aligned} \tag{3.59}$$

3.2.4 Holographic Transport

In this section we compute the transport coefficients derived in the last section from holography. One of the big advantages of gauge/gravity duality is that in order to derive the dynamical properties of a strongly coupled theory (with gravity dual) only relatively easy computations are needed as we see in this section. Again we concentrate on the results since a detailed calculation of this kind will be presented in chapter 4.

In the following only $\delta A_x(t,r)$ and $\delta g_{tx}(t,r)$ fluctuations are considered on top of the background metric and vector field given in section 3.2. Thus only the optical (electrical) conductivity and the thermoelectric effect introduced above, are derived.

Our goal in this section is to compute the Green's functions associated to the different transport coefficients shown in equation (3.59) from holography. To compute retarded Green's functions in gauge/gravity duality the procedure developed in [44] is used. However, here we choose slightly different sign conventions. Through this section we work in momentum space, i.e.

$$\Phi_m(x^\mu, r) = \int \frac{\mathrm{d}^{\mathrm{D}}k}{(2\pi)^{\mathrm{D}}} \mathrm{e}^{\mathrm{i}k_\mu x^\mu} \Phi_m(k_\mu, r)\,, \tag{3.60}$$

with Φ_m being some arbitrary field living in the gravity theory. For now it does not matter either if this field includes perturbations or just a background field. Next we define the conjugate momentum to the field $\Phi_m(k_\mu, r)$, i.e.

$$\Pi_m(k_\mu, r) = \frac{\delta S_L[(\Phi_m)_0^B]}{\delta \partial_r \Phi_m(k_\mu, r)} + \frac{\delta S_{\mathrm{bdry}}[(\Phi_m)_0^B]}{\delta\,(\Phi_m)_0^B}\,, \tag{3.61}$$

where S_{bdry} is an appropriate boundary action to render the conjugate momentum finite, i.e. it includes counterterms, and $(\Phi_m)_0^B$ is the value of the non-normalisable mode of $\Phi_m(k_\mu, r)$. With $S[(\Phi_m)_0^B]$ we mean that one has to plug in the solution for $\Phi_m(k_\mu, r)$ subject to the boundary condition $(\Phi_m)_0^B$ into the equation above. Note that one has to be careful in applying this formula to arbitrary fields. For instance, in the case of a scalar field Ψ, as defined in section 3.2.2, the correct definition is $\Phi = r^{-(\Delta-\mathrm{D})}\Psi$. Thus all the fields have to be redefined in a way that the non-normalisable mode is constant at the boundary in order for this approach to work[13]. The expectation value of the dual operator $\langle \mathcal{O}_m \rangle$ can be written in terms of the conjugate momentum, resulting in

$$\langle \mathcal{O}_m \rangle(k_\mu) = \lim_{r\to\infty} \Pi_m(k_\mu, r) = \frac{\delta S_L[(\Phi_m)_0^B]}{\delta\,(\Phi_m)_0^B}\,. \tag{3.62}$$

The theory behind this equation is the Hamilton-Jacobi formulation of classical mechanics (see e.g. [44, 84]). Considering fluctuations to linearised order, i.e. $\Phi_m(k_\mu, r) = \Phi_m^{\mathrm{bkg}}(r) + \delta\Phi_m(k_\mu, r)$, we get an equation very similar to (3.47), however, with δj_m replaced by the non-normalisable mode of the perturbed field, i.e. by $\delta\,(\Phi_m)_0^B\,(k_\mu)$, thus

$$\delta\langle \mathcal{O}_m \rangle(k_\mu) = G^R_{\mathcal{O}_m\mathcal{O}_n}(k_\mu)\,\delta\,(\Phi^n)_0^B\,(k_\mu)\,. \tag{3.63}$$

It is important to remark that to obtain the retarded Green's function the boundary conditions at the black hole horizon matters. We make this statement more

[13] This approach works for the spin 0, 1 and 2 cases. Other cases may be more subtle.

precise below. Let us for now assume that the conditions at the horizon are chosen in a way that the retarded Green's function is obtained. Comparing eq. (3.62) and eq. (3.63) and taking into account that we have linearised with respect to the fluctuation, we obtain

$$G^R_{\mathcal{O}_m\mathcal{O}_n}(k_\mu) = \lim_{r\to\infty} \frac{\delta\Pi_m(k_\mu, r)}{\delta\left(\Phi^n\right)^B_0(k_\mu)} = \lim_{r\to\infty} \frac{\delta\Pi_m(k_\mu, r)}{\delta\Phi_n(k_\mu, r)}\,. \tag{3.64}$$

Some comments are in place: First, since we linearised with respect to the fluctuations the sources $\delta\left(\Phi^n\right)^B_0(k_\mu)$ do not need to be set to zero after taking the functional derivative. The conjugate momentum only depends linearly on the fluctuations. Second, the last equality holds due to the definition of the fields above equation (3.62).

Next we use (3.62) to derive a general formula for the expectation value of the energy-momentum tensor $\langle T^{\mu\nu}\rangle$ and the current $\langle J^\mu\rangle$[14]. The current is straightforward to compute, namely

$$\langle J^\mu\rangle = \lim_{r\to\infty} \frac{\delta S_L}{\delta\partial_r A_\mu} = -\frac{1}{g^2}\sqrt{-g}F^{r\mu}\Big|_{r\to\infty}\,. \tag{3.65}$$

For the s-wave superfluid background solution, using the boundary expansion (3.38), results in[15]

$$\langle\mathcal{J}^t\rangle = -\frac{1}{g^2 L}\phi_1^B\,, \tag{3.67}$$

The conjugate momentum to $g_{\mu\nu}$, i.e. the boundary energy-momentum tensor, is more intricate to compute. First let us remind ourselves that since we are in asymptotically AdS space the metric and its fluctuations behave as (for the boundary at infinity and $\mu\,,\nu \neq r$)

$$g_{\mu\nu} = \frac{r^2}{L^2} g^{(0)}_{\mu\nu}(r)\,, \tag{3.68}$$

with $g^{(0)}_{\mu\nu}(r\to\infty) = (g_{\mu\nu})^B_0$. Thus following (3.62) we obtain

$$\langle T^{\mu\nu}\rangle = \frac{S_L[g_0^B]}{\delta\left(g_{\mu\nu}\right)^B_0} = \lim_{r\to\infty}\frac{S_L[g_0^B]}{\delta g^{(0)}_{\mu\nu}} = \lim_{r_B\to\infty}\left(\frac{r_B}{L}\right)^2\sqrt{-\gamma}\frac{1}{\sqrt{-\gamma}}\frac{S_L[g_0^B]}{\delta\gamma_{\mu\nu}}\,, \tag{3.69}$$

where $\gamma_{\mu\nu}$ is the induced metric on the boundary, i.e. $\gamma_{\mu\nu} = g_{\mu\nu}|_{r_B} = (r_B^2/L^2)g^{(0)}_{\mu\nu}(r_B)$ and $S_L[g_0^B]$ is the on-shell action. In principle r_B could be any constant r-slice

[14] We denote by $\mathcal{J}$ and $\mathcal{T}$ the equilibrium expectation values only, while J and T include the equilibrium values plus fluctuations.

[15] In the unbroken phase introduced before, the AdS Reissner-Nordström case in D = 3, we obtain for the background current

$$\langle\mathcal{J}^t\rangle = \frac{r_H}{g^2L^2}\mu\,, \tag{3.66}$$

in perfect agreement with eq. (2.57) (using $z = L^2/r$).

of the foliated asymptotically AdS space, to stress this point we use r_B instead of r here. Furthermore we used that $\delta\gamma_{\mu\nu}/\delta g^{(0)}_{\mu\nu}(r_B) = (r_B^2/L^2)$. The reason for rewriting this expression is to use a well-known result from Brown and York [85] together with the appropriate counter terms (cf. [86,87] and the discussion in the next chapter) to obtain the field theory energy-momentum tensor

$$\langle T^{\mu\nu}\rangle = \frac{1}{\kappa^2}\lim_{r\to\infty}\left(\frac{r}{L}\right)^2\sqrt{-\gamma}\left(K^{\mu\nu} - \gamma^{\mu\nu}K + \frac{\mathrm{D}-1}{L}\right), \tag{3.70}$$

where the extrinsic curvature K_{AB} is defined as

$$K_{AB} = -\frac{1}{2}P_A{}^C P_B{}^D\left(\nabla_C n_D + \nabla_D n_C\right), \tag{3.71}$$

with the outward-point normal vector and the projector being

$$n_A dx^A = \sqrt{g_{rr}}\mathrm{d}r \quad \text{and} \quad P_{AB} = g_{AB} - n_A n_B\,, \tag{3.72}$$

respectively. The induced metric $\gamma_{\mu\nu}$ and the extrinsic curvature tensor $K_{\mu\nu}$ on the boundary are the pull-back of P_{AB} and K_{AB}, respectively. In the coordinates we use through out this thesis this is always equivalent to $\gamma_{\mu\nu} \equiv P_{\mu\nu}$ and $K_{\mu\nu} \equiv K_{AB}$, with A, $B \neq r$.

Note that more counterterms have to be added to the equation above, depending on the background metric and the fluctuations considered. In addition, it is important to remark that in the way $\langle T^{\mu\nu}\rangle$ and $\langle J^\mu\rangle$ are defined we could in principle compute it on every r-slice r_B and not only at the AdS boundary, i.e. for $r_B \to \infty$. For instance, we could compute the flow of these operators along the r-direction. However, a word of caution is in order. The counterterms, which in the case of $T^{\mu\nu}$ is $(\mathrm{D}-1)/L$ are only valid at the AdS boundary. To compute the correct r flow we would need to compute the corresponding "flow" of the counterterms, which is very challenging and to the author's knowledge has not been done so far. The methods used in [87] to derive the counterterms only work at the AdS boundary, since one of the central points is to rewrite the metric in terms of Fefferman-Graham coordinates, which in full generality is only possible close to the AdS boundary.

For the s-wave superfluid background solution, using the boundary expansion (3.38), we obtain[16]

$$\begin{aligned}\langle \mathcal{T}^{tt}\rangle &= -\frac{1}{\kappa^2 L}N_1^B \text{ and}\\ \langle \mathcal{T}^{xx}\rangle = \langle \mathcal{T}^{yy}\rangle &= -\frac{1}{2\kappa^2 L}N_1^B\,,\end{aligned} \tag{3.74}$$

[16] In the unbroken phase introduced before, the AdS Reissner-Nordström case in D = 3, we obtain for the background energy-momentum tensor

$$\langle \mathcal{T}^{tt}\rangle = \frac{\mu^2 r_H}{2g^2L^2} + \frac{r_H^3}{\kappa^2 L^4} \quad \text{and} \quad \langle \mathcal{T}^{xx}\rangle = \langle \mathcal{T}^{yy}\rangle = \frac{\mu^2 r_H}{4g^2L^2} + \frac{r_H^3}{2\kappa^2 L^4}\,. \tag{3.73}$$

where either ψ_1^B or ψ_2^B was set to zero. For the case of $\psi_1^B \neq 0$ additional counterterms have to be added (cf. [57]). It is interesting that even in the broken phase the energy-momentum tensor is still traceless, i.e. $-\langle \mathcal{T}^{tt} \rangle + \langle \mathcal{T}^{xx} \rangle + \langle \mathcal{T}^{yy} \rangle = 0$, implying that the dual theory is still conformal (cf. section 2.1.2).

Now we add the fluctuations to this background. In addition we explain the relation between the boundary conditions at the horizon and the Green's functions. We look at the perturbations $\delta A_x(k_\mu, r)$ and $\delta g_{tx}(k_\mu, r)$. The linearised equations of motion for this fields are

$$\begin{aligned} &\delta A_x'' + \left(\frac{N'}{N} - \frac{\chi'}{2}\right)\delta A_x' + \left(-\frac{2g^2q^2\psi^2}{N} - \frac{2\kappa^2 e^\chi \phi'^2}{g^2 N} + \frac{\omega^2 e^\chi}{N^2}\right)\delta A_x = 0\,, \\ &4\frac{\kappa^2}{g^2}\phi'\delta A_x + \delta g_{tx}' - \frac{2\delta g_{tx}}{r} = 0\,, \end{aligned} \tag{3.75}$$

where we set $\vec{k} = 0$. At the AdS boundary this fields have the expansion

$$\begin{aligned} \delta A_x(r \to \infty) &= (A_x)_0^B + (A_x)_1^B \frac{L}{r} \text{ and} \\ \delta g_{tx}(r \to \infty) &= \frac{r^2}{L^2}(g_{tx})_0^B + (g_{tx})_1^B \frac{L}{r}\,, \end{aligned} \tag{3.76}$$

where $(g_{tx})_1^B$ actually depends on $(A_x)_0^B$, however, the explicit form is not important. In order to apply the formalism developed above we use $\delta\xi_{tx} = g^{xx}\delta g_{tx}$ instead of δg_{tx}. This way a constant non-normalisable mode is obtained.

To solve the equations (3.75) we still have to fix conditions at the horizon. The expansions of the fields at the horizon are

$$\begin{aligned} \delta A_x(r \to r_H) &= \left(\frac{r}{r_H} - 1\right)^{-\mathrm{i}\frac{\omega}{4\pi T}} \sum_{j=0}^{n} (A_x)_j^H \left(\frac{r}{r_H} - 1\right)^j \text{ and} \\ \delta\xi_{tx}(r \to r_H) &= \left(\frac{r}{r_H} - 1\right)^{-\mathrm{i}\frac{\omega}{4\pi T}} \sum_{j=0}^{n} (\xi_{tx})_j^H \left(\frac{r}{r_H} - 1\right)^j\,, \end{aligned} \tag{3.77}$$

where we used $\delta\xi_{tx}$ instead of g_{tx}, while T denotes the Hawking temperature. The only independent parameter is $(A_x)_0^H$ which can be set to 1. Note that in principle there is a second expansion to the equations (3.75) with a prefactor $(r/r_H - 1)^{\mathrm{i}\omega/(4\pi T)}$. However, we set all the corresponding expansion coefficients to zero since this solution corresponds to outgoing boundary conditions at the black hole horizon, i.e. the black hole would emit information. The condition with the minus sign, which we choose, corresponds to ingoing boundary condition at the black hole horizon, i.e. information can only fall into the black hole. This is equivalent to the dissipation of energy, opposed to the generation of energy. Thus the choice of boundary conditions at the horizon sets half of the free parameters to zero. In addition it fixes the kind of field theory Green's function, since the

ingoing condition leads to the retarded Green's function while the outgoing condition results in the advanced Green's function (cf. [69, 88, 89]).

Next we compute the Green's functions associated with the fluctuations δA_x and $\delta\xi_{tx}$. The corresponding conjugate momenta are

$$\begin{aligned}\Pi_T^{tx}(\omega,r) &= \frac{2r^3}{\kappa^2 L^4}\mathrm{e}^{\frac{\chi}{2}}\left(1-\frac{r}{L\sqrt{N}}\right)\delta\xi_{tx}(\omega,r) - \mathrm{e}^{\frac{\chi}{2}}\frac{r^2\phi'}{g^2L^2}\delta A_x(\omega,r)\\ \Pi_J^{x}(\omega,r) &= -\frac{\mathrm{e}^{-\frac{\chi}{2}}N}{g^2}\delta A_x'(\omega,r) - \mathrm{e}^{\frac{\chi}{2}}\frac{r^2\phi'}{g^2L^2}\delta\xi_{tx}(\omega,r)\,,\end{aligned} \tag{3.78}$$

where we set again $\vec{k}=0$ and prime denotes ∂_r. Therefore the field theory operators are

$$\begin{aligned}\langle T^{tx}\rangle(\omega) &= -\langle\mathcal{T}^{tt}\rangle\,(\xi_{tx})_0^B\,(\omega) - \langle\mathcal{J}^t\rangle\,(A_x)_0^B\,(\omega) \text{ and}\\ \langle J^x\rangle(\omega) &= \frac{1}{L^2g^2}\,(A_x)_1^B\,(\omega) - \langle\mathcal{J}^t\rangle\,(\xi_{tx})_0^B\,(\omega)\,,\end{aligned} \tag{3.79}$$

where besides the background expansion (3.38) we also used (3.76). Comparing this results with equation (3.63) enables us to write down the Green's function matrix for these fluctuations

$$\begin{pmatrix}\langle J^x\rangle(\omega)\\ \langle T^{tx}\rangle(\omega)\end{pmatrix} = \begin{pmatrix}\frac{1}{L^2g^2}\frac{(A_x)_1^B(\omega)}{(A_x)_0^B(\omega)} & -\langle\mathcal{J}^t\rangle\\ -\langle\mathcal{J}^t\rangle & -\langle\mathcal{T}^{tt}\rangle\end{pmatrix}\begin{pmatrix}(A_x)_0^B\,(\omega)\\ (\xi_{tx})_0^B\,(\omega)\end{pmatrix}. \tag{3.80}$$

Note that $(A_x)_1^B\,(\omega)$ can only depend linearly on $(A_x)_0^B\,(\omega)$. This comes from the fact that ingoing boundary conditions were chosen at the horizon by which one of the free parameters of a linear second order differential equation was set to zero. Thus $(A_x)_0^B\,(\omega)$, the only free parameter left, is an overall factor of the solution, which can be scaled out.

Finally, we make contact to the dual field theory by comparing this results to our findings in section 3.2.3. By identifying δA_x in section 3.2.3 with $(A_x)_0^B$ above and similarly δg_{tx} with $(\xi_{tx})_0^B$ [17], we are able to compute the transport coefficients (3.59) holographically, i.e.

$$\begin{aligned}\sigma(\omega) &= -\frac{\mathrm{i}}{\omega}\frac{1}{L^2g^2}\frac{(A_x)_1^B\,(\omega)}{(A_x)_0^B\,(\omega)}\,,\\ T\alpha(\omega) &= \frac{\mathrm{i}}{\omega}\langle\mathcal{J}^t\rangle - \mu\sigma(\omega) \text{ and}\\ T\bar{\kappa}(\omega) &= \frac{\mathrm{i}}{\omega}\left(\langle\mathcal{T}^{tt}\rangle + \langle\mathcal{T}^{xx}\rangle - 2\mu\langle\mathcal{J}^t\rangle\right) + \mu^2\sigma(\omega)\,.\end{aligned} \tag{3.81}$$

[17] Since $\delta g_{tx} = (r/L)^2\delta\xi_{tx}$ we can identify $\delta\xi_{tx}$ with $g_{tx}^{(0)}$ in eq. (3.69).

One term was added by hand, namely $\langle \mathcal{T}^{xx} \rangle$ in the last equation, which is a contact term originating from the fluctuation of the projector $P^{\mu\nu}$ in equation (3.41)[18].

Now we can integrate equation (3.75) using for instance *Mathematica* and read off the boundary expansions (3.76) to compute $\sigma(\omega)$. In figure 3.3, taken from [55], the real part of the conductivity is plotted with respect to the reduced frequency $\omega/\langle \mathcal{O}_i \rangle$. There are a few points which are noteworthy. At zero frequency there is a delta peak which arises in part from the superconducting behaviour[19], then there is a gap for frequencies lower than a certain value ω_g. ω_g divided by the temperature is roughly of the order 8 which is a value close to the findings in high-T_c superconductors. Thus, there is hope that maybe holography can model this kind of superconductors. However, note that the gap here is not a real gap, since in the $T \to 0$ limit the real conductivity does not vanish [90]. Therefore the analogy does not entirely hold. This is opposed to the case for the p-wave (see next chapter). For large frequencies the asymptotic behaviour agrees with the expectation value of a conformal field theory in 3 dimensions (see section 4.2.7.1 for more comments on this fact). Finally note that the superconductors from holography are weakly gauged superconductor, thus the Meissner Effect cannot be derived directly. However, it is seen indirectly from the currents it induces in the superconducting material (cf. [90]).

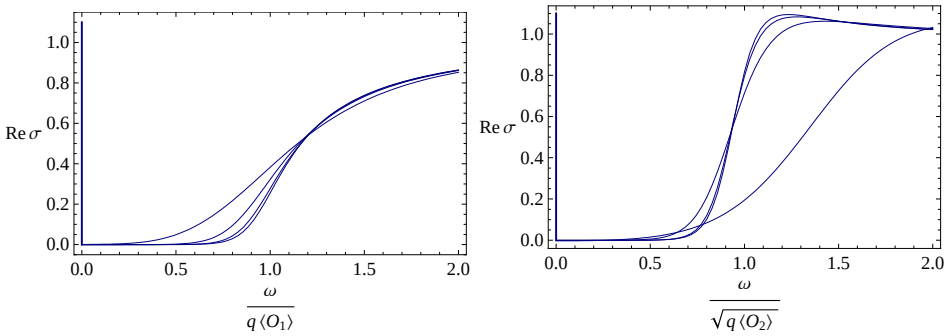

Figure 3.3: Real part of the conductivity for both condensates as a function of reduced frequency for different values of q. Note that both solutions show the typical frequency gap. Source: [55]

[18] To first order in fluctuations $P^{\mu\nu} = g^{\mu\nu} - \delta g^{\mu\nu} + u^\mu u^\nu$, where we used that the inverse of $\hat{g}_{\mu\nu} = g_{\mu\nu} + \delta g_{\mu\nu}$ is $\hat{g}^{\mu\nu} = g^{\mu\nu} - \delta g^{\mu\nu}$. This insures that we obtain $\hat{g}^{\mu\lambda}\hat{g}_{\lambda\nu} = \delta^\mu{}_\nu + \mathcal{O}(\delta^2)$.

[19] There is a second contribution to the delta peak originating from the momentum conservation in this system, we comment more on that in section 4.2.7.1.

Chapter 4

The Holographic p-wave Superfluid

In this chapter we discuss a generalisation of the holographic s-wave superconductor, namely the holographic p-wave superconductor[1]. In this model, apart from the $U(1)$ also the $SO(3)$ rotational symmetry is broken spontaneously.

The search for anisotropic and/or inhomogeneous solutions in the context of gauge/gravity duality recently gained a lot of attention [60,61,91], since condensed matter systems are generically governed by an underlying lattice, e.g. high-T_c superconductors [92]. The system discussed in this chapter is probably the simplest implementation of anisotropy. Due to its relative simplicity, it is technically feasible to study many different aspects of the model, for instance hydrodynamic effects, i.e. low energy excitations about the thermodynamic equilibrium. In this thesis we concentrate on these properties of the holographic p-wave superconductor.

We find that, due to the broken symmetries, many interesting transport effects which are known from crystals and other condensed matter systems, can be modelled. The most remarkable result observed in holographic models relates to the universal behaviour[2] of the ratio between shear viscosity and entropy density $\eta/s = 1/(4\pi)$ at strong coupling. The value was first computed in [42][3]. By now it is known to be a generic result in field theories with a dual isotropic two derivative Einstein gravity description. In section 4.2.7.5 we show that by breaking the rotational invariance a temperature dependent ratio is obtained. This is

[1] As stated before in the holographic context we use superfluid and superconductor interchangeably.

[2] Universal quantities, i.e. quantities which are dimensionless and independent of the number of colours, allow for a comparison between results from gauge/gravity duality and experiment. Note that in nature the number of colours is usually small.

[3] For a supersymmetric generalisation of η/s see [93].

the first example of a deviation from universality at leading order in $1/N$ and $1/\lambda$, where λ is the 't Hooft coupling (cf. [1, 2]).

Besides η/s, we find two distinct electrical conductivities (see sections 4.2.7.1 and 4.2.7.2). Whereas the conductivity perpendicular to the symmetry breaking vector condensate behaves as expected, the other direction displays interesting features: Apart from the expected gap for small frequencies and the correct large frequency limit, we observe a broad peak at very small frequencies, which resembles a Drude behaviour. Normally, to obtain the latter the translational symmetry has to be broken. Interestingly, our solution does not implement this in an obvious way.

Finally, the coupling between energy-momentum tensor and different currents which are present in the setup, resemble three effects known as thermoelectric, flexoelectric and piezoelectric effect. The first one has been observed before in the context of gauge/gravity duality and it describes the coupling between heat and charge transport. The other two effects were first seen in [2, 3] (cf. sections 4.2.7.5 and 4.2.7.6). The flexoelectric effect relates the polarisation of a liquid crystal to mechanical bending, while the piezoelectric effect generates a current through mechanical squeezing.

This chapter is structured as follows: first we introduce the holographic p-wave superfluid and discuss the thermodynamic properties (section 4.1), followed by a discussion about the fluctuations on top of this solution (section 4.2). In the latter section we first present the technical aspects of the calculations (see sections 4.2.1 to 4.2.6) followed by the physical interpretation of the results (section 4.2.7). This chapter is based on the author's publications [1–3].

4.1 Holographic Setup and Equilibrium

The starting point to generated the holographic p-wave superfluid is a $SU(2)$ Einstein-Yang-Mills theory in $(4+1)$-dimensional asymptotically AdS space. Taking the full backreaction of the gauge field on the geometry into account, this system was first described in [50], while the probe limit was discussed in [47]. The action is given by

$$S_L^{\text{pwave}} = \int \mathrm{d}^5x\,\sqrt{-g}\,\left[\frac{1}{2\kappa^2}\,(R-\Lambda) - \frac{1}{4g^2}\,F^a_{AB}F^{aAB}\right] + S_{\text{bdy}}\,, \tag{4.1}$$

where we use the same conventions as in the chapters before, while here, g denotes the $SU(2)$ Yang-Mills coupling constant. The boundary terms S_{bdy} are the same as in section 2.4.1, with $\mathrm{D} = 4$, i.e.

$$S_{\text{bdy}} = -\frac{1}{2\kappa^2}\int_{\partial AdS}\mathrm{d}^4x\sqrt{-\gamma}\left(-2K + \frac{6}{L}\right)\,, \tag{4.2}$$

with K the trace of the extrinsic curvature, defined in eq. (3.71), and γ the induced metric on the AdS boundary (cf. equation (3.72) and below). The $SU(2)$ field strength F^a_{AB} is given by

$$F^a_{AB} = \partial_A A^a_B - \partial_B A^a_A + \epsilon^{abc} A^B_A A^c_B \,, \tag{4.3}$$

where ϵ^{abc} is the totally antisymmetric tensor with $\epsilon^{123} = +1$. The A^a_A are the components of the gauge field, $A = A^a_A \tau^a \mathrm{d}x^A$, where τ^a are the $SU(2)$ generators, related to the Pauli matrices by $\tau^a = \sigma^a/2\mathrm{i}$. Moreover, it is also convenient to define

$$\alpha \equiv \frac{\kappa}{g} \,, \tag{4.4}$$

which determines how strongly the vector fields influence the AdS_5 geometry. Note that α is a free parameter of the theory, since the model discussed here is not a top-down model. That is, the 5 dimensional theory is not embedded into a 10 dimensional superstring theory. Embedding the theory would fix most of the free parameters (cf. for instance [94] for the AdSRN an s-wave case and [48,49] for the probe p-wave model with two D7-branes). In this chapter we rather work in the bottom-up approach, whereby allowing for a free choice of the field content and of some of the parameters in the system. The prize we pay for this simplification is with an uncertainty about the field content of the dual theory. This makes it harder to understand and interpret the results obtained. Nevertheless, by symmetry arguments and by analogy to the D7-brane system, we are able to identify most of the results from a field theoretic point of view.

The resulting Einstein and Yang-Mills equations from the action above are

$$R_{AB} + \frac{4}{L^2} g_{AB} = \left(T_{AB} - \frac{1}{3} T_C{}^C g_{AB} \right) \,, \tag{4.5}$$

$$\nabla_A F^{aAB} = -\epsilon^{abc} A^B_A F^{cAB} \,, \tag{4.6}$$

where the Yang-Mills stress-energy tensor T_{AB} is

$$T_{AB} = \alpha^2 \left(F^a_{CA} F^{aC}{}_B - \frac{1}{4} g_{AB} F^a_{CD} F^{aCD} \right) \,. \tag{4.7}$$

Note that we pulled the gravitational constant κ into the definition of the energy momentum tensor. We stick to this unusual choice since the results are characterised in terms of different values of α.

Next we examine a solution to these equations, which break some of the symmetries of this system. Moreover, we find that for certain choices of boundary conditions the AdSRN solution is recovered (cf. section 2.4.2).

4.1.1 Hairy Black Hole Solution

In this section we search for a solution to the equations of motion (4.5) and (4.6) which breaks some of the gauge and rotational symmetries, under which the action 4.1 is invariant. A priori the action does not change under $SU(2)$ gauge transformations and the diffeomorphisms of AdS_5. This translates into a dual field theory, which is invariant under the full conformal symmetry in 4 dimensional Minkowski space and under a global $SU(2)$ (flavour) symmetry (see discussions in chapters 2 and 3). However, since we want a dual field theory at finite temperature and finite charge density, i.e. with a global $U(1)$ symmetry[4], gravity solutions with a black hole and a non-trivial gauge field profile are considered. In analogy to the AdS Reissner-Nordström case the time component of one of the gauge fields is chosen to have a profile in the radial AdS direction, where we are free to choose which of the flavour directions to take. Our choice is the 3 direction, thus $A_t^3 = A_t^3(r)$. This solution explicitly breaks the $SU(2)$ invariance to a $U(1)$ gauge symmetry. Apart from that, the black hole solution is still invariant under the full $SO(3)$ rotational symmetry in the x, y, z directions. This solution correspond exactly to the AdS Reissner-Nordström black hole (see below). Next we go one step further and break some of the remaining symmetries. Remember the discussion about the stability of the AdSRN in section 3.2, the same applies here. While in that section the condensation of a scalar field was considered (holographic s-wave superconductor), which led to a new stable solution with a spontaneously broken $U(1)$ symmetry. Here we examine the next simpler possibility, namely the condensation of a vector field (cf. [47]). This not only breaks the $U(1)$ symmetry, but the rotational invariance as well. We will see that the breaking of the $SO(3)$ leads to very interesting effects, especially when considering fluctuations about the thermal equilibrium. That is, when computing hydrodynamic transport properties of this solution.

The solutions of interest here are called hairy black hole solutions. The corresponding gauge field ansatz is (c.f. [47, 50])

$$A = \phi(r)\tau^3 \mathrm{d}t + w(r)\tau^1 \mathrm{d}x\,, \tag{4.8}$$

where we denote r to be the radial AdS direction. The vector condensate $w(r)$ is known as the vector hair of the AdS black hole. This ansatz guarantees that by setting $w(r) \equiv 0$ the well-known AdS Reissner-Nordström solution is recovered (see section 2.4.2 and the discussion below).

The dual operator to $A_t^3(r) = \phi(r)$ is the charge density $\langle \mathcal{J}_t^3 \rangle$, which is the only non-vanishing component of the $U(1)$ charge current $\langle \mathcal{J}_\mu^3 \rangle$ in the dual field theory.

[4]The charge density is the time component of a conserved current, which, following Noether's theorem, is related to a continuous symmetry [77].

With a non-vanishing $A^1_x(r) = w(r)$ component, a dual operator $\langle \mathcal{J}^1_x \rangle$ is generated, which, as stated above, not only breaks the $U(1)$ symmetry but also the $SO(3)$ rotational symmetry. Thus a $SO(2)$ rotational symmetry around the x-axis and a $\mathbb{Z}_2$ parity symmetry $P_{\|}$: $x \to -x$ and $w \to -w$ is left. Throughout this chapter we call the x-axis the preferred direction. Finally we want the $U(1)$ and rotational symmetry to be broken spontaneously in the dual field theory. Thus a solution with non-trivial $w(r) \neq 0$ in the bulk and the boundary condition $w(r \to \partial\text{AdS}) = 0$ is chosen (cf. discussions in section 3.2.2). Therefore the dual operator $\langle \mathcal{J}^1_x \rangle \neq 0$, the vector condensate, gets a expectation value without being sourced explicitly. That is, the symmetries are broken spontaneously and the expectation value is generated dynamically. A consistent ansatz for the metric in agreement with the symmetry discussions above is [50, 95]

$$\mathrm{d}s^2 = -N(r)\sigma(r)^2\mathrm{d}t^2 + \frac{1}{N(r)}\mathrm{d}r^2 + \frac{r^2}{f(r)^4}\mathrm{d}x^2 + r^2 f(r)^2\left(\mathrm{d}y^2 + \mathrm{d}z^2\right), \tag{4.9}$$

with $N(r) = \frac{r^2}{L^2} - \frac{2m(r)}{r^2}$. In the following we denote the position of the horizon as r_H. The AdS boundary is at $r \to \infty$. This choice of coordinates corresponds to (2.13) and the conventions used in chapter 3. Note that this ansatz is consistent with a diagonal bulk energy-momentum tensor (4.7), as it is the case for the choice of gauge fields.

Inserting everything into the Einstein and Yang-Mills equations yields five equations of motion for $m(r)$, $\sigma(r)$, $f(r)$, $\phi(r)$, $w(r)$ and one constraint equation. The dynamical equations can be rewritten as (prime denotes $\frac{\partial}{\partial r}$)

$$\begin{aligned}
m' &= \frac{\alpha^2 r f^4 w^2 \phi^2}{6N\sigma^2} + \frac{\alpha^2 r^3 \phi'^2}{6\sigma^2} + N\left(\frac{r^3 f'^2}{f^2} + \frac{\alpha^2}{6} r f^4 w'^2\right), \\
\sigma' &= \frac{\alpha^2 f^4 w^2 \phi^2}{3rN^2\sigma} + \sigma\left(\frac{2rf'^2}{f^2} + \frac{\alpha^2 f^4 w'^2}{3r}\right), \\
f'' &= -\frac{\alpha^2 f^5 w^2 \phi^2}{3r^2 N^2 \sigma^2} + \frac{\alpha^2 f^5 w'^2}{3r^2} - f'\left(\frac{3}{r} - \frac{f'}{f} + \frac{N'}{N} + \frac{\sigma'}{\sigma}\right), \\
\phi'' &= \frac{f^4 w^2 \phi}{r^2 N} - \phi'\left(\frac{3}{r} - \frac{\sigma'}{\sigma}\right), \\
w'' &= -\frac{w\phi^2}{N^2\sigma^2} - w'\left(\frac{1}{r} + \frac{4f'}{f} + \frac{N'}{N} + \frac{\sigma'}{\sigma}\right).
\end{aligned} \tag{4.10}$$

The equations of motion are invariant under the following four scaling transfor-

mations,

$$
\begin{aligned}
&(I) && \sigma \to \lambda\sigma\,, && \phi \to \lambda\phi, && && \\
&(II) && f \to \lambda f\,, && w \to \lambda^{-2} w, && && \\
&(III) && r \to \lambda r\,, && m \to \lambda^4 m\,, && w \to \lambda w\,, && \phi \to \lambda\phi\,, \\
&(IV) && r \to \lambda r\,, && m \to \lambda^2 m\,, && L \to \lambda L\,, && \phi \to \frac{\phi}{\lambda}\,, \qquad \alpha \to \lambda\alpha\,,
\end{aligned}
$$

where in each case λ is some real positive number. Using (I) and (II) we can set the boundary values of both $\sigma(r)$ and $f(r)$ to one, leading to the usual asymptotically AdS spacetime. With (III) it is possible to set r_H to one. However, we retain r_H as a bookkeeping factor to restore the temperature dependence of the dual operators (cf. discussions in the next section). Finally, later we will use (IV) to set the AdS radius L to one.

As mentioned above the AdSRN is also a solution of this system, namely for

$$
\begin{aligned}
&w(r) = 0\,, \\
&\phi(r) = \mu\left(1 - \frac{r_H^2}{r^2}\right)\,, \\
&\sigma(r) = 1 = f(r) \text{ and} \\
&N(r) = \left(\frac{r^2}{L^2} - \frac{r_H^2}{r^2}\left(\frac{r_H^2}{L^2} + \frac{2\alpha^2\mu^2}{3}\right) + \frac{2\alpha^2\mu^2 r_H^4}{3r^4}\right)\,.
\end{aligned}
\tag{4.11}
$$

Here the same conventions and coordinates are used as in equation (3.30), with D = 4. As before, the value of $A_t^3(r) = \phi(r)$ at the boundary, namely μ, is the $U(1)$ chemical potential in dual field theory.

Unfortunately no analytic solutions are known for $w(r) \neq 0$ therefore we solve the equations (4.10) using numerical methods. Our method of choice is the shooting method. It is suitable for problems with boundary values instead of initial values. That means that there are values at the horizon r_H as well as at the AdS boundary $r_B \gg 1$ which have to be met[5]. The shooting method takes as input a combination of known and guessed values at one of the boundaries, for conciseness we choose it to be at the horizon r_H. Then we integrate to the boundary r_B and compare the integrated results with the known values. If the values coming from numerical integration do not agree with the demanded values at r_B we change slightly the guessed values at the horizon and integrate again. This procedure is repeated until finally the correct values at the AdS boundary are obtained. We automatise this approach by turning the search for the initial values into a root

[5] r_B is the UV cut off of our solution, since it is from a technical point of view not possible to set $r_B = \infty$.

finding problem and implementing, for instance, the well-known Newton's method.

To realise the methods described above the expansions of the functions near the horizon and the AdS boundary have to be known. Furthermore the thermodynamic quantities of this system are expressed in terms of these expansion coefficients.
Near the horizon, we expand every function in powers of $\left(\frac{r}{r_H}-1\right)^i$ with some constant coefficients. The generic structure of the expansions is[6]

$$F(r)\big|_{r\to r_H} \simeq F_0^H + \left(\frac{r}{r_H}-1\right) F_1^H + \left(\frac{r}{r_H}-1\right)^2 F_2^H + \dots , \tag{4.12}$$

with $F \in \{m, \sigma, f, \phi, w\}$. Two of the coefficients are fixed by

$$\begin{aligned} N(r_H) = 0 \;&\Rightarrow m(r_H) = \frac{r_H^4}{2} \;\text{ and} \\ A_t^3(r_H) = \phi(r_H) &= 0\,. \end{aligned} \tag{4.13}$$

The former is due to the definition of a black hole horizon, while the latter takes into account that the gauge field A has to be well defined at the horizon, i.e. $g^{MN}A_M^a A_N^a < \infty$ (see for example discussions in ref. [90, 96]). The equations of motion then impose relations among all the remaining coefficients.

Near the AdS boundary the expansion reads

$$F(r)\big|_{r\to\infty} \simeq F_0^B + F_2^B \frac{r_H^2}{r^2} + F_4^B \frac{r_H^4}{r^4} + \dots , \tag{4.14}$$

again $F \in \{m, \sigma, f, \phi, w\}$ and we set $f(r=\infty) = \sigma(r=\infty) = 1$ and $w(r=\infty) = 0$. The former is due to our demand for asymptotically AdS spacetime[7] and the latter due to the fact that $U(1)$ symmetry of field theory side is supposed to be broken spontaneously. That is, the dual operator $\mathcal{J}^{1x}$ is not to be sourced (see discussion above (4.9)).

A straightforward exercise shows that only five coefficients are independent at the AdS boundary. Consider the equations of motion (4.10), there are two first order differential equations and three second order ones. Hence we get a total of $3\cdot 2 + 2\cdot 1 = 8$ free parameters. Taking the fixed parameters at the boundary into account ($f_0^B = \sigma_0^B = 1$ and $w_0^B = 0$) and plugging the asymptotic expansion (4.14) into the equations of motion (4.10) leaves us with 5 free parameters, which we choose to be the lowest order ones, i.e.

$$\phi_0^B = \mu,\ \phi_2^B,\ f_4^B,\ w_2^B \;\text{ and }\; m_0^B\,. \tag{4.15}$$

[6] From here on we set $L = 1$ by using the scaling symmetries (IV) above.

[7] As stated before, we fix the values at the boundary to 1 by using the scaling transformations (I) and (II).

We take the chemical potential μ as the independent physical parameter of the theory, i.e. every time a different value is chosen for it we obtain a new set of solutions to the equations of motion and therefore a new thermodynamic configuration of the system. Consequently we use the grand canonical ensemble[8] when computing the thermodynamic properties of the system. The four remaining parameters are determined from the solutions of the equations of motion. They are related to dual field theory quantities, namely ϕ_2^B is proportional to the charge density, w_2^B to the condensate, m_0^B to the energy and f_4^B measures the amount of anisotropy at the UV fixed point. However, we will see that the energy-momentum tensor in equilibrium is insensitive to the rotational symmetry breaking and therefore $f_4^B = 0$.

For the expansion at the boundary up to the first two non-vanishing orders, we get

$$\begin{aligned}
m^B &\simeq m_0^B + m_2^B \frac{r_H^2}{r^2}, \quad \text{with} \quad m_2^B = -\frac{\alpha^2(\phi_2^{B\,2} + w_2^{B\,2})r_H^2}{3}, \\
\sigma^B &\simeq 1 + \sigma_6^B \frac{r_H^6}{r^6}, \quad \text{with} \quad \sigma_6^B = -\frac{2}{9}\frac{\alpha^2 w_2^{B\,2}}{r_H^2}, \\
f^B &\simeq 1 + f_4^B \frac{r_H^4}{r^4}, \\
\phi^B &\simeq \mu + \phi_2^B \frac{r_H^2}{r^2}, \\
w^B &\simeq 0 + w_2^B \frac{r_H^2}{r^2} + w_4^B \frac{r_H^4}{r^4}, \quad \text{with} \quad w_4^B = -\frac{1}{8}\frac{\mu^2 w_2^B}{r_H^2}.
\end{aligned} \tag{4.16}$$

The counting at the horizon is slightly more difficult. Again we start with 8 free parameters due to the structure of the equations of motion ($3 \cdot 2 + 2 \cdot 1$). Not taking into account that we are expanding close to the horizon results in ϕ_0^H, ϕ_1^H, m_0^H, m_1^H, f_0^H, f_1^H, σ_0^H and w_0^H as independent parameters. However, since r_H is the horizon, this fixes $m_0^H = r_H^4/2$ ($N(r_H) = 0$) and $\phi_0^H = 0$ for regularity reasons ($g^{AB}A_A A_B$ should be finite at the horizon). Thus, 6 free parameters are left. Note that the horizon r_H is fixed by the remaining expansion coefficients. However, we rather choose r_H to be a free parameter and fix m_1^H instead. Therefore, now r_H, ϕ_1^H, f_0^H, f_1^H, σ_0^H and w_0^H are free. Finally, these choices set $f_1^H = 0$, while ϕ_1^H can be used to scan through different temperatures. Therefore at the horizon there are 5 independent parameters left. They are

$$r_H, \;\; \phi_1^H, \;\; \sigma_0^H, \;\; f_0^H \;\; \text{and} \;\; w_0^H \,. \tag{4.17}$$

To solve the equations (4.10) explicitly using numerical methods we set $r_H = 1$.

[8] In the grand canonical ensemble the chemical potential is fixed (cf. section 2.4.2).

The explicit form of the near-horizon expansions for the different fields are

$$\begin{aligned} m^H &\simeq \frac{r_H^4}{2} + \left(\frac{r}{r_H} - 1\right) m_1^H, \quad \text{with} \quad m_1^H = \frac{\alpha^2 {\phi_1^H}^2}{6{\sigma_0^H}^2} r_H^2 \,, \\ \sigma^H &\simeq \sigma_0^H + \left(\frac{r}{r_H} - 1\right) \sigma_1^H \,, \\ f^H &\simeq f_0^H + \left(\frac{r}{r_H} - 1\right)^2 f_2^H \,, \\ \phi^H &\simeq 0 + \left(\frac{r}{r_H} - 1\right) \phi_1^H + \left(\frac{r}{r_H} - 1\right)^2 \phi_2^H \,, \\ w^H &\simeq w_0^H + \left(\frac{r}{r_H} - 1\right)^2 w_2^H \,. \end{aligned} \tag{4.18}$$

Note that we have not stated explicitly the dependency of the coefficients σ_1^H, f_2^H, ϕ_2^H and w_2^H on the free parameters, since the quantities we present here do not depend on them.

The shooting method relies on finding the correct value for the remaining 4 parameters at the horizon, while setting $r_H = 1$ using (III), for a given $\mu = \mu_0$, so that $f_0^B = \sigma_0^B = 1$ and $w_0^B = 0$ are met at the boundary. Finally, the 4 independent expansion coefficients at the boundary can be read off by fitting the resulting numeric functions to the expansions series (4.16).

4.1.2 Thermodynamics

Next we extract thermodynamic information about the dual field theory (most of the results of this section were already presented in [50]) in the same way done for the AdS Reissner-Nordström solution (cf. section 2.4.2 and section 3.2.4). The relevant quantities are given in terms of the expansion coefficient of the fields at the horizon and at the boundary. For convenience we use the scaling transformation (III) to make the r_H dependence explicitly and render the remaining fields dimensionless. We thus define the dimensionless functions $\tilde{m}(r) \equiv m(r)/r_H^4$, $\tilde{\phi}(r) \equiv \phi(r)/r_H$ and $\tilde{w}(r) \equiv w(r)/r_H$, while $f(r)$ and $\sigma(r)$ are already dimensionless.

We work in the grand canonical ensemble, with fixed chemical potential μ, similar to the case of the AdS Reissner-Nordström solution studied at the end of chapter 2.

The temperature and entropy is obtained from horizon data. The temperature T is given by the Hawking temperature of the black hole,

$$T = \frac{N'(r_H)\sigma(r_H)}{4\pi} = \frac{\sigma_0^H}{12\pi}\left(12 - \alpha^2 \frac{\left(\tilde{\phi}_1^H\right)^2}{{\sigma_0^H}^2}\right) r_H \,, \tag{4.19}$$

where the first equal sign is equivalent to (2.46). Note that (c.f. expansion (4.18))

$$m'(r_H) = \frac{1}{r_H} m_1^H = \frac{\alpha^2 (\phi_1^H)^2}{6(\sigma_0^H)^2} r_H = \frac{\alpha^2 (\tilde{\phi}_1^H)^2}{6(\sigma_0^H)^2} r_H^3 \tag{4.20}$$

was used. In what follows we often convert from r_H to T simply by inverting the equation above.

The entropy S is given by the Bekenstein-Hawking entropy of the black hole,

$$S = \frac{2\pi}{\kappa_5^2} A_H = \frac{2\pi V_3}{\kappa_5^2} r_H^3 = \frac{2\pi^4}{\kappa_5^2} V_3 T^3 \frac{12^3 {\sigma_0^H}^3}{\left(12{\sigma_0^H}^2 - (\tilde{\phi}_1^H)^2 \alpha^2\right)^3}\,, \tag{4.21}$$

where A_H denotes the area of the horizon and $V_3 = \int \mathrm{d}^3 x$ (cf. section 2.4.1).

The next quantity we compute is the grand potential Ω (cf. section 2.4.2), which is the object of interest in the grand canonical ensemble in order to find stable vacua. As before, Ω is identified with T times the on-shell bulk action in Euclidean signature S_E^{pwave} (cf. section 2.4.2), with a compactified Euclidean time direction with period $1/T$. We denote the Euclidean bulk action as S_E^{pwave} and $S_{E,\text{on-shell}}^{\text{pwave}}$ for its on-shell value. Our solution is always static, hence $S_{E,\text{on-shell}}^{\text{pwave}}$ always includes an integration over the time direction, producing a factor of $1/T$. $S_{E,\text{on-shell}}^{\text{pwave}}$ includes a bulk term, a Gibbons-Hawking boundary term and counterterms,

$$S_{E,\text{on-shell}}^{\text{pwave}} = S_{\text{bulk}}^{\text{pwave}} + S_{\text{GH}}^{\text{pwave}} + S_{\text{CT}}^{\text{pwave}}\,. \tag{4.22}$$

$S_{\text{bulk}}^{\text{pwave}}$ and $S_{\text{GH}}^{\text{pwave}}$ exhibit divergences, which are cancelled by the counterterms in $S_{\text{CT}}^{\text{pwave}}$. To regulate these divergencies we introduce an UV cut off $r = r_B$, with r_B large but finite. Ultimately the regulator is removed by taking $r_B \to \infty$.

Plugging the ansatz for the metric and the gauge fields into the action we obtain the explicit on-shell form of the three terms (see also [50])

$$\begin{aligned}
S_{\text{bulk}}^{\text{pwave}} &= \frac{V}{T\kappa_5^2} \frac{1}{2f(r)^2} r N(r)\sigma(r)\partial_r(r^2 f(r)^2)\Big|_{r=r_B}\,,\\
S_{\text{GH}}^{\text{pwave}} &= -\frac{V}{T\kappa_5^2} N(r)\sigma(r) r^3 \left(\frac{N'(r)}{2N(r)} + \frac{\sigma'(r)}{\sigma(r)} + \frac{3}{r}\right)\Big|_{r=r_B}\,,\\
S_{\text{CT}}^{\text{pwave}} &= \frac{3V}{T\kappa_5^2} r^3 \sqrt{N(r)}\sigma(r)\Big|_{r=r_B}\,.
\end{aligned} \tag{4.23}$$

To derive these results the extrinsic curvature and induced metric, defined as in equation (3.71) and below, was used.

Finally, we can use equation (2.48) to determine Ω as

$$\Omega = T S_{E,\text{on-shell}}^{\text{pwave}}\Big|_{r_B\to\infty} = \frac{\pi^4}{\kappa^2} V_3 T^4 \frac{12^4 {\sigma_0^H}^4}{\left(12{\sigma_0^H}^2 - (\tilde{\phi}_1^H)^2 \alpha^2\right)^4} \left(\tilde{m}_0^B + 4 f_4^B\right)\,, \tag{4.24}$$

where again the result is expressed in terms of expansion coefficients of the functions defined at the end of last section.

To compute the charge density $\langle \mathcal{J}^{3t} \rangle$ and the condensate $\langle \mathcal{J}^{1x} \rangle$ we take the same approach as developed in section 3.2.4, generalised to non-Abelian gauge fields. We obtain

$$\langle J^{a\mu} \rangle = \lim_{r_B \to \infty} \frac{\delta S^{\text{pwave}}_{L,\text{on-shell}}}{\delta \partial_r A^a_\mu} = \lim_{r \to \infty} -\frac{1}{g^2} \sqrt{-g} F^{a\, r\mu} \tag{4.25}$$

Using the AdS boundary expansions (4.16), the charge density and the condensate read

$$\begin{aligned} \langle \mathcal{J}^{3t} \rangle &= -\frac{2}{g^2} \phi_2^B r_H^2 = -\frac{2\pi^3}{g^2} T^3 \frac{12^3 {\sigma_0^H}^3}{\left(12 {\sigma_0^H}^2 - \left(\tilde{\phi}_1^H\right)^2 \alpha^2\right)^3} \tilde{\phi}_2^B \quad \text{and} \\ \langle \mathcal{J}^{1x} \rangle &= \frac{2}{g^2} w_2^B r_H^2 = \frac{2\pi^3}{g^2} T^3 \frac{12^3 {\sigma_0^H}^3}{\left(12 {\sigma_0^H}^2 - \left(\tilde{\phi}_1^H\right)^2 \alpha^2\right)^3} \tilde{w}_2^B \,, \end{aligned} \tag{4.26}$$

respectively.

The expectation value of the stress-energy tensor of the CFT is derived in section 3.2.4. We rewrite it here with the spacetime indices down,

$$\begin{aligned} \langle T_{\mu\nu} \rangle &= \lim_{r_B \to \infty} \frac{\sqrt{-\gamma}}{r_B^2} \frac{1}{\sqrt{-\gamma}} \frac{\delta S^{\text{pwave}}_{L,\text{on-shell}}}{\delta \gamma^{\mu\nu}} = \\ &= \lim_{r_B \to \infty} \left[\frac{1}{\kappa_5^2} \frac{\sqrt{-\gamma}}{r_B^2} \left(K_{\mu\nu} - K^\rho{}_\rho \gamma_{\mu\nu} + 3\, \gamma_{\mu\nu} \right) \right] , \end{aligned} \tag{4.27}$$

where the extrinsic curvature is defined in (3.71). Note that contrary to the result in section 3.2.4, here we divide by a factor of r^2, since the differentiation is with respect to $\delta\gamma^{\mu\nu}$ and not $\delta\gamma_{\mu\nu}$. The non-trivial components of the energy-momentum are

$$\begin{aligned} \langle \mathcal{T}_{tt} \rangle &= 3 \frac{r_H^4}{\kappa^2} \tilde{m}_0^B = 3 \frac{\pi^4}{\kappa^2} T^4 \frac{12^4 {\sigma_0^H}^4}{\left(12 {\sigma_0^H}^2 - \left(\tilde{\phi}_1^H\right)^2 \alpha^2\right)^4} \tilde{m}_0^B \,, \\ \langle \mathcal{T}_{xx} \rangle &= \frac{r_H^4}{\kappa^2} \left(\tilde{m}_0^B - 8 f_4^B \right) = \\ &= \frac{\pi^4}{\kappa^2} T^4 \frac{12^4 {\sigma_0^H}^4}{\left(12 {\sigma_0^H}^2 - \left(\tilde{\phi}_1^H\right)^2 \alpha^2\right)^4} \left(\tilde{m}_0^B - 8 f_4^B \right) , \\ \langle \mathcal{T}_{yy} \rangle = \langle \mathcal{T}_{zz} \rangle &= \frac{r_H^4}{\kappa^2} \left(\tilde{m}_0^B + 4 f_4^B \right) = \\ &= \frac{\pi^4}{\kappa^2} T^4 \frac{12^4 {\sigma_0^H}^4}{\left(12 {\sigma_0^H}^2 - \left(\tilde{\phi}_1^H\right)^2 \alpha^2\right)^4} \left(\tilde{m}_0^B + 4 f_4^B \right) . \end{aligned} \tag{4.28}$$

All the other components vanish identically, i.e. the net momentum of the fluid is zero. This result is guaranteed by our ansatz for the gauge field which implies a

diagonal Yang-Mills stress-energy tensor and a diagonal metric.

Since the dual field theory is supposed to describes a conformal[9] fluid, the energy-momentum tensor is expected to be traceless. This is easily checked by plugging the above quantities into the equation $\langle \mathcal{T}_{tt} \rangle = \langle \mathcal{T}_{xx} \rangle + \langle \mathcal{T}_{yy} \rangle + \langle \mathcal{T}_{zz} \rangle$. Therefore the broken solution is still conformal and the only physical parameter in the dual field theory is the ratio μ/T.

For $\tilde{m}_0^B = \frac{1}{2} + \frac{\alpha^2 \tilde{\mu}^2}{3}$, $\sigma_0^h = 1$, $\tilde{\phi}_1^h = 2\tilde{\mu}$, $f_2^B = 0$, and $\tilde{\phi}_1^B = -\tilde{\mu}$ the correct thermodynamic properties of the Reissner-Nordström black hole are recovered (see results in section 3.2.4).

For solutions with nonzero $\langle \mathcal{J}^{1x} \rangle$, the $SO(3)$ rotational symmetry is broken to $SO(2)$. From the results presented above, eq. (4.28), we may expect that $\langle \mathcal{T}_{xx} \rangle \neq \langle \mathcal{T}_{yy} \rangle = \langle \mathcal{T}_{zz} \rangle$. However, it turns out that the numerical solution is consistent with $f_4^B = 0$, also in the broken case. Furthermore analytic double expansions in small values of the condensate and α^2 confirmed this result[10]. In addition the authors of [97] showed that generic stationary black hole solutions (possibly breaking rotational or translational symmetries) with gravity coupled to a $U(1)$ gauge field in asymptotically AdS spacetime have an isotropic dual energy-momentum-tensor in the UV. However, in the next sections it will become apparent that at the level of small deviations from the thermal equilibrium the effect of the rotational symmetry breaking becomes important.
In the diagrams 4.1, 4.2 and 4.3 we show the grand canonical potential, the entropy and $\langle \mathcal{J}^{1x} \rangle$, respectively, for two different values of α: $\alpha = 0.316$ and $\alpha = 0.447$. For temperatures $T < T_c$ it is evident that there are more than one solution to the equations of motion. Note that T_c is the temperature at which, for $\alpha < \alpha_c = 0.365 \pm 0.001$, $\langle \mathcal{J}^{1x} \rangle \neq 0$, while for $\alpha > \alpha_c$ the situation is more complicated. We discuss this case below. One of the solutions is always the analytically known AdS Reissner-Nordström black hole. The second solution has a non-vanishing vacuum expectation value for the current $\langle \mathcal{J}^{1x} \rangle \neq 0$, i.e. there is a condensate in the system and the $U(1)$ and $SO(3)$ symmetries are broken. For temperatures $T > T_c$ the AdSRN solution describes the thermodynamic equilibrium.

As pointed out in [50] for values of α below $\alpha_c = 0.365 \pm 0.001$ there is a second order phase transition, recognisable by the discontinuity in the first derivative of the entropy at T_c (see fig. 4.2(a)). Moreover, by looking at the grand potential

[9] It is a conformal fluid, since we are analysing a gravity theory in asymptotically AdS, see discussion in section 2.4.

[10] The author is thankful to Ann-Kathrin Straub for pointing this out.

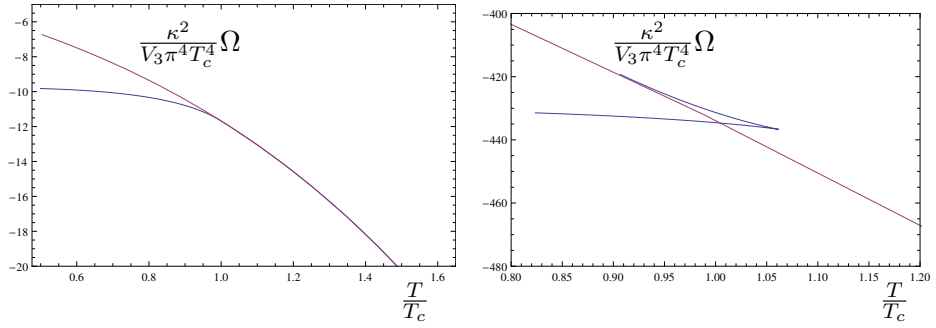

(a) (b)

Figure 4.1: This plot shows the grand potential Ω versus the temperature T for the α values: (a) $\alpha = 0.316 < \alpha_c$ and (b) $\alpha = 0.447 > \alpha_c$. The red line is the solution for a vanishing $\langle J^{1x} \rangle$, the blue line for the solution with a condensate. We see that in figure (a) for $T < T_c$ the solution with non-vanishing condensate is the energetically preferred one. For $T > T_c$ there is only one solution without a condensate, i.e. at $T = T_c$ there is a phase transition. In figure (b) the solution with non vanishing condensate is multi-valued. Nevertheless, the physical state in which the system is in, is above T_c the red line, i.e. the solution without condensate, and only at $T \leq T_c$ the solution with condensate is energetically favourable. Cf. [50]

Ω (see fig. 4.1(a)) it is evident that the solution with $\langle \mathcal{J}^{1x} \rangle \neq 0$ is energetically favourable to the one with vanishing expectation value (see discussions in chapter 3).

For the case $\alpha > \alpha_c$ we see a kink in the grand potential at $T \simeq T_c$ (see fig. 4.1(b)), which is characteristic for first order phase transitions. Note that $\langle \mathcal{J}^{1x} \rangle \neq 0$ also at temperatures above T_c. The reason for that is that we define T_c at the point where the solution with non-vanishing current becomes energetically favourable in comparison to the Reissner-Nordström solution and not at the highest temperature where the solution with condensate is mathematically possible.

The solution with non-vanishing $\langle \mathcal{J}^{1x} \rangle$ dynamically brakes the $U(1)$ symmetry and at the same time leads to a breaking of the $SO(3)$ symmetry to a $SO(2)$ symmetry. Therefore $\langle \mathcal{J}^{1x} \rangle$ can be seen as the order parameter for this phase transition. The critical exponent of this parameter seems to agree with the standard mean field value of $1/2$ (for the second order transition) (see [50] and section 3.2.4).

To interpret these results, we have to keep in mind that there is no net momentum flow. However, $\langle \mathcal{J}^{1x} \rangle$ is a non-vanishing current, i.e. we have a system with a charge flow without mass transport. Such a system can possibly be described by spinorial degrees of freedom fixed to a lattice. In the case of the Reissner-

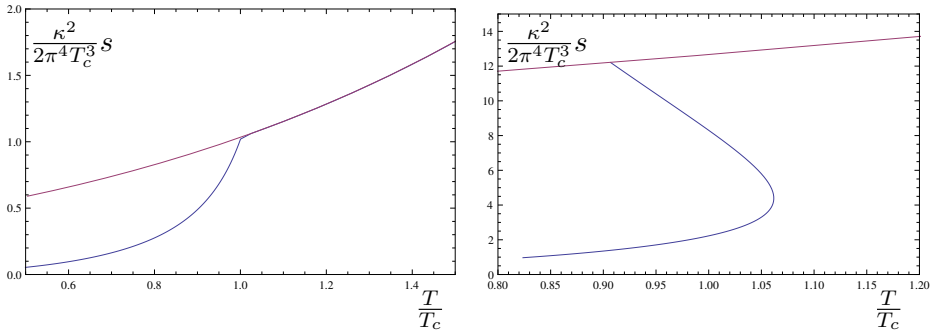

Figure 4.2: This plot shows the entropy S versus the temperature T for the α values: 4.1(a) $\alpha = 0.316 < \alpha_c$ and 4.1(b) $\alpha = 0.447 > \alpha_c$. The red line is the solution for a vanishing $\langle \mathcal{J}^{1x} \rangle$, the blue line for the solution with a condensate. In figure 4.2(a) we see that for the energetically preferred solution, i.e. $\langle \mathcal{J}^{1x} \rangle \neq 0$, the curve at $T = T_c$ is continuous but not differentiable, i.e. for $\alpha < \alpha_c$ we have a second order phase transition. On the other hand, in figure 4.2(b) we see that there is a jump at $T = T_c$ between the energetically preferred solutions, i.e. for $\alpha > \alpha_c$ we have a first order phase transition. Cf. [50]

Nordström solution the spins have no preferred direction. However, in the broken phase they do. Due to fixed position of the spins there is no mass transport and therefore no net momentum transport, i.e. $\langle \mathcal{T}_{ti} \rangle = 0$, with $i \in \{x, y, z\}$. The condensation can be seen as a correlation between the spins, with the correlation length increasing with the decrease of temperature. Alternatively, due to the symmetries in this system there are some similarities to liquid crystals which in the nematic phase also align along one preferred direction [54]. The last interpretation, we present, is motivated by the discussion in the context of a broken phase in D3/D7 systems [48,49]. In this system two probe D7-branes are embedded into $AdS_5 \times S^5$. The resulting DBI action includes an $SU(2)$ Yang-Mills term and a similar condensation process as we see here occurs. However, since this system is a top-down-model the dual field theory is known and in that theory the condensate corresponds to a ρ meson, which condenses. That is $\langle J^{1x} \rangle \propto \bar{u}\gamma^x d + \bar{d}\gamma^x u$, where u and d corresponds to the up- and down-quark spinors, while γ_μ are the gamma matrices.

For a better understanding and interpretation of the results it would be helpful to determine the $T \to 0$ limit of this solution. The $T \to 0$ limit is interesting, since it describes the dual field theory at its IR fixed point. Fixed points are governed by universal behaviours and thus it may be helpful to identify the correct class of systems described here. Note that we expect a stable IR fixed point in our solution, since the entropy density seems to tend to zero for decreasing temperatures (cf. fig. 4.2). However, for small values of the temperature in comparison to the

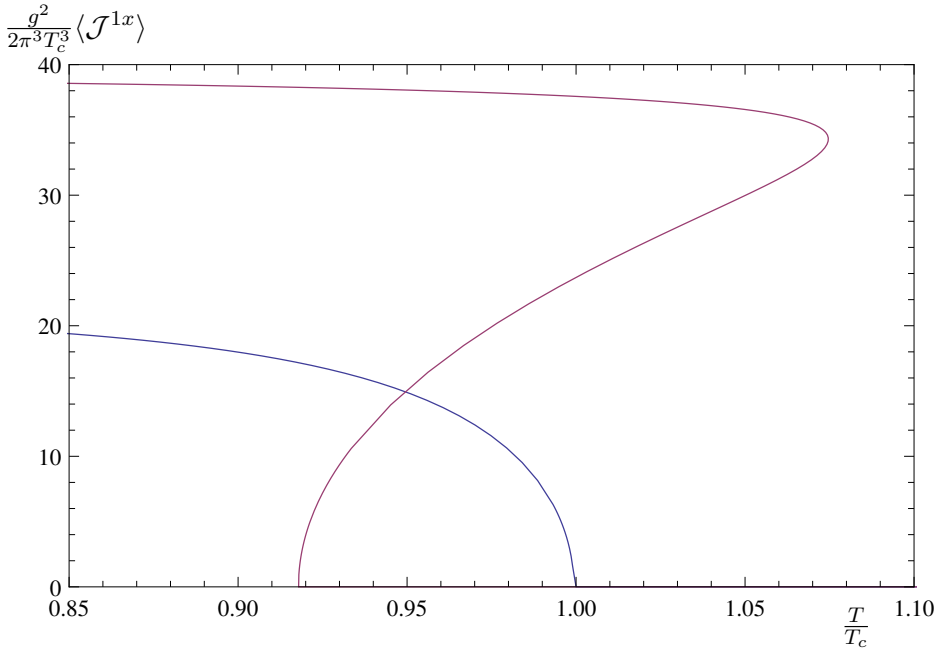

Figure 4.3: This plot shows the condensate $\langle \mathcal{J}^{1x}\rangle$ versus the temperature T for two values of α, namely, the red line is computed for $\alpha = 0.447 > \alpha_c$ and the blue line for $\alpha = 0.316 < \alpha_c$. Furthermore the solution for $\alpha = 0.447$ was scaled with a factor 1/5. $\langle \mathcal{J}^{1x}\rangle$ is the order parameter of the phase transition, for the case $\alpha < \alpha_c$ (blue line) it was shown in [50] that the critical exponent is 1/2. The red line is multi-valued for certain regions of the plot. Bellow T_c it takes the topmost values, jumping down to zero for $T > T_c$, which is a consequence of the first order phase transition. Cf. [50]

chemical potential the solutions obtained by numerical methods become numerically unstable. Nevertheless there is one approach described in [98], where they start at zero temperature and construct a domain wall solution of this setup in the broken phase. However, as described in chapter 5, depending on the parameters one could possibly flow to different IR fixed points. Assuming there are different fixed points, then the authors of [98] would have computed one of them.

To summarise the findings above we present an overview plot in figure 4.5 of the different phases depending on μ/T and α. For $\alpha \leq \alpha_c = 0.365$, the phase transition is second order while for larger values of α the transition becomes first order. The critical temperature decreases as we increase the parameter α. The broken phase is thermodynamically preferred in the blue and red region while in the white region the Reissner-Nordström black hole is favoured. The Reissner-Nordström black hole is unstable in the blue region and the phase transition from the white to the blue region is second order. In the red region, the Reissner-Nordström black hole is still stable, however the state with non-zero condensate is preferred. The transition from the white to the red region is first order. In the green region we cannot trust the numerics. At zero temperature, the data is

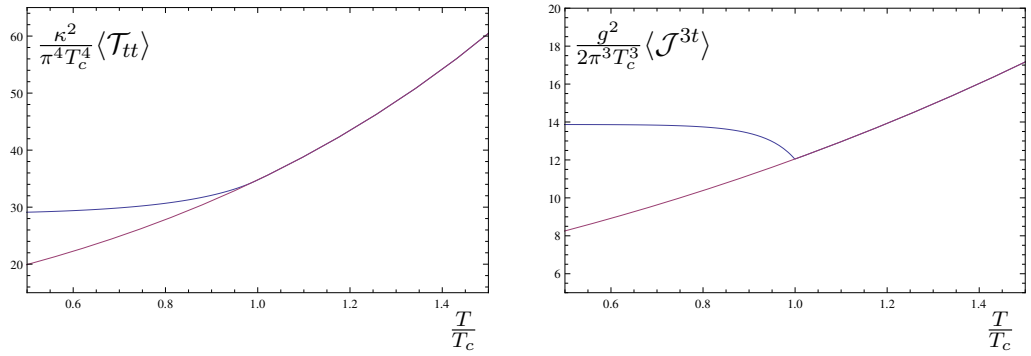

(a) (b)

Figure 4.4: The energy density $\langle \mathcal{T}_{tt}\rangle$ (a) and the charge density $\langle \mathcal{J}^{3t}\rangle$ (b) over the reduced temperature T/T_c for $\alpha = 0.316$. The red line is the solution without a condensate and the blue line the solution with $\langle \mathcal{J}^{1x}\rangle \neq 0$ below T_c. Note that $\langle \mathcal{J}^{3t}\rangle$ describes the total charge in the bulk. Thus, we see that in the broken solution some of the black hole charge is wandering into the bulk. Source: [2]

obtained as described in [98, 99].

4.2 Perturbations about Equilibrium

In this section we study the response of the holographic p-wave superfluid to small perturbations. On the gravity side these perturbations are given by fluctuations of the metric $h_{MN}(x^\mu, r)$ and the gauge field $a^a_M(x^\mu, r)$. Thus we study in total 14 physical modes: 5 from the massless graviton in 5 dimensions and 3×3 from the massless vectors in five dimensions. Due to time and spatial translation invariance in the Minkowski directions, the fluctuations can be decomposed into their Fourier modes

$$\begin{aligned} h_{MN}(x^\mu, r) &= \int \frac{\mathrm{d}^4 k}{(2\pi)^4} \mathrm{e}^{\mathrm{i} k_\mu x^\mu}\, \hat{h}_{MN}(k^\mu, r)\,, \\ a^a_M(x^\mu, r) &= \int \frac{\mathrm{d}^4 k}{(2\pi)^4} \mathrm{e}^{\mathrm{i} k_\mu x^\mu}\, \hat{a}^a_M(k^\mu, r)\,. \end{aligned} \tag{4.29}$$

To simplify notations we drop the hat on the fields in momentum space, which we use from now on if not stated otherwise.

4.2.1 Characterisation of Fluctuations

In general we have to introduce two spatial momenta: one longitudinal to the condensate $k_\parallel$ and one perpendicular to the condensate $k_\perp$, i. e. $k^\mu = (\omega, k_\parallel, k_\perp, 0)$, in order to fully describe the perturbations. Introducing the momentum perpendicular to the condensate breaks the remaining rotational symmetry $SO(2)$ down to the discrete $\mathbb{Z}_2$ parity transformation $P_\perp$: $k_\perp \to -k_\perp$ and $x_\perp \to -x_\perp$. Thus introducing this momentum forbids the usual classification of the fluctuations in

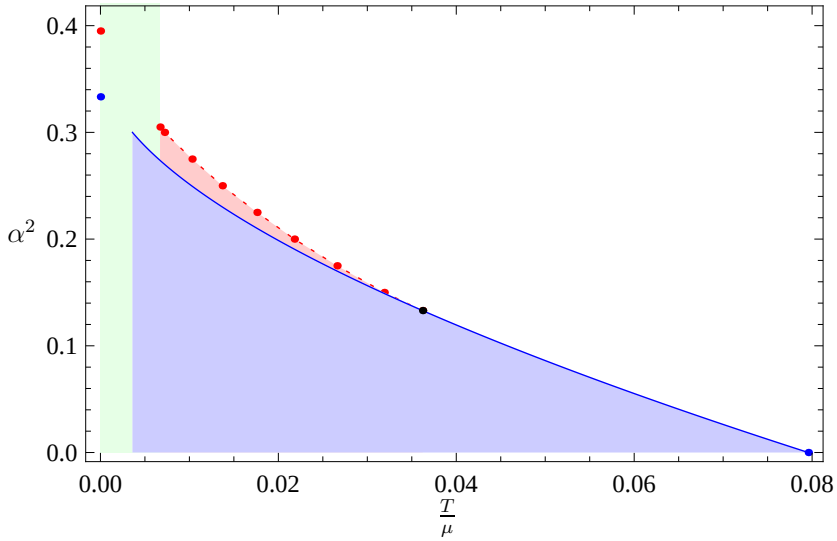

Figure 4.5: The phase structure of the theory: In the blue and red region the broken phase is the thermodynamically preferred phase while in the white region the Reissner-Nordström black hole is the ground state. In the blue region the Reissner-Nordström black hole is unstable and the transition from the white to the blue region is second order. In the red region the Reissner-Nordström black hole is still stable. The transition form the white to the red region is first order. The black dot determines the critical point where the order of the phase transition changes. In the green region we cannot trust the numerics. Source: [2]

different helicity states of the little group, since the symmetry group just consists of discrete groups at best $P_{\parallel} \times P_{\perp}$. We do not study this case further in this thesis. However a momentum exclusively in the direction longitudinal to the condensate or zero spatial momentum preserves the $SO(2)$ rotational symmetry such that we can classify the fluctuations according to their transformation under this $SO(2)$ symmetry (see table 4.1). The modes of different helicity decouple from each other. The momentum longitudinal to the condensate, however, breaks the longitudinal parity invariance $P_{\parallel}$.

4.2.2 Gauge Fixing

To obtain the physical modes of the system we have to fix the gauge freedom. We choose a gauge where $a_r^a \equiv 0$ and $h_{Mr} \equiv 0$. Thus the equations of motion for these fields become constraints. These constraints fix the unphysical fluctuations in each helicity sector and allow only the physical modes to fluctuate. The physical modes are constructed by enforcing invariance under the residual gauge transformations subject to the constraints $\delta a_r^a = 0$ and $\delta h_{Mr} = 0$.

	dynamical fields	constraints	# physical modes
helicity 2	$h_{yz}, h_{yy} - h_{zz}$	none	2
helicity 1	$h_{ty}, h_{xy}; a_y^a$	h_{yr}	4
	$h_{tz}, h_{xz}; a_z^a$	h_{zr}	4
helicity 0	$h_{tt}, h_{xx}, h_{yy} + h_{zz}, h_{xt}; a_t^a, a_x^a$	$h_{tr}, h_{xr}, h_{rr}; a_r^a$	4

Table 4.1: Classifications of the fluctuations according to their transformation under the $SO(2)$ group. The constraints are given by the equations of motion for the fields which are set to zero due the fixing of the gauge freedom: $a_r^a \equiv 0$ and $h_{rM} \equiv 0$. The number of physical modes is obtained by the number of dynamical fields minus the number of constraints. Due to $SO(2)$ invariance the fields in the first and second line of the helicity one fields can be identified. Source: [2]

4.2.2.1 Ansatz

We begin the construction of gauge invariant fields by examining the relevant diffeomorphism and $SU(2)$ gauge transformations of the metric functions and the Yang-Mills fields. Under diffeomorphism the fields transform as

$$\begin{aligned} \mathcal{L}_\Sigma g_{AB} &= \nabla_A \Sigma_B + \nabla_B \Sigma_A = \partial_A \Sigma_B + \partial_B \Sigma_A - 2\Gamma^C_{AB}\Sigma_c \,, \\ \mathcal{L}_\Sigma A^a_A &= \Sigma^C \nabla_C A^a_A + A^a_C \nabla_A \Sigma^C = \Sigma^C \partial_C A^a_A + A^a_C \partial_A \Sigma^C \,, \end{aligned} \tag{4.30}$$

where $\mathcal{L}_\Sigma$ is the Lie derivative along Σ and Γ^C_{AB} are the Christoffel symbol.
The $SU(2)$ transformation only affects the gauge fields, therefore we do not take the metric fluctuations into account. A field in the adjoint $SU(2)$ representation transforms under the $SU(2)$ as

$$\delta_\Lambda a^a_A = \nabla_A \Lambda^a + \epsilon^{abc} A^B_A \Lambda^c \,. \tag{4.31}$$

The combination of these transformation leads to

$$\begin{aligned} \delta g_{AB} &= \partial_A \Sigma_B + \partial_B \Sigma_A - 2\Gamma^C_{AB}\Sigma_c \,, \\ \delta A^a_A &= \Sigma^C \partial_C A^a_A + A^a_C \partial_A \Sigma^C + \nabla_A \Lambda^a + \epsilon^{abc} A^B_A \Lambda^c \,. \end{aligned} \tag{4.32}$$

Hence, in our case, a generic infinitesimal transformation acting on a perturbed solution is given in terms of the 8 parameters $\{\Sigma^M, \Lambda^a\}$.

To compute the transformations of the fluctuations we start by defining

$$\begin{aligned} \hat{g}_{AB} &= g_{AB} + h_{AB} \,, \\ \hat{A}^a_A &= A^a_A + a^a_A \,, \end{aligned} \tag{4.33}$$

where g_{AB} and A^a_A are the background fields of the hairy black hole solution (cf. sec. 4.1.1), which are completely fixed and there is now gauge ambiguity left. The fluctuations h_{MN} and a^a_M are our dynamical fields. Thus, for instance the variation of the fluctuation field defined as $\xi_t = g^{tt} h_{tt}$ is given by

$\delta\xi_t = g^{tt}\delta h_{tt} = g^{tt}\delta\hat{g}_{tt}$. Furthermore, they are of the same order as the parameters Σ^A and Λ^a, i.e. if we expand in powers of perturbations, the infinitesimal generators and the fluctuations are treated equally.

In order to shorten the expressions during the derivation of the physical modes, we rewrite the background metric (4.9) in terms of

$$\begin{aligned} \mathrm{d}s^2 &= g_{MN}\mathrm{d}x^M\mathrm{d}y^N = \\ &= -c_1(r)^2\mathrm{d}t^2 + c_2(r)^2\mathrm{d}x^2 + c_3(r)^2(\mathrm{d}y^2+\mathrm{d}z^2) + c_4(r)^2\mathrm{d}r^2\,, \end{aligned} \tag{4.34}$$

the only non-zero components of the background Yang-Mills field are $A^3_t = \phi(r)$ and $A^1_x = w(r)$. From here on we work in momentum space, i.e.

$$\begin{aligned} \Sigma^M(x^\mu, r) &= \int \frac{\mathrm{d}^4k}{(2\pi)^4}\, \mathrm{e}^{ik_\mu x^\mu}\Sigma^M(k^\mu, r), \\ \Lambda^a(x^\mu, r) &= \int \frac{\mathrm{d}^4k}{(2\pi)^4}\, \mathrm{e}^{ik_\mu x^\mu}\Lambda^a(k^\mu, r), \end{aligned} \tag{4.35}$$

where $k^\mu = (\omega, k_\parallel, 0, 0)$. To make the equations more legible from now on we set $k_\parallel = k$.

Thus the variations of the h_{Mr} components of the metric and the a^a_r components of the Yang-Mills field under an infinitesimal transformation (4.32) acting on a perturbed background solution are, up to first order contributions,

$$\begin{aligned} \delta h_{tr} &= -i\omega {c_4}^2\Sigma^r + {c_1}'\Sigma^t - c_1\partial_r\Sigma^t, \\ \delta h_{xr} &= ik{c_4}^2\Sigma^r + {c_2}^2\partial_r\Sigma^x, \\ \delta h_{yr} &= {c_3}^2\partial_r\Sigma^y, \\ \delta h_{zr} &= {c_3}^2\partial_r\Sigma^z, \\ \delta h_{rr} &= 2c_4\left({c_4}'\Sigma^r + c_4\partial_r\Sigma^r\right), \\ \delta a^1_r &= w\partial_r\Sigma^x + \partial_r\Lambda^1, \\ \delta a^2_r &= \partial_r\Lambda^2, \\ \delta a^3_r &= -\frac{\phi}{c_1}\partial_r\Sigma^t + \partial_r\Lambda^3. \end{aligned}$$

It is easy to convince ourselves that by carefully choosing Σ_A and Λ^a δh_{Mr} and δa^a_r can be set to vanish. The residual gauge freedom corresponds to any further transformation of the form (4.32) that, while keeping the above components null, changes the rest of the dynamical fields. The physical modes on the other hand, which we derive in the next section, are invariant under these transformations.

The solutions to $\delta h_{Mr} = 0$, $\delta a^a_r = 0$ can be written in terms of 8 constants

$\{K_M, \Lambda_0^a\}$ as

$$\begin{aligned}
\Sigma^t(\omega,k,r) &= -K_t c_1 - i\omega K_r c_1 A, \quad \text{with } A = \int \mathrm{d}r \frac{c_4}{{c_1}^2}\,,\\
\Sigma^x(\omega,k,r) &= K_x - ikK_r B, \quad \text{with } B = \int \mathrm{d}r \frac{c_4}{{c_2}^2}\,,\\
\Sigma^y(\omega,k,r) &= K_y\,,\\
\Sigma^z(\omega,k,r) &= K_z\,,\\
\Sigma^r(\omega,k,r) &= \frac{K_r}{c_4}\,,\\
\Lambda^1(\omega,k,r) &= ikK_r C_w + \Lambda_0^1, \quad \text{with } C_w = \int \mathrm{d}r \frac{c_4 w}{{c_2}^2}\\
\Lambda^2(\omega,k,r) &= \Lambda_0^2\\
\Lambda^3(\omega,k,r) &= -K_t\phi - i\omega K_r\left(\phi A - C_\phi\right) + \Lambda_0^3, \quad \text{with } C_\phi = \int \mathrm{d}r \frac{c_4\phi}{{c_1}^2}\,.
\end{aligned} \tag{4.36}$$

Next we build the physical fields out of linear combination of all the remaining fluctuations.

4.2.2.2 The Physical Fields

The helicity two fluctuations, $\Xi = g^{yy}h_{yz}$ and $h_{yy} - h_{zz}$ are already invariant under (4.32), i.e.

$$\begin{aligned}
\delta\Xi &= g^{yy}\delta h_{yz} = 0\,,\\
\delta(h_{yy} - h_{zz}) &= 0\,.
\end{aligned} \tag{4.37}$$

Thus there is nothing left to do in this sector. The helicity one fluctuations transform as

$$\begin{aligned}
\delta h_{xy} &= \mathrm{i}k{c_3}^2 K_y\,,\\
\delta h_{ty} &= -\mathrm{i}\omega{c_3}^2 K_y\,,\\
\delta a_y^a &= 0\,.
\end{aligned} \tag{4.38}$$

Hence the a_y^a are physical, while the invariant combination of the other two gives the physical mode $\Psi = g^{yy}(\omega h_{xy} + k h_{ty})$, where for technical reasons we multiplied with a background metric component (cf. discussion in section 3.2.4). Summarising, we obtain for these modes

$$\begin{aligned}
&\text{helicity two:} \quad \Xi = g^{yy}h_{yz},\ h_{yy} - h_{zz}\,,\\
&\text{helicity one:} \quad \Psi = g^{yy}(\omega h_{xy} + k h_{ty});\ a_y^a\,.
\end{aligned} \tag{4.39}$$

Note that the same applies to the z components, which behave in exactly the same way as the y components, since there is a $SO(2)$ symmetry in the yz-plane.

Next we arrange the helicity zero fields[11] ξ_{tx}, ξ_t, ξ_x, ξ_y, ξ_z, a_x^a and a_t^a in different linear combinations, with r-dependent coefficients τ_n, so that the combinations are invariant under residual gauge transformations. That is

$$\delta\Phi = \sum_{a=1}^{3}(\tau_a \delta a_x^a + \tau_{3+a}\delta a_t^a) + \tau_7\delta\xi_{tx} + \tau_8\delta\xi_t + \tau_9\delta\xi_x + \tau_{10}\delta\xi_y + \tau_{11}\xi_z = 0\,, \quad (4.40)$$

where we call the physical modes Φ_i, with $i \in \{1,2,3,4\}$. Note that from table 4.1 we know that we should expect 4 invariant fields. Due to the structure of the equations we also get the helicity 2 mode $\xi_y - \xi_z$ here.

The helicity zero fluctuations transform under the residual gauge transformations as

$$\begin{aligned}
\delta\xi_{tx} &= -\mathrm{i}\omega K_x + \mathrm{i}k\frac{{c_1}^2}{{c_2}^2}K_t - \omega k\left(B + \frac{{c_1}^2}{{c_2}^2}A\right)K_r\,,\\
\delta\xi_t &= 2\mathrm{i}\omega K_t + \left(\frac{2{c_1}'}{c_1 c_4} - 2\omega^2 A\right)K_r\,,\\
\delta\xi_x &= 2\mathrm{i}kK_x + \left(\frac{2{c_2}'}{c_2 c_4} + 2k^2 B\right)K_r\,,\\
\delta\xi_y &= \frac{2{c_3}'}{c_3 c_4}K_r\,,\\
\delta\xi_z &= \frac{2{c_3}'}{c_3 c_4}K_r\,,\\
\delta a_x^1 &= \mathrm{i}k\Lambda_0^1 + \mathrm{i}kwK_x + \left(\frac{w'}{c_4} + k^2(wB - C_w)\right)K_r\,,\\
\delta a_t^1 &= -\mathrm{i}\omega\Lambda_0^1 - \phi\Lambda_0^2 - \mathrm{i}\omega wK_x - \omega k(wB - C_w)K_r\,,\\
\delta a_x^2 &= \mathrm{i}k\Lambda_0^2 - w\Lambda_0^3 - \mathrm{i}\omega wC_\phi K_r\,,\\
\delta a_t^2 &= -\mathrm{i}\omega\Lambda_0^2 + \phi\Lambda_0^1 + \mathrm{i}k\phi C_w K_r\,,\\
\delta a_x^3 &= \mathrm{i}k\Lambda_0^3 + w\Lambda_0^2 - \mathrm{i}k\phi K_t + \omega k(\phi A - C_\phi)K_r\,,\\
\delta a_t^3 &= -\mathrm{i}\omega\Lambda_0^3 + \mathrm{i}\omega\phi K_t + \left(\frac{\phi'}{c_4} - \omega^2(\phi A - C_\phi)\right)K_r\,.
\end{aligned} \quad (4.41)$$

Plugging everything into equation (4.40) results in 6 algebraic equations, since (4.32) has to vanish independently for all values of K_i and Λ_0^a. Thus, we can solve for 6 of the τ_n coefficients in terms of the other five. The solution gives the most general gauge invariant combination and it is independent of $\{A, B, C_w, C_\phi\}$.

What we call the four physical fields, Φ_i, are chosen as a set of linear independent fields invariant under residual diffeomorphisms and $SU(2)$ transformations. The linear combinations are not entirely fixed, but there is some freedom left. We

[11] We use $\xi_y = g^{yy}h_{yy}$, $\xi_z = g^{yy}h_{zz}$, $\xi_x = g^{xx}h_{xx}$, $\xi_t = g^{tt}h_{tt}$ and $\xi_{tx} = g^{xx}h_{tx}$.

choose

$$\begin{aligned}
\Phi_1 =& a_x^1 - \frac{\mathrm{i}k}{\phi} a_t^2 + \frac{k^2}{w\phi} a_t^3 + \frac{k\omega}{w\phi} a_x^3 + \frac{kw}{\omega}\xi_{tx} - \frac{k^2 f^4 N w \sigma^2}{2r^2\omega^2}\xi_t + \\
&+ \frac{k^2 f^5 w^2 \sigma\phi\left(\sigma N' + 2N\sigma'\right) - 2r^2\omega^2 f\left(w\phi w' + k^2\phi'\right)}{8r\omega^2 w\phi\left(f + rf'\right)}(\xi_y + \xi_z)\,, \\
\Phi_2 =& a_x^2 + \frac{\mathrm{i}\left(-k^2 + w^2\right)}{\omega w} a_t^3 - \frac{\mathrm{i}k}{w} a_x^3 - \frac{\mathrm{i}w\phi}{2\omega}\xi_t + \\
&+ \frac{\mathrm{i}rf\left(w^2\phi\left(\sigma N' + 2N\sigma'\right) + 2N\left(k^2 - w^2\right)\sigma\phi'\right)}{8\omega N w\sigma\left(f + rf'\right)}(\xi_y + \xi_z)\,, \\
\Phi_3 =& \xi_x + \frac{2k}{\omega}\xi_{tx} - \frac{k^2 f^4 N\sigma^2}{r^2\omega^2}\xi_t + \\
&+ \frac{4r^2\omega^2 f' - 2r\omega^2 f + k^2 f^5\sigma\left(\sigma N' + 2N\sigma'\right)}{4r\omega^2\left(f + rf'\right)}(\xi_y + \xi_z)\,, \\
\Phi_4 =& a_x^3 - \frac{w\phi}{\omega^2 - \phi^2} a_t^1 - \frac{\mathrm{i}\omega w}{\omega^2 - \phi^2} a_t^2 + \frac{w^2\phi}{\omega^2 - \phi^2}\xi_{tx} - \frac{k f^4 N w^2\sigma^2\phi}{2r^2\omega\left(\omega^2 - \phi^2\right)}\xi_t + \\
&+ \frac{k}{\omega} a_t^3 + \frac{kf\left(f^4 w^2\sigma\phi\left(\sigma N' + 2N\sigma'\right) + 2r^2\left(-\omega^2 + \phi^2\right)\phi'\right)}{8r\omega\left(\omega^2 - \phi^2\right)\left(f + rf'\right)}(\xi_y + \xi_z)\,,
\end{aligned} \tag{4.42}$$

with

$$\xi_y = g^{yy}h_{yy},\ \xi_z = g^{yy}h_{zz},\ \xi_x = g^{xx}h_{xx},\ \xi_t = g^{tt}h_{tt},\ \xi_{tx} = g^{xx}h_{tx}\,. \tag{4.43}$$

As already mentioned above with this approach we get a fifth physical mode, which, however, transforms as a helicity two state, namely $\xi_y - \xi_z$. Using this definition of the physical modes makes the identification between the Green's functions and the transport coefficients later on easier (cf. section 4.2.7). Note that at the level of the equations of motion, we still work with all fields and only when determining the Green's function the linear combinations derived above are used to obtain physically sensible results.

4.2.3 Equations of Motion and Asymptotic Behaviour

In the following we will focus on the response exclusively to time dependent perturbations, i. e. $k^\mu = (\omega, 0, 0, 0)$. In this case, in addition to the $SO(2)$ symmetry, $P_\parallel$ parity is conserved which allows us to decouple some of the physical modes in the different helicity blocks. In this section we write down the equations of motion for the fluctuations and determine the corresponding asymptotic behaviours.

4.2.3.1 Equations of Motion

The equations of motion are easily derived by expanding the equations of motion (4.5) up to first order in fluctuations. The corresponding equation for the helicity two mode $\Xi = g^{yy}h_{yz}$ reads

$$\Xi'' + \left(\frac{1}{r} + \frac{4r}{N} - \frac{r\alpha^2\phi'^2}{3N\sigma^2}\right)\Xi' + \frac{\omega^2}{N^2\sigma^2}\Xi = 0\,. \tag{4.44}$$

This is the equation of a minimally coupled scalar field. We will see below that due to this fact the value of the corresponding transport coefficient, namely the shear viscosity, is immediately known.

Due to the parity $P_\parallel$, the helicity one modes split into two blocks where the modes of the first block are even while the modes of the second block are odd under $P_\parallel$. The equations of motion for the helicity one even block are

$$\begin{aligned} 0 &= a_y^{3\prime\prime} + \left(\frac{1}{r} - \frac{2f'}{f} + \frac{N'}{N} + \frac{\sigma'}{\sigma}\right) a_y^{3\prime} + \left(\frac{\omega^2}{N^2\sigma^2} - \frac{f^4 w^2}{r^2 N} - \frac{2\alpha^2\phi'^2}{N\sigma^2}\right) a_y^3 \,, \\ 0 &= \Psi_t' + \frac{2\alpha^2\phi'}{r^2 f^2} a_y^3 \,, \end{aligned} \tag{4.45}$$

while the ones of the odd block read

$$\begin{aligned} 0 =& \Psi_x'' + \left(\frac{1}{r} + \frac{4r}{N} + \frac{6f'}{f} - \frac{r\alpha^2\phi'^2}{3N\sigma^2}\right)\Psi_x' + \frac{2\alpha^2 w'}{r^2 f^2} a_y^{1\prime} + \frac{\omega^2}{N^2\sigma^2}\Psi_x \\ &+ \frac{2i\alpha^2\omega w\phi}{r^2 f^2 N^2\sigma^2} a_y^2 - \frac{2\alpha^2 w\phi^2}{r^2 f^2 N^2\sigma^2} a_y^1 \,, \\ 0 =& a_y^{1\prime\prime} + \left(\frac{1}{r} - \frac{2f'}{f} + \frac{N'}{N} + \frac{\sigma'}{\sigma}\right) a_y^{1\prime} - f^6 w'\Psi_x' \\ &+ \left(\frac{\omega^2}{N^2\sigma^2} + \frac{\phi^2}{N^2\sigma^2}\right) a_y^1 - \frac{2i\omega\phi}{N^2\sigma^2} a_y^2, \\ 0 =& a_y^{2\prime\prime} + \left(\frac{1}{r} - \frac{2f'}{f} + \frac{N'}{N} + \frac{\sigma'}{\sigma}\right) a_y^{2\prime} \\ &+ \left(\frac{\omega^2}{N^2\sigma^2} + \frac{\phi^2}{N^2\sigma^2} - \frac{f^4 w^2}{r^2 N}\right) a_y^2 + \frac{2i\omega\phi}{N^2\sigma^2} a_y^1 - \frac{i\omega f^6 w\phi}{N^2\sigma^2}\Psi_x \,. \end{aligned} \tag{4.46}$$

where $\Psi_t = g^{yy}h_{ty}$ and $\Psi_x = g^{yy}h_{xy}$. Notice that following our discussion of section 4.2.2, in the first block there is only one physical mode a_y^3 while the value of the other field Ψ_t is given by the constraint (4.45). The same is true for the second block, since in the gauge invariant fields (4.39) h_{ty} drops out for $k_\parallel = 0$ and we are left with the three physical modes $\Psi_x = \Psi$, a_y^1 and a_y^2.

Finally, the same arguments are also valid for the helicity zero fields. We obtain a parity even block containing the fields ξ_t, ξ_x, ξ_y, ξ_z, a_x^1, a_x^2, a_t^3 and a parity odd block with ξ_{tx}, a_t^1, a_t^2, a_x^3. Due to their length we omit the equations here, but rather present them in appendix A. However, note that here the counting of the second and first order differential equations agrees as well with the number of physical fields we derived for this sector in the section before. We come back to this point in the next section when deriving the asymptotic behaviour of the fields.

4.2.3.2 Asymptotic Behaviour

Next we derive the behaviour of the fluctuation fields $\{F(r)\}$ at the horizon and at the boundary from the equations of motion stated above. To compute the real-

time retarded Green's functions [88,100], besides regularity[12], we have to fulfil the incoming boundary conditions at the horizon. The ansatz used to compute the behaviour of the fields close to r_H is

$$F(r)\big|_{r\to r_H} = \left(\frac{r}{r_H}-1\right)^{\beta}\sum_{i\geq 0} F_i^h \left(\frac{r}{r_H}-1\right)^{i}. \tag{4.47}$$

We obtain two possibilities for β, namely

$$\beta = \pm \mathrm{i}\frac{\omega}{4\pi T}, \tag{4.48}$$

with T the temperature defined in equation (4.19). This corresponds to the incoming as well as outgoing boundary condition at the horizon. We choose the solution with the "$-$" sign which corresponds to the incoming boundary condition. As stated before, this corresponds to the dissipation of energy and leads us to the retarded Green's function (see [88] and discussion in section 3.2.4).

On the other hand, our ansatz at the boundary is similar to the one used for the background calculation in section 3.2.4 and 4.1. However, here we have to add logarithmic terms to get a consistent solution (cf. [101]). Therefore our ansatz is

$$F(r)\big|_{r\to\infty} = \sum_{i\geq 0}\left(F_i^B + \hat{F}_i^B \ln\left(\frac{r_H}{r}\right)\right)\left(\frac{r_H}{r}\right)^{i}. \tag{4.49}$$

The helicity two case, Ξ, is simple, since there is only one equation and the incoming boundary condition at the horizon. Due to the incoming condition one of the free parameters at the horizon is set to zero, leaving one free parameter $(\Xi)_0^H$. At the AdS boundary we are left with 2 free parameters,$(\Xi)_0^B$ and $(\Xi)_4^B$. Now if we choose a value for $(\Xi)_0^H$, the equation of motion is fully determined and we can integrate to the boundary and read of the boundary values of Ξ.

The helicity one case is slightly more complicated. For the parity even case the equations (4.45) have 3 independent expansion coefficients at the boundary (4 free parameters from the 2 second order differential equations minus 1 free parameter due to the constraint). We choose them to be $\left(a_y^3\right)_0^B$, $\left(a_y^3\right)_2^B$ and $\left(\Psi_t\right)_0^B$. As before, at the horizon the independent parameters were already halved by choosing the incoming boundary condition. From the remaining two parameters we can get rid of one by using the constraint equation (4.45). Hence one free parameter at the horizon is left, namely $\left(a_y^3\right)_0^H$. When solving these equations numerically we set $\left(a_y^3\right)_0^H = 1$ and scan through different values of ω. We can perform similar considerations for the parity odd block (equations (4.46)) of the helicity one fields. We do not have any constraint, just three fields and their corresponding equations of

[12]The condition $\phi(r_H) = 0$ at the horizon guarantees regularity, also at the level of fluctuations. Thus, even with all fluctuations switched on, there is no need for any further constraint.

motion. Therefore at the boundary there are six independent parameters, namely $\left(a_y^1\right)_0^B$, $\left(a_y^1\right)_2^B$, $\left(a_y^2\right)_0^B$, $\left(a_y^2\right)_2^B$, $\left(\Psi_x\right)_0^B$ and $\left(\Psi_x\right)_4^B$. At the horizon we have $\left(\Psi_x\right)_0^H$, $\left(a_y^1\right)_0^H$, $\left(a_y^2\right)_0^H$. Again three free parameters at the horizon are fixed by the incoming boundary condition. As before, by choosing the values for all fields at the horizon the system is fully determined.

In the helicity zero case, the equations of motion for the fluctuation fields can again be distributed into two blocks. In the first block (parity odd), there are 5 independent expansion coefficients at the boundary (8 free parameters from the 4 second order differential equations minus 3 free parameters due to the constraints). We choose them to be $(\xi_{tx})_0^B$, $\left(a_t^1\right)_0^B$, $\left(a_t^2\right)_0^B$, $\left(a_x^3\right)_0^B$ and $\left(a_x^3\right)_2^B$. The boundary condition at the horizon leaves us with half of the independent parameters, i.e. 4. We can get rid of another 3 by using the constraint equations. Hence just one free parameter is left at the horizon. For the parity even block there are also 3 constraints, but we are dealing with 7 fields, each with its own second order differential equation. Therefore at the boundary we get $14 - 3 = 11$ independent parameters, namely $(\xi_y)_0^B$, $(\xi_z)_0^B$, $(\xi_x)_0^B$, $(\xi_t)_0^B$, $\left(a_x^1\right)_0^B$, $\left(a_x^2\right)_0^B$, $\left(a_t^3\right)_0^B$, $\left(a_x^1\right)_2^B$, $\left(a_x^2\right)_2^B$, $(\xi_y)_4^B$ and $(\xi_z)_4^B$. At the horizon, as before, we already fixed 7 free parameters by choosing the incoming boundary condition. There are $7 - 3 = 4$ free parameters that fully determines the system of equations.

Next we explicitly present the expansions at the boundary, since the Green's functions and the corresponding transport coefficients are expressed in terms of these (cf. section 4.2.5). Note that the metric fluctuation expansion coefficients are dimensionless, while the coefficients of the gauge field fluctuations have r_H dimension one. We cut the expansion after the last order which is relevant for the computation of the Green's functions.

Helicity two mode:

$$\Xi = (\Xi)_0^B + \frac{\omega^2}{4r^2}(\Xi)_0^B + \left(r_H^4 (\Xi)_4^B - \frac{\omega^4}{16}(\Xi)_0^B \ln\frac{r_H}{r}\right)\frac{1}{r^4} \tag{4.50}$$

Helicity one parity even modes:

$$\begin{aligned} a_y^3 &= \left(a_y^3\right)_0^B + \left(r_H^2 \left(a_y^3\right)_2^B - \frac{1}{2}\omega^2 \left(a_y^3\right)_0^B \ln\frac{r_H}{r}\right)\frac{1}{r^2}, \\ \Psi_t &= (\Psi_t)_0^B - \alpha^2 \phi_2^B \left(a_y^3\right)_0^B \frac{r_H^2}{r^4} \end{aligned} \tag{4.51}$$

Helicity one parity odd modes:

$$
\begin{aligned}
a_y^1 &= \left(a_y^1\right)_0^B + \frac{r_H^2}{r^2}\left(a_y^1\right)_2^B \\
&\quad - \frac{1}{2}\left(\omega^2\left(a_y^1\right)_0^B - 2\mathrm{i}\omega\mu\left(a_y^2\right)_0^B + \mu^2\left(a_y^1\right)_0^B\right)\frac{1}{r^2}\ln\frac{r_H}{r}\,, \\
a_y^2 &= \left(a_y^2\right)_0^B + \frac{r_H^2}{r^2}\left(a_y^2\right)_2^B \\
&\quad - \frac{1}{2}\left(\omega^2\left(a_y^2\right)_0^B + 2\mathrm{i}\omega\mu\left(a_y^1\right)_0^B + \mu^2\left(a_y^2\right)_0^B\right)\frac{1}{r^2}\ln\frac{r_H}{r}\,, \\
\Psi_x &= \left(\Psi_x\right)_0^B + \frac{\omega^2}{4r^2}\left(\Psi_x\right)_0^B + \left(r_H^4\left(\Psi_x\right)_4^B - \frac{\omega^4}{16}\left(\Psi_x\right)_0^B\ln\frac{r_H}{r}\right)\frac{1}{r^4}
\end{aligned}
\tag{4.52}
$$

Helicity zero parity even modes:

$$
\begin{aligned}
\xi_y &= \left(\xi_y\right)_0^B + \omega^2\frac{2\left(\xi_y\right)_0^B - \left(\xi_x\right)_0^B - \left(\xi_z\right)_0^B}{12}\frac{1}{r^2} \\
&\quad + \left(r_H^4\left(\xi_y\right)_4^B - \frac{1}{48}\omega^4\left(\left(\xi_y\right)_0^B - \left(\xi_x\right)_0^B - \left(\xi_z\right)_0^B\right)\ln\frac{r_H}{r}\right)\frac{1}{r^4}\,, \\
\xi_z &= \left(\xi_z\right)_0^B + \omega^2\frac{2\left(\xi_z\right)_0^B - \left(\xi_x\right)_0^B - \left(\xi_y\right)_0^B}{12}\frac{1}{r^2} \\
&\quad + \left(r_H^4\left(\xi_z\right)_4^B - \frac{1}{48}\omega^4\left(\left(\xi_z\right)_0^B - \left(\xi_x\right)_0^B - \left(\xi_y\right)_0^B\right)\ln\frac{r_H}{r}\right)\frac{1}{r^4}\,, \\
\xi_x &= \left(\xi_x\right)_0^B + \omega^2\frac{2\left(\xi_x\right)_0^B - \left(\xi_y\right)_0^B - \left(\xi_z\right)_0^B}{12}\frac{1}{r^2} + \left(-r_H^4\left(\left(\xi_y\right)_4^B + \left(\xi_z\right)_4^B\right)\right. \\
&\quad + \alpha^2 r_H^2 w_2^B\left(-\left(a_x^1\right)_0^B + \mathrm{i}\frac{\mu}{\omega}\left(a_x^2\right)_0^B\right) + \left(2f_4^B - m_0^B\right)\left(\xi_x\right)_0^B \\
&\quad - \left(f_4^B + m_0^B\right)\left(\left(\xi_y\right)_0^B + \left(\xi_y\right)_0^B\right) \\
&\quad \left. - \frac{1}{48}\omega^4\left(2\left(\xi_x\right)_0^B - \left(\xi_y\right)_0^B - \left(\xi_z\right)_0^B\right)\ln\frac{r_H}{r}\right)\frac{1}{r^4}\,, \\
\xi_t &= \left(\xi_t\right)_0^B + \omega^2\frac{\left(\xi_y\right)_0^B + \left(\xi_z\right)_0^B + \left(\xi_x\right)_0^B}{6}\frac{1}{r^2} + \left(\left(f_4^B + m_0^B\right)\left(\left(\xi_y\right)_0^B + \left(\xi_z\right)_0^B\right)\right. \\
&\quad \left.\alpha^2 r_H^2 w_2^B\left(\left(a_x^1\right)_0^B - \mathrm{i}\frac{\mu}{\omega}\left(a_x^2\right)_0^B\right) + \left(-2f_4^B + m_0^B\right)\left(\xi_x\right)_0^B\right)\frac{1}{r^4}\,, \\
a_x^1 &= \left(a_x^1\right)_0^B + \frac{r_H^2}{r^2}\left(a_x^1\right)_2^B - \frac{1}{2}\left(\left(\mu^2+\omega^2\right)\left(a_x^1\right)_0^B - 2\mathrm{i}\mu\omega\left(a_x^2\right)_0^B\right)\frac{1}{r^2}\ln\frac{r_H}{r}\,, \\
a_x^2 &= \left(a_x^2\right)_0^B + \frac{r_H^2}{r^2}\left(a_x^2\right)_2^B - \frac{1}{2}\left(\left(\mu^2+\omega^2\right)\left(a_x^2\right)_0^B + 2\mathrm{i}\mu\omega\left(a_x^1\right)_0^B\right)\frac{1}{r^2}\ln\frac{r_H}{r}\,, \\
a_t^3 &= \left(a_t^3\right)_0^B + \left(-\frac{\mathrm{i}}{\omega}w_2^B\left(a_x^2\right)_0^B - \frac{1}{2}\phi_2^B\left(2\left(\xi_y\right)_0^B + \left(\xi_x\right)_0^B - \left(\xi_t\right)_0^B\right)\right)\frac{r_H^2}{r^2}
\end{aligned}
\tag{4.53}
$$

Helicity zero parity odd modes:

$$\begin{aligned}
a_t^1 &= \left(a_t^1\right)_0^B + \frac{\left(\omega^2 \left(\xi_{tx}\right)_0^B - \left(a_x^3\right)_0^B \mu - \left(\xi_{tx}\right)_0^B \mu^2\right) w_2^B}{\omega^2 - \mu^2} \frac{r_H^2}{r^2} \\
&\quad - \frac{\left(\left(a_t^1\right)_0^B \mu + \mathrm{i}\omega \left(a_t^2\right)_0^B\right) \phi_2^B}{\omega^2 - \mu^2} \frac{r_H^2}{r^2} \,, \\
a_t^2 &= \left(a_t^2\right)_0^B + \frac{-\mathrm{i}\omega \left(a_x^3\right)_0^B w_2^B + \left(\left(a_t^2\right)_0^B \mu - \mathrm{i}\omega \left(a_t^1\right)_0^B\right) \phi_2^B}{\mu^2 - \omega^2} \frac{r_H^2}{r^2} \,, \\
a_x^3 &= \left(a_x^3\right)_0^B + \left(r_H^2 \left(a_x^3\right)_2^B - \frac{1}{2}\omega^2 \left(a_x^3\right)_0^B \ln \frac{1}{r^2}\right) \frac{1}{r^2} \,, \\
\xi_{tx} &= \left(\xi_{tx}\right)_0^B - \alpha^2 \left(a_x^3\right)_0^B \phi_2^B \frac{r_H^2}{r^4}
\end{aligned} \tag{4.54}$$

We use (4.16) for the background fields.

4.2.4 Counterterms

Before computing the Green's functions, we have to determine the counterterms which render the solution finite at the AdS boundary (cf. eq. (3.61)). The algorithmic generation of such counter terms goes under the name holographic renormalisation [101].

The boundary part S_{bdy} of the action (4.1) does not have any influence on the equations of motion, but it ensure that the action is finite on-shell. It includes the Gibbons-Hawking boundary term, which renders the variational problem with Dirichlet boundary conditions to be well-defined, and additional terms, the counterterm action S_{CT}, needed to cancel divergences. Thus, the full action is

$$S = \frac{1}{2\kappa^2} \int \mathrm{d}^5x \sqrt{-g} \left[R - \Lambda - \frac{\alpha^2}{2} F^a_{MN} F^{aMN}\right] + \frac{1}{\kappa^2} \int \mathrm{d}^4x \sqrt{-\gamma}\, K + S_{\mathrm{CT}} \,. \tag{4.55}$$

A systematic way to compute the counterterms was derived in [87]. For a nice review see [101]. Note that for us it is enough to follow the lead of [101, 102], use the terms calculated there and adapt them to the non-Abelian case at hand.

First we start by determining the on-shell action $S^{\mathrm{pwave}}_{L,\text{on-shell}}$ to second order in the fluctuations. For the background on-shell action see section 4.1.2. To guarantee better legibility we split the action into the different modes, i.e.

$$\begin{aligned}
S^{\text{on-shell}}_{\text{helicity 2}} =& \frac{1}{\kappa^2} \int \frac{\mathrm{d}^4k}{(2\pi)^4} \Bigg\{ -\frac{1}{4} r^3 N \sigma \Xi \Xi' \\
&+ r^3 N \sigma \left(\frac{3}{2\sqrt{N}} - \frac{1}{r} + \frac{f'}{2f} - \frac{N'}{4N} - \frac{\sigma'}{2\sigma}\right) \Xi^2 \Bigg\} \Bigg|_{r=r_B} \,,
\end{aligned} \tag{4.56}$$

$$
\begin{aligned}
&S^{\text{on-shell}}_{\text{hel.0, bl.1}} = \\
&= \frac{1}{\kappa^2}\int \frac{\mathrm{d}^4k}{(2\pi)^4}\left\{\frac{r^5}{4f^4\sigma}\xi_{tx}{\xi_{tx}}' + \frac{r^3\alpha^2}{2\sigma}\left(a_t^1{a_t^1}' + a_t^2{a_t^2}'\right) - \frac{r\alpha^2 f^4 N\sigma}{2}a_x^3{a_x^3}'\right. \\
&\left. + \left(\frac{3r^4}{2f^4\sigma} - \frac{3r^5}{2f^4\sigma\sqrt{N}}\right){\xi_{tx}}^2 - \frac{r^3\alpha^2}{2\sigma}\xi_{tx}\left(w'a_t^1 + \phi' a_x^3\right)\right\}\Bigg|_{r=r_B},
\end{aligned}
\tag{4.57}
$$

$$
\begin{aligned}
&S^{\text{on-shell}}_{\text{hel.0, bl.2}} = \\
&= \frac{1}{\kappa^2}\int \frac{\mathrm{d}^4k}{(2\pi)^4}\left\{\frac{r^3N\sigma}{4}\xi_y{\xi_y}' - \frac{r\alpha^2f^4N\sigma}{2}\left(a_x^1{a_x^1}' + a_x^2{a_x^2}'\right) + \frac{r^3\alpha^2}{2\sigma}a_t^3{a_t^3}'\right. \\
&- \frac{3r^2N\sigma}{8}{\xi_t}^2 - \frac{r^2}{8f}\left(2fN\sigma + \frac{fr\sigma N'}{2} + fNr\sigma' + 2Nr\sigma f'\right){\xi_x}^2 \\
&+ \frac{r^3N\sigma}{4}\xi_y\left({\xi_t}' + {\xi_x}'\right) + \frac{r^2}{4f}\left(5fN\sigma - rN\sigma f' + \frac{rf\sigma N'}{2} + rfN\sigma'\right)\xi_y\xi_t \\
&+ \frac{r^3N\sigma}{4}\left(\xi_t + \xi_x\right){\xi_y}' + \frac{r^2}{2f}\left(2fN\sigma + \frac{rN\sigma f'}{2} + \frac{rf\sigma N'}{2} + rfN\sigma'\right)\xi_y\xi_x \\
&+ \frac{r^3N\sigma}{8}\left(\xi_t{\xi_x}' + \xi_x{\xi_t}'\right) + \frac{r^2}{8f}\left(5fN\sigma + 2rN\sigma f' + \frac{rf\sigma N'}{2} + rfN\sigma'\right)\xi_t\xi_x \\
&\left. - \frac{r\alpha^2f^4N\sigma w'}{4}a_x^1\left(\xi_t - \xi_x + 2\xi_y\right) - \frac{r^3\alpha^2\phi'}{4\sigma}a_t^3\left(\xi_t - \xi_x - 2\xi_y\right)\right\}\Bigg|_{r=r_B}
\end{aligned}
\tag{4.58}
$$

and

$$
\begin{aligned}
&S^{\text{on-shell}}_{\text{helicity 1}} = \\
&= \frac{1}{\kappa^2}\int \frac{\mathrm{d}^4k}{(2\pi)^4}\left\{\frac{r^5f^2}{4\sigma}\Psi_t{\Psi_t}' - \frac{1}{4}r^3f^6N\sigma\Psi_x{\Psi_x}'\right. \\
&- \frac{r\alpha^2N\sigma}{2f^2}\left(a_y^1{a_y^1}' + a_y^2{a_y^2}' + a_y^3{a_y^3}'\right) + \frac{3r^4f^2}{2\sigma}\left(1 - \frac{r}{\sqrt{N}}\right){\Psi_t}^2 \\
&+ \frac{r^3f^6N\sigma}{2}\left(\frac{3}{\sqrt{N}} - \frac{2}{r} - \frac{2f'}{f} - \frac{N'}{2N} - \frac{\sigma'}{\sigma}\right){\Psi_x}^2 \\
&\left. + \frac{r\alpha^2f^4N\sigma w'}{2}a_y^1\Psi_x - \frac{r^3\alpha^2\phi'}{2\sigma}a_y^3\Psi_t\right\}\Bigg|_{r=r_B},
\end{aligned}
\tag{4.59}
$$

where we again use r_B us an UV cut off of the theory.

By plugging the expansions at the AdS boundary, (4.50), (4.51), (4.52), (4.53) and (4.54), into the boundary actions (4.56), (4.59), (4.57) and (4.58), we obtain the non-renormalized on-shell action, $S_{\text{on-shell}} = \frac{1}{\kappa^2}\int \frac{\mathrm{d}^4k}{(2\pi)^4}\,\mathcal{L}_{r_B}$, where the integrand $\mathcal{L}_{r_B}$ is written in terms of the free parameters of the boundary expansions. Here we concentrate on the divergent parts only. The terms that have to be cancelled by the counterterms are the ones with explicit $1/r_B^a$ dependence, with $a \geq 1$. These

are $\frac{\mathcal{L}^{\rm Div}_{r_B}}{r_H^4} =$

$$
\begin{aligned}
=&+\frac{2}{r_H^4}\ln\frac{r_H}{r_B}\Bigg[+\frac{\omega^4}{48}\left((\xi_y)_0^{B^2}+(\xi_x)_0^{B^2}-2\,(\xi_y)_0^{B}\,(\xi_x)_0^{B}\right)\\
&+\frac{1}{32}\omega^4\left((\Xi)_0^{B^2}+(\Psi_x)_0^{B^2}\right)-\frac{\alpha^2\omega^2}{4}\big(a_x^3\big)_0^{B^2}\\
&-\frac{\alpha^2\left(\mu^2-\omega^2\right)}{4}\left(\big(a_x^1\big)_0^{B^2}+\big(a_x^2\big)_0^{B^2}\right)+\mathrm{i}\alpha^2\mu\omega\left(a_x^1\right)_0^{B}\left(a_x^2\right)_0^{B}\\
&+\mathrm{i}\alpha^2\omega\mu\big(a_y^1\big)_0^{B}\big(a_y^2\big)_0^{B}+\frac{1}{4}\alpha^2\Bigg(\omega^2\left(\big(a_y^1\big)_0^{B^2}+\big(a_y^2\big)_0^{B^2}+\big(a_y^3\big)_0^{B^2}\right)\\
&+\mu^2\left(\big(a_y^1\big)_0^{B^2}+\big(a_y^2\big)_0^{B^2}\right)\Bigg)\Bigg].
\end{aligned}
\tag{4.60}
$$

For the construction of the counterterms, first we need to define the induced metric $\gamma_{\mu\nu}$ on the $r = r_B$ plane,

$$
\gamma_{\mu\nu}=\frac{\partial x^M}{\partial\tilde{x}^\mu}\frac{\partial x^N}{\partial\tilde{x}^\nu}g_{MN}(r)\bigg|_{r=r_B}. \tag{4.61}
$$

Next we examine possible covariant counterterms by following [101, 102]. They are composed of a combination of $R[\gamma]$, $R_{\mu\nu}[\gamma]$ and $F^a_{\mu\nu}$ (i.e. the Ricci scalar, Ricci tensor and field strength on the induced surface). Possible covariant combinations of the three terms and the determinant of the induced metric are $\sqrt{-\gamma}$, $\sqrt{-\gamma}R[\gamma]$, $\sqrt{-\gamma}R[\gamma]^2$, $\sqrt{-\gamma}R^{\mu\nu}[\gamma]R_{\mu\nu}[\gamma]$ and $\sqrt{-\gamma}F^a_{\mu\nu}F^{a\mu\nu}$. The coefficients in front of them can be guessed by requiring the divergences to vanish in the complete action. Their expansions for $r_B \gg 1$ are

$$
\begin{aligned}
\sqrt{-\gamma}R[\gamma]\Big|_{r_B}=&\frac{r_B^2\omega^2}{2}\left[(\Xi)_0^{B^2}+(\Psi_x)_0^{B^2}-(\xi_y)_0^{B^2}-2\,(\xi_y)_0^{B}\,(\xi_x)_0^{B}\right]\\
&+\frac{\omega^4}{12}\Big(3(\Xi)_0^{B^2}+3(\Psi_x)_0^{B^2}+(\xi_y)_0^{B^2}+(\xi_x)_0^{B^2}\\
&\qquad-2\,(\xi_y)_0^{B}\,(\xi_x)_0^{B}\Big),\\
\sqrt{-\gamma}R[\gamma]^2\Big|_{r_B}=&\omega^4\left(4(\xi_y)_0^{B^2}+(\xi_x)_0^{B^2}+4\,(\xi_y)_0^{B}\,(\xi_x)_0^{B}\right),\\
\sqrt{-\gamma}R^{\mu\nu}[\gamma]R_{\mu\nu}[\gamma]\Big|_{r_B}=&\frac{\omega^4}{2}\Big((\Xi)_0^{B^2}+(\Psi_x)_0^{B^2}+3(\xi_y)_0^{B^2}+(\xi_x)_0^{B^2}\\
&\qquad+2\,(\xi_y)_0^{B}\,(\xi_x)_0^{B}\Big)\quad\text{and}
\end{aligned}
\tag{4.62}
$$

$$
\begin{aligned}
\sqrt{-\gamma}F^a_{\mu\nu}F^{a\mu\nu}\Big|_{r_B}=&-2\omega^2\left(\big(a_x^3\big)_0^{B^2}+\big(a_y^3\big)_0^{B^2}\right)\\
&-2\left(\mu^2+\omega^2\right)\left(\big(a_x^1\big)_0^{B^2}+\big(a_x^2\big)_0^{B^2}+\big(a_y^1\big)_0^{B^2}+\big(a_y^2\big)_0^{B^2}\right)\\
&+8\mathrm{i}\mu\omega\left(\big(a_x^1\big)_0^{B}\big(a_x^2\big)_0^{B}+\big(a_y^1\big)_0^{B}\big(a_y^2\big)_0^{B}\right).
\end{aligned}
\tag{4.63}
$$

By comparing these terms to the ones in (4.60), it can be checked that by adding the real space action

$$S_{\rm CT} = -\frac{1}{\kappa^2}\int \mathrm{d}^4x\,\sqrt{-\gamma}\,\left(3+\frac{1}{4}R[\gamma]+\left(\frac{1}{24}R[\gamma]^2-\frac{1}{8}R^{\mu\nu}[\gamma]R_{\mu\nu}[\gamma]\right.\right.\\ \left.\left.+\frac{\alpha^2}{4}F^a_{\mu\nu}F^{a\mu\nu}\right)\ln\frac{r_H}{r_B}\right)\Bigg|_{r_B\gg 1} \tag{4.64}$$

to the action $S_L^{\rm pwave}$ (4.1) we get a divergence-free theory (up to second order in the fluctuations) for $r_B \gg 1$. Now we have all the ingredients to compute the finite retarded Green's functions for the different fluctuations.

4.2.5 Green's functions

In this section we determine the retarded Green's functions G of the stress-energy tensor $T^{\mu\nu}$ and the currents $J^{a\mu}$, namely (small Latin letters refer to the flavour directions and small Greek letters to the field theory spacetime directions)

$$\begin{aligned}
G^{\mu\nu,\rho\sigma}(k) &= -\mathrm{i}\int \mathrm{d}t\mathrm{d}^3x\,\mathrm{e}^{-\mathrm{i}k_\mu x^\mu}\,\theta(t)\langle[T^{\mu\nu}(t,\vec{x}),T^{\rho\sigma}(0,0)]\rangle\,,\\
G^{a\mu,b\nu}(k) &= -\mathrm{i}\int \mathrm{d}t\mathrm{d}^3x\,\mathrm{e}^{-\mathrm{i}k_\mu x^\mu}\,\theta(t)\langle[J^{a\mu}(t,\vec{x}),J^{b\nu}(0,0)]\rangle\,,\\
G^{\mu\nu,a\rho}(k) &= -\mathrm{i}\int \mathrm{d}t\mathrm{d}^3x\,\mathrm{e}^{-\mathrm{i}k_\mu x^\mu}\,\theta(t)\langle[T^{\mu\nu}(t,\vec{x}),\mathcal{J}^{a\rho}(0,0)]\rangle\,,\\
G^{a\rho,\mu\nu}(k) &= -\mathrm{i}\int \mathrm{d}t\mathrm{d}^3x\,\mathrm{e}^{-\mathrm{i}k_\mu x^\mu}\,\theta(t)\langle[J^{a\rho}(t,\vec{x}),T^{\mu\nu}(0,0)]\rangle\,.
\end{aligned} \tag{4.65}$$

$T^{\mu\nu}$ and $J^{a\mu}$ are the full stress-energy tensor and current, respectively. Thus they include the equilibrium parts, $\langle\mathcal{T}^{\mu\nu}\rangle$ and $\langle\mathcal{J}^{a\mu}\rangle$, as well as the corresponding dissipative parts which arise due to the inclusion of fluctuations in our model. We use the approach determined in section 3.2.4. That is, we compute the conjugate momentum Π_m, which in our case corresponds to the boundary charge current and energy-momentum tensor,

$$\begin{aligned}
\langle J^{a\mu}\rangle &= \left(-\frac{\sqrt{-g}}{g^2}F^{ar\mu}+\frac{S_{\rm CT}^{\text{on-shell}}}{\delta\left(A^a_\mu\right)^B_0}\right)\Bigg|_{r\to\infty}\,,\\
\langle T^{\mu\nu}\rangle &= \left(\frac{r^2\sqrt{-\gamma}}{\kappa^2}\left(K^{\mu\nu}-\gamma^{\mu\nu}K+\frac{\mathrm{D}-1}{L}\right)+\frac{S_{\rm CT}^{\text{on-shell}}}{\delta\left(g_{\mu\nu}\right)^B_0}\right)\Bigg|_{r\to\infty}
\end{aligned} \tag{4.66}$$

and then use

$$G^R_{\mathcal{O}_m\mathcal{O}_n}(k_\mu) = \lim_{r\to\infty}\frac{\delta\Pi_m(k_\mu,r)}{\delta\left(\Phi^n\right)^B_0(k_\mu)} = \lim_{r\to\infty}\frac{\delta\Pi_m(k_\mu,r)}{\delta\Phi_n(k_\mu,r)} \tag{4.67}$$

to determine the corresponding Green's function. Note that in the current we use the full metric g_{AB} rather than the induced metric $\gamma_{\mu\nu}$, this is not a typo (cf. section 3.2.4). Finally we use $S_{\rm CT}^{\text{on-shell}}$ as in equation (4.64) with the terms given by

(4.62). We do not show this explicitly, however, all divergence cancel exactly.

Next we present the Green's functions sorted by helicity. We constraint ourselves to just stating the result. The physical interpretation and the identification of transport coefficients of the dual field theory is left for section 4.2.7. Note that the metric fluctuation expansion coefficients are dimensionless and the gauge field fluctuations expansion coefficient have r_H dimension one.

4.2.5.1 Helicity two mode

The non-trivial helicity two mode displayed in table 4.1 is $h_{yz} = g_{yy}\Xi$. Using the the formalism above we obtain for the energy momentum tensor

$$\begin{aligned}\langle T^{yz}\rangle(\omega) &= \frac{2r_H^4}{\kappa^2}(\Xi)_4^B(\omega) + \frac{1}{\kappa^2}\left(-\left(4f_4^B + m_0^B\right)r_H^4 - \frac{5\omega^4}{32}\right)(\Xi)_0^B(\omega) = \\ &= \frac{2r_H^4}{\kappa^2}\Xi_4^B(\omega) - \left(\langle \mathcal{T}^{yy}\rangle + \frac{5\omega^4}{32\kappa^2}\right)(\Xi)_0^B(\omega)\,.\end{aligned} \tag{4.68}$$

The corresponding Green's function is

$$G^{yz,yz}(\omega) = \left(\frac{2r_H^4}{\kappa^2}\frac{(\Xi)_4^B(\omega)}{(\Xi)_0^B(\omega)} - \langle \mathcal{T}^{yy}\rangle - \frac{5\omega^4}{32\kappa^2}\right), \tag{4.69}$$

where $\langle \mathcal{T}^{yy}\rangle$ is the equilibrium contribution given by the pressure P (cf. section 4.1.2). As we will see in section 4.2.7.4, the Green's function of this helicity mode will lead to a shear viscosity component with universal behaviour, i.e. $\eta_{yz}/s = 1/4\pi$.

4.2.5.2 Helicity one modes

The helicity one modes displayed in table 4.1 are discussed next. As pointed out before, due to the parity $P_\parallel$ transformations, the helicity one modes split into two blocks where the modes of the first block are even while the modes of the second block are odd under $P_\parallel$. In the first block there is only one physical mode a_y^3, while the value of the other field Ψ_t is given by the constraint (4.45). This can also be seen in the gauge invariant fields (4.39) since h_{ty} drops out for $k_\parallel = 0$. The other three physical modes appear in the second block where Ψ_x for $k_\parallel = 0$.

Block 1 - Parity even For the parity even block of the helicity one modes we obtain ($\perp$ stands for either y or z)

$$\begin{aligned}
\langle T^{t\perp}\rangle(\omega) &= \frac{2r_H^2\phi_2^B}{g^2}\left(a_\perp^3\right)_0^B(\omega) - \frac{3m_0^B}{\kappa^2}\left(\Psi_t\right)_0^B(\omega) = \\
&= -\langle\mathcal{J}^{3t}\rangle\left(a_\perp^3\right)_0^B(\omega) - \langle\mathcal{T}^{tt}\rangle\left(\Psi_t\right)(\omega), \\
\langle J^{3\perp}\rangle(\omega) &= \frac{2r_H^2}{g^2}\left(a_\perp^3\right)_2^B(\omega) + \frac{2r_H^2\phi_2^B}{g^2}\left(\Psi_t\right)_0^B(\omega) - \frac{\omega^2}{2g^2}\left(a_\perp^3\right)_0^B(\omega) = \\
&= \frac{2r_H^2}{g^2}\left(a_\perp^3\right)_2^B(\omega) - \langle\mathcal{J}^{3t}\rangle\left(\Psi_t\right)_0^B(\omega) - \frac{\omega^2}{2g^2}\left(a_\perp^3\right)_0^B(\omega).
\end{aligned} \tag{4.70}$$

Using

$$\begin{pmatrix}\langle J^{3\perp}\rangle(\omega)\\ \langle T^{t\perp}\rangle(\omega)\end{pmatrix} = \begin{pmatrix}G^{3\perp,3\perp}(\omega) & G^{3\perp,t\perp}(\omega)\\ G^{t\perp,3\perp}(\omega) & G^{t\perp,t\perp}(\omega)\end{pmatrix}\begin{pmatrix}\left(a_\perp^3\right)_0^B(\omega)\\ \left(\Psi_t\right)_0^B(\omega)\end{pmatrix}, \tag{4.71}$$

the Green's functions read

$$\begin{pmatrix}G^{3\perp,3\perp}(\omega) & G^{3\perp,t\perp}(\omega)\\ G^{t\perp,3\perp}(\omega) & G^{t\perp,t\perp}(\omega)\end{pmatrix} = \begin{pmatrix}\frac{2r_H^2}{g^2}\frac{\left(a_\perp^3\right)_2^B(\omega)}{\left(a_\perp^3\right)_0^B(\omega)} - \frac{\omega^2}{2g^2} & -\langle\mathcal{J}^{3t}\rangle\\ -\langle\mathcal{J}^{3t}\rangle & -\langle\mathcal{T}_{tt}\rangle\end{pmatrix}. \tag{4.72}$$

This result agrees exactly with the result we obtained before in the holographic s-wave superfluids (see section 3.2.4). The symmetry breaking of the rotational symmetry has no effect on these modes. As discussed before, the coupling between the current $\langle J^{3\perp}\rangle$ and the momentum $\langle T^{t\perp}\rangle$ is known as the thermoelectric effect which we will study in section 4.1.2.

Block 2 - Parity odd The response due to the fluctuations $a_\perp^1$, $a_\perp^2$ and $\Psi_x = g^{xx}h_{xy}$ is given by

$$\begin{aligned}
\langle J^{1\perp}\rangle =& \frac{2r_H^2}{g^2}\left(a_\perp^1\right)_2^B - \frac{\left(\mu^2+\omega^2\right)}{2g^2}\left(a_\perp^1\right)_0^B + \frac{\mathrm{i}\mu\omega}{g^2}\left(a_\perp^2\right)_0^B \\
&- \frac{2r_H^2 w_2^B}{g^2}\left(\Psi_x\right)_0^B = \\
=& \frac{2r_H^2}{g^2}\left(a_\perp^1\right)_2^B - \frac{\left(\mu^2+\omega^2\right)}{2g^2}\left(a_\perp^1\right)_0^B + \frac{\mathrm{i}\mu\omega}{g^2}\left(a_\perp^2\right)_0^B \\
&- \langle\mathcal{J}^{1x}\rangle\left(\Psi_x\right)_0^B, \\
\langle J^{2\perp}\rangle =& \frac{2r_H^2}{g^2}\left(a_\perp^2\right)_2^B - \frac{\left(\mu^2+\omega^2\right)}{2g^2}\left(a_\perp^2\right)_0^B - \frac{\mathrm{i}\mu\omega}{g^2}\left(a_\perp^1\right)_0^B, \\
\langle T^{x\perp}\rangle =& \frac{2r_H^4}{\kappa^2}\left(\Psi_x\right)_4^B - \frac{5}{\kappa^2}\left(-\left(-8f_4^B + m_0^B\right)r_H^4 + \frac{\omega^4}{32}\right)\left(\Psi_x\right)_0^B = \\
=& \frac{2r_H^4}{\kappa^2}\left(\Psi_x\right)_4^B - \left(\langle\mathcal{T}^{xx}\rangle + \frac{5\omega^4}{32\kappa^2}\right)\left(\Psi_x\right)_0^B.
\end{aligned} \tag{4.73}$$

Due to the length of the expressions from now on we do not state the ω dependence explicitly. Again we define the Green's functions as

$$\begin{pmatrix} \langle J^{1\perp} \rangle \\ \langle J^{2\perp} \rangle \\ \langle T^{x\perp} \rangle \end{pmatrix} = \begin{pmatrix} G^{1\perp,1\perp} & G^{1\perp,2\perp} & G^{1\perp,x\perp} \\ G^{2\perp,1\perp} & G^{2\perp,2\perp} & G^{2\perp,x\perp} \\ G^{x\perp,1\perp} & G^{x\perp,2\perp} & G^{x\perp,x\perp} \end{pmatrix} \begin{pmatrix} \left(a_\perp^1\right)_0^B \\ \left(a_\perp^2\right)_0^B \\ \left(\Psi_x\right)_0^B \end{pmatrix} , \tag{4.74}$$

where the matrix of Green's functions is given by

$$\begin{pmatrix} \frac{2r_H^2}{g^2}\frac{\left(a_\perp^1\right)_2^B}{\left(a_\perp^1\right)_0^B} - \frac{\mu^2+\omega^2}{2g^2} & \frac{2r_H^2}{g^2}\frac{\left(a_\perp^1\right)_2^B}{\left(a_\perp^2\right)_0^B} + \frac{\mathrm{i}\omega\mu}{g^2} & \frac{2r_H^2}{g^2}\frac{\left(a_\perp^1\right)_2^B}{\left(\Psi_x\right)_0^B} - \langle \mathcal{J}_1^x \rangle \\ \frac{2r_H^2}{g^2}\frac{\left(a_\perp^2\right)_2^B}{\left(a_\perp^1\right)_0^B} - \frac{\mathrm{i}\omega\mu}{g^2} & \frac{2r_H^2}{g^2}\frac{\left(a_\perp^2\right)_2^B}{\left(a_\perp^2\right)_0^B} - \frac{\mu^2+\omega^2}{2g^2} & \frac{2r_H^2}{g^2}\frac{\left(a_\perp^2\right)_2^B}{\left(\Psi_x\right)_0^B} \\ \frac{2r_H^4}{\kappa^2}\frac{\left(\Psi_x\right)_4^B}{\left(a_\perp^1\right)_0^B} - \langle \mathcal{J}_1^x \rangle & \frac{2r_H^4}{\kappa^2}\frac{\left(\Psi_x\right)_4^B}{\left(a_\perp^2\right)_0^B} & \frac{2r_H^4}{\kappa^2}\frac{\left(\Psi_x\right)_4^B}{\left(\Psi_x\right)_0^B} - \langle \mathcal{T}^{xx} \rangle - \frac{5\omega^4}{32\kappa^2} \end{pmatrix} . \tag{4.75}$$

Note that here it has to be taken into account that all the physical fields are sourcing each other. Thus the ratios in the off-diagonal components have to be included. We explain the notation above by means of an example, namely let us set the initial conditions $\left(a_\perp^1\right)_0^H = 0 = (\Psi_x)_0^H$ and $\left(a_\perp^2\right)_0^H = 1 r_H$ [13] at the horizon. Since the equations are coupled (cf. eq. (4.46)), we not only obtain non-trivial values for $\left(a_\perp^2\right)_2^B$, but also for $\left(a_\perp^1\right)_2^B$ and $(\Psi_x)_4^B$. Hence, for instance, in the $1,2$ component the ratio $\left(a_\perp^1\right)_2^B / \left(a_\perp^2\right)_0^B$ is proportional to the Green's function describing the mixing of the corresponding dual operators. In section 4.2.6 an algorithm to compute these correlators using numerical methods is presented.

Due to the breaking of rotational symmetry we see a new coupling between the currents $\langle J^{1\perp} \rangle$, $\langle J^{2\perp} \rangle$ and the stress tensor $\langle T^{x\perp} \rangle$ in this subset of the fluctuations. This new coupling generates some interesting new physical effect: it induces a non-universal behaviour of the ratio between shear viscosity to entropy density (opposed to the yz case shown above) and a flexoelectric effect known from nematic crystals. We present the interpretation of these effects in our setup in a later section.

4.2.5.3 Helicity zero modes

The Green's functions related to the helicity zero modes are the most challenging ones to obtain. Not only because there are more fields involved than in any other block, but rather since here two effects we saw separately in the helicity one case have to be combined, namely the coupling of physical modes to physical modes and to non-dynamical fields. Besides, the relevant physical modes, which were

[13] We have to include one power of r_H to get the units right. In case of a non-vanishing metric fluctuation at the horizon we do not have to multiply the 1 by r_H, since these fields are dimensionless.

derived in section 4.2.2, are far more complicated than the ones of the other cases. At least, for $k = 0$ these modes can be split into two blocks, one transforming oddly (block 1) and the other evenly (block 2) under $P_{\|}$.

Block 1 - Parity odd The first block is composed by the modes $\{a_t^1, a_t^2, a_x^3, \xi_{tx} = g_{xx}h_{tx}\}$. The corresponding conjugate momenta are

$$\begin{aligned}
\langle J^{1t}\rangle =&\frac{1}{(\omega^2-\mu^2)}\left(\frac{2r_H^2\phi_2^B}{g^2}\left(\mu\left(a_t^1\right)_0^B+\mathrm{i}\omega\left(a_t^2\right)_0^B\right)\right.\\
&\left.+\frac{2r_H^2 w_2^B}{g^2}\mu\left(a_x^3\right)_0^B\right)=\\
=&\frac{1}{(\omega^2-\mu^2)}\left(-\langle\mathcal{J}^{3t}\rangle\left(\mu\left(a_t^1\right)_0^B+\mathrm{i}\omega\left(a_t^2\right)_0^B\right)+\mu\langle\mathcal{J}^{1x}\rangle\left(a_x^3\right)_0^B\right),\\
\langle J^{2t}\rangle =&\frac{1}{(\omega^2-\mu^2)}\left(\frac{2r_H^2\phi_2^B}{g^2}\left(\mathrm{i}\omega\left(a_t^1\right)_0^B-\mu\left(a_t^2\right)_0^B\right)\right.\\
&\left.+\frac{2r_H^2 w_2^B}{g^2}\mathrm{i}\omega\left(a_x^3\right)_0^B\right)=\\
=&\frac{1}{(\omega^2-\mu^2)}\left(-\langle\mathcal{J}^{3t}\rangle\left(\mathrm{i}\omega\left(a_t^1\right)_0^B-\mu\left(a_t^2\right)_0^B\right)+\mathrm{i}\omega\langle\mathcal{J}^{1x}\rangle\left(a_x^3\right)_0^B\right),\\
\langle J^{3x}\rangle =&\frac{2r_H^2}{g^2}\left(a_x^3\right)_2^B-\frac{\omega^2}{2g^2}\left(a_x^3\right)_0^B+\frac{2r_H^2\phi_2^B}{g^2}\left(\xi_{tx}\right)_0^B=\\
=&\frac{2r_H^2}{g^2}\left(a_x^3\right)_2^B-\frac{\omega^2}{2g^2}\left(a_x^3\right)_0^B-\langle\mathcal{J}^{3t}\rangle\left(\xi_{tx}\right)_0^B,\\
\langle T^{tx}\rangle =&-\frac{3m_0^B r_H^4}{\kappa^2}\left(\xi_{tx}\right)_0^B+\frac{2r_H^2\phi_2^B}{g^2}\left(a_x^3\right)_0^B=\\
=&-\langle\mathcal{T}^{tt}\rangle\left(\xi_{tx}\right)_0^B-\langle\mathcal{J}^{3t}\rangle\left(a_x^3\right)_0^B.
\end{aligned}\tag{4.76}$$

Before we continue to compute the Green's functions there is one subtlety that needs to be addressed. As discussed in section 4.2.2, there is a residual gauge freedom left which has to be taken into account to obtain physically sensible observables. Using the gauge transformations given in (4.41) for $k = 0$ and setting $K_t = K_r = \Lambda_0^3 = 0$, since they do not affect the fields discussed in this block, we obtain the unique gauge invariant linear combination

$$\Phi_4 = a_x^3 + w\frac{\mathrm{i}\omega a_t^2+\phi a_t^1-w\phi\xi_{tx}}{\phi^2-\omega^2}\tag{4.77}$$

The boundary expansion of Φ_4 is

$$\begin{aligned}
\Phi_4(r)|_{r->\infty} \simeq&\left(\Phi_4\right)_0^B+\left(\Phi_4\right)_2^B\frac{r_H^2}{r^2}=\\
=&\left(a_x^3\right)_0^B+\left(\left(a_x^3\right)_2^B+w_2^B\frac{\mu\left(a_t^1\right)_0^B+\mathrm{i}\omega\left(a_t^2\right)_0^B}{\mu^2-\omega^2}\right)\frac{r_H^2}{r^2},
\end{aligned}\tag{4.78}$$

where we used the boundary expansion (4.54) of the fields a_t^1, a_t^2, a_x^3 and ξ_{tx}. Note that terms with $\ln(r_H/r)$ are not of interest here, since the expectation values

were already regularised. The important fact is that the coefficient of $(r_H/r)^2$ is gauge invariant by construction, while $\left(a_x^3\right)_2^B$ is not. Thus to obtain a physical Green's function, i.e. which is invariant under gauge transformations, it has to be proportional to the ratio $(\Phi_4)_2^B / (\Phi_4)_0^B$, rather than $\left(a_x^3\right)_2^B / \left(a_x^3\right)_0^B$. An easy way to implement this, is by adding and subtracting the missing terms to the current $\langle J^{3x}\rangle$, that is

$$\begin{aligned}\langle J^{3x}\rangle =&\frac{2r_H^2}{g^2}\left(\left(a_x^3\right)_2^B + w_2^B\frac{\mu\left(a_t^1\right)_0^B + \mathrm{i}\omega\left(a_t^2\right)_0^B}{\mu^2-\omega^2}\right)\\ &-\left(\frac{2r_H^2 w_2^B}{g^2}\frac{\mu\left(a_t^1\right)_0^B + \mathrm{i}\omega\left(a_t^2\right)_0^B}{\mu^2-\omega^2}\right)+\cdots =\\ =&\frac{2r_H^2}{g^2}(\Phi_4)_2^B - \langle\mathcal{J}^{1x}\rangle\left(\frac{\mu\left(a_t^1\right)_0^B + \mathrm{i}\omega\left(a_t^2\right)_0^B}{\mu^2-\omega^2}\right)+\dots ,\end{aligned} \tag{4.79}$$

where the ellipsis stands for the remaining terms of the relevant equation in (4.76). In addition the adding of this zero renders our Green's function matrix symmetric. It is defined by

$$\begin{pmatrix}\langle J^{1t}\rangle\\ \langle J^{2t}\rangle\\ \langle J^{3x}\rangle\\ \langle T^{tx}\rangle\end{pmatrix} = \begin{pmatrix}G^{1t,1t} & G^{1t,2t} & G^{1t,3x} & G^{1t,tx}\\ G^{2t,1t} & G^{2t,2t} & G^{2t,3x} & G^{2t,tx}\\ G^{3x,1t} & G^{3x,2t} & G^{3x,3x} & G^{3x,tx}\\ G^{tx,1t} & G^{tx,2t} & G^{tx,3x} & G^{tx,tx}\end{pmatrix}\begin{pmatrix}\left(a_t^1\right)_0^B\\ \left(a_t^2\right)_0^B\\ (\Phi_4)_0^B\\ \left(\xi_{tx}\right)_0^B\end{pmatrix},$$

which explicitly written in terms of the field theory expectation values is

$$\mathcal{G}_{(1)}(\omega) = \begin{pmatrix}\frac{\mu}{\mu^2-\omega^2}\langle\mathcal{J}^{3t}\rangle & \frac{\mathrm{i}\omega}{\mu^2-\omega^2}\langle\mathcal{J}^{3t}\rangle & \frac{-\mu}{\mu^2-\omega^2}\langle\mathcal{J}^{1x}\rangle & 0\\ \frac{-\mathrm{i}\omega}{\mu^2-\omega^2}\langle\mathcal{J}^{3t}\rangle & \frac{\mu}{\mu^2-\omega^2}\langle\mathcal{J}^{3t}\rangle & \frac{\mathrm{i}\omega}{\mu^2-\omega^2}\langle\mathcal{J}^{1x}\rangle & 0\\ \frac{-\mu}{\mu^2-\omega^2}\langle\mathcal{J}^{1x}\rangle & \frac{-\mathrm{i}\omega}{\mu^2-\omega^2}\langle\mathcal{J}^{1x}\rangle & G^{3x,3x}(\omega) & -\langle\mathcal{J}^{3t}\rangle\\ 0 & 0 & -\langle\mathcal{J}^{3t}\rangle & -\langle\mathcal{T}^{tt}\rangle\end{pmatrix}. \tag{4.80}$$

The matrix is completely determined by the equilibrium solution, except for one entry, namely the correlator generated by Φ_4, which in terms of the parity odd helicity zero modes reads

$$\begin{aligned}G^{3x,3x}(\omega) =&\frac{2r_H^2}{g^2}\frac{(\Phi_4)_2^B}{(\Phi_4)_0^B} - \frac{\omega^2}{2g^2} =\\ =&\frac{2r_H^2}{g^2}\frac{1}{(a_x^3)_0^B}\left(\left(a_x^3\right)_2^B + w_2^B\frac{\mu\left(a_t^1\right)_0^B + i\omega\left(a_t^2\right)_0^B}{\mu^2-\omega^2}\right) - \frac{\omega^2}{2g^2}.\end{aligned} \tag{4.81}$$

Thus all entries of $\mathcal{G}_{(1)}$ are gauge invariant.

Block 2 - Parity even The fields left to discuss are $\{a_t^3, a_x^2, a_x^1, \xi_t, \xi_y, \xi_x\}$, which transform evenly under the parity transformation $P_{\|}$. Again we first state the conjugate momenta at the boundary associated to these fields, that is[14]

$$\begin{aligned}
\langle J^{1x}\rangle =&\frac{2r_H^2}{g^2}\left(a_x^1\right)_2^B - \frac{\left(\mu^2+\omega^2\right)}{2g^2}\left(a_x^1\right)_0^B + \frac{\mathrm{i}\mu\omega}{g^2}\left(a_x^2\right)_0^B \\
&+ \frac{r_H^2 w_2^B}{g^2}((\xi_t)_0^B - (\xi_x)_0^B + (\xi_\perp)_0^B) = \\
=&\frac{2r_H^2}{g^2}\left(a_x^1\right)_2^B - \frac{\left(\mu^2+\omega^2\right)}{2g^2}\left(a_x^1\right)_0^B + \frac{\mathrm{i}\mu\omega}{g^2}\left(a_x^2\right)_0^B \\
&+ \frac{1}{2}\langle\mathcal{J}^{1x}\rangle((\xi_t)_0^B - (\xi_x)_0^B + (\xi_\perp)_0^B)\,, \\
\langle J^{2x}\rangle =&\frac{2r_H^2}{g^2}\left(a_x^2\right)_2^B - \frac{\mathrm{i}\mu\omega}{g^2}\left(a_x^1\right)_0^B - \frac{\left(\mu^2+\omega^2\right)}{2g^2}\left(a_x^2\right)_0^B\,, \\
\langle J^{3t}\rangle =&\frac{2\mathrm{i}r_H^2 w_2^B}{g^2\omega}\left(a_x^2\right)_0^B = \frac{\mathrm{i}}{\omega}\langle\mathcal{J}^{1x}\rangle\left(a_x^2\right)_0^B\,, \\
\langle T^{tt}\rangle =&\frac{r_H^4}{2\kappa^2}\left(8f_4^B - m_0^B\right)(\xi_x)_0^B + \frac{r_H^4}{2\kappa^2}\left(-4f_4^B - m_0^B\right)(\xi_\perp)_0^B \\
&- \frac{3m_0^B r_H^4}{2\kappa^2}(\xi_t)_0^B - \frac{2r_H^2 w_2^B}{g^2}\left(a_x^1\right)_0^B + \frac{2\mathrm{i}\mu r_H^2 w_2^B}{g^2\omega}\left(a_x^2\right)_0^B = \\
=&-\frac{1}{2}\langle\mathcal{T}^{xx}\rangle(\xi_x)_0^B - \frac{1}{2}\langle\mathcal{T}^{yy}\rangle(\xi_\perp)_0^B - \frac{1}{2}\langle\mathcal{T}^{tt}\rangle(\xi_t)_0^B \\
&- \langle\mathcal{J}^{1x}\rangle\left(a_x^1\right)_0^B + \frac{\mathrm{i}\mu}{\omega}\langle\mathcal{J}^{1x}\rangle\left(a_x^2\right)_0^B\,,
\end{aligned} \tag{4.82}$$

and

$$\begin{aligned}
\langle T^{xx}\rangle =&-\frac{2r_H^4}{\kappa^2}(\xi_\perp)_4^B(\omega) + \frac{r_H^4}{2\kappa^2}\left(-8f_4^B + m_0^B\right)(\xi_t)_0^B(\omega) \\
&+ \frac{r_H^4}{\kappa^2}\left(8f_4^B - \frac{5m_0^B}{2}\right)(\xi_x)_0^B(\omega) - \frac{r_H^4}{\kappa^2}\left(6f_4^B + \frac{3m_0^B}{2}\right)(\xi_\perp)_0^B(\omega) \\
&- \frac{2r_H^2 w_2^B}{g^2}\left(a_x^1\right)_0^B(\omega) + \frac{2\mathrm{i}\mu r_H^2 w_2^B}{g^2\omega}\left(a_x^2\right)_0^B(\omega)\,, \\
\langle T^{yy}\rangle =&\frac{2r_H^4}{\kappa^2}(\xi_y)_4^B + \frac{r_H^4}{2\kappa^2}\left(4f_4^B + m_0^B\right)\left((\xi_t)_0^B + (\xi_x)_0^B + (\xi_z)_0^B - (\xi_y)_0^B\right)\,, \\
\langle T^{zz}\rangle =&\frac{2r_H^4}{\kappa^2}(\xi_z)_4^B + \frac{r_H^4}{2\kappa^2}\left(4f_4^B + m_0^B\right)\left((\xi_t)_0^B + (\xi_x)_0^B + (\xi_y)_0^B - (\xi_z)_0^B\right)\,,
\end{aligned} \tag{4.83}$$

where $\xi_\perp = \xi_y + \xi_z$. In the last two cases we have not identified the background expansion coefficients with the corresponding expectation values, since the gauge fixing changes many of the numerical prefactors.

The second block is composed by the modes $\{a_t^3,\, a_x^2,\, a_x^1,\, \xi_t,\, \xi_y,\, \xi_z,\, \xi_x\}$, which combine to three physical fields. The combinations were defined in (4.42). However,

[14]For legibility reasons, we do not state the terms with higher powers of ω, since they are of no interest to us.

in this section we choose $k = 0$, in which case they reduce to (again $\xi_\perp = \xi_y + \xi_z$)

$$\begin{aligned}
\Phi_1 &= a_x^1 - \frac{rfw'}{4\,(f+rf')}\xi_\perp\,,\\
\Phi_2 &= a_x^2 + \frac{\mathrm{i}w}{\omega}a_t^3 - \frac{\mathrm{i}w\phi}{2\omega}\xi_t + \frac{\mathrm{i}rfw\,(2\phi N\sigma' + \phi N'\sigma - 2\phi' N\sigma)}{8\omega N\sigma\,(f+rf')}\xi_\perp\\
\Phi_3 &= \xi_x + \frac{2rf' - f}{2(f+rf')}\xi_\perp\,,
\end{aligned} \tag{4.84}$$

As in the previous case, we have to recast the conjugate momenta to get gauge invariant Green's functions. To fix the gauge freedom, we first examine the boundary expansion of Φ_1, Φ_2 and Φ_3, namely

$$\begin{aligned}
\Phi_1 &= \left(a_x^1\right)_0^B + \left(\left(a_x^1\right)_2^B + \frac{w_2^B}{2}\left(\xi_\perp\right)_0^B\right)\frac{r_H^2}{r^2}\,,\\
\Phi_2 &= \left(a_x^2\right)_0^B + \left(\left(a_x^2\right)_2^B + \mathrm{i}\frac{w_2^B}{\omega}\left(a_t^3\right)_0^B - \mathrm{i}\frac{w_2^B\mu}{2\omega}\left(\left(\xi_t\right)_0^B - \mathrm{i}\frac{1}{2}\left(\xi_\perp\right)_0^B\right)\right)\frac{r_H^2}{r^2}\,,\\
\Phi_3 &= \left(\xi_x\right)_0^B - \frac{1}{2}\left(\xi_\perp\right)_0^B + \left(-\frac{3}{2}\left(\xi_\perp\right)_4^B - \alpha^2 w_2^B\left(a_x^1\right)_0^B + \mathrm{i}\frac{\alpha^2 w_2^B\mu}{\omega}\left(a_x^2\right)_0^B\right.\\
&\quad\left. + \left(2f_4^B - m_0^B\right)\left(\xi_x\right)_0^B - \left(7f_4^B + m_0^B\right)\left(\xi_\perp\right)_0^B\right)\frac{r_H^4}{r^4}\,.
\end{aligned} \tag{4.85}$$

Next we identify the expansion above with the expansion coefficients of the fields, i.e. we can rewrite above expressions in terms of

$$\begin{aligned}
\Phi_1 &= \left(\Phi_1\right)_0^B + \left(\Phi_1\right)_2^B\frac{r_H^2}{r^2}\,,\\
\Phi_2 &= \left(\Phi_2\right)_0^B + \left(\Phi_2\right)_2^B\frac{r_H^2}{r^2} \quad \text{and}\\
\Phi_3 &= \left(\Phi_3\right)_0^B + \left(\Phi_3\right)_4^B\frac{r_H^4}{r^4}\,.
\end{aligned} \tag{4.86}$$

Due to the form of the asymptotic behaviour shown above, from here on we redefine our fields in the following way

$$\begin{aligned}
\xi_p(\omega, r) &= \xi_x(\omega, r) + \frac{1}{2}\left(\xi_y(\omega, r) + \xi_z(\omega, r)\right)\,,\\
\xi_m(\omega, r) &= \xi_x(\omega, r) - \frac{1}{2}\left(\xi_y(\omega, r) + \xi_z(\omega, r)\right)\,.
\end{aligned} \tag{4.87}$$

In addition, a rotation of the a_x^1, a_x^2 fluctuations is performed into

$$a_x^+(\omega, r) = a_x^1(\omega, r) + \mathrm{i}\,a_x^2(\omega, r)\,, \quad a_x^-(\omega, r) = a_x^1(\omega, r) - \mathrm{i}\,a_x^2(\omega, r)\,. \tag{4.88}$$

Accordingly, we rotate the corresponding physical fields into $\Phi_\pm = \Phi_1 \pm \mathrm{i}\,\Phi_2$, so that their respective boundary values coincide with those of $a_x^\pm$. This parametrisation is more convenient, since the a_x^+ and a_x^- fields transform in the fundamental representation of the unbroken $U(1)$. That is, they behave in a similar fashion

as electrically charged vector mesons do under the $U(1)_{\rm em}$ or alternatively the W bosons in the Standard Model. To make contact with the unbroken phase, we keep the parametrisation also in the broken phase. Notice that these fields are conjugate of one another: $(a^{\pm}(\omega))^* = a^{\mp}(-\omega)$.

Next the gauge invariant Green's functions are again constructed by adding a zero in the same way done above for the parity odd block. However, to secure readability we omit the steps in between (they are the same as before) and jump directly to the result.

The Green's function matrix of this block is

$$\begin{pmatrix} \langle J^{3t}\rangle \\ \langle J^{x}_{+}\rangle \\ \langle J^{x}_{-}\rangle \\ \langle \frac{1}{2}\left(T^{xx}-T^{\perp\perp}\right)\rangle \\ \langle \frac{1}{2}\left(T^{xx}+T^{\perp\perp}\right)\rangle \\ \langle T^{tt}\rangle \end{pmatrix} = \mathcal{G}_{(2)} \begin{pmatrix} \left(a^3_t\right)^B_0 \\ \left(\Phi_+\right)^B_0 \\ \left(\Phi_-\right)^B_0 \\ \left(\Phi_3\right)^B_0 \\ \left(\xi_p\right)^B_0 \\ \left(\xi_t\right)^B_0 \end{pmatrix} , \tag{4.89}$$

where $T^{\perp\perp} = T^{xx} + T^{yy}$ and the entries are denoted by

$$\mathcal{G}_{(2)} = \begin{pmatrix} G^{3t,3t} & G^{3t,x}_{+} & G^{3t,x}_{-} & G^{3t,m} & G^{3t,p} & G^{3t,t} \\ G^{x,3t}_{+} & G^{x,x}_{+,+} & G^{x,x}_{+,-} & G^{x,m}_{+} & G^{x,p}_{+} & G^{x,t}_{+} \\ G^{x,3t}_{-} & G^{x,x}_{-,+} & G^{x,x}_{-,-} & G^{x,m}_{-} & G^{x,p}_{-} & G^{x,t}_{-} \\ G^{m,3t} & G^{m,x}_{+} & G^{m,x}_{-} & G^{m,m} & G^{m,p} & G^{m,t} \\ G^{p,3t} & G^{p,x}_{+} & G^{p,x}_{-} & G^{p,m} & G^{p,p} & G^{p,t} \\ G^{t,3t} & G^{t,x}_{+} & G^{t,x}_{-} & G^{t,m} & G^{t,p} & G^{t,t} \end{pmatrix} . \tag{4.90}$$

Some comments are in order explaining the expectation values of equation (4.89) and the notation we use. Regarding the former, we derive $\langle \frac{1}{2}\left(T^{xx}-T^{\perp\perp}\right)\rangle$ and $\langle \frac{1}{2}\left(T^{xx}+T^{\perp\perp}\right)\rangle$ in section 4.2.7.3. Regarding the notation, note that the index m is related to Φ_3 field, since $(\Phi_3)^B_0 = (\xi_m)^B_0$. Furthermore the $\frac{x}{\pm}$ indices are related to the Φ_+ and Φ_- fields. Here all entries are functions of the background, except for the sector containing the physical fields and their couplings, which has to be computed numerically. This part of the Green's function matrix depends on the

boundary values (4.86). The different entries are

$$
\begin{aligned}
&G^{3t,3t} = G^{3t,m} = G^{3t,p} = G^{3t,t} = G^{m,3t} = G^{p,3t} = G^{t,3t} = 0\\
&G^{3t,x}_{+} = G^{x,3t}_{+} = \frac{1}{2\omega}\langle \mathcal{J}^{1x}\rangle\\
&G^{3t,x}_{-} = G^{x,3t}_{-} = -\frac{1}{2\omega}\langle \mathcal{J}^{1x}\rangle\\
&G^{x,p}_{+} = G^{p,x}_{+} = -\frac{\omega-\mu}{4\omega}\langle \mathcal{J}^{1x}\rangle\\
&G^{x,t}_{+} = G^{t,x}_{+} = \frac{\omega-\mu}{2\omega}\langle \mathcal{J}^{1x}\rangle\\
&G^{x,p}_{-} = G^{p,x}_{-} = -\frac{\omega+\mu}{4\omega}\langle \mathcal{J}^{1x}\rangle\\
&G^{x,t}_{-} = G^{t,x}_{-} = \frac{\omega+\mu}{2\omega}\langle \mathcal{J}^{1x}\rangle\\
&G^{m,p} = G^{p,m} = \frac{3}{8}\left(\langle \mathcal{T}^{tt}\rangle - 2\langle \mathcal{T}^{xx}\rangle\right)\\
&G^{m,t} = G^{t,m} = -\frac{1}{4}\left(\langle \mathcal{T}^{tt}\rangle - 2\langle \mathcal{T}^{xx}\rangle\right)\\
&G^{p,t} = G^{t,p} = \frac{1}{4}\langle \mathcal{T}^{tt}\rangle\\
&G^{p,p} = -\frac{3}{8}\langle \mathcal{T}^{tt}\rangle\\
&G^{t,t} = -\frac{1}{2}\langle \mathcal{T}^{tt}\rangle
\end{aligned}
\tag{4.91}
$$

$$
\begin{aligned}
G^{x,x}_{\pm,\pm}(\omega) &= \frac{2r_H^2}{g^2}\frac{(\Phi_\pm)_2^B(\omega)}{(\Phi_\pm)_0^B(\omega)} + \frac{1}{4g^2}(\omega\pm\mu)^2\,,\\
G^{x,x}_{\pm,\mp}(\omega) &= \frac{2r_H^2}{g^2}\frac{(\Phi_\pm)_2^B(\omega)}{(\Phi_\mp)_0^B(\omega)}\,,\\
G^{m,x}_{\pm}(\omega) &= \frac{4r_H^4}{3\kappa^2}\frac{(\Phi_3)_4^B(\omega)}{(\Phi_\pm)_0^B(\omega)} + \frac{\omega\mp\mu}{12\omega}\langle \mathcal{J}_1^x\rangle\,,\\
G^{x,m}_{\pm}(\omega) &= \frac{r_H^2}{g^2}\frac{(\Phi_\pm)_2^B(\omega)}{(\Phi_3)_0^B(\omega)} + \frac{\omega\mp\mu}{12\omega}\langle \mathcal{J}_1^x\rangle\,,\\
G^{m,m}(\omega) &= \frac{4r_H^4}{3\kappa_5^2}\frac{(\Phi_3)_4^B(\omega)}{(\Phi_3)_0^B(\omega)} + \frac{1}{3}\left(7\langle \mathcal{T}^{yy}\rangle + \langle \mathcal{T}^{xx}\rangle\right) - \frac{5}{4}\langle \mathcal{T}^{tt}\rangle\,.
\end{aligned}
\tag{4.92}
$$

4.2.6 Generating the Solutions

In this section we describe how to solve the equations of motion using numerical methods in *Mathematica*[15]. All the equations we solve in this chapter are ordinary first or second order linear differential equations. Therefore the built-in numerical solver function *NDsolve* is sufficient for our purpose.

The solving of the equations for the helicity two mode (section 4.2.5.1), the parity odd helicity one modes (first part of section 4.2.5.2) and the parity odd helicity

[15]Wolfram Mathematica

zero modes (first part of section 4.2.5.3) is straight forward. Complications arise in the remaining two parity even helicity one and zero blocks, since here we have to deal with a mixing of the different physical modes. This is known under operator mixing described in [103].

In the easier cases, there is exactly one free parameter for each block at the horizon (c.f. section 4.2.3.2), i.e. $(\Xi)_0^H$, $\left(a_y^3\right)_0^H$ and $\left(a_x^3\right)_0^H$. This is a consequence of our choice of incoming boundary conditions and the amount of physical fields present in each sector. We can set all this expansion coefficients to 1 since they only determine a overall scaling of the resulting function. Now we integrate to the boundary and fit the corresponding boundary expansion (see equations (4.52) and (4.54)) to the numerical result obtained. Finally we plug this expansion coefficients into the corresponding Green's functions derived in section 4.2.5, i.e. into the equations (4.69), (4.72) and (4.80). The results are discussed in the next section.

Next we review the algorithm to compute Green's function matrices in the case of operator mixing. For concreteness we present the algorithm for the second block of the helicity one fields where the fluctuations a_y^1, a_y^2 and Ψ_x mix (cf. second part of section 4.2.5.2). However, the same methodology applies to the relevant helicity zero block as well.

We start by defining the boundary conditions at the horizon for the vector $\Lambda^{\mathrm{T}}(r) = \left(a_y^1(r), a_y^2(r), \Psi_x(r)\right)$. On the one hand we demand incoming boundary conditions (cf. eq. (4.47)), that is

$$\Lambda_{(a)}^I(r \to r_H) \simeq \left(\frac{r}{r_H} - 1\right)^{-\frac{i\omega}{4\pi T}} \left(e_{(a)}^I + \dots\right) , \tag{4.93}$$

where the index I refers to the three fields a_y^1, a_y^2 and Ψ_x. Since 3 coupled second order differential equations have to be solved with incoming boundary conditions chosen at the horizon, we are left with three free parameters. We choose three linear independent conditions for these parameters. This generates three linear independent solutions for each function $a_y^1(r)$, $a_y^2(r)$ and $\Psi_x(r)$. The reasoning behind this approach is that the fields not only gain a non-trivial profile along the r direction if the field is switched on at the horizon but also through the coupling with the other fields. That is, if we choose, for instance, $\left(a_y^1\right)_0^H = 1$ while the other two parameters vanish, we still get non-trivial solutions for $a_y^2(r)$ and $\Psi_x(r)$. This solutions depend linearly on $\left(a_y^1\right)_0^B \propto \left(a_y^1\right)_0^H$, since the differential equations are linear in the fluctuations. It is important to remark that $\left(a_y^2\right)_0^B$ and $(\Psi_x)_0^B$ both vanish, since they are only proportional to $\left(a_y^2\right)_0^H$ and $(\Psi_x)_0^B$, respectively. Nevertheless, in general, the subleading terms are present. Note that from this solutions the off-diagonal terms in the Green's function matrix (4.75)

are gained. In order to generate all the possible solutions at once, we choose the three linear independent conditions at the horizon and plug our choices into the vectors $e_{(1)}$, $e_{(2)}$ and $e_{(3)}$, where we use

$$e_{(1)}^{\mathrm{T}} = (1,0,0)\,, \quad e_{(2)}^{\mathrm{T}} = (0,1,0)\,, \quad e_{(3)}^{\mathrm{T}} = (0,0,1)\,. \tag{4.94}$$

Each vector $e_{(1)}$ generates one solution for each field. Note that different choices are possible, however, we get the best numerical result (with least numerical error) using these set of vectors. Next the resulting functions are collected in a 3 by 3 matrix $H(r)$ defined by

$$H^I{}_a(z) = \Lambda^I_{(a)}(r)\,, \tag{4.95}$$

with $I = 1,2,3$ and $a = 1,2,3$. We also need the matrix

$$\mathcal{H}(r) = H(r)H(r_B)^{-1}\,, \tag{4.96}$$

which divides the fields by their value at the boundary.

By taking the derivative of this matrix with respect to r, we obtain $\mathcal{H}'(r) = H'(r)\cdot H(r_B)^{-1}$. This is nothing else but the holographic Green's function (4.75) up to some powers of r, which come from taking the derivative. Remember that the boundary expansions of the fields look like $a+b/r^i$. To obtain the Green's function matrix we have to multiply $\mathcal{H}'(r)$ by a matrix $A(r)$ which contains the correct powers of r to cancel the ones discussed above. For the case we are discussing here, $A(r)$ is given by

$$A(r_B) = \begin{pmatrix} -r_B^3 & 0 & 0 \\ 0 & -r_B^3 & 0 \\ 0 & 0 & -\frac{r_B^5}{2} \end{pmatrix}\,, \tag{4.97}$$

with r_B the value of the UV cut off. Note that when performing the computation on a computer we cannot take $r_B \to \infty$, however, a very big number is chosen, so that the numerical error is small.

Finally we obtain

$$G^R(\omega) = \lim_{r_B\to\infty} A(\omega, r_{\mathrm{bdy}})\mathcal{H}'(\omega, r_{\mathrm{bdy}})\,, \tag{4.98}$$

where $G^R(\omega)$ corresponds to, e.g., equation (4.75), up to contact terms. Note that we have to subtract the counterterms, determined in section 4.2.4, by hand to render our results finite.

Using the procedure described above, we automatically get the full Green's function matrices (up to counterterms) (4.75) and (4.92). For the latter there is another subtlety that has to be taken into account, namely that the physical fields are a

linear combination of the solutions. However, this is easily fixed by adding the leading and subleading terms of the solutions in the way shown in equation (4.85). The explicit results for the different modes are shown in the next section.

4.2.7 Transport Properties – Physical Interpretation

In this section we extract the transport properties of the holographic p-wave superfluid from the correlation functions in section 4.2.3. We split our analysis into distinct transport phenomena. We start with the thermoelectric effect perpendicular and parallel to the condensate. Then we discuss the different components of the shear viscosity tensor and the results we obtain for them holographically. Finally, we present the flexoelectric and piezoelectric effects originating from the coupling between flavour currents and energy-momentum tensor.

4.2.7.1 Thermoelectric Effect perpendicular to the Condensate

As discussed for the s-wave case in chapter 3, we can relate the results of (4.71) to the thermoelectric effect found in some condensed matter materials. We begin with the well known connection between electric $\langle J^{3\perp}\rangle = \langle J^{\perp}\rangle$[16] and thermal $\langle Q^{\perp}\rangle = \langle T^{t\perp}\rangle - \mu\langle J^{\perp}\rangle$ transport perpendicular to the condensate direction, i.e.

$$\begin{pmatrix}\langle J^{\perp}\rangle\\ \langle Q^{\perp}\rangle\end{pmatrix} = \begin{pmatrix}\sigma^{\perp\perp} & T\alpha^{\perp\perp}\\ T\alpha^{\perp\perp} & T\bar{\kappa}^{\perp\perp}\end{pmatrix}\begin{pmatrix}E_{\perp}\\ -(\nabla_{\perp}T)/T\end{pmatrix}, \tag{4.99}$$

where the electric field $E_{\perp}$ and the thermal gradient $-\nabla_{\perp}T/T$ are related to the background values of the gauge field $\left(a^3_{\perp}\right)^B_0$ and the metric $(\Psi_t)^B_0$. This identification is equivalent to the one in section 3.2.3,

$$\begin{aligned} E_{\perp} &= \mathrm{i}\omega\left(\left(a^3_{\perp}\right)^B_0 + \mu\,(\Psi_t)^B_0\right),\\ -\frac{\nabla_{\perp}T}{T} &= \mathrm{i}\omega\,(\Psi_t)^B_0\ . \end{aligned} \tag{4.100}$$

Putting everything together and comparing the relation of the electric and thermal transport to the corresponding equations for $\langle J^{\perp}\rangle$ and $\langle T^{t\perp}\rangle$ in (4.71), we can identify the coefficients in (4.99) as

$$\begin{aligned} \sigma^{\perp\perp} &= -\frac{\mathrm{i}G^{\perp,\perp}_{3,3}}{\omega} = -\frac{1}{g^2}\frac{\mathrm{i}}{\omega}\left(2r_H^2\frac{\left(a^3_{\perp}\right)^B_1}{\left(a^3_{\perp}\right)^B_0} - \frac{\omega^2}{2}\right),\\ T\alpha^{\perp\perp} &= -\frac{\mathrm{i}}{\omega}\left(G_3^{\perp t\perp} - \mu G^{\perp,\perp}_{3,3}\right) = \frac{\mathrm{i}}{\omega}\langle\mathcal{J}^t_3\rangle - \mu\sigma^{\perp\perp},\\ T\bar{\kappa}^{\perp\perp} &= -\frac{\mathrm{i}}{\omega}\left(G^{t\perp,t\perp} + \mu^2 G^{\perp,\perp}_{3,3}\right) = \frac{\mathrm{i}}{\omega}\langle\left(\mathcal{T}_{tt}\right\rangle - 2\mu\langle\mathcal{J}^t_3\rangle) + \mu^2\sigma^{\perp\perp}. \end{aligned} \tag{4.101}$$

These results are in agreement with all our findings in the s-wave case. Thus we interpret this result again as a description of the simultaneous transport of charge

[16] We use the index $\perp$ for either y or z. Note that all quantities are the same in both cases.

and heat (or energy). This means that an electric field not only leads to a current, but also to a heat flux and, conversely, a temperature gradient leads to an electric current in addition to a heat flux. Note that in this subset we do not observe any effect of the breaking of the rotational symmetry since all the fields are in the transverse direction to the condensate.

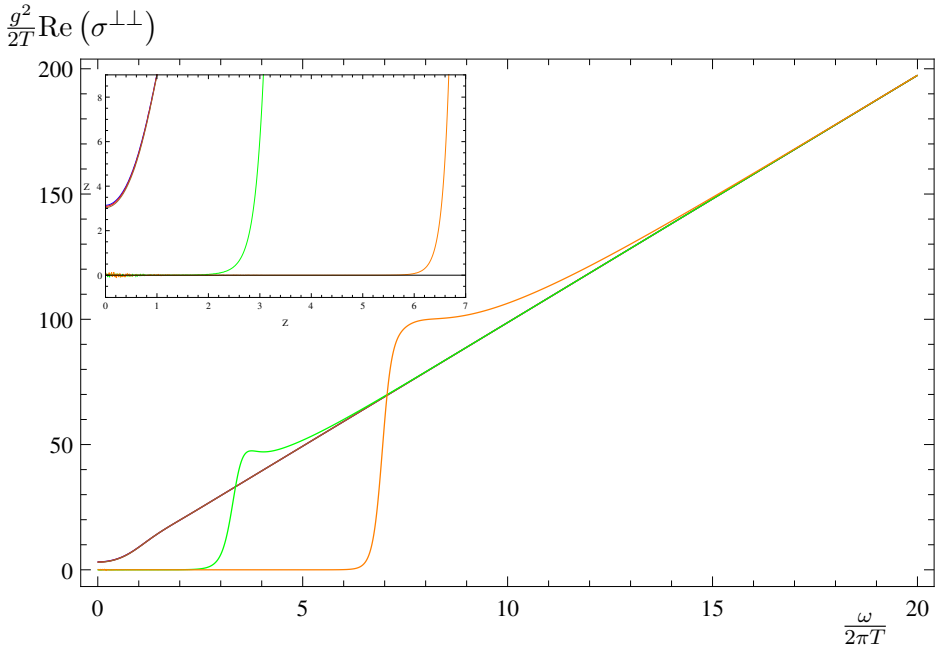

Figure 4.6: Real part of the conductivity $\mathrm{Re}(\sigma^{\perp\perp})$ over the frequency $\omega/(2\pi T)$ for $\alpha = 0.032$. The color coding is as follows: blue $T = \infty$, red $T = 1.34T_c$, brown $T = 1.00T_c$, green $T = 0.40T_c$, orange $T = 0.19T_c$. Note that the three curves with the highest temperature, blue, red and brown, are nearly on top of each other. The agreement of the curves in the $\omega \to 0$ limit is due to the small change in the strength of the Drude peak with temperature. Below T_c, the superfluid contribution to the delta peak at $\omega = 0$ is turned on and we obtain larger deviations from the $T = \infty$ curve, since the area below the curves has to be the same for all temperatures (sum rule). Furthermore the value for $\omega \to 0$ clearly asymptotes to 0 with decreasing temperature. Source: [2]

In figure 4.6, 4.7 and 4.8 we plot our numerical results for $\mathrm{Re}(\sigma^{\perp\perp})$ versus the reduced frequency $\omega/(2\pi T)$ for different values of α as defined in (4.4), namely $\alpha = 0.032 < \alpha_c$, $\alpha = 0.316 \lesssim \alpha_c$ and $\alpha = 0.447 > \alpha_c$, respectively. For large frequencies, i. e. $\omega \gg 2\pi T$, the conductivity depends linearly on the frequency (e.g. [104]),

$$\mathrm{Re}(\sigma^{\perp\perp}) \to \frac{\alpha^2}{{\kappa_5}^2}\pi\omega \qquad \text{for} \qquad \omega \gg 2\pi T\,. \tag{4.102}$$

We expect this behaviour on dimensional grounds, and as a consequence of the conformal symmetry in our system[17]. For temperatures $T < T_c$ we see a gap

[17] There is no lattice spacing which would spoil the high frequency behaviour.

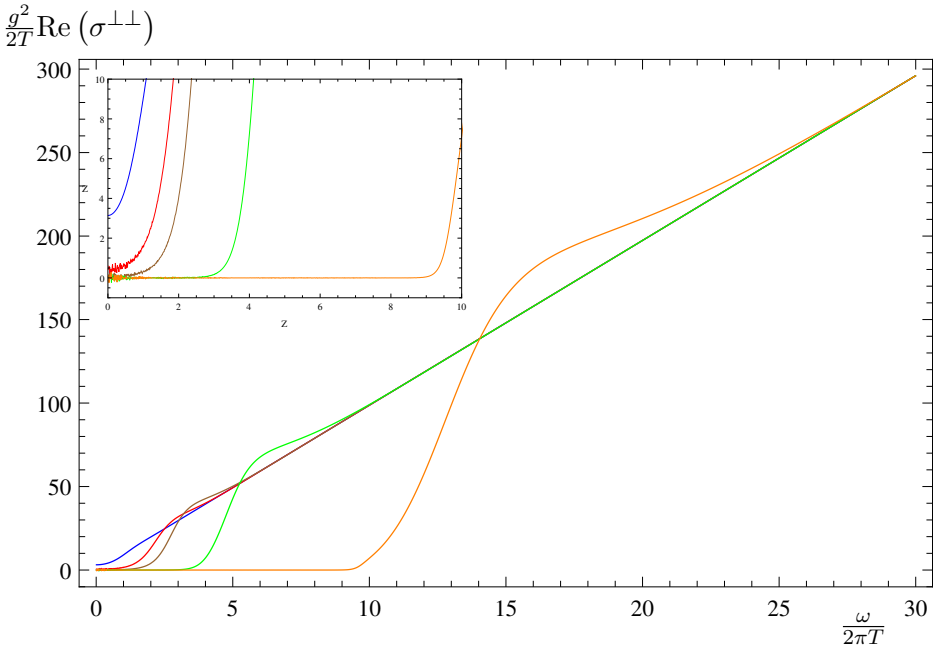

Figure 4.7: Real part of the conductivity $\mathrm{Re}(\sigma^{\perp\perp})$ over the frequency $\omega/(2\pi T)$ for $\alpha = 0.316$. The color coding is as follows: blue $T = \infty$, red $T = 1.00T_c$, brown $T = 0.88T_c$, green $T = 0.50T_c$, orange $T = 0.19T_c$. In this plot we see that the Drude peak has already a much stronger dependence on the temperature than in the $\alpha = 0.032$ case, since the blue and the red curve can be clearly distinguished. Below T_c the contributions of the superfluid phase to the delta peak leads again to a tendency of the curve to vanish for frequencies in the gap region, since the area below the curves have to be the same for all temperatures (sum rule). Source: [2]

opening up at small frequencies. The size of the gap increases as the temperature decreases. This gap is expected from superconductors. It ends at a frequency ω_g with a sharp increase of the conductivity. Beyond the gap the conductivity at temperature $T < T_c$ is larger than the corresponding values at temperatures $T > T_c$, such that the small temperature conductivities approach the asymptotic behaviour (4.102) from above (cf. [47–49]).

The value of $\mathrm{Re}(\sigma^{\perp\perp})$ at $\omega = 0$ approaches zero with decreasing temperature. Below T_c the tendency for this part of the conductivity to vanish increases. Nevertheless, we still find finite values even below T_c. However, these values are exponentially suppressed (c.f. [55]). In [98] it is shown that in the limit $T \to 0$ there is a hard gap, i. e. the value for the conductivity becomes zero. Thus in the p-wave, we can interpret the region between $\omega = 0$ and ω_g as a gap, opposed to the s-wave case (cf. [90]). Finally, we observe that an increase in α leads to a stronger suppression of the real part of the conductivity in the gap region.

Due to the sum rule for the conductivity, i.e. the frequency integral over the real

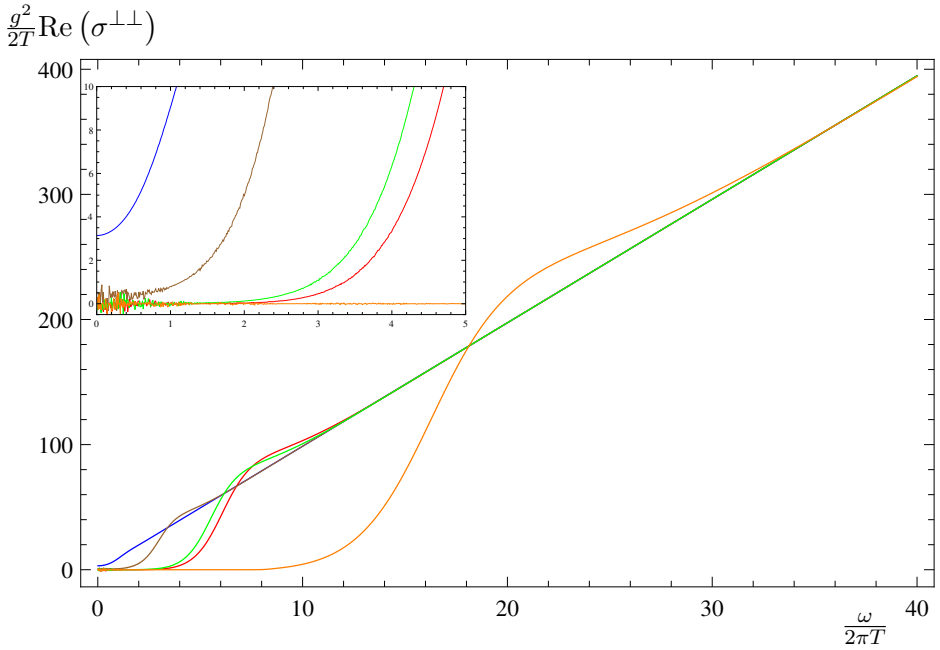

Figure 4.8: Real part of the conductivity $\mathrm{Re}(\sigma^{\perp\perp})$ over the frequency $\omega/(2\pi T)$ for $\alpha = 0.447$. The color coding is as follows: blue $T = \infty$, brown $T = 1.95T_c$, green $T = 1.00T_c$, red $T = 0.91T_c$, orange $T = 0.34T_c$. Again we see the same tendency as before for the curve to vanish at $\omega \to 0$ for decreasing temperatures. The strength of the Drude peak has a strong dependence on the temperatures, since the blue and the brown curve are quite far apart (both curves were computed for temperatures above T_c). Source: [2]

part of the conductivity is constant for all temperatures, a delta peak has to form at zero frequency which contains the "missing area" of the gaped region. The strength of the delta peak has two contributions: the first is proportional to what we call the perpendicular superfluid density $n_s^\perp$ in analogy to the behaviour found in superconductors (see [73]), $\mathrm{Re}(\sigma^{\perp\perp}) \sim \alpha^2/\kappa^2\ \pi n_s^\perp \delta(\omega)$ and appears only for temperatures below T_c. The second contribution is a consequence of the translation invariance of our system (c.f. [57]), the Drude peak, and appears for all temperatures.

The delta peak appears in the imaginary part of the conductivity as a pole. We can see this from Kramers-Kronig relation (see [55]), which leads to

$$\mathrm{Im}(\sigma^{\perp\perp}) \simeq \frac{A_D(\alpha, T)}{\omega} + \frac{A_s^\perp(\alpha)}{\omega}\left(1 - \frac{T}{T_c}\right), \tag{4.103}$$

for $T \lesssim T_c$, with $A_s^\perp(\alpha)\left(1 - \frac{T}{T_c}\right) \propto n_s^\perp$ and A_D parametrising the contribution from the Drude peak. In figure 4.9 we present the imaginary part of the conductivity $\omega\mathrm{Im}(\sigma^{\perp\perp})$ versus the frequency $\omega/(2\pi T)$ for $\alpha = 0.316$ and different temperatures. We see that $\omega\mathrm{Im}(\sigma^{\perp\perp})$ takes finite values for $\omega \to 0$ and $T < \infty$. The finite values above T_c are due to the Drude peak, i.e. the A_D part of (4.103).

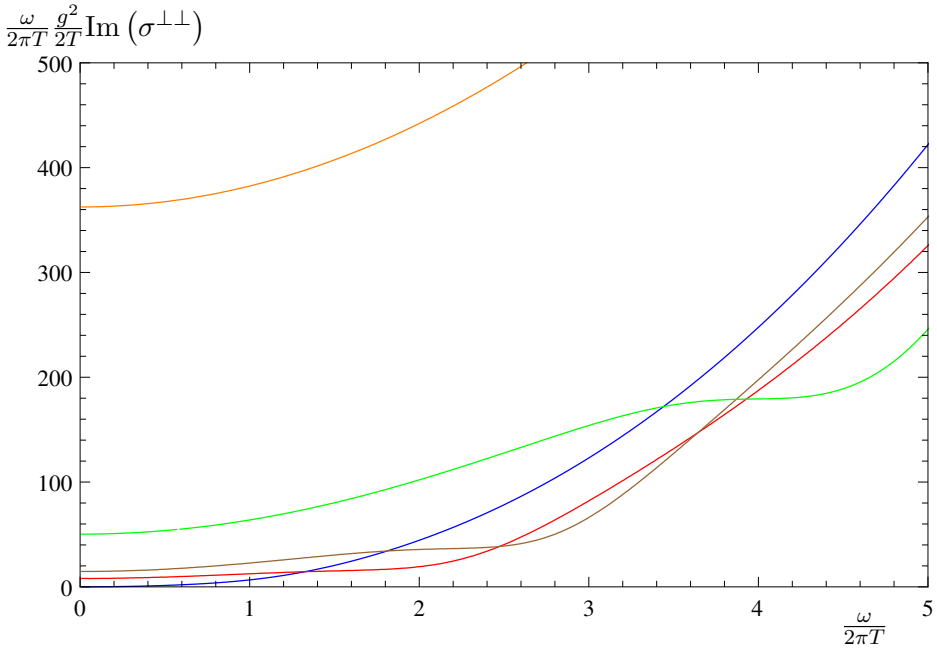

Figure 4.9: Imaginary part of the conductivity $\omega\mathrm{Im}(\sigma^{\perp\perp})$ over the frequency $\omega/(2\pi T)$ for $\alpha = 0.316$. The color coding is as follows: blue $T = \infty$, red $T = 1.00T_c$, brown $T = 0.88T_c$, green $T = 0.50T_c$, orange $T = 0.19T_c$. The curves in this plot have a constant value for $\frac{\omega}{2\pi T} \to 0$, which is determined by the δ-peak in the real part of the conductivity by the Kramers-Kronig relation. The values for this constant are, in the same order as the temperatures above: 0, 8.0, 14.7, 50.3 and 362.4. Note that we already see a finite value for $T = 1.00T_c$, this is due to the Drude peak. Below T_c the values at $\omega = 0$ are due to two contributions, first the Drude peak, as before, and second due to the superfluid density. Source: [2]

Below T_c we see a further contribution from the superfluid density. By analysing the temperature dependence of $\lim_{\omega\to 0}\omega\mathrm{Im}(\sigma^{\perp\perp})$, we get a smooth curve, which is, however, not differentiable at T_c, i.e. it behaves as equation (4.103) anticipates. Note that A_D and $A_s^{\perp}$ have a non trivial dependence on α. Finally, as expected, there is an increase in the superfluid density with decreasing temperature.

4.2.7.2 Thermoelectric Effect parallel to the Condensate

Similar to the presentation above, we see the thermoelectric effect parallel to the condensate as well, i.e. we look at charge transport and temperature gradients in the x direction. This is related to the first block of helicity zero states presented in section 4.2.5.3. However, in the case at hand, there is a slight complication in comparison to the last section due to a further coupling of the a_t^1 and a_t^2 fields to a_x^3 and to h_{tx} (see section 4.2.5.3).

We start again by relating the field theoretical quantities E_x and $\nabla_x T$ to the

corresponding boundary values of the dual fields $(\Phi_4)_0^B$ and $(\xi_{tx})_0^B$. As before we obtain

$$\begin{aligned} E_x &= \mathrm{i}\omega \left[(\Phi_4)_0^B + \mu \, (\xi_{tx})_0^B \right] , \\ -\frac{\nabla_x T}{T} &= \mathrm{i}\omega \, (\xi_{tx})_0^B \, . \end{aligned} \tag{4.104}$$

This modes source the charge current $\langle J^x \rangle = \langle J^{3x} \rangle$ in direction of the condensate and the heat flux $\langle Q^x \rangle = \langle T^{tx} \rangle - \mu \langle J^x \rangle$, respectively. The relation of these currents to the corresponding electrical field and temperature gradient defines the conductivity matrix (c.f. equation (4.99))

$$\begin{pmatrix} \langle J^x \rangle \\ \langle Q^x \rangle \end{pmatrix} = \begin{pmatrix} \sigma^{xx} & T\alpha^{xx} \\ T\alpha^{xx} & T\bar{\kappa}^{xx} \end{pmatrix} \begin{pmatrix} E_x \\ -(\nabla_x T)/T \end{pmatrix} . \tag{4.105}$$

Comparing this matrix to the lower right corner of the one in (4.80), we are able to identify the electric, thermal and thermoelectric conductivity related to the retarded Green's functions in the following way

$$\begin{aligned} \sigma^{xx} &= -\frac{\mathrm{i}}{\omega} G^{x,x}_{3,3} \, , \\ T\alpha^{xx} &= -\frac{\mathrm{i}}{\omega} \left(G^{xtx}_3 - \mu G^{x,x}_{3,3} \right) = \frac{\mathrm{i}}{\omega} \langle \mathcal{J}^t_3 \rangle - \mu \sigma^{xx} \, , \\ T\bar{\kappa}^{xx} &= -\frac{\mathrm{i}}{\omega} \left(G^{tx,tx} - 2\mu G^{xtx}_3 + \mu^2 G^{x,x}_{3,3} \right) = \frac{\mathrm{i}}{\omega} \left(\langle \mathcal{T}_{tt} \rangle - 2\mu \langle \mathcal{J}^t_3 \rangle \right) + \mu^2 \sigma^{xx} \, . \end{aligned} \tag{4.106}$$

The rest of the matrix (4.80) shows the response of the system due to the a^1_t, a^2_t fluctuations. Here we see the difference to the case discussed in the previous section, which arises due to the breaking of the rotational symmetry. In [47], the a^1_t, a^2_t fluctuation fields are interpreted as generating a rotation of the charge density in direction $\langle J^{1t} \rangle$ and $\langle J^{2t} \rangle$, however without changing its magnitude. The chemical potential then tries to pull the charge density back to $\langle J^{3t} \rangle$

The complete transport matrix of this block then reads

$$\begin{pmatrix} \langle \mathcal{J}^t_1 \rangle \\ \langle J^t_2 \rangle \\ \langle J^x \rangle \\ \langle Q^x \rangle \end{pmatrix} = \begin{pmatrix} \sigma^{t,t}_{1,1} & \sigma^{t,t}_{1,2} & \sigma^{t,x}_{1,3} & -\mu\sigma^{t,x}_{1,3} \\ \sigma^{t,t}_{2,1} & \sigma^{t,t}_{2,2} & \sigma^{t,x}_{2,3} & -\mu\sigma^{t,x}_{2,3} \\ \sigma^{x,t}_{3,1} & \sigma^{x,t}_{3,2} & \sigma^{xx} & T\alpha^{xx} \\ -\mu\sigma^{x,t}_{3,1} & -\mu\sigma^{x,t}_{3,2} & T\alpha^{xx} & T\bar{\kappa}^{xx} \end{pmatrix} \begin{pmatrix} i\omega a^1_t \\ i\omega a^2_t \\ E_x \\ -\frac{\nabla_x T}{T} \end{pmatrix} , \tag{4.107}$$

where each of the transport coefficients is simply related to the corresponding Green's function by $\sigma = -\mathrm{i}G/\omega$. We will now focus on the electric conductivity σ^{xx}, all the other components can either be obtained from it or are given by background fields (cf. (4.80)).

The numerical results for σ^{xx} are shown in figures 4.10 and 4.11 for $\alpha = 0.316 < \alpha_c$. As it is the case for the conductivity perpendicular to the condensate, the results for other values of α do not show any significant qualitative difference therefore we do not present them in this thesis.

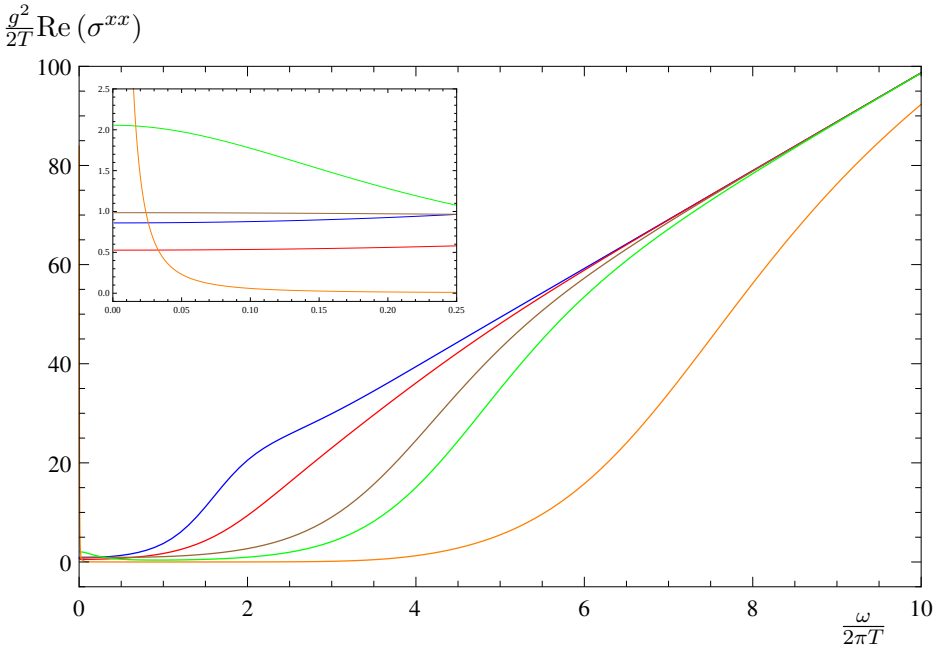

Figure 4.10: Real part of the conductivity $\mathrm{Re}(\sigma^{xx})$ over the frequency $\omega/(2\pi T)$ for $\alpha = 0.316$. The color coding is as follows: blue $T = 1.63T_c$, red $T = 0.98T_c$, brown $T = 0.88T_c$, green $T = 0.78T_c$, orange $T = 0.50T_c$. There is a delta peak at strictly $\omega = 0$, not noticeable in this figure, as dictated by the sum rule (the area below the curves has to be the same for any T). Source: [3]

Let us discuss the similarities and differences between σ^{xx} and $\sigma^{\perp\perp}$. The curve of the real part of σ^{xx} (fig. 4.10) shows the correct asymptotic behaviour for large frequencies [104], i. e. the real part is proportional to the frequency for all temperatures. More precisely, for $\omega \gg T$ we have (cf. section above)

$$\mathrm{Re}(\sigma^{xx}) \to \frac{\alpha^2}{\kappa_5^2}\pi\omega\,. \tag{4.108}$$

Both $\mathrm{Re}(\sigma^{xx})$ and $\mathrm{Re}(\sigma^{\perp\perp})$ have the same behaviour in the large frequency limit. In this limit all the effects due to finite temperature, finite chemical potential and symmetry breaking become negligible and we obtain the expected result for a conformal field theory.

For decreasing frequencies we see that the conductivity decreases until nearly vanishing. This sharp decrease is a known feature of superconductors. It is present for all temperatures, not only for $T < T_c$. However, for smaller temperatures the

decrease starts at larger values of ω. It is by far not as sharp as in $\sigma^{\perp\perp}$, and there are some qualitative differences: The bump before decreasing is absent for σ^{xx}. Thus the asymptotic value at large frequencies is approached by the curves from below, rather than from above, as it is the case for $\mathrm{Re}(\sigma^{\perp\perp})$. Besides, up to numerical inaccuracy, the conductivities do not seem to vanish for any frequency, for temperatures above $0.5T_c$. In comparison, the transverse conductivity has a far stronger temperature suppression in the gaped region. However, below $0.5T_c$ the situation seems to change dramatically as is explained in the next paragraph.

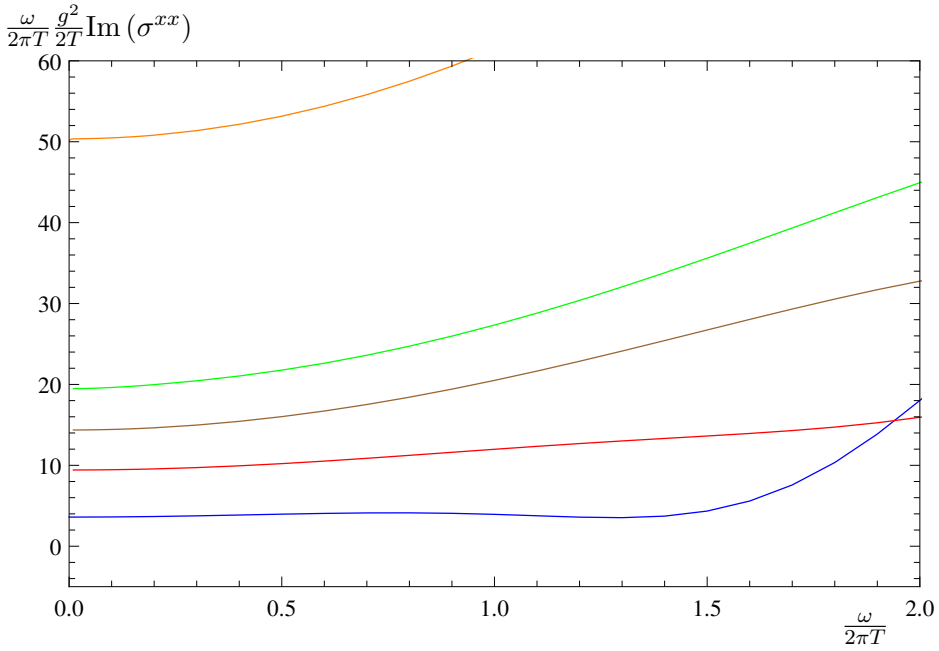

Figure 4.11: Imaginary part of the conductivity times the frequency, $\omega\mathrm{Im}(\sigma^{xx})$ over the frequency $\omega/(2\pi T)$ for $\alpha = 0.316$. The color coding is as follows: blue $T = 1.63T_c$, red $T = 0.98T_c$, brown $T = 0.88T_c$, green $T = 0.78T_c$, orange $T = 0.50T_c$. The curves tend to a constant value as $\omega \to 0$, which indicates the presence of a pole at the origin. This is related to the delta peak in the real part of σ^{xx}. Source: [3]

The real part of σ^{xx}, as opposed to the perpendicular case, increases again for small but finite frequencies and reaches a finite value in the $\omega \to 0$ limit, as seen in the zoomed region of figure 4.10. This increase of the real part in the zero frequency limit is due to a quasinormal mode which moves up the imaginary axis in the complex frequency plane (see the blue arrow in figure 4.20) and seems to reach the origin $\omega = 0$ at temperatures around $0.5T_c$. The increase we see towards the $\omega \to 0$ limit comes from the projection of the quasinormal mode onto the real frequency axis. Since the quasinormal mode moves in direction of the origin, this bump increases with decreasing temperature. Unfortunately it is challenging to compute the exact temperature when the mode arrives at the origin, since we have

to rely on numerical calculations. Nevertheless, for temperatures below $0.5T_c$ it seems that a pole is formed and at the same time the real part of the conductivity is more strongly suppressed at finite small frequencies in comparison to cases of temperatures above $0.5T_c$ (see the green and orange curve in zoomed region of figure 4.10). It seems that somewhere around $0.5T_c$, due to the quasinormal mode at the origin, the conductivity behaviour in direction of the condensate changes. It is challenging to understand this behaviour from a dual field theoretical point of view, since we do not know explicitly the dual field theory. At the time of writing we could not identify any real system with this behaviour. However, the broad peak in figure 4.10 resembles a Drude like behaviour (see for instance [105]). This would mean that besides some rotational breaking also the translational invariance is somehow spoiled. It would be very interesting to further examine the similarities and differences to a conventional Drude model.

Due to the pole in the imaginary part of the conductivity (see fig. 4.11) and the Kramers-Kronig relation [55] we know that at $\omega = 0$ the real part must have a delta peak. Again there are two main contributions to the prefactor of this delta peak, which depend on the temperature. Accordingly the pole in the imaginary part can be expressed as

$$\lim_{\omega\to 0} \omega \,\mathrm{Im}\left(\sigma^{xx}\right) \simeq A_D(\alpha, T) + A_s^x(\alpha)\left(1 - \frac{T}{T_c}\right) . \tag{4.109}$$

This is similar to the perpendicular case. In fact, the first contribution A_D is again a consequence of translational invariance in our system. The second contribution, A_s^x, appears when temperatures decrease below T_c. This prefactor is expected to be connected to the superfluid density n_s^x, which we expect to differ from $n_s^\perp$, since we do not have an isotropic condensate. In addition the values of $\lim_{\omega\to 0} \omega \,\mathrm{Im}\left(\sigma^{xx}\right)$ and $\lim_{\omega\to 0} \omega \,\mathrm{Im}\left(\sigma^{xx}\right)$ for values of $T \lesssim T_c$ differ from each other. Unfortunately we can not determine $n_s^\perp$ and n_s^x, since we do not know the contribution of A_D explicitly, neither do we know if A_D is the same in both cases.

The properties of the two components of the conductivities we state here are very similar to the ones found in the non-backreacted case (see [47]). Therefore corrections due to the backreaction seem to be rather small.

4.2.7.3 Viscosity Tensor in Anisotropic Fluids

Before we present our results for the components of the viscosity tensor in the isotropic and transversely isotropic case, i.e. a fluid with a $SO(2)$ rotational symmetry, we derive the general form of the energy-momentum tensor up to first order in fluctuations.

The equilibrium energy-momentum tensor plus its dissipative contribution $\Pi_{\mu\nu}$ is given by (cf. discussion in section 3.2.3)

$$T_{\mu\nu} = e u_\mu u_\nu + P\, P_{\mu\nu} + \Pi_{\mu\nu}\,, \tag{4.110}$$

with e the energy density, P the pressure u^μ the 4-velocity and $P_{\mu\nu} = \eta_{\mu\nu} + u_\mu u_\nu$, where $\eta_{\mu\nu}$ is the flat metric. Next we consider small fluctuations around the flat metric, i. e. $g_{\mu\nu} = \eta_{\mu\nu} + \epsilon h_{\mu\nu}(x^\mu)$. This leads to corrections of $T_{\mu\nu}$, which we take up to first order in ϵ into account and collect them in $\Pi_{\mu\nu}$. We derive the general form of $\Pi^{\mu\nu}$ in agreement with the symmetries below. However, there is a second contribution of order ϵ coming from the projector $P_{\mu\nu}$, which is not included in $\Pi^{\mu\nu}$. It is given by

$$\tilde{P}_{\mu\nu} = P_{\mu\nu} + \epsilon h_{\mu\nu}\,. \tag{4.111}$$

When computing $T_{\mu\nu}$ to order ϵ we not only have to take the transport coefficients we obtain from $\Pi_{\mu\nu}$ into account but also the contributions coming from $\tilde{P}_{\mu\nu}$, i.e.

$$T_{\mu\nu} = e u_\mu u_\nu + P\, P_{\mu\nu} + \epsilon P\, h_{\mu\nu} + \Pi_{\mu\nu}\,. \tag{4.112}$$

Note that in section 4.1.2 we found that the equilibrium energy-momentum tensor for the p-wave is isotropic therefore we can apply the same reasoning described above to that case. The kind of contributions we just discussed leads to contact terms in the Green's functions (cf. [57]).

In general, viscosity refers to the dissipation of energy due to some internal motion [106]. For an internal motion which describes a general translation or a general rotation, the dissipation is zero. Thus the dissipation depends on the gradient of the velocities u^μ in the combination $u_{\mu\nu} = \frac{1}{2}\left(\nabla_\mu u_\nu + \nabla_\nu u_\mu\right)$, and we may define a general dissipation function $\Xi = \frac{1}{2}\eta^{\mu\nu\lambda\rho} u_{\mu\nu} u_{\lambda\rho}$, where $\eta^{\mu\nu\lambda\rho}$ defines the viscosity tensor [107]. Its symmetries are given by

$$\eta^{\mu\nu\lambda\rho} = \eta^{\nu\mu\lambda\rho} = \eta^{\mu\nu\rho\lambda} = \eta^{\lambda\rho\mu\nu}\,. \tag{4.113}$$

The part of the stress tensor which is dissipative due to viscosity is defined as

$$\Pi^{\mu\nu} = -\frac{\partial \Xi}{\partial u_{\mu\nu}} = -\eta^{\mu\nu\lambda\rho} u_{\lambda\rho}\,. \tag{4.114}$$

In the case of a fluid in the rest frame $u^t = 1$, and to satisfy the Landau frame condition $u_\mu \Pi^{\mu\nu} = 0$, the stress energy tensor (and the viscosity tensor, correspondingly) must have non-zero components only in the spatial directions $i, j, \ldots = \{x, y, z\}$. In the most general case, only 21 independent components of η_{ijkl} appear in the expressions above.

For the particular case of an isotropic fluid, the tensor can be recast in terms of only 2 independent components. They are usually parametrised by the shear viscosity η and the bulk viscosity ζ, so that the dissipative part of the stress tensor can be expressed as $\Pi^{ij} = -2\eta(u^{ij} - \frac{1}{3}\delta^{ij}u^l_l) - \zeta u^l_l \delta^{ij}$ (see [107]).

For a transversely isotropic fluid, there are 5 independent components of η^{ijkl}. Without loss of generality, we choose the symmetry axis to be the x-axis. The non-zero components are parametrized by

$$\begin{aligned} &\eta^{xxxx} = \zeta_x + \frac{4}{3}\lambda\,, && \eta^{yyyy} = \eta^{zzzz} = \zeta_y + \frac{\lambda}{3} + \eta_{yz}\,, \\ &\eta^{xxyy} = \eta^{xxzz} = -\frac{2}{3}\lambda\,, && \eta^{yyzz} = \zeta_y + \frac{\lambda}{3} - \eta_{yz}\,, \\ &\eta^{yzyz} = \eta_{yz}\,, && \eta^{xyxy} = \eta^{xzxz} = \eta_{xy}\,. \end{aligned} \tag{4.115}$$

The non-zero off-diagonal components of the stress tensor are

$$\begin{aligned} &\Pi^{xy} = -2\eta_{xy}u_{xy} = -\frac{\mathrm{i}\omega}{2}\eta_{xy}h_{xy}\,, \qquad \Pi^{xz} = -2\eta_{xy}u_{xz} = -\frac{\mathrm{i}\omega}{2}\eta_{xy}h_{xz}\,, \\ &\Pi^{yz} = -2\eta_{yz}u_{yz} = -\frac{\mathrm{i}\omega}{2}\eta_{yz}h_{yz}\,. \end{aligned} \tag{4.116}$$

Here we used that small fluctuations $h_{\mu\nu}$ about the flat metric are translated into

$$\begin{aligned} \nabla_a u_b = -\Gamma^\lambda_{ab}u_\lambda = \Gamma^t_{ab} &= \frac{1}{2}g^{tt}\left(\partial_a g_{tb} + \partial_b g_{at} - \partial_t g_{ab}\right) = \\ &= \frac{1}{2}\partial_t g_{ab} = -\epsilon\frac{\mathrm{i}\omega}{2}h_{ab}\,, \end{aligned} \tag{4.117}$$

where a, b run over the spatial directions x, y, z and we used that $u^\mu = (1,0,0,0)$ and $h_{ab}(x^\mu) = \mathrm{e}^{-\mathrm{i}\omega t}h_{ab}$. From now on we neglect ϵ since it should be clear from the context which order we are considering. Due to the rotational symmetry in the yz-plane $\eta_{xy} = \eta_{xz} \equiv \eta_{x\perp}$.

In the consideration which led to (4.115) we only include contributions to the stress tensor due to the dissipation via viscosity. Thus we find the terms in the constitutive equations which depend on the velocity gradient of the normal fluid u_μ only. In general, there could also be terms depending on the derivatives of the Goldstone boson fields $v_\mu = \partial_\mu\varphi$, i.e. on the superfluid velocity and on the velocity of the director (since our condensate sets a direction we also call it a director in analogy to the expressions used in [108]), which may contribute to the dissipative part of the stress tensor.
However, these terms do not contribute to the off-diagonal components of the energy-momentum tensor because (1) a shear viscosity due to the superfluid velocity leads to a non-positive divergence of the entropy current [106, 109], and (2) no rank two tensor can be formed out of degrees of freedom of the director if the gradients of the director vanish [108]. In our case, the second argument is fulfilled

since the condensate is homogeneous and the fluctuations depend on time only. Even though these degrees of freedom will generate additional transport coefficients, they do not change the shear viscosities, so we can use Kubo's formulae (see 3.2.3) which give the shear viscosities in terms of the stress energy correlation functions.

Next we discuss the other components we displayed in (4.115). Let us consider a conformal fluid, so that $\zeta_x = \zeta_y = 0$ (this can easily be shown using the tracelessness condition of the stress-energy tensor, i. e. $\Pi^a{}_a = 0$, with $a = x, y, z$). The usual way to perturb a system in thermal equilibrium is to switch on small perturbations of the background fields and add these sources to the action. Here we are interested in the metric fluctuations about the flat Minkowski metric, i. e. the terms of interest here are

$$\begin{aligned} &\Pi^{xx}h_{xx} + \Pi^{yy}h_{yy} + \Pi^{zz}h_{zz} = \\ &\qquad = +i\omega\frac{2}{3}\lambda\left(h_{xx} - \frac{1}{2}\left(h_{yy}+h_{zz}\right)\right)^2 + i\omega\frac{\eta_{yz}}{2}\left(h_{yy}-h_{zz}\right)^2 . \end{aligned} \tag{4.118}$$

To derive the right hand side we use equations (4.114) and (4.115), as well as $u_{aa} = -\frac{i\omega}{2}h_{aa}$, with $a = x, y, z$ and the rest frame choice $u^\mu = (1, 0, 0, 0)$. Applying the same calculation to the isotropic case we obtain

$$\begin{aligned} &\Pi^{xx}h_{xx} + \Pi^{yy}h_{yy} + \Pi^{zz}h_{zz} = \\ &\qquad = +\frac{i\omega}{3}\eta\left(\left(h_{xx}-h_{yy}\right)^2 + \left(h_{xx}-h_{zz}\right)^2 + \left(h_{yy}-h_{zz}\right)^2\right) \\ &\qquad = +i\omega\frac{2}{3}\eta\left(h_{xx} - \frac{1}{2}\left(h_{yy}+h_{zz}\right)\right)^2 + i\omega\frac{\eta}{2}\left(h_{yy}-h_{zz}\right)^2 . \end{aligned} \tag{4.119}$$

Note that in the isotropic case there is only one shear viscosity η. The purpose of the rewriting of the latter case is to show the connection to the transversely isotropic case. This rewriting shows that at a phase transition between an isotropic and transversely isotropic material, λ turns into the isotropic shear viscosity η, explaining the behaviour we see in figure 4.17 (see section below). Note that this computation takes place on the field theory side. Therefore the metric we need to lower and raise indices is the flat Minkowski metric.

It is easy to show that the left hand side of equation (4.118) is equivalent to

$$\begin{aligned} &\Pi^{xx}h_{xx} + \Pi^{yy}h_{yy} + \Pi^{zz}h_{zz} = \\ &\qquad = \frac{1}{2}\left(\Pi^{xx} - \left(\Pi^{yy}+\Pi^{zz}\right)\right)\left(h_{xx} - \frac{1}{2}\left(h_{yy}+h_{zz}\right)\right) \\ &\qquad\quad + \frac{1}{2}\left(\Pi^{xx} + \left(\Pi^{yy}+\Pi^{zz}\right)\right)\left(h_{xx} + \frac{1}{2}\left(h_{yy}+h_{zz}\right)\right) \\ &\qquad\quad + \frac{1}{2}\left(\Pi^{yy}-\Pi^{zz}\right)\left(h_{yy}-h_{zz}\right) . \end{aligned} \tag{4.120}$$

The next step is to apply linear response theory (c.f. section 3.2.3) and relate the field theory two point functions to the corresponding Green's function we obtain from gravity. We show the identification on a case by case study. In the following sections we discuss the different terms we introduced in (4.116) and (4.120). Note that the Green's function of the dissipative part of the second term of (4.120) is zero, thus we only find contact terms for this component (cf. (4.91)). Finally the last term of (4.120) corresponds to the helicity two mode and is related to the shear viscosity η_{yz}, which we discuss in the next section.

4.2.7.4 Universal Shear Viscosity

Now we have the necessary background to properly interpret our results for the energy-momentum correlators. We first consider the helicity two mode h_{yz}. It is well known that, in the isotropic case, the corresponding component of the energy-momentum tensor may be written as (cf. section 4.2.7.3 and [42, 44, 110])

$$\langle T^{yz} \rangle = -(P + \mathrm{i}\omega\eta_{yz}) h_{yz} \,. \tag{4.121}$$

Using (4.112) and (4.116) we see that this is still correct in the transversely symmetric case we are studying here. The result also takes the form of the gravity calculation (4.69)[18]. Thus the shear viscosity is given by the well-known Kubo formula

$$\eta_{yz} = -\lim_{\omega\to 0} \frac{1}{\omega} \mathrm{Im}\left(G^{yz,yz}\right) = -\lim_{\omega\to 0} \frac{1}{\omega} \frac{2r_h^4}{\kappa_5^2} \frac{\Xi_4^B(\omega)}{\Xi_0^B(\omega)} \,. \tag{4.122}$$

The value for η_{yz} we obtain by evaluating the corresponding equations of motion (4.44) is within numerical uncertainty consistent with $1/(4\pi)s$, with s the entropy density (4.21). This value for the shear viscosity was coined the universal value, since it is found in all strongly coupled field theories dual to isotropic two derivative gravity [42, 44, 110]. In [42] it was conjectured that

$$\frac{\eta}{s} = \frac{1}{4\pi} \frac{\hbar}{k_B} \,, \tag{4.123}$$

with $\hbar$ Planck's constant and k_B Boltzmann's constant, is a lower bound for all fluids found in nature. From here on we call this bound the Kovtun, Son and Starinets (KSS) bound. The common fluids we know from our daily life, e.g. water, have viscosities far above this value. However, strikingly, the value measured in quark-gluon plasma seems to be very close to the conjectured lower bound of $1/4\pi$ [46]. This is a strong hint that the quark-gluon plasma is a strongly coupled phase of QCD.

Actually, we can also proof our result analytically following [44]. In the $\omega \to 0$ limit the equation of motion (4.44) corresponds to $\partial_r \Pi = 0$, with Π the conjugate

[18] We do not see an ω^4-term, as in (4.69), in the linear hydrodynamic description since this term corresponds to a higher order term with four derivatives.

momentum to the field $\Xi = g^{yy}h_{yz}$. It was shown in [44] that a constant profile along radial AdS direction is the decisive condition in order for the ratio between shear viscosity and entropy density have to take the universal value,

$$\frac{\eta_{yz}}{s} = \frac{1}{4\pi}\,. \tag{4.124}$$

The reason for the applicability of the proof and the result described above lies in the fact that this subset of the fluctuations is not influenced by the rotational symmetry breaking. The fluctuation h_{yz} is transverse to the condensate.

4.2.7.5 Non-Universal Shear Viscosity and Flexoelectric Effect

Next we study the remaining three components of the helicity one modes, $\langle J_1^{\perp}\rangle$, $\langle J_2^{\perp}\rangle$ and $\langle T^{x\perp}\rangle$ as given by (4.74).

Non-Universal Shear Viscosity We first focus on $\langle T^{x\perp}\rangle$, which for $\left(a_{\perp}^{1}\right)_0^B = \left(a_{\perp}^{2}\right)_0^B = 0$ can be translated into the following dual field theory behaviour (see section 4.2.7.3)

$$\langle T^{x\perp}\rangle = -P\, h_{x\perp} - i\omega\eta_{x\perp}h_{x\perp}\,, \tag{4.125}$$

where $\eta_{x\perp}$ is the second shear viscosity which is present in a transversal isotropic fluid (see section 4.2.7.3) and with $P = \langle \mathcal{T}^{xx}\rangle$ as defined in (4.28). Here we see again that we can apply the Kubo formula to determine the shear viscosity $\eta_{x\perp}$,

$$\eta_{x\perp} = -\lim_{\omega\to 0}\frac{1}{\omega}\mathrm{Im}\left(G^{x\perp,x\perp}\right)\,, \tag{4.126}$$

where $G^{x\perp,x\perp}$ is given by equation (4.75). This shear viscosity has a non-trivial temperature dependence even in the large N and large 't Hooft coupling limit and is therefore not universal. In fig. 4.12 we compare our numerical results for the ratio of the shear viscosity $\eta_{x\perp}$ to the entropy density s with the universal behaviour of the shear viscosity η_{yz} for different values of α. We see that in the normal phase $T \geq T_c$, the two shear viscosities coincide as required in an isotropic fluid. In addition, the ratio of shear viscosity to entropy density is universal. In the superfluid phase $T < T_c$, the two shear viscosities deviate from each other and $\eta_{x\perp}$ is non-universal. However, it is exciting that $\eta_{x\perp}/s \geq 1/4\pi$, such that the KSS bound on the ratio of shear viscosity to entropy density [42] is still valid. Interestingly it was shown in [111] that in an axion-dilaton-gravity setup this bound can be violated to leading order in 't Hooft coupling and $1/N$. In this setup the violation is also due to a rotational symmetry breaking, however, there they explicitly break it with an anisotropic axion. On a computational basis the only difference between their setup and ours is that in our case $f(r) \geq 1$ and in theirs $f(r) \leq 1$, with $f(r)$ defined in equation (4.9). It would be interesting to further study the difference between both approaches and understand why one leads to an increase and the other to a decrease of the ratio with decreasing temperature

in comparison to the isotropic case.

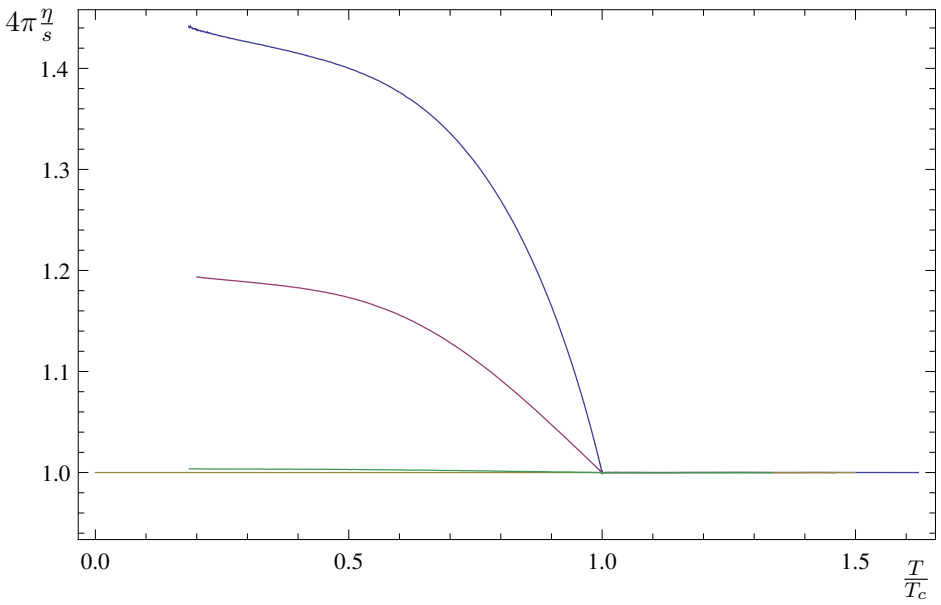

Figure 4.12: Ratio of shear viscosities η_{yz} and $\eta_{x\perp}$ to entropy density s over the reduced temperature T/T_c for different values of the ratio of the gravitational coupling constant to the Yang-Mills coupling constant α. The colour coding is as follows: In yellow, η_{yz}/s for all values of α; while the curve for $\eta_{x\perp}/s$ is plotted in green for $\alpha = 0.032$, red for $\alpha = 0.224$ and blue for $\alpha = 0.316$. The shear viscosities coincide and are universal in the normal phase $T \geq T_c$. However in the superfluid phase $T < T_c$, the shear viscosity η_{yz} has the usual universal behaviour while the shear viscosity $\eta_{x\perp}$ is non-universal. Source: [2]

The difference between the two viscosities in the superfluid phase is controlled by α as defined in (4.4). In the probe limit where $\alpha = 0$, the shear viscosities also coincide in the superfluid phase. By increasing the backreaction of the gauge fields, i. e. rising α, the deviation between the shear viscosities becomes larger in the superfluid phase as shown in fig. 4.12. If α is larger than the critical value $\alpha_c = 0.365$ found in [50] (see fig. 4.5) where the phase transition to the superfluid phase becomes first order (cf. 4.1.2), the shear viscosities are also multivalued close to the phase transition as seen in fig. 4.13. Since there is a maximal α denoted by $\alpha_{\max} = 0.628$ for which the superfluid phase exists (see fig. 4.5), we expect that the deviation of the shear viscosity $\eta_{x\perp}$ from its universal value is maximal for this $\alpha_{\max}$. Unfortunately numerical calculations for large values of α are very challenging such that we cannot present satisfying numerical data for this region. It is interesting that also the deviations due to 't Hooft coupling and N corrections are bounded. In this case the bound is determined by causality [112].

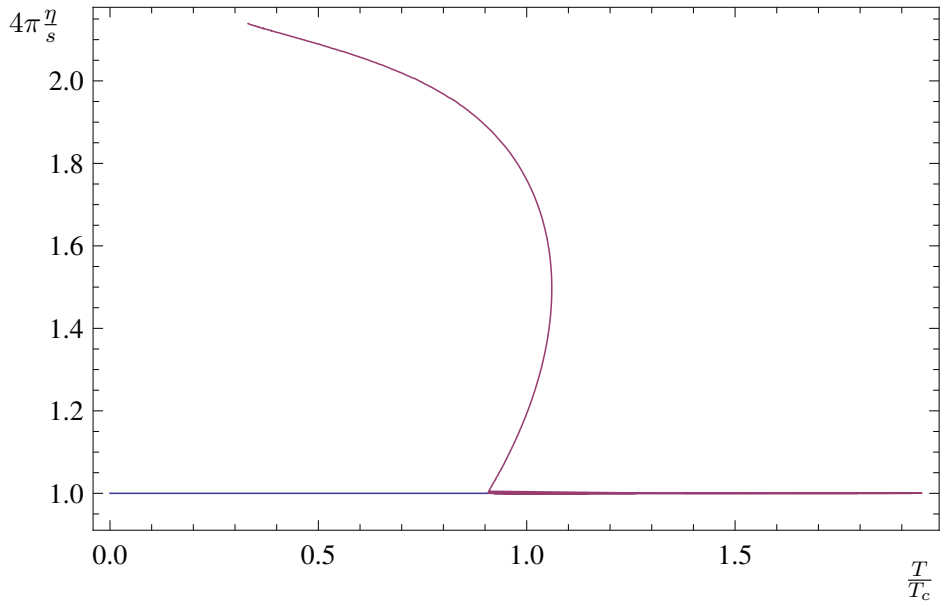

Figure 4.13: Ratio of shear viscosities η_{yz} (blue) and $\eta_{x\perp}$ (red) to entropy density s over the reduced temperature T/T_c for $\alpha = 0.447$, which is larger than the critical value where the phase transition becomes first order: The shear viscosities coincide in the normal phase $T \geq T_c$ and are universal. In the superfluid phase $\eta_{x\perp}$ is non-universal. Close to the phase transition, it is multivalued as expected for a first order phase transition. Source: [2]

In addition, close to the critical temperature, we find numerically that for $\alpha < \alpha_c$

$$1 - 4\pi\frac{\eta_{x\perp}}{s} \propto \left(1 - \frac{T}{T_c}\right)^{\beta} \quad \text{with} \quad \beta = 1.00 \pm 3\% \,. \tag{4.127}$$

Interestingly, the value of β appears to be independent of α. This result has been confirmed by an analytic calculation in [113].
The non-universality of the shear viscosity can be understood in the following way. For the $\eta_{x\perp}$ component, the relevant equation of motion (4.46) in the $\omega \to 0$ limit includes also non-vanishing source terms besides the derivative of the conjugate momentum Π_x of Ψ_x, i.e. $\partial_r \Pi_x =$ source. This is in contrast to the equation of motion which leads to the η_{yz} component. Note that the source term depends on the condensate w and the fluctuation $a^1_\perp$ and vanishes if the condensate w vanishes. Hence, as we confirm numerically in fig. 4.12, when the condensate is absent (i.e. for the $T > T_c$ case) we obtain again the universal result, since in this case the same proof as described above for the helicity two mode applies.

Flexoelectric Effect For $h_{x\perp} = 0$, we obtain flavor charge transport, i. e. a flavour field $a^{1,2}_\perp$ generates a flavour current $\langle J^{1,2\,\perp}\rangle$. In the unbroken phase it is useful to combine the fields $a^{1,2}_\perp$ in the way $a^{\pm}_\perp = a^1_\perp \pm \mathrm{i}a^2_\perp$ since they transform in the fundamental representation of the $U(1)$ symmetry and are complex conjugate

to each other. To make contact to the unbroken phase, we also use this definition in the broken phase.
Using the following definition for the currents $\langle J_\pm\rangle = 1/2\,(\langle J_1\rangle \pm \mathrm{i}\langle J_2\rangle)$, the full transport matrix becomes

$$\begin{pmatrix}\langle J_+^\perp\rangle\\ \langle J_-^\perp\rangle\\ \langle T^{x\perp}\rangle\end{pmatrix} = \begin{pmatrix} G_{+,+}^{\perp,\perp} & G_{+,-}^{\perp,\perp} & G_{+}^{\perp,x\perp}\\ G_{-,+}^{\perp,\perp} & G_{-,-}^{\perp,\perp} & G_{-}^{\perp,x\perp}\\ G^{x\perp,\perp}_{\ +} & G^{x\perp,\perp}_{\ -} & -\langle T_{xx}\rangle - \mathrm{i}\omega\eta_{x\perp}\end{pmatrix}\begin{pmatrix}a_\perp^+\\ a_\perp^-\\ h_{x\perp}\end{pmatrix}, \tag{4.128}$$

where the flavor conductivities are given by

$$\begin{aligned}
G_{\pm,\pm}^{\perp,\perp}(\omega) &= \frac{1}{4}\left[G^{1\perp,1\perp}(\omega) + G^{2\perp,2\perp}(\omega) \mp \mathrm{i}\left(G^{1\perp,2\perp}(\omega) - G^{2\perp,1\perp}(\omega)\right)\right]\\
&= \frac{r_H^2}{2g^2}\left(\frac{\left(a_\perp^1\right)_2^B}{\left(a_\perp^1\right)_0^B} + \frac{\left(a_\perp^2\right)_2^B}{\left(a_\perp^2\right)_0^B} - \frac{(\mu\mp\omega)^2}{2}\right.\\
&\qquad\left. \mp\mathrm{i}\left(\frac{\left(a_\perp^1\right)_2^B}{\left(a_\perp^2\right)_0^B} - \frac{\left(a_\perp^2\right)_2^B}{\left(a_\perp^1\right)_0^B}\right)\right),\\
G_{\pm,\mp}^{\perp,\perp}(\omega) &= \frac{1}{4}\left[G^{1\perp,1\perp}(\omega) - G^{2\perp,2\perp}(\omega) \pm \mathrm{i}\left(G^{1\perp,2\perp}(\omega) + G^{2\perp,1\perp}(\omega)\right)\right]\\
&= \frac{r_H^2}{2g^2}\left(\frac{\left(a_\perp^1\right)_2^B}{\left(a_\perp^1\right)_0^B} - \frac{\left(a_\perp^2\right)_2^B}{\left(a_\perp^2\right)_0^B} \pm \mathrm{i}\left(\frac{\left(a_\perp^1\right)_2^B}{\left(a_\perp^2\right)_0^B} + \frac{\left(a_\perp^2\right)_2^B}{\left(a_\perp^1\right)_0^B}\right)\right),\\
G^{x\perp,\perp}_{\ \pm}(\omega) &= \frac{1}{2}\left[G^{x\perp,1\perp}(\omega) \mp \mathrm{i}G^{x\perp,2\perp}(\omega)\right] =\\
&= -\frac{\langle\mathcal{J}_1^x\rangle}{4} + \frac{r_H^4}{\kappa^2}\left(\frac{\left(\Psi_x\right)_4^B}{\left(a_\perp^1\right)_0^B} \mp \mathrm{i}\frac{\left(\Psi_x\right)_4^B}{\left(a_\perp^2\right)_0^B}\right),\\
G_{\pm}^{\perp,x\perp}(\omega) &= \frac{1}{2}\left[G^{1\perp,x\perp}(\omega) \pm \mathrm{i}G^{2\perp,x\perp}(\omega)\right] =\\
&= -\frac{\langle\mathcal{J}_1^x\rangle}{4} + \frac{r_H^2}{g^2}\left(\frac{\left(a_\perp^1\right)_2^B}{\left(\Psi_x\right)_0^B} \pm \mathrm{i}\frac{\left(a_\perp^2\right)_2^B}{\left(\Psi_x\right)_0^B}\right).
\end{aligned} \tag{4.129}$$

First note that for $\mu = 0$ where the $SU(2)$ symmetry is restored, i. e. $a^1 \equiv a^2$, the Green's function is diagonal and $G_{+,+}^{\perp,\perp} = G_{-,-}^{\perp,\perp} = G^{3\perp,3\perp}$. In the unbroken phase, $G_{+,-}^{\perp,\perp} = G_{-,+}^{\perp,\perp} \equiv 0$ is still valid for $\mu \neq 0$, since the $a^\pm$ do not couple to each other, while $G_{+,+}^{\perp,\perp} \neq G_{-,-}^{\perp,\perp}$ for $\mu \neq 0$. In the unbroken as well as in the broken phase we find

$$\begin{aligned}
&G_{-,-}^{\perp,\perp}(\omega) = G_{+,+}^{\perp,\perp}(-\omega)^*, && G_{+,-}^{\perp,\perp}(\omega) = G_{-,+}^{\perp,\perp}(-\omega)^*,\\
&G_{+}^{\perp,x\perp}(\omega) = G_{-}^{\perp,x\perp}(-\omega)^* \quad\text{and}\quad && G^{x\perp,\perp}_{\ +}(\omega) = G^{x\perp,\perp}_{\ -}(-\omega)^*,
\end{aligned} \tag{4.130}$$

as expected since $a^1(\omega) = \left(a^1(-\omega)\right)^*$, $a^2(\omega) = \left(a^2(-\omega)\right)^*$ and $\Psi_x(\omega) = (\Psi_x(-\omega))^*$.

In figure 4.14 we plot the real and imaginary parts of $G_{\pm,\pm}^{\perp,\perp}(\omega)$. We see in fig. 4.14(c) and 4.14(d), showing $\mathrm{Im}(G_{\pm,\pm}^{\perp,\perp})$, that for temperatures $T > T_c$, the

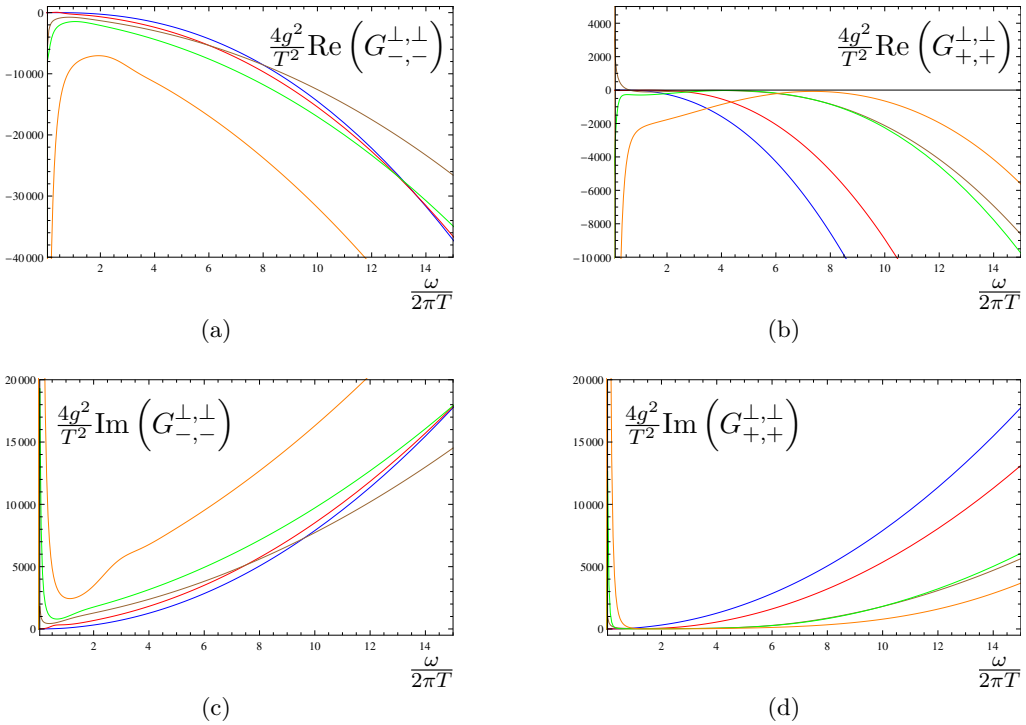

Figure 4.14: These plots show the real and imaginary part of the correlators $G^{\perp,\perp}_{\pm,\pm}$ versus the reduced frequency $\omega/(2\pi T)$ for $\alpha = 0.316$ at different temperatures: $T = \infty$ blue line, $T = 3.02T_c$ red line, $T = 1.00T_c$ brown line, $T = 0.88T_c$ green line and $T = 0.50T_c$ orange line. Source: [2]

quasinormal modes tend towards the origin (in these plots we see their projection on the real axis) (see e. g. [47, 114] and figure 4.20). For $T \leq T_c$ we see a pole at the origin which is due to the massless Goldstone modes. These Goldstone modes are related to rotations of the director $\langle \mathcal{J}^{1x} \rangle$ in real space which are generated by the fluctuations $a^1_\perp$ [19]. Furthermore, as expected for large frequencies, the Green's function grows proportional to ω^2 in the $\pm\pm$ components, the same as for the correlator $G^{3\perp,3\perp}$. In figure 4.14 the correlators for the different temperatures do not seem to have the same asymptotic behavior. However, in this case we have contribution from terms such as $\omega\mu$, i.e. of first order in ω, which are not existent in the $G^{3\perp,3\perp}$ component. Hence to see that all correlators have the same limit, larger values of ω have to be considered. Even not present in our figures we verified numerically that the asymptotics of the correlators at different temperatures agree. Furthermore, in this context, we check that the fluctuations $a^\pm_\perp$, which are unstable in the normal phase, are stabilised in the broken phase for $T < T_c$, i.e. the quasinormal modes of these perturbations stay in the lower half plane. Thus, the preferred direction induced by the current $\langle \mathcal{J}^{1x} \rangle$ is stable.

[19] The other Goldstone mode is related to the change of the phase of the condensate and correspond to the fluctuation a^2_x, see section 4.2.7.6.

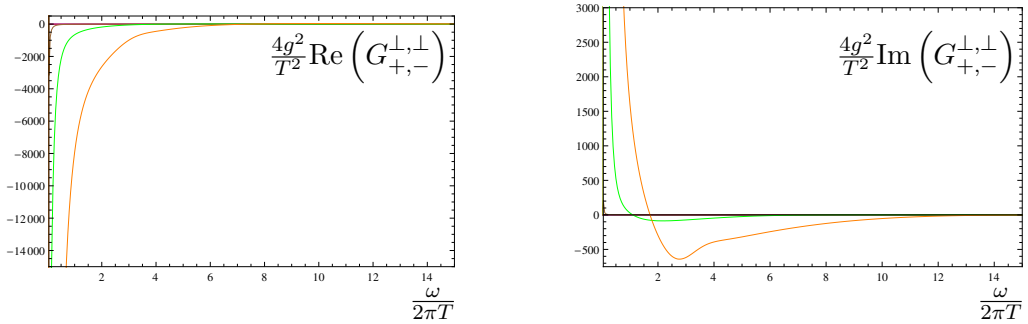

(a) (b)

Figure 4.15: These plots show the real and imaginary part of the correlator $G^{\perp,\perp}_{+,-}$ versus the reduced frequency $\omega/(2\pi T)$ for $\alpha = 0.316$ at different temperatures: $T = \infty$ blue line, $T = 3.02T_c$ red line, $T = 1.00T_c$ brown line, $T = 0.88T_c$ green line and $T = 0.50T_c$ orange line. The curves for the temperatures above T_c are exactly zero for all frequencies. Source: [2]

In figure 4.15 we plot $G^{\perp,\perp}_{+,-}(\omega)$. We see that this correlator vanishes for $T > T_c$ since the $a^{\pm}_{\perp}$ do not couple in the unbroken phase. Furthermore, below T_c, a pole at $\omega = 0$ due to the Nambu-Goldstone mode appears. We do not show $G^{\perp,\perp}_{-,+}(\omega)$ since $G^{\perp,\perp}_{+,-}$ and $G^{\perp,\perp}_{-,+}$ look alike. Nevertheless, there is a difference between them in the broken phase. The difference arises from the contributions to the correlators due to the mixed terms, $G^{1\perp,2\perp}$ and $G^{2\perp,1\perp}$, in the corresponding equation in (4.129). However, these are suppressed in relation to $G^{1\perp,1\perp}$, which contains the Goldstone mode in the broken phase.

Finally, in figure 4.16 we show $G^{\perp,x\perp}_{\pm}(\omega)$. Note that the contribution of $\langle \mathcal{J}^x_1 \rangle$ to the real parts of the correlators is not included in the corresponding plots since it just shifts the curves by a constant. Furthermore, we have that $\mathrm{Im}(G^{\perp,x\perp}_{\pm}) = \mathrm{Im}(G^{x\perp,\perp}_{\pm})$ and $\mathrm{Re}(G^{\perp,x\perp}_{\pm}) - \mathrm{const} = \mathrm{Re}(G^{x\perp,\perp}_{\pm})$, i.e. there is a constant offset between the real parts of these correlators. We expect that this constant offset is generated by the term $\left(\Psi_x\right)^B_4(\omega)/\left(a^1_{\perp}\right)^B_0(\omega)$ which may be constant in the limit $\omega \to 0$ since $a^1_{\perp}$ has a normal mode at $\omega = 0$ and the subleading term of Ψ_x is probably not sourced in this case. To check this claim one ansatz is to compute analytically a double expansion in terms of small α and small condensate, following [113]. However, it turns out that it is very hard to push the expansion far enough to see the relevant terms, which would explain the observations described above. In the unbroken phase these correlators vanish since the differential equations of the corresponding fields decouple. In the broken phase the correlators present a rich structure, which we cannot fully address. However, it seems that the coupling between the $a^{\pm}_{\perp}$ flavor fields and the strain $h_{x\perp}$ generates new excitations which appear as bumps in the curves.

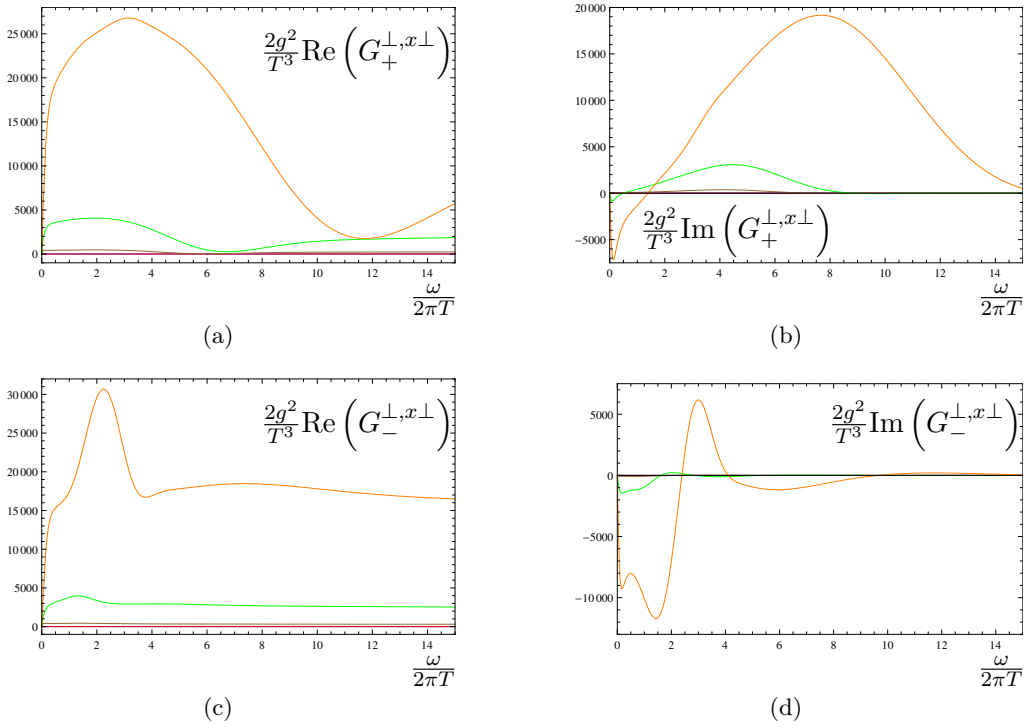

Figure 4.16: These plots show the real and imaginary part of the correlators $G_{\pm}^{\perp,x\perp}$ versus the reduced frequency $\omega/(2\pi T)$ for $\alpha = 0.316$ at different temperatures: $T = \infty$ blue line, $T = 3.02T_c$ red line, $T = 1.00T_c$ brown line, $T = 0.88T_c$ green line and $T = 0.50T_c$ orange line. The curves for the temperatures above T_c are exactly zero for all frequencies. Source: [2]

These correlators arise from the coupling between the stress $\langle T^{x\perp}\rangle$ and the flavour fields $a_{\perp}^{\pm}$ as well as the currents $\langle J_{\pm}^{\perp}\rangle$ and the strain $h_{x\perp}$ described in (4.128). From a field theoretic point of view this coupling introduces an effect which is similar to the flexoelectric effect known from nematic crystals [54] and only appears in fluids with broken rotational symmetry. We have a current $\langle \mathcal{J}^{1x}\rangle$ in a favoured direction in the background which interacts with the flavour fields $a_{\perp}^{\pm}$. This interaction induces a force on the current which pushes the current in its perpendicular direction generating the stress $\langle T^{x\perp}\rangle$. In the similar way, a strain $h_{x\perp}$ introduces an inhomogeneity in the current $\langle \mathcal{J}^{1x}\rangle$ resulting in a flavour field $a_{\perp}^{\pm}$ which generates the currents $\langle J_{\pm}^{\perp}\rangle$.

4.2.7.6 Viscosities and Flavour Transport Coefficients

The last remaining block contains the modes which transform as scalars under the $SO(2)$ symmetry and are even under the parity transformation $\langle \mathcal{J}_x^1\rangle \to -\langle \mathcal{J}_x^1\rangle$. It includes the fields a_x^1, a_x^2, a_t^3, $\xi_t = g^{tt}h_{tt}$, $\xi_x = g^{xx}h_{xx}$ and $\xi_{\perp} = g^{yy}h_{yy} + g^{yy}h_{zz}$. Similarly to the parity odd block (section 4.2.7.2), these fields form 3 physical modes, Φ_1, Φ_2 and Φ_3 (see (4.42)). It turns out that it is more sensible to consider

this fields in terms of $\Phi_\pm = \Phi_1 \pm i\Phi_2$, since they transform fundamentally under the $U(1)$ in the unbroken phase.

Transport Coefficient associated to a Normal Stress Difference In the presence of anisotropy, besides the two shear viscosities η_{yz} and $\eta_{x\perp}$, there are three other independent coefficients. However, in a conformal fluid, two of them, ζ_x and ζ_y, vanish due to the tracelessness condition of the energy-momentum tensor in conformal theories (see section 4.2.7.3). The remaining nonzero component, λ, is related to the normal stress difference as we will discuss next.

The two point function $G^{m,m}$ (see equation (4.90)) generated by the bulk field Φ_3 can be related to the Green's function obtained from the first term in equation (4.120) by

$$\begin{aligned} G^{m,m}(\omega) = &\lim_{|\vec{k}|\to 0} \int \mathrm{d}t\, \mathrm{d}^3x e^{-\mathrm{i}k_\mu x^\mu} \theta(t) \times \\ &\left\langle \left[\frac{1}{2}\left(T^{xx}(t,\vec{x}) - \left(T^{\perp\perp}(t,\vec{x})\right)\right), \frac{1}{2}\left(T^{xx}(0,0) - \left(T^{\perp\perp}(0,0)\right)\right)\right]\right\rangle . \end{aligned} \tag{4.131}$$

Using Kubo's formula we obtain the connection to the transport coefficient λ, defined in (4.115), i. e.

$$\lambda = \lim_{\omega\to 0} \frac{3}{2\omega} \operatorname{Im} G^{m,m}(\omega) . \tag{4.132}$$

As discussed in section 4.2.7.3 there is no λ in the isotropic phase. However, the corresponding transport coefficient in the unbroken phase is just the shear viscosity η (compare equations (4.118) and (4.119)). Therefore we can match λ to η at the phase transition.

In the broken phase λ is the transport coefficient related to the normal stress difference, that is, the difference of the diagonal components of the stress tensor, $\langle \frac{1}{2}\left(T^{xx} - T^{\perp\perp}\right)\rangle$. Generically, whenever an incompressible material is squeezed between two surfaces by applying normal stresses, it will tend to expand along the directions parallel to these surfaces (e.g. normal radial squeezing on a cylinder is expected to lengthen its shape on the vertical direction). In figure 4.17 we see that with decreasing temperature it becomes more and more difficult to deform the material, since the energy cannot be dissipated that easily anymore.

Piezoelectric effect The remaining part of the transport matrix (4.91), which we now discuss is

$$\begin{pmatrix} \langle J^x_+ \rangle \\ \langle J^x_- \rangle \\ \langle \frac{1}{2}(T^{xx} - 2T^{\perp\perp})\rangle \end{pmatrix} = \begin{pmatrix} G^{x,x}_{+,+} & G^{x,x}_{+,-} & G^{x\,m}_{+} \\ G^{x,x}_{-,+} & G^{x,x}_{-,-} & G^{x\,m}_{-} \\ G^{m\,x}_{+} & G^{m\,x}_{-} & G^{m,m} \end{pmatrix} \begin{pmatrix} \Phi^+_\perp \\ \Phi^-_\perp \\ \Phi_3 \end{pmatrix} . \tag{4.133}$$

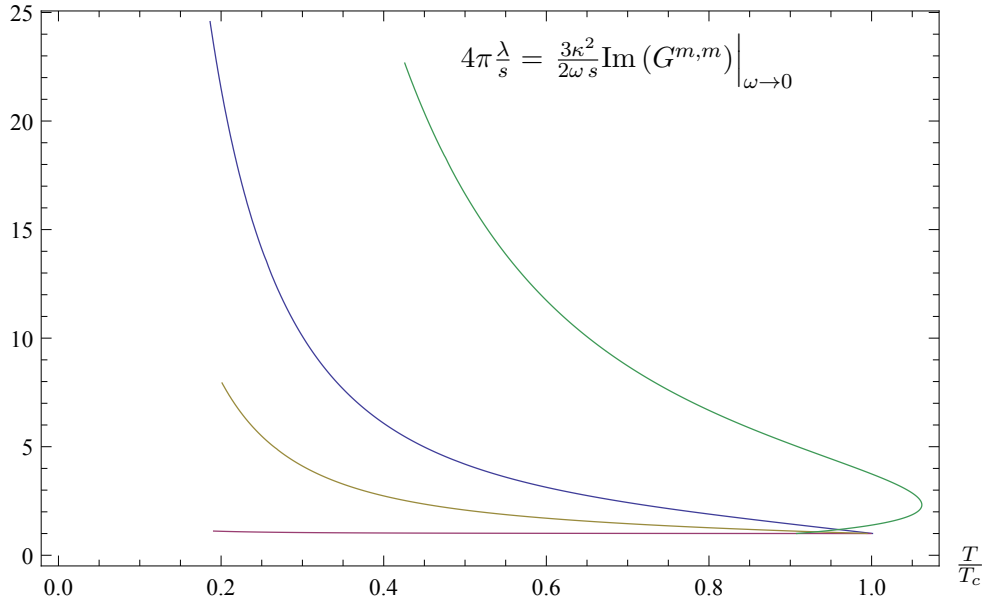

Figure 4.17: We plot $\frac{\lambda}{s}$ over the temperature T/T_c for $\alpha = 0.032$ (red), $\alpha = 0.224$ (yellow), $\alpha = 0.316$ (blue) and $\alpha = 0.447$ (green). Note that $\alpha = 0.447 > \alpha_c$ and therefore the phase transition is first order leading to multiple values near the phase transition. All curves tend to $1/(4\pi)$ at T_c, since in the unbroken phase λ corresponds to the isotropic shear viscosity η. Source: [3]

For the explicit form of this matrix see equation (4.92). The transport properties presented here show similarities to an effect known as piezoelectric effect found in crystals [54]. This effect describes the generation of an electric current due to the squeezing or elongation of a crystal, or the generation of a mechanical strain due to an external electric field. A coupling between a normal stress difference and (flavour) currents that resembles this effect is found in this block. Note that the piezoelectric effect was also found in the context of black branes in [115].

In the same way we find a coupling between the stress tensor and the gauge fields perpendicular to the condensate, we find here an analogous coupling between $a_x^{\pm}$ and the diagonal elements of the energy-momentum tensor, and correspondingly between the diagonal metric fluctuations and the flavour currents $\langle J_{\pm}^x \rangle$ (cf. equation (4.91)). In the field theory this may be related to a current (in our case a flavour current) being affected by, or generating, mechanical stress (piezoelectric effect).

In figures 4.18 and 4.19 we plot the real and imaginary part of $G^{x,x}_{\pm,\pm}$ and $G^{x,x}_{\pm,\mp}$ over the reduced frequency $\omega/(2\pi T)$, for several values of the temperature, or equivalently of the chemical potential μ. Again, we find the symmetry relations

$$G^{x,x}_{-,-}(\omega) = G^{x,x}_{+,+}(-\omega)^*\,, \qquad G^{x,x}_{+,-}(\omega) = G^{x,x}_{-,+}(-\omega)^*\,,$$

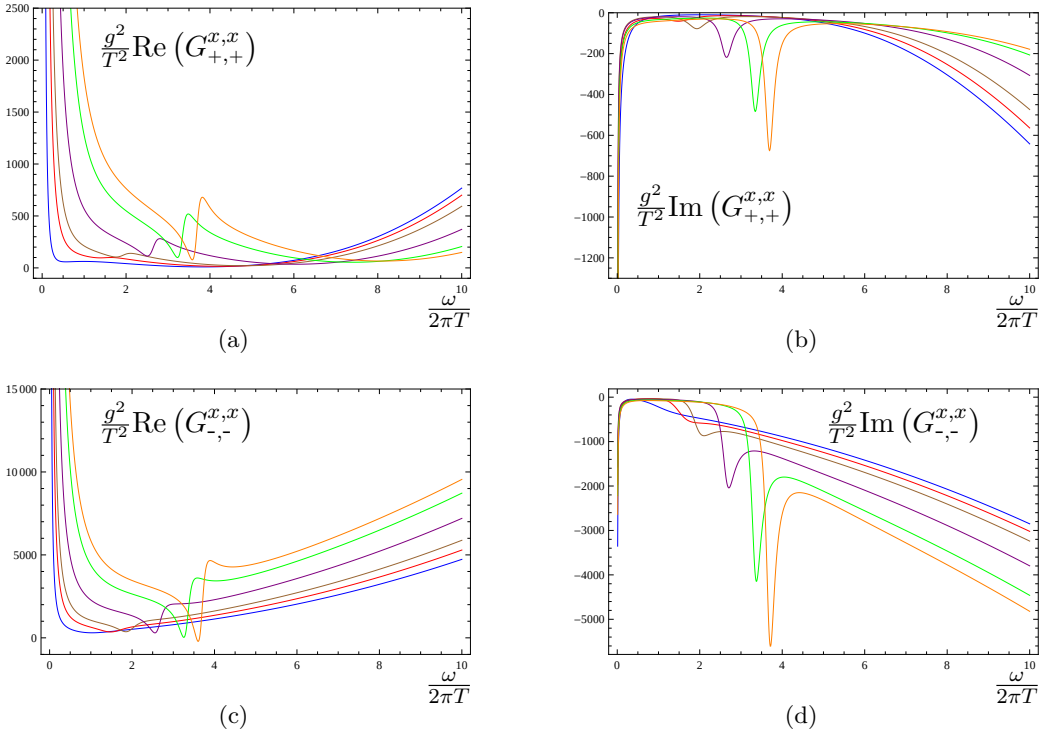

Figure 4.18: These plots show the real and imaginary part of the correlators $G^{x,x}_{\pm,\pm}$ versus the reduced frequency $\omega/(2\pi T)$ for $\alpha = 0.316$ at different temperatures: blue $T = 0.98T_c$, red $T = 0.88T_c$, brown $T = 0.78T_c$, purple $T = 0.62T_c$, green $T = 0.50T_c$, orange $T = 0.46T_c$. Source: [3]

$$G^{x,x}_{-,-}(\omega) = G^{x,x}_{+,+}(-\omega)^*\,, \qquad G^{x,x}_{+,-}(\omega) = G^{x,x}_{-,+}(-\omega)^*\,,$$

as we did in the study of helicity one modes above. This was expected from the fact that $(\Phi_+(\omega))^* = \Phi_-(-\omega)$, $(\Phi_-(\omega))^* = \Phi_+(-\omega)$ and $(\Phi_3(\omega))^* = \Phi_3(-\omega)^*$.

In figure 4.21 we plot the $G^{m,x}_{\pm}$, whose imaginary parts are identical to those of $G^{x,m}_{\pm}$, and whose real parts are similar, except for small frequencies compared to the temperature.

Notice that many of the curves in figs. 4.18 to 4.21 show a pole at $\omega = 0$. To understand why, remember that the formation of $\langle \mathcal{J}^{1x} \rangle$ selects a preferred direction in flavour space, spontaneously breaking the $SO(3)$ and $U(1)_3$ symmetries. As a consequence of this, the a^2_x field becomes one of the three massless Goldstone modes arising from the spontaneous symmetry breaking[20]. This common pole reflects the Goldstone mode in all of the correlators presented here. When plotting the quasinormal modes in the complex frequency plane we see this pole at the origin. In the unbroken case the quasinormal modes tend towards this point (see figure 4.20). In fact, although it is not apparent in figs. 4.19 and 4.21, the

[20]The other two Goldstone modes, a^1_y and a^1_z, corresponding to the breaking of the $SO(3)$ were discussed in the last section.

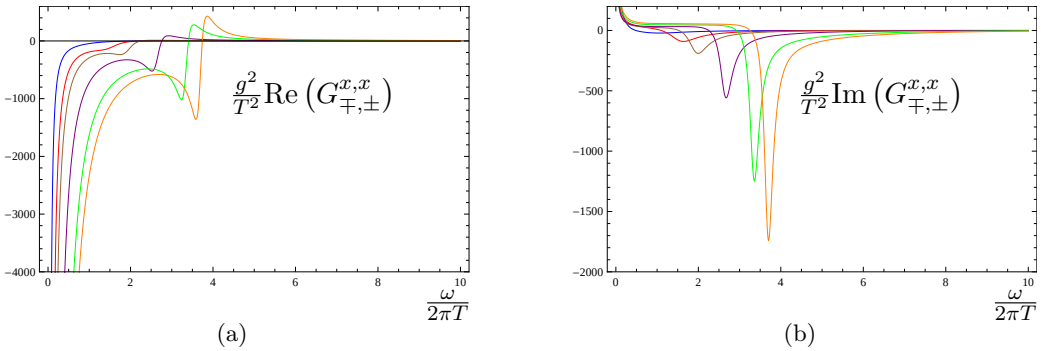

(a) (b)

Figure 4.19: These plots show the real and imaginary part of the correlator $G^{x,x}_{+,-}$, or equivalently $G^{x,x}_{-,+}$, versus the reduced frequency $\omega/(2\pi T)$ for $\alpha = 0.316$ at different temperatures: blue $T = 0.98T_c$, red $T = 0.88T_c$, brown $T = 0.78T_c$, purple $T = 0.62T_c$, green $T = 0.50T_c$, orange $T = 0.46T_c$. Source: [3]

correlators vanish completely in the unbroken phase $T > T_c$, since in this limit the equations of motion of the bulk fields decouple.

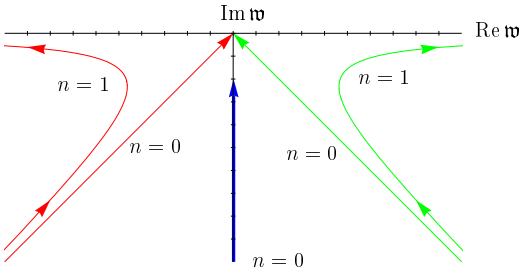

Figure 4.20: This figure, taken from [48], shows the different quasinormal modes in the D3/D7 system in the complex frequency plane. Here $\mathfrak{w} = \omega/(2\pi T)$. The red and green curves show the modes of the fluctuations which correspond to $\Phi_\pm$ in our setup and the blue curve corresponds to our Φ_4. It is interesting to see that the backreaction and the bottom up approach we pursue in the system at hand behave in a very similar fashion as the D3/D7 probe setup. Note however, that there is one difference: due to the backreaction and consequently the rotational symmetry breaking in the superfluid phase, the $a^\pm_y$ decouple from the $\Phi_\pm$, contrary to what happens in the D3/D7 mode. Moreover, we only see the red and green modes in the $\Phi_\pm$ sector and not in the $a^\pm_y$ sector (see [2] for a treatment of this modes). Source: [48]

In addition to the pole, we see the formation of a bump located at the same value of the frequency for all Green's functions. These bumps arise due to higher quasinormal mode excitations. With decreasing temperature, they move in the direction of smaller values of the negative imaginary parts and larger real parts of the frequencies. Therefore they become more accentuated with decreasing temperature. Nevertheless, the quasinormal modes stay in the lower half complex frequency plane for all values of the temperatures we are able to check. It would

be very interesting to see if the system is still stable if we switch on finite momentum. Perhaps in that case it is possible to find a transition to the phases known as spatially modulated phases, which were studied in [116–119]. The behaviour of the quasinormal modes is very similar to the one found in the D3/D7 model in [48] (see figure 4.20), where they are interpreted as mesonic excitations. However, since we do not have a precise knowledge of the field theory side, this interpretation should be treated with care. Furthermore, since our dual field theory is strongly coupled, quasiparticle excitations are probably not the correct description anymore.

The Green's functions $G^{x,x}_{\pm,\pm}$ (c.f. fig. 4.18) seem to have the wrong asymptotic values, however, as described in the helicity one section this is just a consequence of the small frequency range displayed here. Actually, they do asymptote to the same value for all temperatures in the limit of large frequencies. However this veils the interesting details at low frequency, therefore we do not show it here. Nevertheless, the large frequency limit is proportional to ω^2, in agreement with the underlying CFT.

Finally, note that the real parts of $G^{x,m}_{\pm}$ and $G^{m,x}_{\pm}$ are not symmetric to each other. In the latter one we see poles in the $\omega \to 0$ limit. This poles are due to the fact that in the $G^{m,x}_{\pm}$ case we are dividing by the boundary value of $\Phi_{\pm}$, which contains the (massless) Goldstone mode a^2_x and therefore vanishes at $\omega = 0$, whereas in the $G^{x,m}_{\pm}$ case we divide by the boundary value of Φ_3, whose quasinormal mode is not located at the origin and thus should not vanish. A better interpretation of this behaviour can only be accounted for in a analytic treatment, e.g., for small values of α and the condensate (see e.g. [120]).

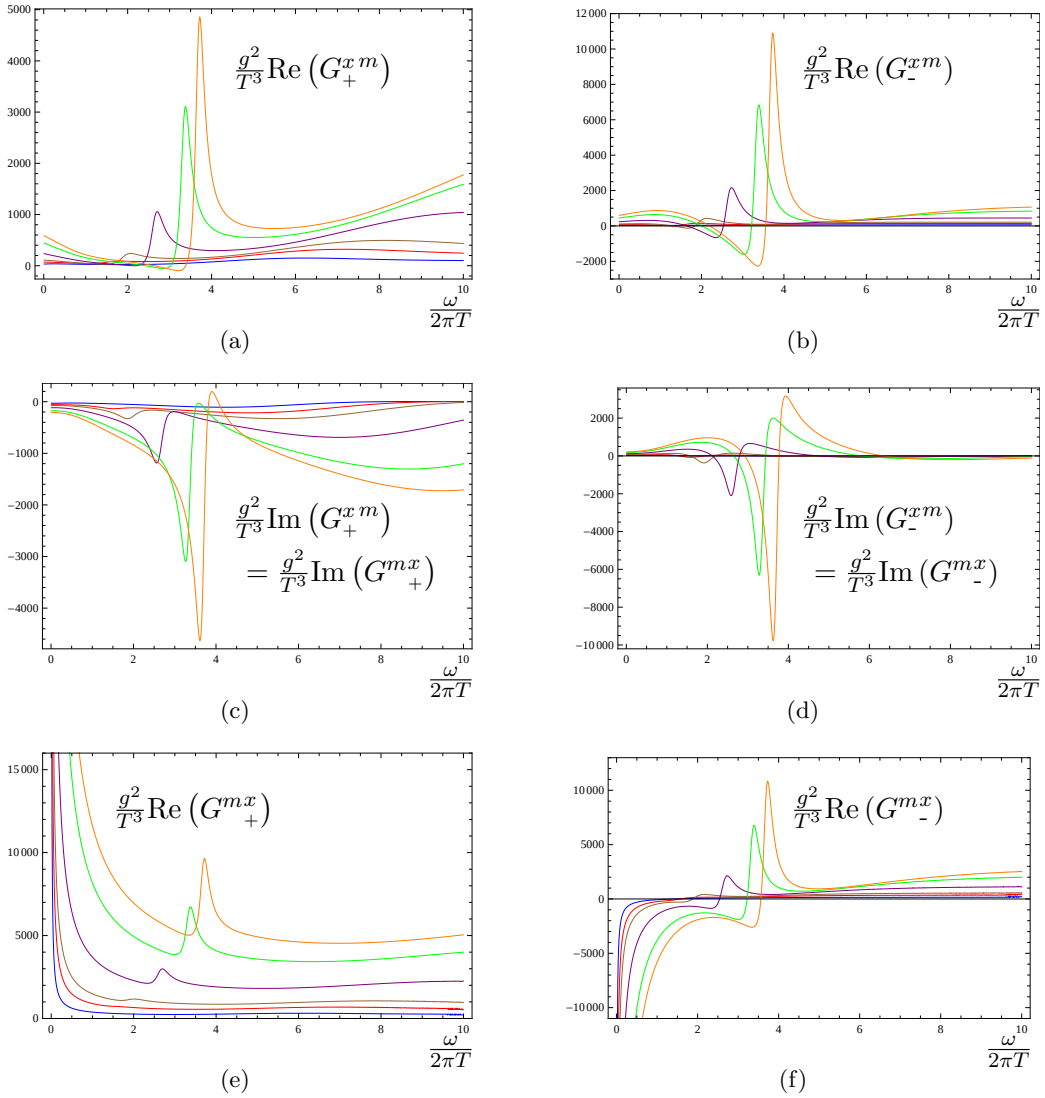

Figure 4.21: These plots show the real and imaginary part of the correlators $G_{\pm}^{x\,m}$ versus the reduced frequency $\omega/(2\pi T)$ for $\alpha = 0.316$ at different temperatures: blue $T = 0.98T_c$, red $T = 0.88T_c$, brown $T = 0.78T_c$, purple $T = 0.62T_c$, green $T = 0.50T_c$, orange $T = 0.46T_c$. We are not showing $G^{m\,x}_{\pm}$ because their imaginary parts are identical. Their real parts, however, show a different low frequency behaviour. Source: [3]

Chapter 5

Entanglement Entropy in Scaling Geometries

In this chapter our main focus lays on the computation of holographic entanglement entropy in scaling geometries. We concentrate on one example of a scaling geometry with very "fermionic" properties, i.e. it allows for low energy excitations at finite momentum. This is precisely the property of a Fermi surface, namely excitations at a finite Fermi momentum k_F.

In [121] the authors claim that it is possible to study Fermi surfaces holographically by examining the holographic entanglement entropy. The conjecture states that a Fermi surface leads to a logarithmic dependence of the entanglement entropy on the relevant length scale of an entangling shape. However, this last point is still vividly discussed. In this thesis we cannot find any sign of a logarithmic dependence, although the geometry has fermionic characteristics.

The entangling shapes discussed in this chapter are a strip, disc and annulus. Remarkably we find that in the scaling geometry mentioned above the strip and the annulus undergo a phase transition, while the sphere does not. This is an interesting feature seen in other geometries as well (see [64]). The phase transitions strongly resemble results computed in confining geometries [122, 123]. However, it is important to stress that our geometry is not confining.

In the first section of this chapter we discuss the scaling geometry and its UV completion in terms of asymptotically AdS (see section 5.1). In the second part we briefly introduce entanglement entropy and its holographic counterpart (see section 5.2). Finally, in section 5.3 we show our results for the holographic entanglement entropy of a strip, disc and annulus computed in one specific scaling geometry. The first and the last main section of this chapter are based on work published by the author in [4].

5.1 Einstein-Maxwell-Dilaton Theory

In the chapters 3 and 4 we studied the instabilities of AdS Reissner-Nordström which led to dynamical symmetry breaking and new stable and thermodynamically preferred solutions with a condensate. However we did not analyse the different possible ground states of these theories at $T = 0$. For the s-wave case this was done in [124, 125]. The authors find that depending on the potential of the scalar field (cf. eq. (3.26)) and the ratio between the gravitational constant κ^2 and the Maxwell coupling g^2, different ground states are possible. In this chapter we interpret the flow along the radial AdS direction as the RG flow of the dual field theory. In this spirit we interpret the different ground states as IR fixed point of the dual field theory. Thus, in the s-wave different scalar potentials lead to a flow to different IR fixed points.

In this section we discuss a second approach to generate a flow into new IR fixed points, which in the field theory will correspond to turning on relevant operators at the UV fixed point. One holographic realisation of this deformation is done in the framework of Einstein-Maxwell-Dilaton systems (see [70] and references therein), where the Dilaton plays the role of the relevant deformation.

The motivation to consider Einstein-Maxwell-Dilaton systems is to study condensed matter applications. In order for a setup to be interesting for these kind of applications it has to include a finite charge density. As we saw in chapter 3, this is related to a gauge field in the bulk, which is dual to a conserved $U(1)$ charge current in the field theory. One possible solution is the AdS Reissner-Nordström black hole. However, as we saw in section 3.2 in the $T \to 0$ limit the geometry describing the ground state of the dual theory is $\mathrm{AdS}_2 \times \mathbb{R}^{\mathrm{D}-1}$. As discussed there, the problem with this IR fixed point is the large finite entropy density at zero temperature (see also [70]). This violates the third law of thermodynamics and is not in agreement with experimental results seen in condensed matter physics. Therefore this state is considered to be unstable. We would like to generate new IR fixed points which do not suffer from this illness. As described above, besides considering the condensation of operators in the bulk, a second possibility to tackle this issue is to add relevant deformations to the UV theory. This translates into a dilatonic field in the Einstein-Maxwell action. By doing so we generate new geometries in the bulk (IR geometries) which in the $T \to 0$ limit have, possibly, vanishing entropy. A second interesting property of these new IR fixed points are emergent non-trivial scaling behaviours. That is, the radial AdS direction, time and the spatial field theory coordinates scale different from each other. This translates into the scaling properties of the dual field theory. Hence these IR geometries are also called scaling geometry. This way it is also possible to construct

non-relativistic fixed points of strongly coupled theories (see for instance [126]). We consider one of these geometries in the following.

We study a concrete solution to the Einstein-Maxwell-Dilaton theory. We start with the analysis of the IR geometry, i.e. the geometry far away from the AdS boundary. This geometry is thought of describing the IR fixed point of a dual field theory. Concretely, the scaling properties of the geometry can be translated into the dynamical critical exponent $\tilde{z}$ and the hyperscaling violation parameter θ (see e.g. [127])[1]. After determining the IR geometry we compute the corresponding AdS completion. That is, we build a $\mathrm{D}+1$ dimensional spacetime which for values $z \gg z_F$ takes the form of the IR geometry and for $z \ll z_F$ is asymptotically $\mathrm{AdS}_{\mathrm{D}+1}$. Here z_F is a scale we introduce to distinguish between the IR and UV regions of the spacetime. Note that opposed to the last two chapters here we work again with z coordinates (cf. equation (2.14)), i.e. the AdS boundary is at $z = 0$.

5.1.1 IR Solution

The relevant action in this chapter is the Einstein-Maxwell-Dilaton (EMD) action

$$S_L^{\mathrm{EMD}} = \int d^{\mathrm{D}+1}x\sqrt{-g}\left(\frac{1}{2\kappa^2}R - \frac{Z(\Phi)}{4g^2}F_{AB}F^{AB} - \frac{1}{2\kappa^2}(\partial\Phi)^2 - \frac{V(\Phi)}{2\kappa^2 L^2}\right), \quad (5.1)$$

with the effective gauge coupling and scalar potential (for the IR geometry) given by

$$Z(\Phi) = Z_0^2 \mathrm{e}^{\alpha\Phi} \quad \text{and} \quad V(\Phi) = -V_0^2 \mathrm{e}^{-\beta\Phi}\,. \quad (5.2)$$

Z_0, V_0, α and β are constants characterising the theory. A few remarks are in order. First, in this chapter we work with a slightly different convention as used in chapter 3 (cf. action (3.26)). That is, the field Φ is a real scalar field, it is not charged under the $U(1)$ gauge symmetry and we pulled out the gravitational constant κ^2. Second, the form of the effective gauge coupling and the scalar potential are motivated by effective actions arising in the low energy limit of string theories [58]. These kinds of theories were coined in [58] "Effective Holographic Theories".

[1] θ can be seen as an effective spatial dimensionality, while the critical scaling exponent $\tilde{z}$ measures the anisotropic scaling between the time and spatial directions.

Applying the standard techniques, we obtain the equations of motion

$$\begin{aligned}
&\partial_A(\sqrt{-g}\, Z(\Phi)F^{AB}) = 0\,,\\
&\partial_A(\sqrt{-g}\,\partial^A\Phi) = \frac{\kappa^2}{4g^2}\sqrt{-g}\frac{\partial Z}{\partial\Phi}F_{CD}F^{CD} + \frac{1}{2L^2}\sqrt{-g}\frac{\partial V}{\partial\Phi}\,,\\
&R_{AB} - \frac{1}{2}Rg_{AB} = \kappa^2 T_{AB}\,,\\
&\quad \text{with}\\
&T_{AB} = \frac{1}{\kappa^2}\left(\partial_A\Phi\partial_B\Phi - \frac{g_{AB}}{2}\left((\partial\Phi)^2 + \frac{V(\Phi)}{L^2}\right)\right) +\\
&\qquad + \frac{1}{4g^2}\left(4\,Z(\Phi)\,F_{AC}F_B{}^C - Z(\Phi)\,g_{AB}F_{CD}F^{CD}\right)\,.
\end{aligned} \tag{5.3}$$

These equations admit the solution [63, 128]

$$\begin{aligned}
&\mathrm{d}s^2 = \frac{L^2}{z^2}\left(-f(z)\mathrm{d}t^2 + g(z)\mathrm{d}z^2 + \sum_{i=1}^{d}\mathrm{d}x_i^2\right)\,,\\
&\text{with } f(z) = f_0\, z^{-\frac{2d(\tilde{z}-1)}{d-\theta}} \text{ and } g(z) = g_0\, z^{\frac{2\theta}{d-\theta}}\,,\\
&A_t(z) = \frac{gL}{\kappa}h(z)\,,\ \text{with } h(z) = h_0\, z^{-d-\frac{d\tilde{z}}{d-\theta}}\,,\ \text{and}\\
&\Phi(z) = \sqrt{d\frac{d\tilde{z}-d-\theta}{d-\theta}}\log z\,,
\end{aligned} \tag{5.4}$$

where we use $d = \mathrm{D} - 1$,

$$\theta = \frac{d^2\beta}{\alpha + (d-1)\beta} \quad \text{and} \quad \tilde{z} = 1 + \frac{\theta}{d} + 4\frac{(d(d-\theta)+\theta)^2}{d^2(d-\theta)\alpha^2}\,. \tag{5.5}$$

Finally, the remaining constants g_0 and h_0 are obtained by plugging the above functions into the equations of motion (5.3). We get

$$\begin{aligned}
g_0 &= \frac{d^2(d+\tilde{z}-\theta-1)(d+\tilde{z}-\theta)}{V_0^2(d-\theta)^2} \ \text{and}\\
h_0^2 &= f_0\,\frac{\tilde{z}-1}{Z_0^2(d+\tilde{z}-\theta)}\,,
\end{aligned} \tag{5.6}$$

while f_0 can be fixed by embedding this geometry into asymptotically AdS space-time.

It is easy to see that the solution (5.4) under $z \to \lambda^{(d-\theta)/d}z$ has the scaling property

$$t \to \lambda^{\tilde{z}}t\,, \quad x_i \to \lambda x_i\,, \quad \mathrm{d}s \to \lambda^{\theta/d}\mathrm{d}s\,. \tag{5.7}$$

Another very important quantity which is influenced by the scaling behaviour of the coordinates is the entropy S, which scales as [128]

$$S \propto T^{\frac{d-\theta}{\tilde{z}}}\,. \tag{5.8}$$

Thus, depending on the values of the dynamical critical exponent $\tilde{z}$ and the hyperscaling violation parameter θ, the entropy vanishes in the limit $T \to 0$.

Before continuing, some comments on a few interesting values of θ and $\tilde{z}$ are in order. If we take $\theta = 0$ and $\tilde{z} = 1$ the proper distance is invariant under scale transformations, and the time and spatial directions scale in the same way. The IR geometry corresponds to $\mathrm{AdS}_{\mathrm{D}+1}$. However, possibly with a different AdS radius L_{IR} in comparison to the UV. The field theories dual to this geometries are relativistic conformal field theories. That is, the RG flow is between a relativistic conformal field theory in the UV and a relativistic conformal field theory in the IR. The next limit of interest is $\theta = 0$ and $\tilde{z} \to \infty$. This corresponds to the $\mathrm{AdS}_2 \times \mathbb{R}^{\mathrm{D}-1}$ IR geometry, which is the extremal AdS Reissner-Nordström solution (see chapter 3). The final case we would like to mention is $\theta = 0$ and $\tilde{z} = 2$, which corresponds to Lifshitz geometries. These describe dual non-relativistic theories. All these theories with different values for θ and $\tilde{z}$ are potentially very interesting for different applications, see for instance [63] for the analysis of spectral densities in various scaling geometries.

The limit in which we are interested in is

$$\tilde{z} \to \infty\,, \quad \theta \to -\infty\,, \quad \text{while} \quad \eta \equiv -\frac{\theta}{\tilde{z}} > 0 \quad \text{is fixed}\,. \tag{5.9}$$

Plugging this limit into solution (5.4), we obtain

$$\begin{aligned} \mathrm{d}s^2 &= \frac{L^2}{z^2}\left(-\frac{f_0}{z^{2d/\eta}}\mathrm{d}t^2 + \frac{g_0}{z^2}\mathrm{d}z^2 + \sum_{i=1}^{d}\mathrm{d}x_i^2\right)\,, \quad \text{with} \quad g_0 = \frac{d^2}{V_0^2}\left(1+\frac{1}{\eta}\right)^2\,, \\ \Phi &= \sqrt{d}\sqrt{1+\frac{d}{\eta}}\log z \quad \text{and} \\ A_t &= \frac{gL}{\kappa}h(z)\,, \quad \text{with} \quad h(z) = \frac{h_0}{z^{d(1+1/\eta)}} \quad \text{and} \quad h_0 = \frac{\sqrt{f_0}}{Z_0\sqrt{1+\eta}}\,. \end{aligned} \tag{5.10}$$

This spacetime possesses the following scaling properties

$$t \to \lambda t, \quad z \to \lambda^{\eta/d} z, \;\Rightarrow\; \mathrm{d}s \to \lambda^{-\eta/d}\mathrm{d}s\,, \tag{5.11}$$

while the spatial coordinates x_i do not scale at all. Hence the background geometry is conformal to $\mathrm{AdS}_2 \times \mathbb{R}^{\mathrm{D}-1}$. This is made precise by the change of coordinates $z = \xi^{\eta/d}$, leading to

$$\mathrm{d}\tilde{s}^2 = \frac{1}{\xi^{2\eta/d}}\left(-\frac{\mathrm{d}\tilde{t}^2}{\xi^2} + \frac{\mathrm{d}\xi^2}{\xi^2} + \sum_{i=1}^{d}\mathrm{d}\tilde{x}_i^2\right)\,, \tag{5.12}$$

where $\sim$ means that we rescaled the coordinates by constants to make the similarity with $\mathrm{AdS}_2 \times \mathbb{R}^{\mathrm{D}-1}$ explicit. It is important to note that the entropy density S

is sensitive to the conformal factor $\xi^{-2\eta/d}$. Thus, as opposed to the extremal AdS Reissner-Nordström case we obtain a vanishing entropy in the $T \to 0$ limit [63], since

$$S \propto T^{\eta}\,. \tag{5.13}$$

Therefore this choice of $\tilde{z}$ and θ is very interesting for condensed matter applications. In addition, the authors of [63] found that this solution displays fermionic properties in the spectral density, i.e. possibly it models a Fermi surface in the dual field theory. Constructing a Fermi surface holographically was one of the big goals of the gauge/gravity community during the time of writing of this thesis. It is important to note that these surfaces are quite generic in condensed matter systems and are by no means a perturbative result at weak coupling [59, 63]. One of the main characteristics of a Fermi surface is the low energy excitations at finite momenta. Since the spatial field theory directions do not scale in the spacetime (5.10), while the time direction does, it is possible to generate low energy excitations at all momenta. Hence the $\mathrm{AdS}_2 \times \mathbb{R}^{\mathrm{D}-1}$ spacetime, or alternatively, spacetimes conformal to $\mathrm{AdS}_2 \times \mathbb{R}^{\mathrm{D}-1}$ are thought of as the most "fermionic" geometries in holographic systems known to date. Most of the other cases with different scaling properties examined in [63] behave in a rather bosonic way. This is one of our main motivations for analysing the holographic entanglement entropy in this setup (see section 5.3). To have a sensible holographic description, next we compute the AdS completion of the geometry discussed above. This means that we embed (5.10) into an asymptotically AdS spacetime.

5.1.2 UV Completion

To compute the UV completion of the IR geometry discussed in the last section, we follow [121]. Basically it relies on turning around the formula derived before. That is, we define $f_0 = k$ and $g_0 = z_F$ in (5.10) and derive the corresponding scalar potential and effective gauge potential. The next step is to generalise the metric components to obtain asymptotically AdS for $z \ll z_F$ and the IR geometry discussed above for $z \gg z_F$. Here we anticipate the interpretation of z_F as a scale introduced to distinguish between the IR and UV regions of spacetime.
The equations for $\Phi'(z)$, $Z(\Phi)$ and $V(\Phi)$, derived from equations (5.3), are

$$\begin{aligned}
\Phi'(z)^2 =& -\frac{d(g(z)f'(z)+f(z)g'(z))}{zf(z)g(z)}\,,\\
V(\Phi) =& \frac{1}{4f(z)^2g(z)^2}\left[z^2g(z)f'^2(z) - 2df(z)^2(2(d+1)g(z)+zg'(z))+\right.\\
&\left.+zf(z)(zf'(z)g'(z)+2g(z)(2df'(z)-zf''(z)))\right] \text{ and}\\
\frac{1}{Z(\Phi)} =& -\frac{1}{4g^2\kappa^2L^{2-2d}\langle\mathcal{J}^t\rangle^2}\frac{1}{f(z)^2g(z)^2z^{2d-1}}\left[zg(z)f'^2(z)+\right.\\
&\left.+f(z)(zf'(z)g'(z)+2g(z)(df'(z)-zf''(z)))\right]\,,
\end{aligned} \tag{5.14}$$

where we used the general form of the metric in (5.4), i.e. without specifying $f(z)$ and $g(z)$. $\langle \mathcal{J}^t \rangle$ is defined using (3.65) and the first equation in (5.3). However, since here we are using the "z" coordinates we get an additional minus sign in comparison to chapter 3. Thus

$$\langle \mathcal{J}^t \rangle = \frac{L^{d-2}}{g^2} \frac{z^{2-d}}{\sqrt{f(z)g(z)}} Z(\Phi) A_t'(z) = \frac{L^{d-1}}{g\kappa} \frac{z^{2-d}}{\sqrt{f(z)g(z)}} Z(\Phi) h'(z)\,. \tag{5.15}$$

We did not specify any value for z in the definition of the dual charge density since the first equation in (5.3) tells us that this is a conserved quantity along the z direction. Note that we can derive $h'(z)$ in terms of the dual conserved current using this equation. Finally, to be physically sensible we demand $\Phi'(z)^2 \geq 0$ and $Z(\Phi) \geq 0$, which constrains $f(z)$ and $g(z)$ in the equations above. The same constrains are derived using the null energy condition [4, 121]. The former is a consequence of the scalar field being real, while the latter makes sure that the kinetic term of the gauge field has the correct sign.

Now we have all the ingredients we need to compute the full spacetime. Our ansatz is

$$f(z) = \frac{k}{k + z^{2d/\eta}} \quad \text{and} \quad g(z) = \frac{z_F^2}{z^2 + z_F^2}\,, \tag{5.16}$$

with $k > 0$ some arbitrary constant and z_F the scale which separates between the UV and IR. One can check that in the IR, for $z \gg z_F$, the IR geometry of last section is obtained, while for $z = 0$ we get AdS_{d+2} spacetime. By plugging this ansatz into (5.14) results in

$$\begin{aligned}
\Phi'(z)^2 =& \frac{d\left(2kz^2 + z^p\left((p+2)z^2 + pz_F^2\right)\right)}{2z^2\left(z^2+z_F^2\right)(k+z^p)} \\
V(\Phi) =& -\frac{1}{4z_F^2(k+z^p)^2}\Big[4d^2\left(z^2+z_F^2\right)(k+z^p)^2 + \\
&+4d(k+z^p)\left(z_F^2(k+z^p) + pz^p\left(z^2+z_F^2\right)\right) + \\
&+pz^p\left(z^p\left(pz^2+(p+2)z_F^2\right) - 2k\left(pz^2+(p-1)z_F^2\right)\right)\Big] \\
Z(\Phi) =& \frac{4\langle \bar{\mathcal{J}}^t\rangle^2 z_F^2 z^{2d-p}(k+z^p)^2}{2kp\left((d-p)\left(z^2+z_F^2\right)+z_F^2\right) + pz^p\left((2d+p)\left(z^2+z_F^2\right)+2z_F^2\right)}\,,
\end{aligned} \tag{5.17}$$

with $\langle \bar{\mathcal{J}}^t \rangle = g\kappa L^{1-d} \langle \mathcal{J}^t \rangle$ and $p = 2d/\eta$. The requirement for positivity of $Z(\Phi)$ leads to $p < d+1$. Next we examine the near boundary $z \to 0$ limit of these functions, which is

$$\begin{aligned}
\Phi(z) &\simeq \frac{\sqrt{d}}{z_F} z\,, \\
Z(\Phi) &\simeq 2\langle \bar{J}^t \rangle \frac{k d^{\frac{p}{2}-d} z_F^{2d-p}}{p(d-p+1)} \Phi(z)^{2d-p}\,, \\
V(\Phi) &\simeq -d(d+1) - d\Phi(z)^2\,.
\end{aligned} \tag{5.18}$$

The scalar potential close to the boundary corresponds to an AdS spacetime with negative cosmological constant $-d(d+1)/L^2 = -(\mathrm{D}-1)\mathrm{D}/L^2$ and a mass term for the scalar field, with $L^2m^2 = -d$. This mass squared term is above the BF bound $m^2 \geq -(d+1)^2/4$. Thus we conclude that the full geometry

$$\mathrm{d}s^2 = \frac{L^2}{z^2}\left(-\frac{k}{k+z^{2d/\eta}}\mathrm{d}t^2 + \frac{z_F^2}{z^2+z_F^2}\mathrm{d}z^2 + \sum_{i=1}^{d}\mathrm{d}x_i^2\right) \tag{5.19}$$

is a physically sensible solution to the Einstein-Maxwell-Dilaton system, with the potentials and scalar fields given by (5.17).

Before we change gears and introduce entanglement entropy in the next section we would like to add some final comments about this background. In [129] it was shown that it is possible to derive geometries of the form (5.10) in top-down models. That is by consistently truncating a supergravity theory. In their case, however, $\eta = 1$ is fixed. In addition, they can identify the scale z_F as set by the charge density $\langle \mathcal{J}^t \rangle$. However, since there is no other scale in our theory apart from the charge density, or alternatively the chemical potential, we assume that a similar identification is possible here, even though we do not know the precise relation. For the computations in the last section of this chapter we will set $z_F = 1$ and by that effectively fixing the chemical potential to a certain value.

5.2 Holographic Entanglement Entropy

5.2.1 Entanglement Entropy

In this section we give a brief introduction to entanglement entropy from a field theoretic perspective. Most of the material and ideas presented below are based on [121, 130].

Take some quantum mechanical system M at zero temperature. The system is in the ground state $|\Psi\rangle$, which is also non-degenerate. In this case the density matrix ρ is very simple, namely

$$\rho_M = |\Psi\rangle\langle\Psi| \,. \tag{5.20}$$

The von Neumann entropy,

$$S_M = -\mathrm{tr}\left(\rho_M \ln \rho_M\right) \,, \tag{5.21}$$

for this cases vanishes, since the ground state is non-degenerate. Next we divide the system M into to subsystems A and B, where B is the complement of A (see fig. 5.1). The total Hilbert space $\mathcal{H}_M$ decomposes into a direct product of the Hilbert spaces of the two subsystems, i.e. $\mathcal{H}_M = \mathcal{H}_A \otimes \mathcal{H}_B$.

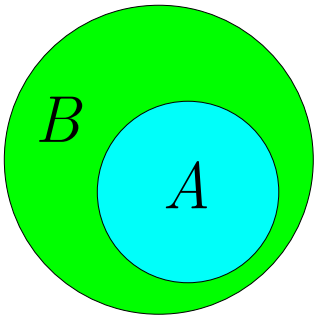

Figure 5.1: Visualisation of entanglement entropy. A system M is divided into two subsystems A and B.

Assume that an observer can only access the degrees of freedom in A. Thus she would only be able to determine the reduced density matrix ρ_A, i.e. the degrees of freedom of B are traced out, thus

$$\rho_A = \mathrm{tr}_B \rho_M \,, \tag{5.22}$$

where tr_B denotes the trace taken over the states living in $\mathcal{H}_B$. The corresponding von Neumann entropy is

$$S_A = -\mathrm{tr}_A \left(\rho_A \ln \rho_A\right) \,. \tag{5.23}$$

This is the entanglement entropy and it accounts for the amount of entanglement between subsystem A and subsystem B. As argued in [130], the entanglement entropy can be seen as a measure for how quantum a system is. Note that by dividing the total system M into the two subsystems we do not change the system in any physical sense, we just draw a symbolic line through it.

Before continuing, let us discuss two small examples to illustrate the concept of entanglement and entanglement entropy. The first example starts with a ground state in the pure state

$$|\Psi\rangle = \frac{1}{\sqrt{2}}\Big(|+\rangle_A|-\rangle_B - |-\rangle_A|+\rangle_B\Big) \,, \tag{5.24}$$

where $+$ and $-$ denotes, for instance, the spin up or down state of an electron or positron. The indices A and B would, in this case, each label one of the two particles. If we stay in the electron-positron picture, this ground state describes a electron-positron system in a spin singlet state. This state could be generate for instance in a pair-production process.
The density matrix of the system is

$$\begin{aligned}\rho =& \frac{1}{2}\Big(\big(|+\rangle_A|-\rangle_B\langle+|_A\langle-|_B\big) - \big(|+\rangle_A|-\rangle_B\langle-|_A\langle+|_B\big) \\ &+ \big(|-\rangle_A|+\rangle_B\langle-|_A\langle+|_B\big) - \big(|-\rangle_A|+\rangle_B\langle+|_A\langle-|_B\big)\Big) \,.\end{aligned} \tag{5.25}$$

A simple computation shows that the von Neumann entropy of this state vanishes. Thus $|\Psi\rangle$ is a pure state. However, what we really want to compute is the entanglement entropy of, e.g., system A. To do so we first trace over system B in ρ and obtain the reduced density matrix

$$\rho_A = \frac{1}{2}\Big(|+\rangle_A\langle+|_A + |-\rangle_A\langle-|_A\Big) \tag{5.26}$$

of system A. The corresponding entanglement entropy is easy to compute. Using (5.23) it reads

$$S_A = -\mathrm{tr}_A\left(\rho_A \ln \rho_A\right) = -\frac{1}{2}\left(\ln\frac{1}{2} + \ln\frac{1}{2}\right) = \ln 2\,. \tag{5.27}$$

This is the maximal value for the entanglement entropy of a two qubit system. Thus states with this property are called maximally entangled states.

In the second example the pure ground state is

$$|\Psi\rangle = \frac{1}{\sqrt{2}}\Big(|+\rangle_A - |-\rangle_A\Big) \otimes \frac{1}{\sqrt{2}}\Big(|+\rangle_B - |-\rangle_B\Big)\,. \tag{5.28}$$

By performing the same steps as before we find that the entanglement entropy of, say, system A vanishes. Thus this two qubit system is not entangled at all.

These examples are very simple, however, they show how entanglement entropy can characterise the entanglement between two subsystems. Furthermore we can easily see that $S_A = S_B$ in above examples. It is clear that in these cases this has to be true since the ground state was symmetric in A and B. However, it is important to note that the statement

$$S_A = S_B \tag{5.29}$$

is true in general if B is the complement of A. This tells us that the entanglement entropy is an intensive quantity. The other important properties of this entropy are subadditivity and strong subadditivity. The former is defined by

$$S_{A_1} + S_{A_2} \geq S_A\,, \tag{5.30}$$

where A_1 and A_2 are submanifolds of A. Note that A_1 and A_2 are not expected to be complementary to each other and they may overlap. The strong subadditivity reads

$$S_{A+B+C} + S_B \leq S_{A+B} + S_{B+C}\,. \tag{5.31}$$

The next step would be to perform the same computations in quantum field theories. However, these are far more intricate and we refer the interested reader to the literature (see e.g. [121, 130, 131] and references therein). Nevertheless, there

are some important results which we need for our later sections. We restrain ourselves to just state them here without derivation, again following the presentation of [130].

In a continuum theory, the entanglement entropy is always divergent and takes the generic form [130]

$$S_A = \gamma \frac{\text{Area}(\partial A)}{\epsilon^{d-1}} + \text{subleading orders}\,, \tag{5.32}$$

where γ is some numerical prefactor depending on the theory, ∂A is the boundary separating A and B (see fig. 5.1) and ϵ is an UV cutoff, for instance, the lattice spacing. This behaviour is called the area law. There are some exceptions to this area law. In a $1+1$ dimensional CFT the entanglement entropy is

$$S_A^{1+1 \text{ dim.}} \propto \ln \frac{l}{\epsilon} + \dots\,, \tag{5.33}$$

where l is the width of A in one distinct spatial dimension. Finally, the last (logarithmic) violation of the area law we need is known to appear in systems with Fermi surfaces [121, 130]. In this case one finds

$$S_A^{\text{Fermi surface}} \propto \left(\frac{l}{\epsilon}\right)^{d-1} \ln \frac{l}{\epsilon} + \dots\,, \tag{5.34}$$

where l is again the typical size of A spanning in all directions and $\epsilon^{-1} \sim k_F$, with k_F the Fermi momentum. As stated in [121], for Fermi momenta smaller than the UV cutoff it is possible to see a Fermi surface in a logarithmic dependence on the typical length of A of the finite parts of the formula above. Note, however, that at the time of writing this last point was still controversially discussed.

Next we show how to compute the entanglement entropy of a field theory with a dual gravity description.

5.2.2 Entanglement Entropy from Holography

In [132], Ryu and Takayanagi proposed a simple way to compute the entanglement entropy for systems with a holographic dual description. In this section we present the conjectured formula and some examples.

The conjectured equation is [132]

$$S_A = \frac{\text{Area}(\gamma_A)}{4G_N^{d+2}}\,, \tag{5.35}$$

(γ_A) is a d dimensional minimal surface in (asymptotically) AdS_{d+2} spacetime with $\partial\gamma_A = \partial A$, where A is the entangling region of the CFT (see figure 5.2).

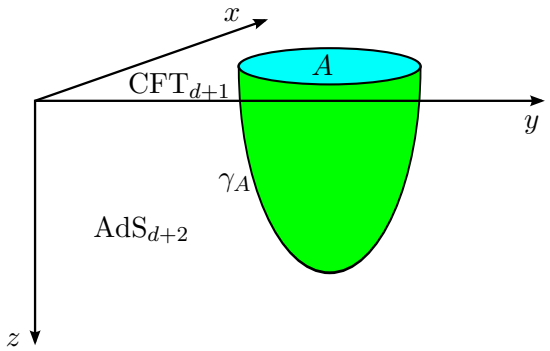

Figure 5.2: The holographic entanglement entropy is computed by minimising the surface γ_A reaching into the AdS bulk.

G_N^{d+2} is the $d+2$ dimensional Newton's constant. The authors of [133] claim to have proven this conjecture for the static case in Einstein-Hilbert gravity, at most minimally coupled to matter. In [130] some examples are computed, where equation (5.35) reproduces exactly known CFT results.

We present some of these examples to explain how to use (5.35). We are interested in simple static entangling geometries at the boundary of pure AdS$_{d+2}$, namely a strip with width l and a disk with radius R. In the following we use the Poincaré z coordinates, i.e.

$$\mathrm{d}s^2 = \frac{L^2}{z^2}\left(-\mathrm{d}t^2 + \mathrm{d}z^2 + \sum_{i=1}^{d}\mathrm{d}x_i^2\right) . \tag{5.36}$$

5.2.2.1 Strip

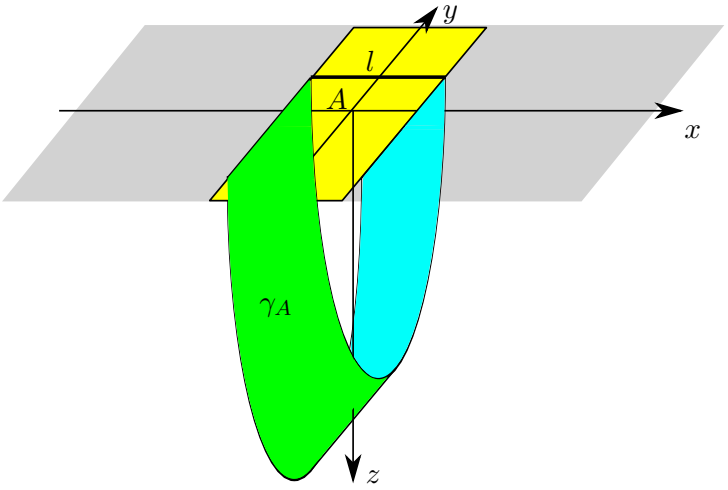

Figure 5.3: The holographic entanglement entropy is computed by minimising γ_A. z is the radial AdS direction, while x and y are spatial field theory coordinates.

In this section we aim to compute the entanglement entropy of a strip in a CFT

dual to pure AdS gravity. The strip has a width l along the $x_1 = x$ direction and in all other directions has length $K \gg l$. As stated above we have to compute the minimal surface γ_A extending from the AdS boundary into the bulk with $\partial\gamma_A = \partial A$ (see fig. 5.3). To do so, we first parametrise the coordinates in terms of the radial AdS coordinate z. Hence the induced metric on γ_A is

$$\mathrm{d}s^2_{\gamma_A} = \frac{L^2}{z^2}\left(\left(1 + x'(z)^2\right)\mathrm{d}z^2 + \sum_{i=2}^{d}\mathrm{d}x_i^2\right). \tag{5.37}$$

The surface area of γ_A is defined as

$$\begin{aligned}\mathrm{Area}(\gamma_A) &= 2\int \mathrm{d}^{d-1}x_i \int_0^{z^*} \mathrm{d}z\, \frac{L^d}{z^d}\sqrt{(1 + x'(z)^2)} = \\ &= 2K^{d-1}L^d \int_0^{z^*} \mathrm{d}z\, \frac{\sqrt{(1 + x'(z)^2)}}{z^d}\,,\end{aligned} \tag{5.38}$$

where z^* is the turning point of γ_A in the AdS bulk. The factor of 2 is due to the fact that the integral only covers half of γ_A with the choice of bounds used above. To compute the minimal surface we use the Euler-Lagrange equation derived from the functional above

$$\frac{\partial}{\partial_z}\left(\frac{x'(z)}{z^d\sqrt{1 + x'(z)^2}}\right) = 0\,. \tag{5.39}$$

Since the right hand side of this equation vanishes, we know that the term in parentheses is conserved. Thus we get

$$x'(z) = \frac{\left(\frac{z}{z^*}\right)^d}{\sqrt{1 - \left(\frac{z}{z^*}\right)^{2d}}}\,. \tag{5.40}$$

This enables us to compute the turning point z^* in terms of the strip width l, since

$$\frac{l}{2} = \int_0^{z^*} \mathrm{d}z\, x'(z) = \sqrt{\pi}\frac{\Gamma\left(\frac{d+1}{2d}\right)}{\Gamma\left(\frac{1}{2d}\right)}z^*\,, \tag{5.41}$$

where $\Gamma(t)$ is the gamma function. Putting everything together and evaluating the integral (5.38) for $d > 1$ leads to

$$\mathrm{Area}(\gamma_A) = \frac{2L^d}{d-1}\left(\frac{K}{\epsilon}\right)^{d-1} - \frac{2^d L^d \pi^{d/2}}{d-1}\left(\frac{K}{l}\right)^{d-1}\left(\frac{\Gamma\left(\frac{d+1}{2d}\right)}{\Gamma\left(\frac{1}{2d}\right)}\right)^d, \tag{5.42}$$

where we expressed z^* in terms of l using equation (5.41). Furthermore, since the integral (5.38) diverges at $z = 0$ we choose a cutoff $\epsilon \ll 1$. Finally, we compute the entanglement entropy S_A^{strip} using equation (5.35), hence for $d > 1$

$$S_A^{\mathrm{strip}} = \frac{1}{4G_N^{d+2}}\left(\frac{2L^d}{d-1}\left(\frac{K}{\epsilon}\right)^{d-1} - \frac{2^d L^d \pi^{d/2}}{d-1}\left(\frac{K}{l}\right)^{d-1}\left(\frac{\Gamma\left(\frac{d+1}{2d}\right)}{\Gamma\left(\frac{1}{2d}\right)}\right)^d\right). \tag{5.43}$$

For the $d = 1$ case it is possible to solve the equation (5.40) directly and obtaining

$$x = -\sqrt{(z^*)^2 - z^2}\,. \tag{5.44}$$

Hence, the final result is $z^* = l/2$ and $\text{Area}(\gamma_A) = 2L \ln\left(\frac{l}{\epsilon}\right)$.
By comparing these results with equations (5.32) and (5.33), we see that the gravity calculations give exactly the behaviour expected from the corresponding field theories.

5.2.2.2 Disc

The next entangling region of interest is a disc/ball of radius R on the field theory side (see fig. 5.2). First we change to polar coordinates in the spatial field theory directions, i.e. $\sum_{i=1}^{d} \mathrm{d}x_i^2 = \mathrm{d}r^2 + r^2 \mathrm{d}\Omega_{d-1}$. Next we determine the induced metric on the surface γ_A, where γ_A is parametrised with respect to the radial AdS coordinate z. Thus we get

$$\mathrm{d}s^2_{\gamma_A} = \frac{L^2}{z^2}\left(\left(1 + r'(z)^2\right)\mathrm{d}z^2 + r^2 \mathrm{d}\Omega_{d-1}\right)\,. \tag{5.45}$$

Following the same steps as before the surface area of γ_A is

$$\text{Area}(\gamma_A) = L^d \text{Vol}(S^{d-1}) \int_0^{z^*} \frac{r^{d-1}}{z^d}\sqrt{1 + r'(z)^2}\,. \tag{5.46}$$

The corresponding Euler-Lagrange equation reads

$$zr(z)r''(z) + (d-1)zr'(z)^4 - dr(z)r'(z)^3 + (d-1)zr'(z)^2 - dr(z)r'(z) = 0\,. \tag{5.47}$$

It is easy to check that

$$r^2 = R^2 - z^2 \tag{5.48}$$

solves this equation. Plugging this solution into (5.46) and using that $z^* = R$ results in

$$\text{Area}(\gamma_A) = L^d \text{Vol}(S^{d-1}) \int_{\epsilon/R}^{1} \mathrm{d}\tilde{z} \frac{\left(1 - \tilde{z}^2\right)^{(d-1)/2}}{\tilde{z}^d}\,, \tag{5.49}$$

with $\tilde{z} = z/R$. Unfortunately it is not possible to derive a closed form for all dimensions. Therefore we stick to the $d = 2$ and 3 case, that is

$$\begin{aligned} \text{Area}(\gamma_A^{d=2}) &= 2\pi L^2 \left(\frac{R}{\epsilon} - \frac{\pi}{2}\right) \quad \text{and} \\ \text{Area}(\gamma_A^{d=3}) &= 4\pi L^3 \left(\frac{1}{2}\left(\frac{R}{\epsilon}\right)^2 - \ln\left(\frac{R}{\epsilon}\right) - \frac{1}{2}\right)\,. \end{aligned} \tag{5.50}$$

Note that for $d = 1$ we get the same result as in the strip case, with $l/2 = R$. The entanglement entropy thus reads

$$\begin{aligned} S_A^{d=2} &= \frac{\pi L^2}{2G_N^4}\left(\frac{R}{\epsilon} - \frac{\pi}{2}\right) \quad \text{and} \\ S_A^{d=3} &= \frac{\pi L^3}{G_N^5}\left(\frac{1}{2}\left(\frac{R}{\epsilon}\right)^2 - \ln\left(\frac{R}{\epsilon}\right) - \frac{1}{2}\right)\,. \end{aligned} \tag{5.51}$$

Here again, the leading divergent behaviour on the gravity side agrees with the results in field theories stated in equation (5.32). For a more general discussion regarding arbitrary dimensions d we refer the interested reader to [130].

5.3 Holographic Entanglement Entropy in IR Scaling Geometries

In this section we use the tools developed above to compute the entanglement entropy of the field theory dual to the scaling geometry discussed in section 5.1.2. First we examine a strip and a disc region solely in the IR limit of this spacetime, since this case is easier to compute. In parts the computation can even be performed analytically. The results we obtain in this limit should agree with the full spacetime calculations for large values of the typical length of an entangling region. This comes from the fact that larger entangling surfaces at the AdS boundary probe farther into the bulk region of the gravity side. An intuitive picture for this is that long distances on the field theory side should be described by the IR limit of the underlying microscopic theory. From a gravity dual description this means that the long distance behaviour at the boundary is encoded by the deep IR geometries, i.e. the geometries far away in the bulk. Next we compute the entanglement entropy for these shapes in the full geometry as well. In addition we consider the annulus. The reason for computing the annulus is that the strip and disc entangling surface behave very differently from each other for large values of their typical lengths. The annulus is thus thought of an interpolating geometry between the other two geometries.

5.3.1 IR Geometry

In this section we calculate the holographic entanglement entropy in the IR limit of the geometry (5.19) for two different entangling surfaces, namely the strip and the disc. For this purpose we consider the case where $g_0 = z_F = 1$ in (5.10),

$$\mathrm{d}s^2 = \frac{L^2}{z^2}\left[-\frac{f_0}{z^p}\mathrm{d}t^2 + \frac{1}{z^2}\mathrm{d}z^2 + \sum_{i=1}^{d}\mathrm{d}x_i^2\right], \quad \text{with } p = 2d/\eta. \tag{5.52}$$

As shown before, this metric is conformal to $AdS_2 \times \mathrm{R}^d$, i.e. for $z = \xi^{2/p}$,

$$\mathrm{d}s^2 = \frac{L^2}{\xi^{\frac{2\eta}{d}}}\left[-\frac{1}{\xi^2}\mathrm{d}t^2 + \frac{1}{\xi^2}\mathrm{d}\xi^2 + \sum_{i=1}^{d}dx_i^2\right]. \tag{5.53}$$

The metric (5.52) is used to calculate the entanglement entropy of the strip, while the metric (5.53) is considered when dealing with the case of the disc. We find that in the IR limit the the boundary separation length of the strip is always constant. We will see that this translates into the fact that in the IR the predominant

minimal surface is two parallel slabs reaching into the bulk. For the sphere case we extract the leading order behaviour in terms of a large disc radius of the entanglement entropy analytically. These results are confirmed by numerical evaluations, in addition the leading order behaviour exhibits an 'area law'.

5.3.1.1 Strip

The strip is defined in the following way (cf. section 5.2.2.1)

$$x_1 \equiv x \in \left[-\frac{l}{2}, \frac{l}{2}\right] , \tag{5.54}$$

with $x_i \in [0, K]$ for $i = 2 \dots d$ and we demand $l \ll K$. The induced metric is given by

$$\mathrm{d}s^2_{\gamma_A} = \frac{L^2}{z^2}\left(\left(\frac{1}{z^2} + x'^2\right)\mathrm{d}z^2 + \sum_{i=2}^{d} \mathrm{d}x_i^2\right) , \tag{5.55}$$

where we have parameterised the minimal surface area γ_A by $x = x(z)$. Thus the minimal surface area reads

$$\begin{aligned} A(\gamma) =& 2\int \frac{L^d}{z^d}\sqrt{\frac{1}{z^2} + x'^2} \\ =& 2L^d K^{d-1}\int \frac{dz}{z^d}\sqrt{\frac{1}{z^2} + x'^2} \, . \end{aligned} \tag{5.56}$$

Since the Lagrangian does not explicitly contain x, there is a conserved quantity (cf. section 5.2.2.2)

$$C = \frac{x'}{z^d\sqrt{\frac{1}{z^2} + x'^2}} , \tag{5.57}$$

which can be recast into

$$x' = \frac{(\frac{z}{z^*})^d}{z\sqrt{1 - (\frac{z}{z^*})^{2d}}}. \tag{5.58}$$

Here z^* denotes the turning point where x' diverges. The boundary separation length l is related to z^* by

$$\frac{l}{2} = \int_0^{z^*} dz \frac{(\frac{z}{z^*})^d}{z\sqrt{1 - (\frac{z}{z^*})^{2d}}}, \tag{5.59}$$

which can be integrated and results in

$$l = l_{\mathrm{crit}} = \frac{\pi}{d} \, . \tag{5.60}$$

Thus the width of the entangling surface is always constant for any value of z^*. The constant boundary separation length has been observed for several other examples as well, i.e. for NS5-branes in [130] and for backgrounds with semi-locality [63, 129]. As argued in [63], this result indicates that a minimal surface

connecting the strip edges at the boundary only exists for a specific separation $l < l_{\text{crit}}$. We will see when repeating this computation in the full geometry that as $l \to l_{\text{crit}}$ the minimal surface drops increasingly farther into the IR. For $l > l_{\text{crit}}$, the disconnected minimal surface, i.e. the solution with $x'(z) = 0$ corresponding to two slabs falling into the IR at constant separation length, dominates. This behaviour is reminiscent of holographic entanglement entropy in confined phases [122], where the connected minimal surface describes the deconfined phase, while the disconnected solution is related to the confined phase. We will see that the overall properties mentioned above holds for the whole geometry.

5.3.1.2 Disc

In this subsection we calculate the holographic entanglement entropy with a spherical entangling surface. For convenience we work with the metric (5.53), which is explicitly conformal to $AdS_2 \times \mathbb{R}^d$. The spherical entangling region is parameterised by $\sum_{i=1}^{d} x_i^2 = R^2$ and the induced metric is given by

$$ds^2_{\gamma_A} = \frac{L^2}{\xi^{\frac{2\eta}{d}}}\left[\left(1+\frac{\xi'^2}{\xi^2}\right)\mathrm{d}\rho^2 + \rho^2 \mathrm{d}\Omega^2_{d-1}\right]. \tag{5.61}$$

We find that the minimal surface area reads (cf. section 5.2.2.2)

$$\begin{aligned} A(\gamma) &= L^d \int d\Omega_{d-1} d\rho \frac{\rho^{d-1}}{\xi^\eta}\sqrt{1+\frac{\xi'^2}{\xi^2}} \\ &= L^d \mathrm{Vol}(\Omega_{d-1}) \int d\rho \frac{\rho^{d-1}}{\xi^\eta}\sqrt{1+\frac{\xi'^2}{\xi^2}}, \end{aligned} \tag{5.62}$$

which leads to the equation of motion

$$\frac{\partial}{\partial\rho}\left(\frac{\rho^{d-1}\xi'}{\xi^{\eta+2}\sqrt{1+\frac{\xi'^2}{\xi^2}}}\right) = -\frac{\rho^{d-1}}{\xi^{\eta+3}\sqrt{1+\frac{\xi'^2}{\xi^2}}}(\eta\xi^2 + (\eta+1)\xi'^2). \tag{5.63}$$

We can estimate the large R behaviour of the solution to the equation above. To do so we choose the ansatz $\xi(\rho) = \lambda e^{-A\rho^B}$, where A, B and λ are constants. Note that in large R limit, most of the hypersurface lies in the near horizon region, hence the metric (5.53) provides an approximate description. The value of λ is fixed by assuming that the crossover from the IR region to the full geometry is at $\rho \sim R$ and $\xi(R) \sim 1$, where the latter is a consequence of $z_F \sim 1$, hence $\lambda = e^{AR^B}$. Plugging this ansatz into the equation (5.63) leads to

$$\eta\rho^4 + \eta A^2 B^2 \rho^{2+2B} - A^3 B^3 (d-1)\rho^{3B} - AB(B+d-2)\rho^{2+B} = 0. \tag{5.64}$$

The values of A and B can be determined by extracting the leading order (large R) behaviour,

$$B = 2 \quad \text{and} \quad A = \frac{\eta}{2(d-1)} \quad \Rightarrow \quad \xi(\rho) = \lambda e^{-\frac{\eta}{2(d-1)}\rho^2}. \tag{5.65}$$

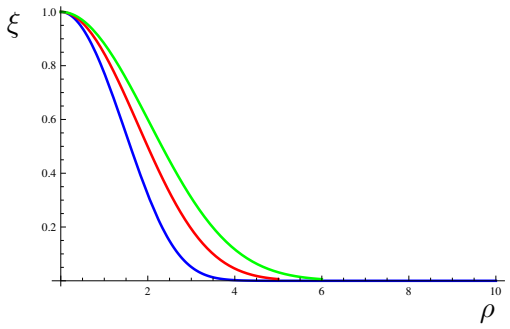

Figure 5.4: The embedding profile $\xi(\rho)$ for a disc entangling surface. ρ is the radial coordinate of the field theory. The blue, red and green curves correspond to the cases $d = 2, 3, 4$ respectively. Source: [4]

The behaviour of $\xi(\rho)$ in different dimension d is plotted in fig. 5.4.

For this case, the holographic entanglement entropy is given by

$$\begin{aligned} S_A^{\text{sphere}} &\propto \int d\rho \frac{\rho^{d-1}}{\xi^\eta} \sqrt{1 + \frac{\xi'^2}{\xi^2}} \\ &\simeq \int d\rho \rho^d e^{A\eta\rho^2} \,. \end{aligned} \tag{5.66}$$

It can be verified that for all dimensions d, the leading order term is R^{d-1}, which means that the area law always holds for large values of R. In particular, we have the following results for $d = 2, 3$,

$$\begin{aligned} &d = 2, \quad S \sim A(\gamma) = R - \frac{1}{R\eta^4} \,, \\ &d = 3, \quad S \sim A(\gamma) = R^2. \end{aligned} \tag{5.67}$$

In fig. 5.5 we compare our leading order results (5.67) with straightforward numerical integration of (5.62). Note that for the $d = 2$ case we use $A_1 = A(\gamma) - R \sim -1/R$, where we compute $A(\gamma)$ numerically by integrating (5.62). In the $d = 3$ case we compare the estimated $A(\gamma)$ in (5.67) with the numerical integration of (5.62). We see that the estimate and the exact numerical integration agree quite well for large values of R. Finally, it is noteworthy that there is no trivial solution $\xi' = 0$ in this case. Thus there is no disconnected phase as in the strip.

5.3.2 Full Geometry

Knowing what to expect for the entanglement entropy in the case of large values of the typical length of the different entangling surfaces, now we go on to compute the entanglement entropy in the full geometry. We find that for a strip entangling shape, the behaviour of the entanglement entropy agrees with the picture proposed in [129], i.e. the boundary separation length l is a smooth function of the turning

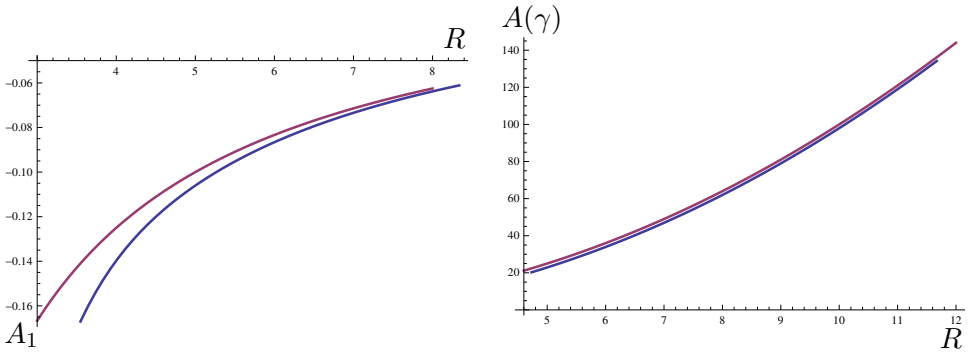

Figure 5.5: The blue curve denotes the numerical solution to (5.62) for $\eta = 1$, while the purple line is the plot of the leading R behaviour of equation (5.67). The left diagram is for the $d = 2$ case, with $A_1 = A(\gamma) - R$. The right one is for $d = 3$. Source: [4]

point and it approaches l_{crit} for large values z^*. In addition, the connected surface dominates when l is sufficiently small and the disconnected surface dominates for $l > l_{\text{crit}}$. In the disc case there is no phase transition. This behaviour is unexpected, since both entangling surfaces probe the same geometry. Unfortunately we can not lift the veil of this mystery here. However, to shed some light on the issue we also compute an annulus entangling region. Before starting with the actual computations, we state the full metric, which was derived in section 5.1.2, since it is used extensively in the following. It reads

$$\mathrm{d}s^2 = \frac{L^2}{z^2}\left(-\frac{k}{k+z^{2d/\eta}}\mathrm{d}t^2 + \frac{z_F^2}{z^2+z_F^2}\mathrm{d}z^2 + \sum_{i=1}^{d}\mathrm{d}x_i^2\right). \tag{5.68}$$

5.3.2.1 Strip

The strip is defined in the same way as before

$$x_1 \equiv x \in \left[-\frac{l}{2}, \frac{l}{2}\right], \text{ with } x_i \in [0, K],\ i = 2 \dots d, \tag{5.69}$$

where $l \ll K$. The induced metric can be read off the solution (5.68)

$$\mathrm{d}s^2_{\gamma_A} = \frac{L^2}{z^2}\left((g(z)+x'^2)\mathrm{d}z^2 + \sum_{i=2}^{d}\mathrm{d}x_i^2\right), \tag{5.70}$$

where we parameterise $x = x(z)$. The minimal surface area is given by

$$\begin{aligned} A(\gamma) &= 2\int \frac{L^d}{z^d}\sqrt{g(z)+x'^2} \\ &= 2L^d K^{d-1}\int \frac{dz}{z^d}\sqrt{g(z)+x'^2}\,. \end{aligned} \tag{5.71}$$

This functional leads to a conserved quantity

$$C = \frac{x'}{z^d\sqrt{g(z)+x'^2}}, \tag{5.72}$$

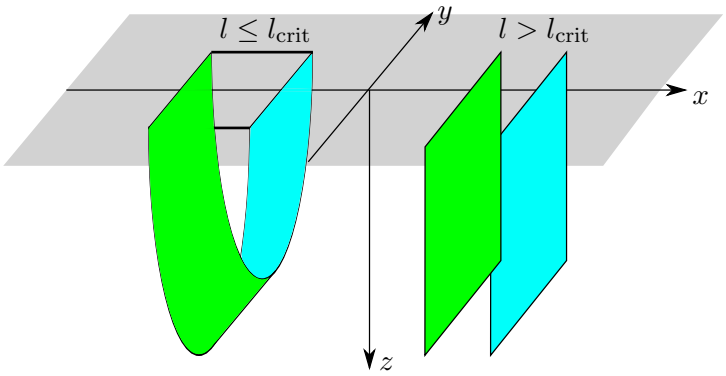

Figure 5.6: Visualisation the two possible solutions for the strip in the scaling geometry.

which we again recast in terms of the turning point z^*, i.e.

$$x' = \frac{\sqrt{g(z)}(\frac{z}{z^*})^d}{\sqrt{1-(\frac{z}{z^*})^{2d}}}\,. \tag{5.73}$$

The boundary separation length is given by integrating this equation, thus

$$\frac{l}{2} = \int_0^{z^*} dz \frac{\sqrt{g(z)}(\frac{z}{z^*})^d}{\sqrt{1-(\frac{z}{z^*})^{2d}}}\,. \tag{5.74}$$

If we plug the IR limit of (5.68) into this equation, i.e. $g(z) = z_F^2/z^2$, the width of the strip is constant and takes the value (cf. the computation above)

$$l = l_{\text{crit}} = \frac{\pi z_F}{d}\,. \tag{5.75}$$

Considering the full solution $g(z) = z_F^2/(z^2+z_F^2)$, we have to integrate

$$l = 2\int_0^{z^*} dz \frac{z_F}{\sqrt{z^2+z_F^2}\sqrt{\left(\frac{z^*}{z}\right)^{2d}-1}}\,, \tag{5.76}$$

to obtain the boundary separation length. Unfortunately this integral can only be solved numerically. In fig. 5.7 we plot $l(z^*)$ for $d = 2, 3$. For all numerical computations we set $z_F = 1$. It is clear from this plot that l is a smooth function of z^*. For small values of z^*, l and l_{crit} differ significantly. However, for z^* sufficiently large, l approaches l_{crit}. Following the RG flow picture, this can be interpreted as probing more and more into the IR. Thus, for increasing values of l we should obtain the result derived in the section above, i.e. $l \to l_{\text{crit}}$. Note that this solution can not go beyond l_{crit}.

To compute the holographic entanglement entropy using equation (5.35) we first determine the minimal surface area $A(\gamma)$ of γ_A. In addition we have to subtract

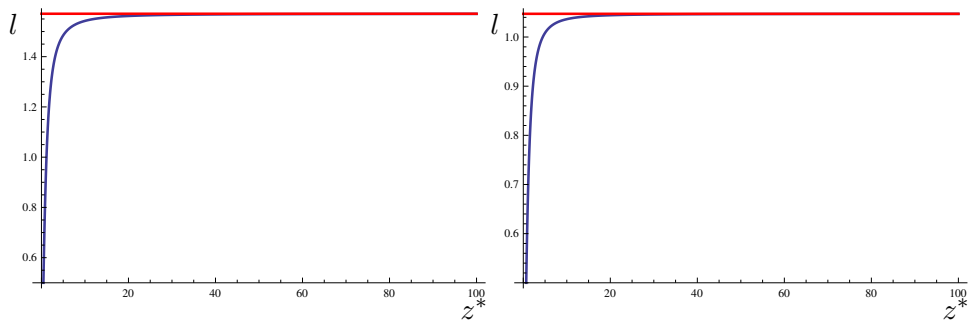

Figure 5.7: We show the boundary separation length of the full solution (blue curve) and the IR solution (red curve). The plot on the left is for the $d = 2$ case and on the right for $d = 3$ case. For both cases l and l_{crit} are significantly different for small values of the turning point z^*. In this case the minimal surface just probes the geometry near the UV. As z^* increases, the minimal surface goes deeper into the IR and l approaches l_{crit}. Source: [4]

the divergent part of the minimal surface. Thus

$$\begin{aligned} A^{\text{con}}_{\text{finite}} =& \frac{1}{2L^d K^{d-1}}(A(\gamma) - A_{\text{div}}) \\ =& \int_0^{z^*} \frac{dz}{z^d} \frac{\sqrt{g(z)}}{1-(\frac{z}{z^*})^{2d}} - \frac{1}{(d-1)\epsilon^{d-1}}\,, \end{aligned} \tag{5.77}$$

and we take the limit $\epsilon \to 0$. The divergent term is the standard result from pure gravity we derived in section 5.2.2.1 (see also [130]). This is a valid approach since our geometry is asymptotically AdS and therefore should have the same dependence on the UV cut off as pure AdS gravity. We plot $A^{\text{strip}}_{\text{finite}}$ in fig. 5.8 for the $d = 2$ and $d = 3$ cases.

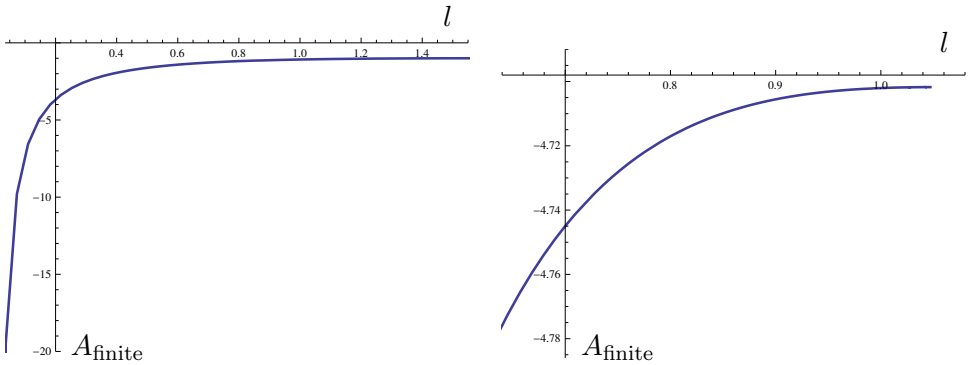

Figure 5.8: Finite part of the holographic entanglement entropy of a strip entangling surface. The plot on the left is for the $d = 2$ case, while the right one is for $d = 3$. As $l \to l_{\text{crit}}$ the entanglement entropy tends to a constant. Source: [4]

The disconnected surface is given by $x' = 0$, so the minimal surface area reads

$$A^{\text{dis}}(\gamma) = L^d K^{d-1} \int \frac{dz}{z^d \sqrt{g(z)}}. \tag{5.78}$$

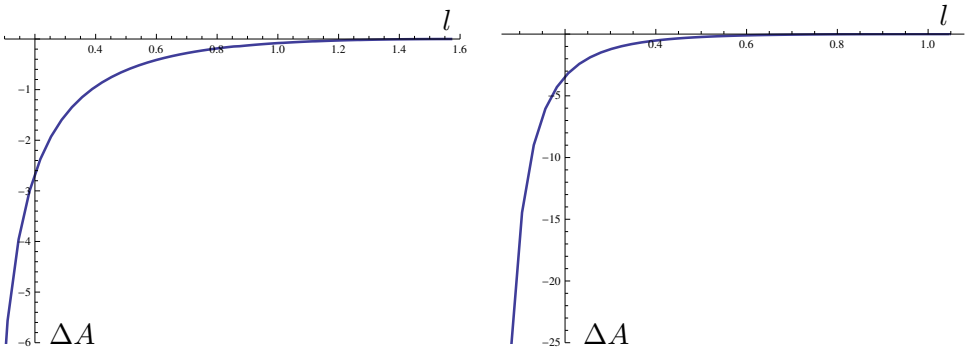

Figure 5.9: The differences between the holographic entanglement entropy of the connected minimal surface and the disconnected one, i.e. $\Delta A = A^{\text{con}}_{\text{finite}} - A^{\text{dis}}_{\text{finite}}$. The plot on the left is for the $d = 2$ case and the one on the right for $d = 3$. When l is sufficiently small, the connected minimal surface dominates. For $l > l_{\text{crit}}$ the disconnected solution dominates. Source: [4]

The behaviour of $\Delta A = A^{\text{con}}_{\text{finite}} - A^{\text{dis}}_{\text{finite}}$ for $d = 2, 3$ is plotted in fig. 5.9, where we again subtracted the divergent term for $A^{\text{dis}}(\gamma)$. It can be seen that when $l < l_{\text{crit}}$, the connected surface dominates. For $l \to l_{\text{crit}}$, the difference between the two solutions tends to zero. Thus the disconnected surface will be the dominant solution for values of the boundary separation length $l > l_{\text{crit}}$. In fig. 5.6 we summarise the finding of this section.

5.3.2.2 Disc

Next we consider the case of a spherical entangling region in the full geometry with polar coordinates at the boundary. The induced metric is given by

$$\mathrm{d}s^2_{\gamma_A} = \frac{L^2}{z^2}\left[\left(g(z) + \rho'^2\right)\mathrm{d}z^2 + \rho^2 \mathrm{d}\Omega^2_{d-1}\right] . \tag{5.79}$$

The minimal surface area reads

$$A_{\gamma_A} = L^d \mathrm{Vol}(\Omega_{d-1}) \int \frac{dz}{z^d} \rho^{d-1} \sqrt{g(z) + \rho'^2}, \tag{5.80}$$

from which we can derive the equation of motion for $\rho(z)$,

$$\partial_z \left(\frac{\rho^{d-1}\rho'}{z^d \sqrt{g(z) + \rho'^2}} \right) = \frac{(d-1)\rho^{d-2}}{z^d} \sqrt{g(z) + \rho'^2}. \tag{5.81}$$

Note that in this case there is no conserved quantity or trivial solution $\rho' = 0$. We solve for $\rho(z)$ numerically by fixing the boundary conditions $\rho(0) = R$, $\rho(z^*) = 0$, where z^* denotes the turning point. The plots for $\rho(z)$ for $d = 2$ and $d = 3$ are shown in fig. 5.10.

In fig. 5.11 we plot the finite part of the holographic entanglement entropy

$$A_{\text{finite}} = \frac{1}{L^d \mathrm{Vol}(\Omega_{d-1})}(A_{\text{sphere}} - A_{\text{div}}), \tag{5.82}$$

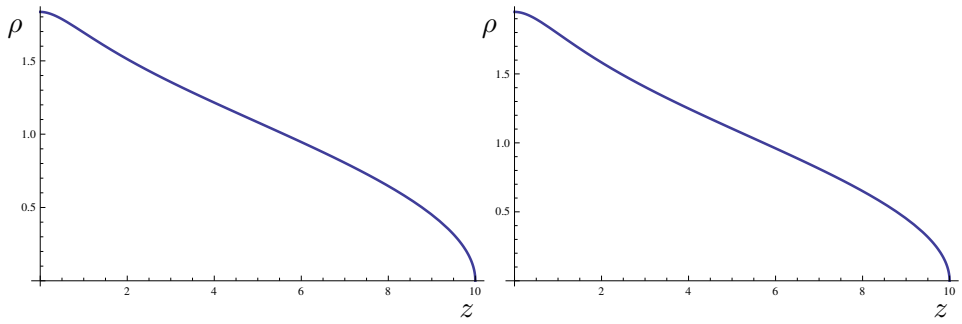

Figure 5.10: The profile of the disc solution. Note that ρ is the radial field theory coordinate and z the radial AdS coordinate. Left: $d = 2$ case; Right: $d = 3$ case. Source: [4]

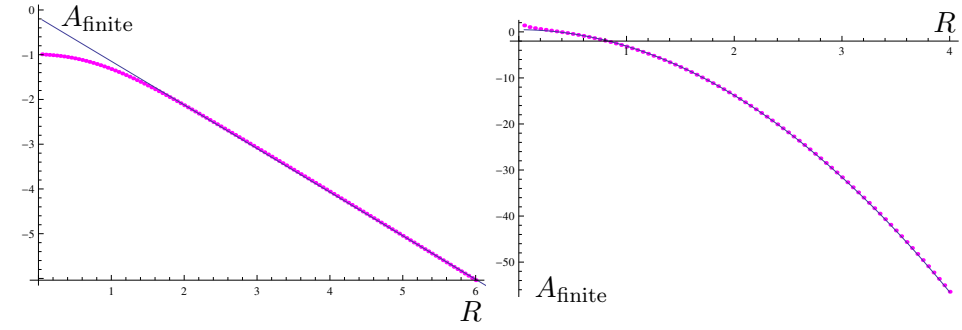

Figure 5.11: Finite part of the holographic entanglement entropy for a spherical entangling region. The plot on the left is the $d = 2$ case, while the right one shows the solution for $d = 3$. The dots are data from numerical evaluations and the curves denote the fits in equation (5.84). Source: [4]

where

$$\begin{aligned} A_{\text{div}} &= \frac{R}{a} \quad \text{for} \quad d = 2 \quad \text{and} \\ A_{\text{div}} &= \frac{R^2}{2a^2} + \frac{1}{2}\log a \quad \text{for} \quad d = 3\,, \end{aligned} \tag{5.83}$$

are the divergencies derived in section 5.2.2.2. The same argumentation as in the strip case holds also here. That is, our geometry corresponds to pure AdS in the UV.

We are interested in the deviation of the finite part of HEE from the area law [129], which can be analysed by performing the fits on the numerical data. The resulting behaviour reads

$$\begin{aligned} A_{\text{finite}} &= -0.171 - 0.975\,R \quad \text{for} \quad d = 2\,, \\ A_{\text{finite}} &= 0.470 - 3.561\,R^2 \quad \text{for} \quad d = 3\,. \end{aligned} \tag{5.84}$$

This indicates that for large values of R the finite part of the holographic entanglement entropy is governed by the area law. This is consistent with the conclusion

in [129], where they compute similar quantities in a string theory embedding of the geometry discussed in section 5.1.2. However, they have to fix $\eta = 1$.

In addition, we cannot find any hint for a phase transition. Rather, with increasing R the turning point z^* diverges exponentially. The divergence is exactly what the authors of [64] find for disc entangling regions in general IR geometries where $g(z) \propto 1/z^2$ (see equation (A5) of their paper, where z_t corresponds to $z(r = 0)$ in our case). Note that the IR geometry discussed in this chapter falls exactly in this class. Interestingly, they argue that the reason for this divergent behaviour is a mass gap in the theory with a continuous spectrum directly on top of the gap. However, in the case at hand this cannot be true, since, as was shown in the first section of this chapter, our IR geometry is dual to $\mathrm{AdS}_2 \times \mathbb{R}^d$ and so there is no scale which could set the gap. Concluding, our case should not have a mass gap neither in the IR nor in the UV.

5.3.2.3 Annulus

From our evaluation of the holographic entanglement entropy for the cases of a strip and a sphere we see a phase transition in the strip case, while no such transition occurs for the sphere case. This behaviour has also been observed in [129], where the background is a charged dilatonic black hole in type IIB supergravity truncated on S^5, whose near horizon geometry is similar to ours with $\eta = 1$.

As argued in [129], a third scale supplied by the anisotropy of the strip should play a role in understanding the phase transition. One way to see this is to consider deforming the sphere entangling surface continuously into an ellipsoid, which finally results in a strip shape entangling region. The phase transition should appear suddenly during this process. However, the ellipsoid is technically quite complex, hence we focus on a simpler case, the annulus, and leave the ellipsoid to future work.

In the annulus case we expect to approximate a sphere in the limit of vanishing inner radius and the strip for both, the inner and outer radius, large in comparison to their difference. We will see that this interpolation between the two geometries does not work out entirely as expected. First we calculate the holographic entanglement entropy for annulus entangling region.

In this case we parametrize $z = z(\rho)$ and obtain the induced metric

$$\mathrm{d}s^2_{\gamma_A} = \frac{L^2}{z^2}\left[\left(1 + g(z)z'^2\right)\mathrm{d}\rho^2 + \rho^2 d\Omega^2_{d-1}\right], \tag{5.85}$$

where prime denotes the partial derivative with respect to ρ.

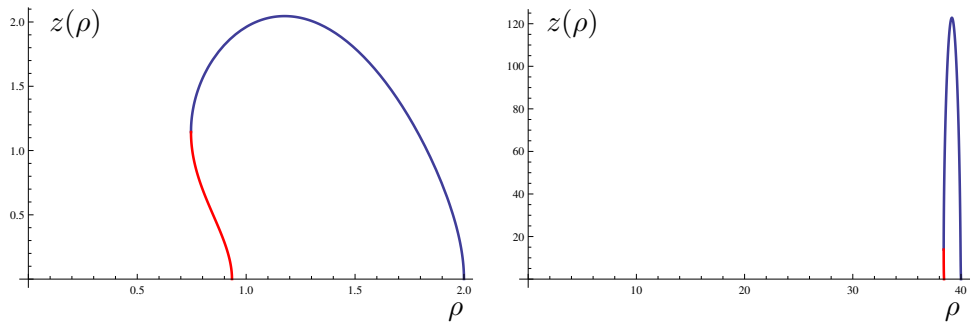

Figure 5.12: Generic connected (annulus) solution. z is the radial AdS coordinate and ρ the radius of the spherical coordinates on the boundary. Both plots are solutions to the equation (5.87) for $d = 2$ and $z_F = 1$. For larger radii ρ_1 and ρ_2 the resulting minimal surface goes deeper into the IR ($z \to \infty$) than it is the case for smaller ones. Note that the solution is not a single valued function, therefore we first generate the blue curve and afterwards search for the matching red one. Source: [4]

The minimal surface area is given by

$$A_{\text{ann}} = L^d \text{Vol}(\Omega_{d-1}) \int d\rho \frac{\rho^{d-1}}{z^d} \sqrt{1 + g(z) z'^2}, \tag{5.86}$$

which leads to the equation of motion

$$\partial_\rho \left(\frac{\rho^{d-1} g(z) z'}{z^d \sqrt{1 + g(z) z'^2}} \right) = -\frac{d\rho^{d-1}}{z^{d+1}} \sqrt{1 + g(z) z'^2} + \frac{\rho^{d-1}}{2z^d} \frac{z'^2}{\sqrt{1 + g(z) z'^2}} \partial_z g(z), \tag{5.87}$$

with boundary condition $z(\rho_1) = z(\rho_2) = \epsilon \to 0$. It is not possible to solve this equation for the whole profile of $z(\rho)$ at once (see blue part of fig. 5.12). What we do instead is to solve the system a second time, however, this time with the parametrisation $\rho(z)$ (see red part of profile in fig. 5.12). Afterwards we numerically invert this result and match both curves.

The finite parts of the minimal surface area are again given by

$$A_{\text{finite}} = \frac{1}{L^d \text{Vol}(\Omega_{d-1})} (A_{\text{ann}} - A_{\text{div}}), \tag{5.88}$$

where we take the divergent terms from [134],

$$\begin{aligned} A_{\text{div}} &= \frac{\rho_1 + \rho_2}{\epsilon}, \quad d = 2, \\ A_{\text{div}} &= \frac{\rho_1^2 + \rho_2^2}{2\epsilon^2} - \frac{1}{2} \log \frac{\rho_1 \rho_2}{a^2}, \quad d = 3. \end{aligned} \tag{5.89}$$

We show generic results for the entanglement entropy for $d = 2$ and $d = 3$ in figures 5.13 and 5.14. There we plot A_{finite} versus the difference of the radii $\Delta\rho = \rho_2 - \rho_1$. We find two connected solutions (deformed annulus, see figure 5.12) for values of $\Delta\rho \leq (\Delta\rho)_{\text{max}}$ and one disconnected solution (two concentric balls) for all values

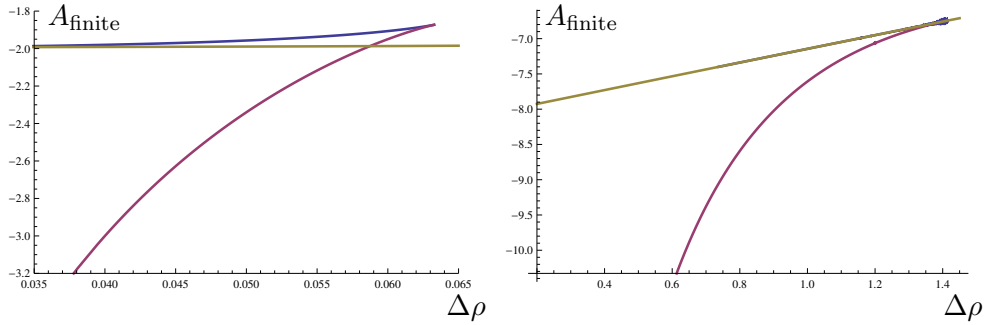

Figure 5.13: Finite part of the annulus entangling region for $d = 2$ versus the difference of the radii $\Delta\rho = \rho_2 - \rho_1$. The left plot has $\rho_2 = 0.1$ and the right one $\rho_2 = 4$ in terms of z_F. Note that for small differences $\Delta\rho \leq (\Delta\rho)_{\text{max}}$ we see different solutions, two connected (deformed annulus) solutions with the lower one being preferred (blue and red) and the concentric balls solution (yellow). The transition between the connected and disconnected solutions at $(\Delta\rho)_{\text{crit}}$ is first order for small values of ρ_2 as becomes obvious from the swallow tail form of the left plot. For larger values of ρ_2 we have a second order transition (see right plot). If $\Delta\rho > (\Delta\rho)_{\text{max}}$ the disconnected solution is the only solution, this behaviour is very similar to the strip case discussed in section 5.3.2.1. To generate these plots we set $z_F = 1$ and the cutoff $a = 0.001$. Source: [4]

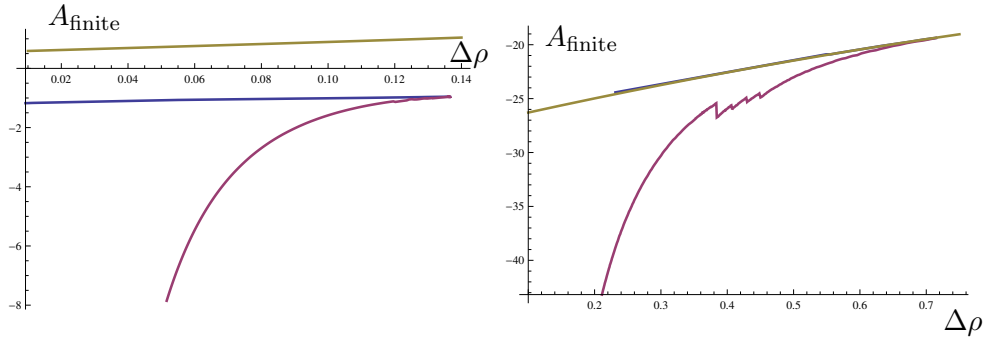

Figure 5.14: Finite part of the annulus entangling region for $d = 3$ versus the difference of the radii $\Delta\rho = \rho_2 - \rho_1$. The left plot has $\rho_2 = 0.3$ and the right one $\rho_2 = 2$ in terms of z_F. Note that for small differences $\Delta\rho \leq (\Delta\rho)_{\text{crit}}$ we see different solutions, two connected (deformed annulus) solutions with the lower one being preferred (blue and red) and the concentric balls solution (yellow). In contrast to the $d = 2$ case we don't find a transition for small values of $\rho_2 < \mathcal{O}(1)$ and a second order one for larger values. For larger values of $\Delta\rho$ the disconnected solution is the only solution, this behaviour is very similar to the strip case discussed in section 5.3.2.1. To generate these plots we set $z_F = 1$ and the cutoff $a = 0.001$. The jagged feature in the right plot is an artifact of the numerical computation and has no physical interpretation. Source: [4]

of $\Delta\rho$. Note that for each value of $\Delta\rho$ the preferred solution is the one with smaller value of A_{finite}. In the $d = 2$ case, at a value $(\Delta\rho)_{\text{crit}}$ a first order transition from the preferred connected to the disconnected solution for small values of the radii and a second order transition for larger ones is found. For $d = 3$ we find a different behaviour: In that case there is no transition for values ρ_1, $\rho_2 < \mathcal{O}(1)$ (the exact value is hard to determine, due to difficult numerical computations), only for larger radii we observe a second order transition. This behaviour is very similar to the strip case discussed in section 5.3.2.1, where there also only exists a connected solution for $l \leq l_{\text{crit}}$, however, there the transition is second order opposed to the case at hand. The analogy goes further: increasing the values of the radii ρ_1, ρ_2 leads to $(\Delta\rho)_{\text{crit}} \to \pi/d$ (c.f. eq. (5.75) with $z_F = 1$). We are not able to check this limit analytically, however our results using numerical methods are in very good agreement with above statement for $d = 2$ and $d = 3$ (see figure 5.15). Looking closer at this limit in $d = 2$, we see the swallow tail becomes smaller turning into a second order transition (see right part of fig. 5.13). From this behaviour we deduce that the annulus tends towards the strip solution for large radii. The other limit, however, where we aim at approximating a sphere, does not work entirely as expected, since for each given pair of radii of the annulus solution, we always find a maximal difference $(\Delta\rho)_{\text{max}}$ between both which is smaller than outer radius ρ_2. Therefore we can at most approximate two concentric spheres, but never one sphere alone. Even this is not always possible, as the small radii $d = 3$ case described above shows. Nevertheless, the similarity in most of the parameter space to the behaviour seen in confining geometries is astonishing (see [122, 123]). It would be interesting to understand if there is a common origin to this resemblance.

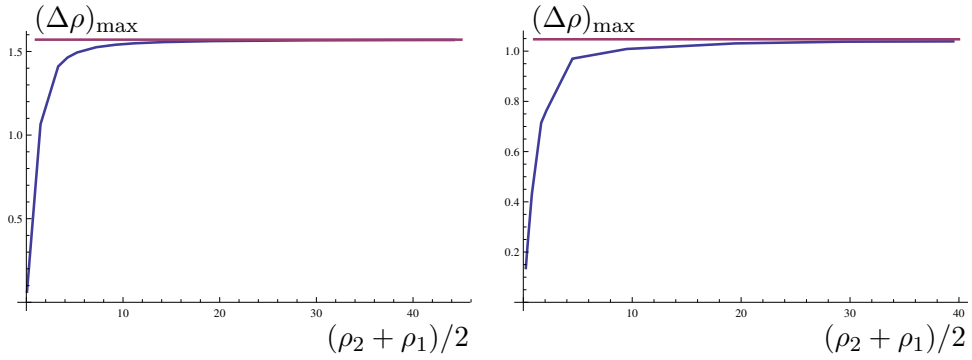

Figure 5.15: We plot the maximal difference between the radii of the connected solution $(\Delta\rho)_{\text{max}}$ versus the middle radius $(\rho_2 + \rho_1)/2$, for $d = 2$ (left) and $d = 3$ (right). It is apparent that $(\Delta\rho)_{\text{max}} \to z_F\pi/d$ (red line), with $z_F = 1$, for larger values of the radii ρ_i. Source: [4]

Finally in the annulus as well as in the strip case $l_{\text{crit}} = \pi z_F/d$ plays an important role governing the phase transition, however, to our knowledge, there is no known dual interpretation of this value. This would be interesting to study further. Since

it is possible to embed the solution described in section 5.1.2 into string theory, at least for the $\eta = 1$ case (see [129]), in principle it should be possible to compute the entanglement entropy in the dual theory, although probably this is not feasible from a technical point of view.

Chapter 6

Conclusion

Universalities play a major role in gauge/gravity duality. At the moment the best understood limit of the duality is the large N and large 't Hooft coupling limit. Thus, sensible quantitative predictions are only possible in terms of dimensionless quantities, without an explicit N dependence.
A second field of application is related to quantum phase transitions. The quantum critical points of different materials can be categorised in terms of a few parameters, for instance, the dynamical critical exponent. Therefore, these points are of universal nature as well. In addition they are described by conformal field theories and some of them seem to be governed by strong coupling. Thus it is natural to expect that gauge/gravity duality can provide some input in this area. In this thesis we saw discussions about both kinds of universalities.

In chapter 4 the first aspect mentioned above was discussed. There, however, we were interested in how to break a universal behaviour, namely the famous ratio between shear viscosity and entropy density. From gauge/gravity duality it was derived that for strongly coupled theories this ratio takes the value $\eta/s = 1/4\pi$. Even though this result is already very close to the measured values for the quark-gluon plasma, to describe any substance found in nature this ratio should be temperature dependent. In this thesis we showed that by breaking the rotational symmetry of a holographic system we can generate such non-universal behaviour.

Besides the shear viscosity, many other transport properties in an anisotropic setup were computed. We found a surprising low frequency behaviour in one of the electrical conductivities of the system, namely a broad Drude peak. This is remarkable, since no translational invariance was broken in any obvious way. In addition, the phase with broken rotational symmetry is also superconducting, i.e. there is a superimposed delta peak on top of the Drude peak.

Due to the coupling between metric and gauge field components, well-known effects from transversely isotropic liquid crystal were induced. Firstly the interaction between flavour currents and off-diagonal stress components resembles the flexoelectric effect, which describes the polarisation of a crystal through mechanical bending. Secondly we see the same structure as in the piezoelectric effect. This effect describes an electrical current due to the squeezing and elongation of a crystal.

Our second main chapter, chapter 5, is related to the universal aspect of quantum phase transitions raised in the first paragraph. There we analysed an IR scaling geometry, i.e. a geometry with a dynamical critical scaling and a hyperscaling violation parameter. The geometry of interest to us was obtained in the limit where the critical scaling and the hyperscaling parameter were send to infinity and minus infinity, respectively, while the ratio of both was kept fixed. This leads to a solution with very fermionic properties, which means low energy excitations at finite momentum and in addition a vanishing entropy at zero temperature. The latter is sensible to describe condensed matter systems, while the former resembles the behaviour close to a Fermi surface.

In this geometry we computed the holographic entanglement entropy for a strip, a disc and an annulus. It is noteworthy that while the strip and the annulus encoded a phase transition for a certain value of the corresponding typical length, the disc did not. Interestingly, in the literature similar effects were observed, however, the explanation put forward there did not apply to our case. Apart from that we could not find any logarithmic area law violation, which may have been related to a Fermi surface.

We see that many of the points discussed in this thesis relate to some kind of universal behaviour. Be it to break it or to find a system describing it. As long as the duality is not better understood in other limits, the search for universalities will be a natural way to continue along. So before we finally conclude we present some future directions arising from this thesis outcome.

Outlook

The holographic p-wave superconductor provides many interesting and feasible directions to follow up on, since it implements anisotropy without the demand for advanced numerical techniques. For once, it would be interesting to switch on a finite momentum along the direction of the condensate. This may lead to momentum induced instabilities [116] and open a door to making contact with the helical phases of black holes, which recently gained much attention [61,118,119]. A second

direction is the computation of the fluid/gravity description of the p-wave. This would not only strengthen the identification of the different transport properties derived in this thesis, but it would at the same time lead to a constitutive equation of a relativistic conformal fluid with broken rotational symmetry. This equation would be valid independently from gauge/gravity duality. Another direction is the inclusion of a time dependent chemical potential, in the spirit of [135], to see how anisotropy influences the time evolution of different modes. Finally, the IR limit of the backreacted p-wave geometry is still an unsolved problem. It would be interesting to see if there are different IR fixed points, besides the domain wall solution of [98], depending on the parameters we choose.

Concerning the holographic entanglement entropy in scaling geometries, a natural extension is to perform a broad survey of the geometries known to have the awkwardly behaving disc entangling surface. Since the entanglement entropy is considered to be sensitive to the spectrum of a theory, it would be very interesting to understand why we see so similar behaviours in so different theories, namely between theories with confinement and without, and with a mass gap and without.

Throughout this thesis we computed various black hole solutions to describe dual superconductors and other condensed matter systems. Nevertheless, one of the big goals of gauge/gravity duality is to understand the duality the other way around. Our hope is that by learning more and more about this simpler direction, some day it will be possible to create a black hole on a lab table.

Acknowledgements

I would like to thank Johanna Erdmenger for her continuous and stimulating support and advice, and for the possibility to work in the inspiring environment of her group. I thank Dieter Lüst for the excellent atmosphere at the Max-Planck-Institute, for reading through this thesis as second referee, and for his incredible short response time concerning email communication.
Moreover, I am grateful to the members of the gauge/gravity group for helping me a lot by proofreading this thesis and, more importantly, for making the last couple of years an unbelievably amazing experience. In particular, I thank Mario Araujo for the relaxing bouldering evenings; Daniel Arean for the idea to wear the party hats; Mario Flory for Kafkaesque discussions; Patrick Kerner for many deep insights; Steffen Klug for various unbelievable stories; Max Newrzella for saving the group's honour during the visit to the Oktoberfest; Da-Wei Pang for the project idea; Charlotte Sleight for valuable tips regarding the English cuisine; Ann-Kathrin Straub for not taking my political instigations seriously; and my two longterm officemates Migael Strydom and Stephan Steinfurt for turning the office into a home.
Furthermore, many thanks go to the IMPRS coordinator Frank Steffen and Monika Goldammer for the organisation of various events during my PhD, and the canteen Team for keeping me healthy over the past years.
I am also very thankful to my parents, Hans Zeller and Gertrud Weber-Zeller, and sisters, Johanna and Barbara Zeller, for always supporting me independently of my communication efforts. Finally, Berit Plumhoff, thank you for always being there for me.

Appendix A

Helicity Zero Equations of Motion

Parity odd

$$0 = \frac{2\alpha^2 f^4 a_t^{1\prime} w'}{r^2} + \frac{2\alpha^2 f^4 a_x^{3\prime} \phi'}{r^2} + \xi_{tx}' \left(-\frac{4f'}{f} - \frac{\sigma'}{\sigma} + \frac{5}{r} \right) - \frac{2\alpha^2 f^4 \xi_{tx} w'^2}{r^2} + \xi_{tx}''$$

$$0 = -\frac{a_t^1 w \phi}{N^2 \sigma^2} - \frac{i\omega a_t^2 w}{N^2 \sigma^2} + a_x^{3\prime\prime} + a_x^{3\prime} \left(\frac{4f'}{f} + \frac{N'}{N} + \frac{\sigma'}{\sigma} + \frac{1}{r} \right) + \frac{\omega^2 a_x^3}{N^2 \sigma^2} + \frac{r^2 \xi_{tx}' \phi'}{f^4 N \sigma^2} + \frac{\xi_{tx} w^2 \phi}{N^2 \sigma^2}$$

$$0 = a_t^{1\prime\prime} + a_t^{1\prime} \left(\frac{3}{r} - \frac{\sigma'}{\sigma} \right) + \frac{a_x^3 f^4 w \phi}{r^2 N} + \xi_{tx} \left(\frac{4f' w'}{f} + \frac{N' w'}{N} + \frac{w\phi^2}{N^2 \sigma^2} + \frac{2\sigma' w'}{\sigma} - \frac{2w'}{r} \right) - \xi_{tx}' w'$$

$$0 = a_t^{2\prime\prime} + a_t^{2\prime} \left(\frac{3}{r} - \frac{\sigma'}{\sigma} \right) - \frac{a_t^2 f^4 w^2}{r^2 N} - \frac{i\omega a_x^3 f^4 w}{r^2 N}$$

$$0 = \frac{2i\alpha^2 f^4 w \phi a_t^{2\prime}}{r^2 \omega} - \frac{2i\alpha^2 a_t^2 f^4 w \phi'}{r^2 \omega} + \frac{2\alpha^2 a_x^3 f^4 \phi'}{r^2} + \xi_{tx}'$$

$$0 = \frac{i\omega a_t^{1\prime}}{\phi} + a_t^{2\prime} - \frac{a_t^2 \phi'}{\phi} - \frac{i\omega \xi_{tx} w'}{\phi}$$

$$0 = \frac{i\phi a_t^{1\prime}}{\omega} - \frac{i a_t^1 \phi'}{\omega} + a_t^{2\prime} + \frac{i f^4 N \sigma^2 w a_x^{3\prime}}{r^2 \omega} - \frac{i a_x^3 f^4 N \sigma^2 w'}{r^2 \omega} + \xi_{tx} \left(\frac{iw\phi'}{\omega} - \frac{i\phi w'}{\omega} \right)$$

Parity even

$$0 = \frac{8\alpha^2 f^4 a_x^{1\prime} w'}{3r^2} - \frac{8\alpha^2 a_x^1 f^4 w \phi^2}{3r^2 N^2 \sigma^2} + \frac{8i\alpha^2 \omega a_x^2 f^4 w \phi}{3r^2 N^2 \sigma^2} + \frac{4\alpha^2 a_t^{3\prime} \phi'}{3N\sigma^2} - \frac{8\alpha^2 a_t^3 f^4 w^2 \phi}{3r^2 N^2 \sigma^2} + \xi_x' \left(-\frac{2f'}{f} - \frac{\alpha^2 r \phi'^2}{3N\sigma^2} + \frac{4r}{N} + \frac{2}{r} \right) + \left(\frac{1}{r} - \frac{2f'}{f} \right) \xi_t' + \left(\frac{1}{r} - \frac{2f'}{f} \right) \xi_y' + \left(\frac{1}{r} - \frac{2f'}{f} \right) \xi_z' + \xi_x \left(\frac{4\alpha^2 f^4 w^2 \phi^2}{3r^2 N^2 \sigma^2} - \frac{4\alpha^2 f^4 w'^2}{3r^2} + \frac{\omega^2}{N^2 \sigma^2} \right)$$

$$
\begin{aligned}
&+\xi_t\left(\frac{4\alpha^2 f^4 w^2\phi^2}{3r^2N^2\sigma^2}-\frac{2\alpha^2\phi'^2}{3N\sigma^2}\right)+\xi_x''\\
0=&-\frac{4\alpha^2 f^4 a_x^{1\prime} w'}{3r^2}+\frac{4\alpha^2 a_x^1 f^4 w\phi^2}{3r^2N^2\sigma^2}-\frac{4i\alpha^2\omega a_x^2 f^4 w\phi}{3r^2N^2\sigma^2}+\frac{4\alpha^2 a_t^{3\prime}\phi'}{3N\sigma^2}+\frac{4\alpha^2 a_t^3 f^4 w^2\phi}{3r^2N^2\sigma^2}\\
&+\xi_y'\left(\frac{f'}{f}-\frac{\alpha^2 r\phi'^2}{3N\sigma^2}+\frac{4r}{N}+\frac{2}{r}\right)+\left(\frac{f'}{f}+\frac{1}{r}\right)\xi_t'+\left(\frac{f'}{f}+\frac{1}{r}\right)\xi_x'+\left(\frac{f'}{f}+\frac{1}{r}\right)\xi_z'\\
&+\xi_x\left(\frac{2\alpha^2 f^4 w'^2}{3r^2}-\frac{2\alpha^2 f^4 w^2\phi^2}{3r^2N^2\sigma^2}\right)+\xi_t\left(-\frac{2\alpha^2 f^4 w^2\phi^2}{3r^2N^2\sigma^2}-\frac{2\alpha^2\phi'^2}{3N\sigma^2}\right)+\frac{\omega^2\xi_y}{N^2\sigma^2}+\xi_y''\\
0=&-\frac{4\alpha^2 f^4 a_x^{1\prime} w'}{3r^2}+\frac{4\alpha^2 a_x^1 f^4 w\phi^2}{3r^2N^2\sigma^2}-\frac{4i\alpha^2\omega a_x^2 f^4 w\phi}{3r^2N^2\sigma^2}+\frac{4\alpha^2 a_t^{3\prime}\phi'}{3N\sigma^2}+\frac{4\alpha^2 a_t^3 f^4 w^2\phi}{3r^2N^2\sigma^2}\\
&+\xi_z'\left(\frac{f'}{f}-\frac{\alpha^2 r\phi'^2}{3N\sigma^2}+\frac{4r}{N}+\frac{2}{r}\right)+\left(\frac{f'}{f}+\frac{1}{r}\right)\xi_t'+\left(\frac{f'}{f}+\frac{1}{r}\right)\xi_x'+\left(\frac{f'}{f}+\frac{1}{r}\right)\xi_y'\\
&+\xi_x\left(\frac{2\alpha^2 f^4 w'^2}{3r^2}-\frac{2\alpha^2 f^4 w^2\phi^2}{3r^2N^2\sigma^2}\right)+\xi_t\left(-\frac{2\alpha^2 f^4 w^2\phi^2}{3r^2N^2\sigma^2}-\frac{2\alpha^2\phi'^2}{3N\sigma^2}\right)+\frac{\omega^2\xi_z}{N^2\sigma^2}+\xi_z''\\
0=&-\frac{4\alpha^2 f^4 a_x^{1\prime} w'}{3r^2}-\frac{8\alpha^2 a_x^1 f^4 w\phi^2}{3r^2N^2\sigma^2}+\frac{8i\alpha^2\omega a_x^2 f^4 w\phi}{3r^2N^2\sigma^2}-\frac{8\alpha^2 a_t^{3\prime}\phi'}{3N\sigma^2}-\frac{8\alpha^2 a_t^3 f^4 w^2\phi}{3r^2N^2\sigma^2}\\
&+\xi_t'\left(\frac{rf'^2}{f^2}+\frac{\alpha^2 f^4 w^2\phi^2}{6rN^2\sigma^2}+\frac{\alpha^2 f^4 w'^2}{6r}-\frac{\alpha^2 r\phi'^2}{2N\sigma^2}+\frac{6r}{N}\right)\\
&+\xi_x'\left(\frac{rf'^2}{f^2}+\frac{\alpha^2 f^4 w^2\phi^2}{6rN^2\sigma^2}+\frac{\alpha^2 f^4 w'^2}{6r}-\frac{\alpha^2 r\phi'^2}{6N\sigma^2}+\frac{2r}{N}-\frac{1}{r}\right)\\
&+\xi_y'\left(\frac{rf'^2}{f^2}+\frac{\alpha^2 f^4 w^2\phi^2}{6rN^2\sigma^2}+\frac{\alpha^2 f^4 w'^2}{6r}-\frac{\alpha^2 r\phi'^2}{6N\sigma^2}+\frac{2r}{N}-\frac{1}{r}\right)\\
&+\xi_z'\left(\frac{rf'^2}{f^2}+\frac{\alpha^2 f^4 w^2\phi^2}{6rN^2\sigma^2}+\frac{\alpha^2 f^4 w'^2}{6r}-\frac{\alpha^2 r\phi'^2}{6N\sigma^2}+\frac{2r}{N}-\frac{1}{r}\right)\\
&+\xi_x\left(\frac{4\alpha^2 f^4 w^2\phi^2}{3r^2N^2\sigma^2}+\frac{2\alpha^2 f^4 w'^2}{3r^2}+\frac{\omega^2}{N^2\sigma^2}\right)+\xi_t\left(\frac{4\alpha^2 f^4 w^2\phi^2}{3r^2N^2\sigma^2}+\frac{4\alpha^2\phi'^2}{3N\sigma^2}\right)\\
&+\frac{\omega^2\xi_y}{N^2\sigma^2}+\frac{\omega^2\xi_z}{N^2\sigma^2}+\xi_t''\\
0=&\,a_x^{1\prime\prime}+a_x^{1\prime}\left(\frac{4f'}{f}-\frac{\alpha^2 r\phi'^2}{3N\sigma^2}+\frac{4r}{N}-\frac{1}{r}\right)+a_x^1\left(\frac{\omega^2}{N^2\sigma^2}+\frac{\phi^2}{N^2\sigma^2}\right)\\
&-\frac{2i\omega a_x^2\phi}{N^2\sigma^2}+\frac{2a_t^3 w\phi}{N^2\sigma^2}-\frac{\xi_t w\phi^2}{N^2\sigma^2}+\frac{1}{2}\xi_t' w'-\frac{1}{2}\xi_x' w'+\frac{1}{2}\xi_y' w'+\frac{1}{2}\xi_z' w'\\
0=&\,\frac{2i\omega a_x^1\phi}{N^2\sigma^2}+a_x^{2\prime\prime}+a_x^{2\prime}\left(\frac{4f'}{f}-\frac{\alpha^2 r\phi'^2}{3N\sigma^2}+\frac{4r}{N}-\frac{1}{r}\right)+a_x^2\left(\frac{\omega^2}{N^2\sigma^2}+\frac{\phi^2}{N^2\sigma^2}\right)\\
&+\frac{i\omega a_t^3 w}{N^2\sigma^2}-\frac{i\omega\xi_t w\phi}{2N^2\sigma^2}-\frac{i\omega\xi_x w\phi}{2N^2\sigma^2}+\frac{i\omega\xi_y w\phi}{2N^2\sigma^2}+\frac{i\omega\xi_z w\phi}{2N^2\sigma^2}\\
0=&-\frac{2a_x^1 f^4 w\phi}{r^2N}+\frac{i\omega a_x^2 f^4 w}{r^2N}+a_t^{3\prime\prime}+a_t^{3\prime}\left(-\frac{2rf'^2}{f^2}-\frac{\alpha^2 f^4 w^2\phi^2}{3rN^2\sigma^2}-\frac{\alpha^2 f^4 w'^2}{3r}+\frac{3}{r}\right)\\
&-\frac{a_t^3 f^4 w^2}{r^2N}+\frac{f^4\xi_x w^2\phi}{r^2N}-\frac{1}{2}\xi_t'\phi'+\frac{1}{2}\xi_x'\phi'+\frac{1}{2}\xi_y'\phi'+\frac{1}{2}\xi_z'\phi'\\
0=&-\frac{if^4 N\sigma^2 w a_x^{2\prime}}{r^2\omega}+\frac{ia_x^2 f^4 N\sigma^2 w'}{r^2\omega}+a_t^{3\prime}-\frac{1}{2}\xi_t\phi'+\frac{1}{2}\xi_x\phi'+\frac{1}{2}\xi_y\phi'+\frac{1}{2}\xi_z\phi'\\
0=&-\frac{2\alpha^2 f^4 a_x^{1\prime} w'}{3r}-\frac{2\alpha^2 a_x^1 f^4 w\phi^2}{3rN^2\sigma^2}+\frac{2i\alpha^2\omega a_x^2 f^4 w\phi}{3rN^2\sigma^2}+\frac{2\alpha^2 r a_t^{3\prime}\phi'}{3N\sigma^2}-\frac{2\alpha^2 a_t^3 f^4 w^2\phi}{3rN^2\sigma^2}
\end{aligned}
$$

$$
\begin{aligned}
&+\xi_x'\left(\frac{r^2f'^2}{3f^2}+\frac{2rf'}{3f}+\frac{\alpha^2f^4w^2\phi^2}{18N^2\sigma^2}+\frac{1}{18}\alpha^2f^4w'^2-\frac{\alpha^2r^2\phi'^2}{18N\sigma^2}+\frac{2r^2}{3N}+\frac{1}{3}\right)\\
&+\xi_y'\left(\frac{r^2f'^2}{3f^2}-\frac{rf'}{3f}+\frac{\alpha^2f^4w^2\phi^2}{18N^2\sigma^2}+\frac{1}{18}\alpha^2f^4w'^2-\frac{\alpha^2r^2\phi'^2}{18N\sigma^2}+\frac{2r^2}{3N}+\frac{1}{3}\right)\\
&+\xi_z'\left(\frac{r^2f'^2}{3f^2}-\frac{rf'}{3f}+\frac{\alpha^2f^4w^2\phi^2}{18N^2\sigma^2}+\frac{1}{18}\alpha^2f^4w'^2-\frac{\alpha^2r^2\phi'^2}{18N\sigma^2}+\frac{2r^2}{3N}+\frac{1}{3}\right)\\
&+\xi_x\left(\frac{\alpha^2f^4w^2\phi^2}{3rN^2\sigma^2}+\frac{\alpha^2f^4w'^2}{3r}+\frac{r\omega^2}{3N^2\sigma^2}\right)+\xi_t\left(\frac{\alpha^2f^4w^2\phi^2}{3rN^2\sigma^2}-\frac{\alpha^2r\phi'^2}{3N\sigma^2}\right)\\
&+\frac{r\omega^2\xi_y}{3N^2\sigma^2}+\frac{r\omega^2\xi_z}{3N^2\sigma^2}+\xi_t'\\
0=&\frac{2\alpha^2a_x^1f^4w'}{r^2}+\frac{2i\alpha^2f^4w\phi a_x^{2\prime}}{r^2\omega}-\frac{2i\alpha^2a_x^2f^4\phi w'}{r^2\omega}\\
&+\xi_x\left(-\frac{rf'^2}{f^2}-\frac{2f'}{f}-\frac{\alpha^2f^4w^2\phi^2}{6rN^2\sigma^2}-\frac{\alpha^2f^4w'^2}{6r}+\frac{\alpha^2r\phi'^2}{6N\sigma^2}-\frac{2r}{N}+\frac{2}{r}\right)\\
&+\xi_y\left(-\frac{rf'^2}{f^2}+\frac{f'}{f}-\frac{\alpha^2f^4w^2\phi^2}{6rN^2\sigma^2}-\frac{\alpha^2f^4w'^2}{6r}+\frac{\alpha^2r\phi'^2}{6N\sigma^2}-\frac{2r}{N}+\frac{2}{r}\right)\\
&+\xi_z\left(-\frac{rf'^2}{f^2}+\frac{f'}{f}-\frac{\alpha^2f^4w^2\phi^2}{6rN^2\sigma^2}-\frac{\alpha^2f^4w'^2}{6r}+\frac{\alpha^2r\phi'^2}{6N\sigma^2}-\frac{2r}{N}+\frac{2}{r}\right)\\
&+\xi_x'+\xi_y'+\xi_z'
\end{aligned}
$$

Bibliography

[1] J. Erdmenger, P. Kerner, and H. Zeller, "Non-universal shear viscosity from Einstein gravity," *Phys.Lett.* **B699** (2011) 301–304, arXiv:1011.5912 [hep-th].

[2] J. Erdmenger, P. Kerner, and H. Zeller, "Transport in Anisotropic Superfluids: A Holographic Description," *JHEP* **1201** (2012) 059, arXiv:1110.0007 [hep-th].

[3] J. Erdmenger, D. Fernandez, and H. Zeller, "New Transport Properties of Anisotropic Holographic Superfluids," *JHEP* **1304** (2013) 049, arXiv:1212.4838 [hep-th].

[4] J. Erdmenger, D.-W. Pang, and H. Zeller, "Holographic entanglement entropy of semi-local quantum liquids," *JHEP* **1402** (2014) 016, arXiv:1311.1217 [hep-th].

[5] J. D. Bekenstein, "Black holes and entropy," *Phys.Rev.* **D7** (1973) 2333–2346.

[6] S. Hawking, "Particle Creation by Black Holes," *Commun.Math.Phys.* **43** (1975) 199–220.

[7] G. 't Hooft, "Dimensional reduction in quantum gravity," arXiv:gr-qc/9310026.

[8] L. Susskind, "The World as a hologram," *J.Math.Phys.* **36** (1995) 6377–6396, arXiv:hep-th/9409089 [hep-th].

[9] J. M. Maldacena, "The large N limit of superconformal field theories and supergravity," *Adv. Theor. Math. Phys.* **2** (1998) 231–252, arXiv:hep-th/9711200.

[10] S. S. Gubser, I. R. Klebanov, and A. M. Polyakov, "Gauge theory correlators from non-critical string theory," *Phys. Lett.* **B428** (1998) 105–114, arXiv:hep-th/9802109.

[11] E. Witten, "Anti-de Sitter space and holography," *Adv.Theor.Math.Phys.* **2** (1998) 253–291, arXiv:hep-th/9802150 [hep-th].

[12] **BICEP2** Collaboration, P. Ade *et al.*, "BICEP2 I: Detection Of B-mode Polarization at Degree Angular Scales," arXiv:1403.3985 [astro-ph.CO].

[13] A. H. Guth, "The Inflationary Universe: A Possible Solution to the Horizon and Flatness Problems," *Phys.Rev.* **D23** (1981) 347–356.

[14] A. D. Linde, "A New Inflationary Universe Scenario: A Possible Solution of the Horizon, Flatness, Homogeneity, Isotropy and Primordial Monopole Problems," *Phys.Lett.* **B108** (1982) 389–393.

[15] A. Albrecht and P. J. Steinhardt, "Cosmology for Grand Unified Theories with Radiatively Induced Symmetry Breaking," *Phys.Rev.Lett.* **48** (1982) 1220–1223.

[16] S. Glashow, "Partial Symmetries of Weak Interactions," *Nucl.Phys.* **22** (1961) 579–588.

[17] S. Weinberg, "A Model of Leptons," *Phys.Rev.Lett.* **19** (1967) 1264–1266.

[18] A. Salam, "Weak and Electromagnetic Interactions," *Conf.Proc.* **C680519** (1968) 367–377.

[19] G. 't Hooft and M. Veltman, "Regularization and Renormalization of Gauge Fields," *Nucl.Phys.* **B44** (1972) 189–213.

[20] **ATLAS** Collaboration, G. Aad *et al.*, "Observation of a new particle in the search for the Standard Model Higgs boson with the ATLAS detector at the LHC," *Phys.Lett.* **B716** (2012) 1–29, arXiv:1207.7214 [hep-ex].

[21] **CMS** Collaboration, S. Chatrchyan *et al.*, "Observation of a new boson at a mass of 125 GeV with the CMS experiment at the LHC," *Phys.Lett.* **B716** (2012) 30–61, arXiv:1207.7235 [hep-ex].

[22] G. Guralnik, C. Hagen, and T. Kibble, "Global Conservation Laws and Massless Particles," *Phys.Rev.Lett.* **13** (1964) 585–587.

[23] F. Englert and R. Brout, "Broken Symmetry and the Mass of Gauge Vector Mesons," *Phys.Rev.Lett.* **13** (1964) 321–323.

[24] P. W. Higgs, "Broken symmetries, massless particles and gauge fields," *Phys.Lett.* **12** (1964) 132–133.

[25] P. W. Higgs, "Broken Symmetries and the Masses of Gauge Bosons," *Phys.Rev.Lett.* **13** (1964) 508–509.

[26] A. Einstein, "Die Grundlage der allgemeinen Relativitätstheorie," *Annalen Phys.* **49** (1916) 769–822.

[27] W. Unruh, "Notes on black hole evaporation," *Phys.Rev.* **D14** (1976) 870.

[28] L. Susskind and J. Lindesay, *An Introduction to Black Holes, Information and the String Theory Revolution: The Holographic Universe*. World Scientific, 2005. `http://books.google.de/books?id=cxJCBRUNmVYC`.

[29] A. Almheiri, D. Marolf, J. Polchinski, and J. Sully, "Black Holes: Complementarity or Firewalls?," *JHEP* **1302** (2013) 062, `arXiv:1207.3123 [hep-th]`.

[30] A. Almheiri, D. Marolf, J. Polchinski, D. Stanford, and J. Sully, "An Apologia for Firewalls," *JHEP* **1309** (2013) 018, `arXiv:1304.6483 [hep-th]`.

[31] J. Polchinski, "Dirichlet Branes and Ramond-Ramond Charges," *Phys. Rev. Lett.* **75** no. 26, (Dec, 1995) 4724–4727.

[32] D. E. Berenstein, J. M. Maldacena, and H. S. Nastase, "Strings in flat space and pp waves from N=4 superYang-Mills," *JHEP* **0204** (2002) 013, `arXiv:hep-th/0202021 [hep-th]`.

[33] J. Polchinski, "Introduction to Gauge/Gravity Duality," `arXiv:1010.6134 [hep-th]`.

[34] O. Aharony, S. S. Gubser, J. M. Maldacena, H. Ooguri, and Y. Oz, "Large N field theories, string theory and gravity," *Phys. Rept.* **323** (2000) 183–386, `arXiv:hep-th/9905111`.

[35] E. D'Hoker and D. Z. Freedman, "Supersymmetric gauge theories and the AdS/CFT correspondence," `arXiv:hep-th/0201253`.

[36] A. Strominger and C. Vafa, "Microscopic origin of the Bekenstein-Hawking entropy," *Phys.Lett.* **B379** (1996) 99–104, `arXiv:hep-th/9601029 [hep-th]`.

[37] E. Zohar, J. I. Cirac, and B. Reznik, "Quantum simulations of gauge theories with ultracold atoms: local gauge invariance from angular momentum conservation," *Phys.Rev.* **A88** (2013) 023617, `arXiv:1303.5040 [quant-ph]`.

[38] P. Hohenberg and B. Halperin, "Theory of Dynamic Critical Phenomena," *Rev.Mod.Phys.* **49** (1977) 435–479.

[39] S. Bhattacharyya, V. E. Hubeny, S. Minwalla, and M. Rangamani, "Nonlinear Fluid Dynamics from Gravity," *JHEP* **0802** (2008) 045, arXiv:0712.2456 [hep-th].

[40] M. Rangamani, "Gravity and Hydrodynamics: Lectures on the fluid-gravity correspondence," *Class.Quant.Grav.* **26** (2009) 224003, arXiv:0905.4352 [hep-th].

[41] A. Chamblin, R. Emparan, C. V. Johnson, and R. C. Myers, "Holography, thermodynamics and fluctuations of charged AdS black holes," *Phys.Rev.* **D60** (1999) 104026, arXiv:hep-th/9904197 [hep-th].

[42] P. Kovtun, D. T. Son, and A. O. Starinets, "Viscosity in strongly interacting quantum field theories from black hole physics," *Phys. Rev. Lett.* **94** (2005) 111601, arXiv:hep-th/0405231.

[43] D. T. Son and A. O. Starinets, "Viscosity, Black Holes, and Quantum Field Theory," *Ann.Rev.Nucl.Part.Sci.* **57** (2007) 95–118, arXiv:0704.0240 [hep-th].

[44] N. Iqbal and H. Liu, "Universality of the hydrodynamic limit in AdS/CFT and the membrane paradigm," *Phys. Rev.* **D79** (2009) 025023, arXiv:0809.3808 [hep-th].

[45] A. O. Starinets, "Quasinormal spectrum and the black hole membrane paradigm," *Phys.Lett.* **B670** (2009) 442–445, arXiv:0806.3797 [hep-th].

[46] U. Heinz, C. Shen, and H. Song, "The viscosity of quark-gluon plasma at RHIC and the LHC," *AIP Conf.Proc.* **1441** (2012) 766–770, arXiv:1108.5323 [nucl-th].

[47] S. S. Gubser and S. S. Pufu, "The gravity dual of a p-wave superconductor," *JHEP* **11** (2008) 033, arXiv:0805.2960 [hep-th].

[48] M. Ammon, J. Erdmenger, M. Kaminski, and P. Kerner, "Superconductivity from gauge/gravity duality with flavor," *Phys. Lett.* **B680** (2009) 516–520, arXiv:0810.2316 [hep-th].

[49] M. Ammon, J. Erdmenger, M. Kaminski, and P. Kerner, "Flavor Superconductivity from Gauge/Gravity Duality," *JHEP* **10** (2009) 067, arXiv:0903.1864 [hep-th].

[50] M. Ammon, J. Erdmenger, V. Grass, P. Kerner, and A. O'Bannon, "On Holographic p-wave Superfluids with Back-reaction," *Phys. Lett.* **B686** (2010) 192–198, arXiv:0912.3515 [hep-th].

[51] J. Erdmenger, M. Haack, M. Kaminski, and A. Yarom, "Fluid dynamics of R-charged black holes," *JHEP* **01** (2009) 055, arXiv:0809.2488 [hep-th].

[52] N. Banerjee, J. Bhattacharya, S. Bhattacharyya, S. Dutta, R. Loganayagam, *et al.*, "Hydrodynamics from charged black branes," *JHEP* **1101** (2011) 094, arXiv:0809.2596 [hep-th].

[53] D. T. Son and P. Surowka, "Hydrodynamics with Triangle Anomalies," *Phys.Rev.Lett.* **103** (2009) 191601, arXiv:0906.5044 [hep-th].

[54] P. de Gennes, *The physics of liquid crystals*. International series of monographs on physics. Clarendon Press, 1974. http://books.google.de/books?id=DTkGJnqykLMC.

[55] S. A. Hartnoll, C. P. Herzog, and G. T. Horowitz, "Holographic Superconductors," *JHEP* **12** (2008) 015, arXiv:0810.1563 [hep-th].

[56] S. A. Hartnoll, C. P. Herzog, and G. T. Horowitz, "Building a Holographic Superconductor," *Phys. Rev. Lett.* **101** (2008) 031601, arXiv:0803.3295 [hep-th].

[57] S. A. Hartnoll, "Lectures on holographic methods for condensed matter physics," *Class. Quant. Grav.* **26** (2009) 224002, arXiv:0903.3246 [hep-th].

[58] C. Charmousis, B. Gouteraux, B. Kim, E. Kiritsis, and R. Meyer, "Effective Holographic Theories for low-temperature condensed matter systems," *JHEP* **1011** (2010) 151, arXiv:1005.4690 [hep-th].

[59] N. Iqbal, H. Liu, and M. Mezei, "Lectures on holographic non-Fermi liquids and quantum phase transitions," arXiv:1110.3814 [hep-th].

[60] G. T. Horowitz, J. E. Santos, and D. Tong, "Optical Conductivity with Holographic Lattices," *JHEP* **1207** (2012) 168, arXiv:1204.0519 [hep-th].

[61] A. Donos, J. P. Gauntlett, and C. Pantelidou, "Competing p-wave orders," *Class.Quant.Grav.* **31** (2014) 055007, arXiv:1310.5741 [hep-th].

[62] M. Cubrovic, J. Zaanen, and K. Schalm, "String Theory, Quantum Phase Transitions and the Emergent Fermi-Liquid," *Science* **325** (2009) 439–444, arXiv:0904.1993 [hep-th].

[63] S. A. Hartnoll and E. Shaghoulian, "Spectral weight in holographic scaling geometries," *JHEP* **1207** (2012) 078, arXiv:1203.4236 [hep-th].

[64] H. Liu and M. Mezei, "Probing renormalization group flows using entanglement entropy," *JHEP* **1401** (2014) 098, arXiv:1309.6935 [hep-th].

[65] C. Johnson, *D-Branes*. Cambridge Monographs on Mathematical Physics. Cambridge University Press, 2006. http://books.google.de/books?id=pnClL_tua_wC.

[66] S. R. Coleman and J. Mandula, "All Possible Symmetries of the S Matrix," *Phys.Rev.* **159** (1967) 1251–1256.

[67] D. Tong, "String Theory," *http://www.damtp.cam.ac.uk/user/tong/string.html* (2009) .

[68] P. Breitenlohner and D. Z. Freedman, "Stability in Gauged Extended Supergravity," *Annals Phys.* **144** (1982) 249.

[69] K. Skenderis and B. C. van Rees, "Real-time gauge/gravity duality: Prescription, Renormalization and Examples," *JHEP* **0905** (2009) 085, arXiv:0812.2909 [hep-th].

[70] S. A. Hartnoll, "Horizons, holography and condensed matter," arXiv:1106.4324 [hep-th].

[71] A. Altland and B. Simons, *Condensed Matter Field Theory*. Cambridge books online. Cambridge University Press, 2010. http://books.google.de/books?id=GpF0Pgo8CqAC.

[72] J. I. Kapusta and C. Gale, *Finite-Temperature Field Theory: Principles and Applications*. Cambridge monographs on mathematical physics. Cambridge University Press, 2006. http://books.google.de/books?id=rll8dJ2iTpsC.

[73] A. Schmitt, "Introduction to superfluidity – Field-theoretical approach and applications," arXiv:1404.1284 [hep-ph].

[74] V. Ginzburg and L. Landau, "On the Theory of superconductivity," *Zh.Eksp.Teor.Fiz.* **20** (1950) 1064–1082.

[75] L. Ryder, *Quantum Field Theory*. Cambridge University Press, 1996. http://books.google.de/books?id=nnuW_kVJ500C.

[76] J. Bardeen, L. Cooper, and J. Schrieffer, "Theory of superconductivity," *Phys.Rev.* **108** (1957) 1175–1204.

[77] M. Peskin and D. Schroeder, *An Introduction To Quantum Field Theory*. Frontiers in physics. Westview Press, 1995. http://books.google.de/books?id=EVeNNcslvX0C.

[78] C. P. Herzog and A. Yarom, "Sound modes in holographic superfluids," *Phys. Rev.* **D80** (2009) 106002, arXiv:0906.4810 [hep-th].

[79] F. Denef and S. A. Hartnoll, "Landscape of superconducting membranes," *Phys. Rev.* **D79** (2009) 126008, arXiv:0901.1160 [hep-th].

[80] N. Mermin and H. Wagner, "Absence of ferromagnetism or antiferromagnetism in one-dimensional or two-dimensional isotropic Heisenberg models," *Phys.Rev.Lett.* **17** (1966) 1133–1136.

[81] P. Kovtun, "Lectures on hydrodynamic fluctuations in relativistic theories," *J.Phys.* **A45** (2012) 473001, arXiv:1205.5040 [hep-th].

[82] J. Bhattacharya, S. Bhattacharyya, S. Minwalla, and A. Yarom, "A Theory of first order dissipative superfluid dynamics," arXiv:1105.3733 [hep-th].

[83] R. Kubo, "Statistical mechanical theory of irreversible processes. 1. General theory and simple applications in magnetic and conduction problems," *J.Phys.Soc.Jap.* **12** (1957) 570–586.

[84] J. de Boer, E. P. Verlinde, and H. L. Verlinde, "On the holographic renormalization group," *JHEP* **0008** (2000) 003, arXiv:hep-th/9912012 [hep-th].

[85] J. D. Brown and J. York, James W., "Quasilocal energy and conserved charges derived from the gravitational action," *Phys.Rev.* **D47** (1993) 1407–1419, arXiv:gr-qc/9209012 [gr-qc].

[86] V. Balasubramanian and P. Kraus, "A stress tensor for anti-de Sitter gravity," *Commun. Math. Phys.* **208** (1999) 413–428, arXiv:hep-th/9902121.

[87] S. de Haro, S. N. Solodukhin, and K. Skenderis, "Holographic reconstruction of spacetime and renormalization in the AdS/CFT correspondence," *Commun. Math. Phys.* **217** (2001) 595–622, arXiv:hep-th/0002230.

[88] D. T. Son and A. O. Starinets, "Minkowski-space correlators in AdS/CFT correspondence: Recipe and applications," *JHEP* **09** (2002) 042, arXiv:hep-th/0205051.

[89] C. P. Herzog and D. T. Son, "Schwinger-Keldysh propagators from AdS/CFT correspondence," *JHEP* **03** (2003) 046, arXiv:hep-th/0212072.

[90] G. T. Horowitz, "Introduction to Holographic Superconductors," arXiv:1002.1722 [hep-th].

[91] Y.-Y. Bu, J. Erdmenger, J. P. Shock, and M. Strydom, "Magnetic field induced lattice ground states from holography," arXiv:1210.6669 [hep-th].

[92] D. Basov and T. Timusk, "Electrodynamics of high- Tc superconductors," *Rev.Mod.Phys.* **77** (2005) 721–779.

[93] J. Erdmenger and S. Steinfurt, "A universal fermionic analogue of the shear viscosity," *JHEP* **1307** (2013) 018, arXiv:1302.1869 [hep-th].

[94] J. P. Gauntlett, J. Sonner, and T. Wiseman, "Quantum Criticality and Holographic Superconductors in M-theory," *JHEP* **1002** (2010) 060, arXiv:0912.0512 [hep-th].

[95] R. Manvelyan, E. Radu, and D. H. Tchrakian, "New AdS non Abelian black holes with superconducting horizons," *Phys. Lett.* **B677** (2009) 79–87, arXiv:0812.3531 [hep-th].

[96] S. Kobayashi, D. Mateos, S. Matsuura, R. C. Myers, and R. M. Thomson, "Holographic phase transitions at finite baryon density," *JHEP* **02** (2007) 016, arXiv:hep-th/0611099.

[97] A. Donos and J. P. Gauntlett, "On the thermodynamics of periodic AdS black branes," *JHEP* **1310** (2013) 038, arXiv:1306.4937 [hep-th].

[98] P. Basu, J. He, A. Mukherjee, and H.-H. Shieh, "Hard-gapped Holographic Superconductors," *Phys. Lett.* **B689** (2010) 45–50, arXiv:0911.4999 [hep-th].

[99] S. S. Gubser, F. D. Rocha, and A. Yarom, "Fermion correlators in non-abelian holographic superconductors," *JHEP* **1011** (2010) 085, arXiv:1002.4416 [hep-th].

[100] D. T. Son and M. A. Stephanov, "QCD at finite isospin density," *Phys. Rev. Lett.* **86** (2001) 592–595, arXiv:hep-ph/0005225.

[101] K. Skenderis, "Lecture notes on holographic renormalization," *Class. Quant. Grav.* **19** (2002) 5849–5876, arXiv:hep-th/0209067.

[102] B. Sahoo and H.-U. Yee, "Electrified plasma in AdS/CFT correspondence," *JHEP* **11** (2010) 095, arXiv:1004.3541 [hep-th].

[103] M. Kaminski, K. Landsteiner, J. Mas, J. P. Shock, and J. Tarrio, "Holographic Operator Mixing and Quasinormal Modes on the Brane," *JHEP* **02** (2010) 021, arXiv:0911.3610 [hep-th].

[104] R. C. Myers, A. O. Starinets, and R. M. Thomson, "Holographic spectral functions and diffusion constants for fundamental matter," *JHEP* **11** (2007) 091, arXiv:0706.0162 [hep-th].

[105] A. Donos and S. A. Hartnoll, "Interaction-driven localization in holography," *Nature Phys.* **9** (2013) 649–655, arXiv:1212.2998.

[106] L. Landau and E. Lifshitz, *Fluid Mechanics*. No. v. 6. Elsevier Science, 1959. http://books.google.de/books?id=CeBbAwAAQBAJ.

[107] L. Landau, L. Pitaevskii, A. Kosevich, and E. Lifshitz, *Theory of Elasticity*. No. v. 7. Elsevier Science, 1984. http://books.google.de/books?id=NXRaWJb4HdkC.

[108] F. M. Leslie, "Some Constitutive Equations For Anisotropic Fluids," *The Quarterly Journal of Mechanics and Applied Mathematics* **19** no. 3, (1966) 357–370.

[109] C. Pujol and D. Davesne, "Relativistic dissipative hydrodynamics with spontaneous symmetry breaking," *Phys. Rev.* **C67** (2003) 014901, arXiv:hep-ph/0204355.

[110] A. Buchel and J. T. Liu, "Universality of the shear viscosity in supergravity," *Phys. Rev. Lett.* **93** (2004) 090602, arXiv:hep-th/0311175.

[111] A. Rebhan and D. Steineder, "Violation of the Holographic Viscosity Bound in a Strongly Coupled Anisotropic Plasma," *Phys.Rev.Lett.* **108** (2012) 021601, arXiv:1110.6825 [hep-th].

[112] A. Buchel and R. C. Myers, "Causality of Holographic Hydrodynamics," *JHEP* **08** (2009) 016, arXiv:0906.2922 [hep-th].

[113] P. Basu and J.-H. Oh, "Analytic Approaches to An-Isotropic Holographic Superfluids," arXiv:1109.4592 [hep-th].

[114] J. Erdmenger, M. Kaminski, P. Kerner, and F. Rust, "Finite baryon and isospin chemical potential in AdS/CFT with flavor," *JHEP* **11** (2008) 031, arXiv:0807.2663 [hep-th].

[115] J. Armas, J. Gath, and N. A. Obers, "Black Branes as Piezoelectrics," *Phys.Rev.Lett.* **109** (2012) 241101, arXiv:1209.2127 [hep-th].

[116] S. Nakamura, H. Ooguri, and C.-S. Park, "Gravity Dual of Spatially Modulated Phase," *Phys.Rev.* **D81** (2010) 044018, arXiv:0911.0679 [hep-th].

[117] H. Ooguri and C.-S. Park, "Spatially Modulated Phase in Holographic Quark-Gluon Plasma," *Phys.Rev.Lett.* **106** (2011) 061601, arXiv:1011.4144 [hep-th].

[118] A. Donos and J. P. Gauntlett, "Holographic striped phases," *JHEP* **1108** (2011) 140, arXiv:1106.2004 [hep-th].

[119] A. Donos and J. P. Gauntlett, "Holographic helical superconductors," *JHEP* **1112** (2011) 091, arXiv:1109.3866 [hep-th].

[120] C. P. Herzog and S. S. Pufu, "The Second Sound of SU(2)," *JHEP* **04** (2009) 126, arXiv:0902.0409 [hep-th].

[121] N. Ogawa, T. Takayanagi, and T. Ugajin, "Holographic Fermi Surfaces and Entanglement Entropy," *JHEP* **1201** (2012) 125, arXiv:1111.1023 [hep-th].

[122] I. R. Klebanov, D. Kutasov, and A. Murugan, "Entanglement as a probe of confinement," *Nucl.Phys.* **B796** (2008) 274–293, arXiv:0709.2140 [hep-th].

[123] A. Pakman and A. Parnachev, "Topological Entanglement Entropy and Holography," *JHEP* **0807** (2008) 097, arXiv:0805.1891 [hep-th].

[124] S. S. Gubser and A. Nellore, "Ground states of holographic superconductors," *Phys.Rev.* **D80** (2009) 105007, arXiv:0908.1972 [hep-th].

[125] G. T. Horowitz and M. M. Roberts, "Zero Temperature Limit of Holographic Superconductors," *JHEP* **11** (2009) 015, arXiv:0908.3677 [hep-th].

[126] M. Taylor, "Non-relativistic holography," arXiv:0812.0530 [hep-th].

[127] S. Sachdev, *Quantum Phase Transitions*. Cambridge University Press, 2011. http://books.google.de/books?id=F3IkpxwpqSgC.

[128] L. Huijse, S. Sachdev, and B. Swingle, "Hidden Fermi surfaces in compressible states of gauge-gravity duality," *Phys.Rev.* **B85** (2012) 035121, arXiv:1112.0573 [cond-mat.str-el].

[129] M. Kulaxizi, A. Parnachev, and K. Schalm, "On Holographic Entanglement Entropy of Charged Matter," *JHEP* **1210** (2012) 098, arXiv:1208.2937 [hep-th].

[130] S. Ryu and T. Takayanagi, "Aspects of Holographic Entanglement Entropy," *JHEP* **0608** (2006) 045, arXiv:hep-th/0605073 [hep-th].

[131] P. Calabrese and J. L. Cardy, "Entanglement entropy and quantum field theory: A Non-technical introduction," *Int.J.Quant.Inf.* **4** (2006) 429, arXiv:quant-ph/0505193 [quant-ph].

[132] S. Ryu and T. Takayanagi, "Holographic derivation of entanglement entropy from AdS/CFT," *Phys.Rev.Lett.* **96** (2006) 181602, arXiv:hep-th/0603001 [hep-th].

[133] A. Lewkowycz and J. Maldacena, "Generalized gravitational entropy," *JHEP* **1308** (2013) 090, arXiv:1304.4926 [hep-th].

[134] T. Hirata and T. Takayanagi, "AdS/CFT and strong subadditivity of entanglement entropy," *JHEP* **0702** (2007) 042, arXiv:hep-th/0608213 [hep-th].

[135] M. Bhaseen, J. P. Gauntlett, B. Simons, J. Sonner, and T. Wiseman, "Holographic Superfluids and the Dynamics of Symmetry Breaking," *Phys.Rev.Lett.* **110** (2013) 015301, arXiv:1207.4194 [hep-th].